Design, Synthesis, and Analysis of Crosslinked Polymeric Nanoparticles for Drug Delivery Applications

A Thesis Submitted by

Luka Blagojevic

In partial fulfilment of the requirements for the degree of

DOCTOR OF PHILOSOPHY

Department of Chemistry
Imperial College London
Molecular Sciences Research Hub
London W12 0BZ
United Kingdom

2023

Declaration of Originality

I, Luka Blagojevic, hereby confirm that the work presented in this document is my own. References to the work of others and instances where assistance was received are clearly acknowledged.

Copyright

The copyright of this thesis rests with the author. Unless otherwise indicated, its contents are licensed under a Creative Commons Attribution-NonCommercial 4.0 International Licence (CC BY-NC).

Under this licence, you may copy and redistribute the material in any medium or format. You may also create and distribute modified versions of the work. This is on the condition that: you credit the author and do not use it, or any derivative works, for a commercial purpose.

When reusing or sharing this work, ensure you make the licence terms clear to others by naming the licence and linking to the licence text. Where a work has been adapted, you should indicate that the work has been changed and describe those changes.

Please seek permission from the copyright holder for uses of this work that are not included in this licence or permitted under UK Copyright Law.

Acknowledgements

Firstly, I would like to thank my supervisor Nazila Kamaly for giving me the opportunity to work on this exciting project and introducing me to the wonderful world of nanoparticles. Through her guidance, I have learned the importance of approaching every difficulty encountered in the research process with courage and a positive attitude. She provided tons of optimism and support throughout this journey; I will always be grateful for this.

I would like to thank Sofia, Jake, Runxin, and all the former members of the Kamaly group. I have learned something from each of you, and I am hopeful to have made a small contribution to making your time spent at Imperial worth remembering. A special thanks go to Rupali Dabas for introducing me to the wonderful world of confocal microscopy, teaching me many valuable lessons, and above all for being the most supportive friend and colleague I had throughout this journey.

I am grateful for the students I helped mentor along the way (Edmund, Nelli, Lisa, Renee). I am hopeful you learned from me as much as I have learned from you. A special thanks goes to Yicheng Wang for her assistance with the scale-up of precursors of polymerisable oligoesters, and her help with the synthesis of nanoparticles containing betamethasone and prednisolone.

I am deeply grateful to everyone who contributed to this project. Many thanks to Lisa Haigh and Malgorzata Puchnarewicz for their assistance with mass spectrometry samples, Pete Haycock and Stuart Elliott for their assistance with endless NMR samples, and Mahmoud Ardakani and Marc Morgan for introducing me to electron microscopy and helping me visualise my nanoparticles.

Many thanks to my friends Paola, Nicky, and Marco. You were my extended family throughout these years and a constant source of support, inspiration, and laughter. I could not imagine my life in London without you.

Finally, I dedicate this thesis to my mum. You are simply the best and I cannot thank you enough for always being there for me.

Abstract

Polymeric nanoparticles are versatile carriers of a range of therapeutic entities and enable the controlled release of these therapies in an increasingly specific spatiotemporal manner. The miniaturisation of clinically advanced degradable polymers such as poly(lactic-*co*-glycolic) acid allowed the establishment of polyester nanoparticles as highly biocompatible golden standards for biomedical applications. Comparatively, synthetic chemistry approaches allow access to crosslinked polymeric nanoparticles via the chemical manipulation of small polymerisable molecules and in doing so, offer the prospect of precise control over drug encapsulation and drug release properties.

The research described in this thesis concerns the synthesis of novel crosslinked polymeric nanoparticles via the radical polymerisation of structurally well-defined building blocks designed around the chemistry of degradable chemical motifs. Firstly, a library of polymerisable oligoesters inspired by sequenced poly(lactic-*co*-glycolic acid) was successfully prepared by stepwise synthesis. Secondly, these polymerisable oligoesters were reacted to form crosslinked polymeric nanoparticles via an unprecedented methodology that enables radical polymerisation and nanoparticle formation processes to occur simultaneously in one pot. Thirdly, the encapsulation of the small-molecule drug dexamethasone was achieved within these novel nanoparticles via a single-step procedure, generating drug-loaded NPs which were found to be stable in the presence of proteins, can be stored as aqueous suspensions at room temperature, and are able to release a fraction of the encapsulated drug *in vitro*. Finally, a disulphide-containing monomer inspired by the chemistry of polymerisable oligoesters is synthesised and reacted to form nanoparticles which are responsive to the presence of glutathione, setting the foundations for the further advancement of the platform towards stimuli-responsive drug delivery systems.

Table of Contents

Chapter 1: Thesis Background and Synopsis **17**

1.1 Drug Delivery Systems **18**

1.2 Nanoparticles for Drug Delivery **19**

1.3 Nanomedicine: Nanoparticles in the Clinic **20**

1.4 Polymeric Nanoparticles **23**

1.4.1 Types of Polymeric Nanoparticles 25

1.4.2 Crosslinked Polymeric Nanoparticles 25

1.4.3 Biocompatibility and Degradation of Polymeric Drug Delivery Systems 27

1.4.4 Mechanisms of Drug Release from Degradable Polymers 28

1.5 Poly(lactic-co-glycolic acid) (PLGA) Nanoparticles **30**

1.5.1 Poly(α-hydroxy acids) 30

1.5.2 PLGA as a Versatile Degradable Polymer 32

1.5.3 PLGA for Drug Delivery 34

1.5.4 PEGylated PLGA 36

1.5.5 PLGA-based Nanoparticles 37

1.6 Stimuli-Responsive Polymeric NPs **39**

1.6.1 Disulphide-containing Nanoparticles 41

1.6.2 Diselenide-containing Nanoparticles 44

1.7 Preparation of Polymeric Nanoparticles **45**

1.7.1 Nanoprecipitation 45

1.7.2 Emulsion-based Methods 48

1.7.3 Crosslinking of Polymers 50

1.7.4 Radical Polymerisation of Monomers 54

1.8 Payload Loading Methods **59**

1.9 Thesis Synopsis **61**

Chapter 2: Design and Synthesis of Oligolactoglycolic Acid Dimethacrylates **62**

2.1 Introduction **63**

2.2 Design of OLGADMAs and Naming Conventions 66

2.3 Synthesis of OLGADMAs 67

2.4 General Considerations Concerning OLGA-based Nanoparticles 77

2.5 Chapter Summary 78

Chapter 3: Synthesis and Analysis of OLGA-based Nanoparticles 79

3.1 Introduction 80

3.2 Initial Work Towards OLGA-based NPs 83

3.2.1 Nanoprecipitation Polymerisation of **OLGADMA 4Aa** 83

3.2.2 Nanoprecipitation Polymerisation of **OLGADMA 4Aa** in the Presence of PEGylated Monomers 86

3.2.3 Influence of the Reaction Duration on the Size of OLGA-based Nanoparticles 93

3.2.4 Influence of the AIBN Concentration on the Size and the Yield of the Nanoparticles 96

3.3 Standard Nanoprecipitation Polymerisation Conditions and Naming Conventions 97

3.4 Synthesis and Analysis of NP4Aa 98

3.5 Synthesis and Analysis of a Library of OLGA-based NPs 101

3.6 Comparative Stability Study of OLGA-based and PLGA-based Nanoparticles 103

3.6.1 Preparation and Analysis of PLGA-based NPs 103

3.6.2 Size Stability at 37 °C 105

3.6.3 ζ-potential Stability at 37 °C 108

3.6.4 pH Stability at 37 °C 109

3.6.5 Analysis of the Stability of **NP4Aa**, **NP4Ab**, and **NP4Bb** via FTIR Spectroscopy 111

3.7 Effect of NP4Aa, NP4Ab, and NP4Bb on Cell Viability In Vitro 112

3.8 Cellular Uptake of Fluorescent NP4Aa 113

3.9 Nanoprecipitation Polymerisation of OLGADMA 4Aa in the Presence of the Water-Soluble Initiator V-50 117

3.10 Chapter Summary **119**

Chapter 4: Synthesis and Analysis of Drug-loaded OLGA-based Nanoparticles **120**

4.1 Introduction **121**

4.2 Initial Work Towards Dexamethasone-loaded OLGA-based Nanoparticles **122**

4.2.1 Stability of Dexamethasone Under Reaction Conditions 122

4.2.2 Optimisation of the Nanoprecipitation Polymerisation of **OLGADMA 4Aa** in the Presence of Dexamethasone 124

4.2.3 Size-modulation of Dexamethasone-loaded Nanoparticles 126

4.3 Standard Procedure for the Synthesis of Dexamethasone-Loaded OLGA-based Nanoparticles and Naming Conventions **127**

4.4 Synthesis and Analysis of DNP4Aa **128**

4.5 Synthesis and Analysis of a Library of Dexamethasone-Loaded OLGA-based Nanoparticles **131**

4.6 Synthesis and Analysis of Dexamethasone-loaded PLGA-based Nanoparticles **133**

4.7 Comparative Drug Release Study **134**

4.8 Stability of DNP4Aa, DNP4Ab, and DNP4Bb in Biological Medium **137**

4.9 Stability of DNP4Aa, DNP4Ab, and DNP4Bb Upon Storage at Room Temperature **139**

4.10 Effect of DNP4Aa, DNP4Ab, and DNP4Bb on Cell Viability In Vitro **141**

4.11 Further Observations Regarding Drug-Loaded OLGA-Based Nanoparticles **142**

4.11.1 Comparison of OLGA-based Nanoparticles Loaded with Dexamethasone, Betamethasone, and Prednisolone 142

4.11.2 Synthesis of OLGA-based Nanoparticles in the Presence of XBD173 . 144

4.12 Chapter Summary **147**

Chapter 5: Work Towards Stimuli-Responsive Crosslinked Polymeric Nanoparticles **148**

5.1 Introduction **149**

5.2 Work Towards Disulphide-Containing Crosslinked Polymeric Nanoparticles **149**

5.2.1 Design and Synthesis of Disulphide **61** 150

5.2.2 Synthesis and Analysis of Disulphide-Containing Crosslinked Polymeric Nanoparticles 151

5.2.3 Preliminary Evaluation of the Stability of Disulphide-Containing Crosslinked Polymeric Nanoparticles in the Presence of Glutathione 154

5.3 Work Towards Diselenide-Containing Crosslinked Polymeric Nanoparticles **158**

5.3.1 Evaluation of the Stability of L-Selenocystine in the Presence of Hydrogen Peroxide 159

5.3.2 Synthesis of Diselenide **63** 161

5.3.3 Proposed Routes Towards Diselenide-Containing Crosslinked Polymeric Nanoparticles 162

5.4 Chapter Summary **164**

Chapter 6: Conclusions and Future Work **165**

Chapter 7: Experimental Section **169**

7.1 General Information **169**

7.1.1 Materials 169

7.1.2 Instrumentation 169

7.1.3 Dynamic Light Scattering (DLS) 169

7.1.4 Electrophoretic Light Scattering (ELS) 170

7.1.5 Transmission Electron Microscopy (TEM) 170

7.1.6 General Synthetic Procedures 170

7.2 Experimental Details for Chapter 2 ..... **173**

7.2.1 Synthesis and Characterisation of OLGADMAs 173

7.3 Experimental Details for Chapter 3 ..... **206**

7.3.1 Influence of the Reaction Duration on the Size of OLGA-based Nanoparticles 206
7.3.2 Standard Nanoprecipitation Polymerisation Conditions 206
7.3.3 Preparation of PLGA-based NPs 207
7.3.4 Comparative Stability Study of OLGA-based and PLGA-based Nanoparticles 207
7.3.5 Effect of **NP4Aa**, **NP4Ab,** and **NP4Bb** on Cell Viability In Vitro 207
7.3.6 Synthesis of Fluorescent **NP4Aa** 208
7.3.7 Cellular Uptake of Fluorescent **NP4Aa** 208
7.3.8 Nanoprecipitation Polymerisation of **OLGADMA 4Aa** in the Presence of the Water-Soluble Initiator V-50 208
7.3.9 Synthesis and Characterisation of **PLGA alt** 209
7.4 Experimental Details for Chapter 4 211
7.4.1 Stability of Dexamethasone Under Typical Nanoprecipitation Polymerisation Conditions 211
7.4.2 Standard Procedure for the Synthesis of Dexamethasone-loaded OLGA-based Nanoparticles 211
7.4.3 Synthesis of Dexamethasone-loaded PLGA-based Nanoparticles 211
7.4.4 Quantitation of Dexamethasone 212
7.4.5 Determination of the Encapsulation Efficiency of Dexamethasone 212
7.4.6 Estimation of the Loading Efficiency of Dexamethasone 212
7.4.7 Comparative Drug Release Study 213
7.4.8 Stability of **DNP4Aa**, **DNP4Ab**, and **DNP4Bb** in Biological Medium 213
7.4.9 Stability of **DNP4Aa**, **DNP4Ab**, and **DNP4Bb** Upon Storage at Room Temperature 213
7.4.10 Synthesis of OLGA-based Nanoparticles in the Presence of XBD173 . 213
7.4.11 Synthesis of PLGA-based Nanoparticles in the Presence of XBD173 . 214
7.4.12 Quantitation of XBD173 214
7.4.13 Estimation of the Encapsulation Efficiency and the Loading Efficiency of XBD173 215
7.4.14 Effect of **DNP4Aa**, **DNP4Ab**, and **DNP4Bb** on Cell Viability In Vitro 215
7.5 Experimental Details for Chapter 5 216
7.5.1 Synthesis and Characterisation of Disulphide **61** 216

7.5.2 Synthesis and Characterisation of Diselenide **63** 217
7.5.3 Synthesis of Disulphide-Containing Crosslinked Polymeric Nanoparticles 219
References 220

Figures

Figure 1. Chronological evolution of drug delivery systems 19
Figure 2. Classification of polymeric NPs according to structure. 25
Figure 3. Structure of a generic crosslinked polymer. 26
Figure 4. Approximation of hydrolysis rates of degradable polymers 27
Figure 5. Mechanisms of drug release from polymeric drug delivery systems 29
Figure 6. Structure of poly(α-hydroxy acids) 30
Figure 7. α,ω-Itaconyl-terminated PLGA-PEG-PLGA macromonomers 34
Figure 8. Chemical structure of glutathione. 42
Figure 9. Examples of functionalised polymers containing the PLGA chemical motif 64
Figure 10. General chemical structure of oligolactoglycolic acid dimethacrylates 65
Figure 11. Proposed structure of OLGA-based NPs. 66
Figure 12. Chemical structures of OLGADMAs synthesised in this work. 67
Figure 13. Protected monomers **1**-**4** 67
Figure 14. DLS analysis of the crude reaction mixture involving **OLGADMA 4Aa** 84
Figure 15. ATR FTIR spectra of **OLGADMA 4Aa** and NPs 85
Figure 16. Chemical structure of PEGylated monomers 87
Figure 17. Intensity-weighted size distribution of NPs prepared from **OLGADMA 4Aa** 88
Figure 18. Stacked sections of ^{1}H NMR of NPs 89
Figure 19. ATR FTIR spectra of **OLGADMA 4Aa**, physical mixture, and NPs 91
Figure 20. C-H stretching region of ATR-FTIR spectra of NPs 92
Figure 21. DLS and ELS analysis of the nanoprecipitation polymerisation reaction 94
Figure 22. ^{1}H NMR analysis of the nanoprecipitation polymerisation reaction. 95
Figure 23. MADLS® analysis of particles prepared using different AIBN concentrations 96
Figure 24. DLS, ELS, and TEM analysis of **NP4Aa** 99
Figure 25. ATR FTIR spectrum of **NP4Aa** 100
Figure 26. DLS analysis of PLGA-based NPs performed over 5 weeks of stability study 106
Figure 27. DLS analysis of OLGA-based NPs performed over 5 weeks of stability study 107
Figure 28. PI of OLGA-based NPs and PLGA-based NPs over 5 weeks of stability study 108
Figure 29. pH of aqueous NP suspensions subjected to 5 weeks of stability study 110
Figure 30. ATR FTIR spectra of NPs during 5 weeks of stability study 111
Figure 31. Normalised HeLa cell viability upon treatment with **NP4Aa**, **NP4Ab**, and **NP4Bb** 112
Figure 32. Confocal microscopy images of cells treated with fluorescent **NP4Aa** (40 μg/mL) 114
Figure 33. Confocal microscopy images of cells treated with fluorescent **NP4Aa** (60 μg/mL) 115
Figure 34. Confocal microscopy images of cells treated with fluorescent **NP4Aa** (100 μg/mL) 116
Figure 35. DLS and ELS analysis of NPs prepared in the presence of the V-50 initiator 118
Figure 36. ATR FTIR of NPs prepared in the presence of the V-50 initiator. 118
Figure 37. ^{1}H NMR spectra of dexamethasone and powders recovered from reaction 123
Figure 38. DLS and ELS analysis of **DNP4Aa** 128

Figure 39. TEM micrograph of **DNP4Aa**. 129
Figure 40. ATR FTIR spectra of dexamethasone and **DNP4Aa**. 130
Figure 41. Cumulative release of dexamethasone from drug-loaded PLGA-based NPs 135
Figure 42. Cumulative release of dexamethasone from drug-loaded OLGA-based NPs 136
Figure 43. Size and PI of **DNP4Aa**, **DNP4Ab**, and **DNP4Bb** after incubation in different media 138
Figure 44. DLS and ELS analysis of aqueous NP suspensions stored at rt 140
Figure 45. Normalised viability of HeLa cells treated with dexamethasone-loaded NPs 141
Figure 46. Chemical structure of dexamethasone, betamethasone, and prednisolone. 142
Figure 47. Chemical structure of XBD173. 144
Figure 48. Analysis of NPs prepared in the presence of XBD173 145
Figure 49. Analysis of PLGA-PEG NPs prepared in the presence of XBD173. 146
Figure 50. TEM micrographs of NPs prepared from disulphide **61** 153
Figure 51. Size-distributions of disulphide-containing NPs incubated with glutathione. 156
Figure 52. Chemical structure of L-selenocystine. 158
Figure 53. ^{77}Se NMR (76 MHz, D_2O/NaOH) spectrum of samples containing L-selenocystine. 160
Figure 54. Chemical structure of the lithium phenyl-2,4,6-trimethylbenzoylphosphinate (LAP) 167

Schemes

Scheme 1. Synthesis of PLGA and Sequenced PLGA 31
Scheme 2. Polymeric micelles formed by self-assembly of PLGA-PEG. 37
Scheme 3. Disintegration of a stimuli-responsive polymeric NP 39
Scheme 4. Building blocks for the synthesis of disulphide-containing polymeric NPs. 43
Scheme 5. Oxidation of diselenides in the presence of hydrogen peroxide 44
Scheme 6. Nanoprecipitation method for the preparation of polymeric NPs. 46
Scheme 7. Emulsion-based methods for the preparation of polymeric NPs. 49
Scheme 8. Preparation of crosslinked polymeric NPs via crosslinking of polymers 51
Scheme 9. Preparation of crosslinked polymeric NPs via click chemistry 52
Scheme 10. Preparation of polymeric NPs via crosslinking of functionalised polymers 53
Scheme 11. Radical crosslinking copolymerisation of vinyl monomers 54
Scheme 12. Protein-templated radical crosslinking copolymerisation 55
Scheme 13. Drug loading methods for polymeric nanoparticles 59
Scheme 14. Synthesis of **OLGADMA 4Aa** 69
Scheme 15. Synthesis of **OLGADMA 4Ab** 70
Scheme 16. Synthesis of **OLGADMA 4Ba** 71
Scheme 17. Synthesis of **OLGADMA 4Bb** 72
Scheme 18. Synthesis of **OLGADMA 6A** 73
Scheme 19. Synthesis of **OLGADMA 6B** 74
Scheme 20. Synthesis of **OLGADMA 8A** 75
Scheme 21. Synthesis of **OLGADMA 8B** 76
Scheme 22. General procedure for the nanoprecipitation polymerisation of OLGADMAs 81
Scheme 23. Nanoprecipitation polymerisation of **OLGADMA 4Aa**. 83
Scheme 24. Nanoprecipitation polymerisation of **OLGADMA 4Aa** in the presence of PEG 86
Scheme 25. Standard conditions for the nanoprecipitation polymerisation. 98
Scheme 26. Synthesis of alternating PLGA. 104
Scheme 27. Nanoprecipitation polymerisation of **OLGADMA 4Aa** in the presence of V-50 117
Scheme 28. Preparation of dexamethasone-loaded OLGA-based NPs 127
Scheme 29. Synthesis of disulphide **61** 151
Scheme 30. Synthesis of disulphide-containing crosslinked polymeric NPs 152
Scheme 31. Synthesis of diselenide **63**. 161
Scheme 32. Proposed routes for the synthesis of diselenide-containing NPs. 162
Scheme 33. Proposed methodology for the synthesis of OLGA-based nanocapsules 167

Tables

Table 1. Examples of polymeric NPs that have entered clinical trials. 24
Table 2. Examples of approved PLGA-based microparticles and implants..... 35
Table 3. Examples of pre-clinical polymeric NPs containing PLGA. 38
Table 4. Examples of nanoprecipitation-based methodologies. 47
Table 5. Drug-loaded polymeric NPs prepared via emulsion-based methods. 50
Table 6. Crosslinked polymeric NPs synthesised by miniemulsion polymerisation..... 56
Table 7. Crosslinked polymeric NPs prepared via microemulsion polymerisation 58
Table 8. DLS and ELS analysis of NPs prepared from **OLGADMA 4Aa**. 87
Table 9. Estimated yields of reactions containing different AIBN concentrations..... 97
Table 10. List of OLGA-based NPs prepared in this work..... 101
Table 11. DLS and ELS analysis of a library of OLGA-based NPs. 102
Table 12. The polymer composition of PLGA-based NPs 104
Table 13. List of PLGA-based NPs prepared in this work 105
Table 14. Encapsulation of dexamethasone 125
Table 15. Analysis of dexamethasone-loaded NPs..... 126
Table 16. List of dexamethasone-loaded OLGA-based NPs..... 131
Table 17. Analysis of dexamethasone-loaded OLGA-based NPs..... 132
Table 18. List of dexamethasone-loaded PLGA-based NPs 133
Table 19. Analysis of dexamethasone-loaded PLGA-based NPs 134
Table 20. NPs prepared in the presence of different glucocorticoids 143
Table 21. Comparison of NPs prepared in the presence of XBD173. 146
Table 22. Analysis of disulphide-based NPs 153
Table 23. Count rates of suspensions containing disulphide-based NPs..... 155
Table 24. Overall yield and isolated amounts of OLGADMAs……..177

Abbreviations

AAm	Acrylamide
AETC	[2-(Acryloyloxy)ethyl]trimethylammonium chloride
AIBN	Azobisisobutyronitrile
APS	Ammonium Persulphate
ATR	Attenuated total reflectance
CCK-8	Cell Counting Kit-8
CuACC	Copper-catalysed azide–alkyne cycloaddition
DCC	Dicyclohexylcarbodiimide
DDS	Drug delivery system
DLS	Dynamic light scattering
DMAP	4-Dimethylaminopyridine
DMEM	Dulbecco's Modified Eagle Medium
DMF	Dimethylformamide
DMSO	Dimethyl sulfoxide
DOSY	Diffusion Ordered Spectroscopy
DTT	Dithiothreitol
EDC HCl	1-Ethyl-3-(3-dimethylaminopropyl)carbodiimide hydrochloride
EE	Encapsulation efficiency
ELS	Electrophoretic light scattering
EMA	European Medicines Agency
FBS	Foetal bovine serum
FDA	Food and Drug Administration
FRET	Förster Resonance Energy Transfer
FTIR	Fourier-transform infrared spectroscopy
GSH	Glutathione
GSSG	Glutathione disulphide
HEMA	2-Hydroxyethyl Methacrylate
IM	Intramuscular administration
IUPAC	International Union of Pure and Applied Chemistry
KPS	Potassium persulphate
LAP	Lithium phenyl-2,4,6-trimethylbenzoylphosphinate

LCST	Lower critical solution temperature
LE	Loading efficiency
MADLS	Multi-angle dynamic light scattering
mPEGA1000	Poly(ethylene glycol) methyl ether acrylate M_n 1000
mPEGMA500	Poly(ethylene glycol) methyl ether methacrylate M_n 500
mRNA	Messenger ribonucleic acid
MWCO	Molecular weight cut-off
MP	Microparticle
NHS	N-Hydroxysuccinimide
NMR	Nuclear Magnetic Resonance
NP	Nanoparticle
OLGADMA	Oligolactoglycolic Acid Dimethacrylate
PCL	Polycaprolactone
PEG	Polyethylene glycol
PEGDA700	Poly(ethylene glycol) diacrylate M_n 700
PEI	Polyethylenimine
PI	Polydispersity index
PLA	Polylactic acid
PLGA	Poly(lactic-co-glycolic acid)
PMMA	Poly(methyl methacrylate)
PS	Polystyrene
PVA	Poly(vinyl alcohol)
ROS	Reactive oxygen species
rpm	Revolutions per minute
SARS-CoV-2	Severe acute respiratory syndrome coronavirus 2
SC	Subcutaneous administration
SDS	Sodium dodecyl sulphate
siRNA	Small interfering RNA
TEMED	Tetramethylethylenediamine
TFA	Trifluoroacetic acid
THF	Tetrahydrofuran
V-50	2,2'-Azobis(2-methylpropionamidine) dihydrochloride

Chapter 1: Thesis Background and Synopsis

1.1 Drug Delivery Systems

Drug delivery strategies enable the conversion of promising therapeutics into successful therapies by means of drug delivery systems (DDSs).[1–4] DDSs are defined as "formulations or devices that enable the introduction of a therapeutic substance in the body and improve its efficacy and safety by controlling the rate, time, and place of the release of drugs in the body".[5] The essential components of DDSs are therefore therapeutic substances and carriers such as particles, formulations or devices.

Current therapeutic substances can be categorised into small-molecule drugs, proteins and peptides, monoclonal antibodies, nucleic acids, and live cells. Delivery strategies have evolved over time to address specific challenges within each therapeutic class. Specifically, small-molecule drug delivery often focuses on improving drug solubility, controlling the release, broadening the activity, and modifying pharmacokinetics with the aim of improving drug bioavailability. With the advent of newer therapeutic modalities, the aim of delivery strategies shifted to improving the stability of the therapeutic (proteins, peptides, nucleic acids), enabling intracellular delivery (nucleic acids), and allowing for viability and expansion (cell therapy).

Drug delivery can be achieved *via* carriers having different compositions, shapes, and dimensions, including macroscopic objects such as drug-releasing implants, microscopic objects such as microparticle depots, and nanoparticles (NPs). For example, Nexplanon® is a long-acting hormonal contraceptive implant consisting of a 4 cm long rod made of ethylene vinyl acetate copolymer containing etonogestrel, which is placed in the patient's upper arm.[6] This delivery modality ensures the release of etonogestrel over a period of three years allowing for prolonged contraception and circumventing daily dosage requirements. Risperdal Consta® contains poly(lactic-*co*-glycolic acid) (PLGA) microspheres with a size of ~100 μm encapsulating the antipsychotic risperidone, which allows for an extended release of the drug upon intramuscular injection.[7] This delivery modality enables a two-week dosing regimen, lower incidence of side effects, and better compliance compared to peroral treatment with risperidone.[8]

Doxil® is a pegylated liposome NP with a size of ~85 nm encapsulating the antineoplastic doxorubicin which demonstrates better cardiac safety and lessened side effects compared to free doxorubicin.[9,10]

Starting from the early 1950s we have witnessed the progressive miniaturisation of drug delivery systems which culminated in substantial clinical advances on the nanoscale, as exemplified by the clinical success of NP-enabled mRNA-based vaccines (Figure 1). Regardless of their size, drug delivery technologies are having a tremendous impact on improving treatment outcomes by "enhancing therapeutic efficacy, reducing toxicity, increasing patient compliance, and enabling entirely new medical treatments".[11]

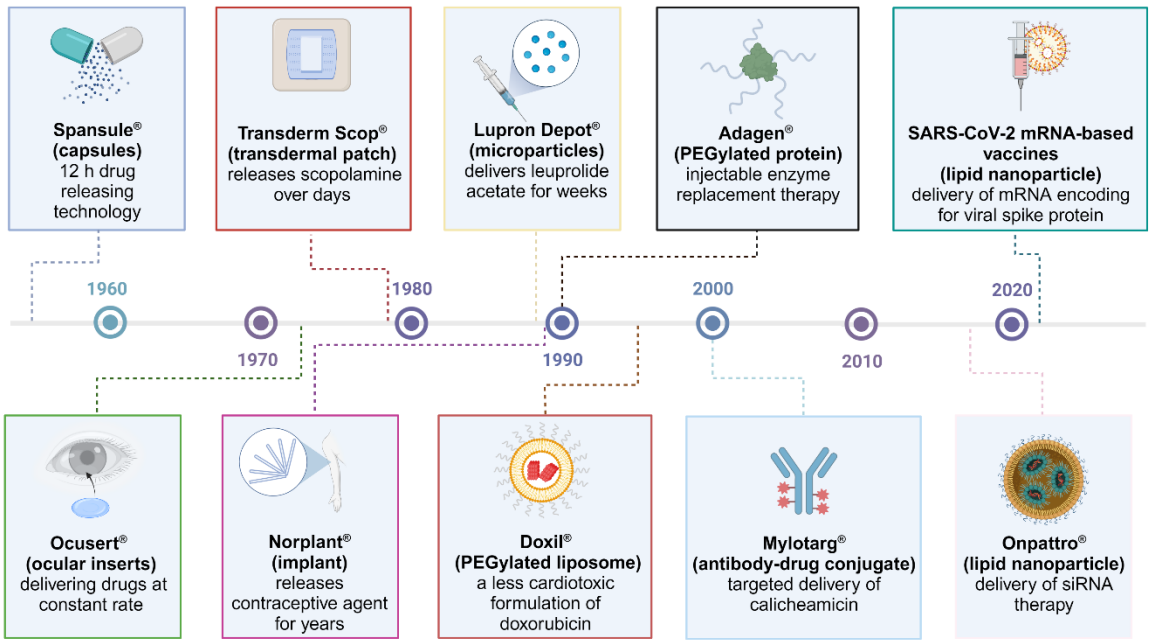


Figure 1. Chronological evolution of drug delivery systems. Figure created using information reported in ref.[12]

1.2 Nanoparticles for Drug Delivery

The IUPAC defines a NP as a particle of any shape with dimensions in the 1×10^{-9} to 1×10^{-7} m range, whereas the upper limit of 100 nm is often considered as the critical cut-off length below which novel nanoscale properties, different from those of the bulk material, arise. This definition can be extended to include particles with dimensions below 500 nm, wherein phenomena such as transparency or turbidity, ultrafiltration,

and stable dispersion are occasionally observed.[13] Alternative size limitations, sometimes reaching 1000 nm, have been proposed for NP classification purposes.[14] A less restrictive definition of NPs is often adopted within the medical field, especially in the context of drug delivery, where particles with diameters exceeding the 100 nm threshold are often required to achieve acceptable drug loadings.[15] Due to the lack of a consensus, the general definition of nanoparticles as "colloidal particles ranging in size from 10 to 1000 nm" will be adopted throughout this work.[16]

NPs for drug delivery consist of "macromolecular materials in which a biologically active material is dissolved, entrapped, encapsulated and/or to which a biologically active material is adsorbed or attached".[16] As drug carriers, NPs can improve the stability and solubility of encapsulated therapeutics, promote transport across membranes, and increase efficacy and safety by prolonging the circulation times.[17] In doing so, NPs can enable new therapies and facilitate the re-evaluation of bioactive molecules considered as debilitated by suboptimal pharmaceutical properties in their free form.[18] Additionally, nanotherapeutics may convey an intrinsic intellectual property advantage, as their manufacturing complexity is able to create significant obstacles in the rapid development of equivalent therapeutics by generic drug companies.[19]

In terms of chemical composition, NPs are roughly categorised into lipid-based, inorganic, and polymeric NPs. Lipid-based NPs are the most common class of FDA-approved nanomedicines due to factors such as biocompatibility, high bioavailability, ability to carry large payloads, and facile formulation.[17,20,21] Inorganic NPs are particularly suitable for imaging applications and photothermal therapies due to their magnetic, radioactive, and plasmonic properties.[22–24] Polymeric NPs are perhaps the most structurally and functionally versatile of the three classes as a variety of NP structures and characteristics are achievable *via* the manipulation of the large pool of natural polymers, synthetic polymers, and polymerisable building blocks.[17]

1.3 Nanomedicine: Nanoparticles in the Clinic

Nanomedicine is a rapidly evolving medical branch that uses nanotechnologies to prevent, monitor and treat diseases.[25,26] Doxil® (PEGylated liposomal doxorubicin) is

regarded as the first approved NP-based therapeutic (FDA, 1995), only preceded by Diprivan® (FDA, 1989), a lipid emulsion of the general anaesthetic propofol containing soybean oil and egg lecithin and nowadays described as “liposomal propofol”.[27,28] A further milestone in the early days of nanomedicine was achieved in 2005 with the approval of Abraxane®, a NP formulation containing the hydrophobic antineoplastic drug paclitaxel bound to albumin.[29]

The advantages of these early nanomedicines over conventional drug therapies mainly reside in improved toxicity profiles. Particularly, the encapsulation of doxorubicin in pegylated liposomes (Doxil®) allows the modification of the pharmacokinetics and biodistribution of doxorubicin, which becomes dominated by the properties of the liposomal carrier due to encapsulation.[30] This in turn results in reduced cardiotoxicity and myelotoxicity compared to free doxorubicin alongside an increased efficacy in certain settings.[31] On the other hand, the main advantage of Abraxane® resides in the solubilising properties of the albumin-based nanoplatform which circumvents the need for the utilisation of toxic excipients such as Cremophor EL and ethanol present in typical paclitaxel formulations, thus enabling a higher dosage of paclitaxel and resulting in an increase in antitumor activity.[32]

Until now, >30 NPs for oral, topical, and systemic administration have been granted approval by regulatory bodies.[21,27,33] Clinical indications of NPs approved by EMA and the FDA include cancer, iron-replacement therapies, anesthesia, fungal infections, macular degeneration, vaccination, and imaging.[23,34–39] Importantly, whilst some would argue that traditional nanomedicines failed to yield marked clinical improvements compared to conventional drugs, the recent approval of nanomedicines such as Onpattro®, Vyxeos®, and Hensify® clearly demonstrates the ability of the nanomedical field to overcome critical therapeutic barriers in ways which are not achievable with conventional medicine.[40,41] For example, nucleic acid-based therapies have the potential to tackle the genetic basis of many diseases and yet suffer delivery difficulties related to degradation by nucleases, immune activation, and cumbersome transmission to cells due to unfavourable physicochemistry.[42] These shortcomings can be addressed by employing chemical modifications and/or delivery technologies such as NPs to enable completely new therapies. Such an approach resulted in the

approval of Onpattro® (FDA, 2018), a first-in-class nucleic acid-based treatment for polyneuropathies resulting from the hereditary disease transthyretin-mediated amyloidosis containing siRNA encapsulated within lipid NPs.[43] A further example is given by Hensify®, a first-in-class product containing radiation-enhancing hafnium oxide NPs for intratumoural administration.[44] Once administered and exposed to ionising radiation, these NPs are capable of augmenting cell damage without adding toxicity to surrounding healthy tissues.

Arguably, the impact of NPs on medicine has never been more evident than with the worldwide clinical introduction of the Pfizer-BioNTech and Moderna SARS-CoV-2 vaccines containing mRNA within lipid NPs.[45] The approval of these vaccines appears to have sparked an explosion of the nanomedicine field, with >35 new NP technologies entering clinical trials in 2021 alone.[21,46] Moreover, these vaccines are predicted to pave the way to the validation and translation of new NPs to the clinic as the administration of billions of doses of mRNA-based SARS-CoV-2 vaccines has initiated what is *de facto* the largest population study of nanomedicine so far.[47]

1.4 Polymeric Nanoparticles

Having origins in the 1960s and pioneered by researchers such as Folkman, Langer, Peppas, Roseman, Heller, Higuchi, Ringsdorf, and Speiser, polymer-based drug delivery evolved into a large medical field encompassing devices such as implants, sutures, microparticles, and NPs as drug carriers.[48–62] Polymeric NPs comprise natural or synthetic polymers and can be prepared through physical or chemical manipulation of polymers or synthesised *via* polymerisation of monomers.[17] Therapeutic polymeric NPs contain a therapeutic substance which can be encapsulated within the core of the NP, entrapped within the polymer matrix, adsorbed on the NP surface, or covalently conjugated to the constituting polymers. Compared to lipids and inorganics, polymers are often considered versatile building blocks for therapeutic NPs due to their stability, high loadings of a variety of therapeutic substances, controllable drug release kinetics, facile functionalisation of the surface with ligands, and because many have demonstrated safety in humans.[63] Compared to liposomes, polymeric NPs are generally more stable *in vivo*, display high drug loadings and allow for both controlled and triggered drug release.[40,64] As carriers for therapeutic substances, classical polymeric NPs are generally capable of [40]:

(i) releasing substances at an experimentally predetermined rate over a prolonged period,
(ii) releasing substances preferentially at target sites, often with controlled release rates,
(iii) maintaining the concentration of substances within therapeutic ranges both in circulation and tissues,
(iv) protecting substances from hepatic inactivation, enzymatic degradation, and rapid clearance *in vivo*.

Moreover, polymeric NPs can be designed to display responsiveness to specific stimuli resulting in the release of the therapeutic payload in a triggered fashion (see 1.6).

Several polymeric NPs have entered clinical trials with cancer treatment being the most frequent application (Table 1).

Product	Therapeutic substance	Polymeric Composition	Phase*	ref
AZD2811	AZD2811	PLA-PEG	II	[65]
BIND-014	docetaxel	PLA-PEG	II	[66]
Genexol®-PM	paclitaxel	PLA-PEG	IV	[67]
NC-6300	epirubicin	PEG-polyaspartate	II	[68]
NC-6004	cisplatin	PEG-poly(glutamic acid)	III	[69]
NC-4016	DACH-platinum	PEG-poly(glutamic acid)	I	[70]
NK105	paclitaxel	PEG-polyaspartate	III	[71]
CriPec	docetaxel	methoxy-poly(ethylene glycol)-*b*-poly[*N*-(2-hydroxypropyl) methacrylamide lactate]	II	[72]
CRLX101	camptothecin	Cyclodextrin-containing polymer	III	[73]
CRLX301	docetaxel	Cyclodextrin-containing polymer	I/II	[74]
PRECIOUS-01	tumour antigen and iNKT cell activator	PLGA	I	[75]

Table 1. Examples of polymeric NPs that have entered clinical trials.[21] * Clinical trial status as of 2021.

1.4.1 Types of Polymeric Nanoparticles

The morphological classification of polymeric NPs diversifies between solid matrix systems called nanospheres, and cavities surrounded by polymeric shells or membranes known as nanocapsules (Figure 2).[17] These can be further classified into subcategories such as polymeric micelles consisting of a hydrophilic shell and a hydrophobic core, polymersomes which are polymeric vesicles with an aqueous core resembling liposomes, dendrimers which are hyperbranched polymers having complex tridimensional architectures, and nano-sized hydrogels named nanogels (Figure 2).[76–83]

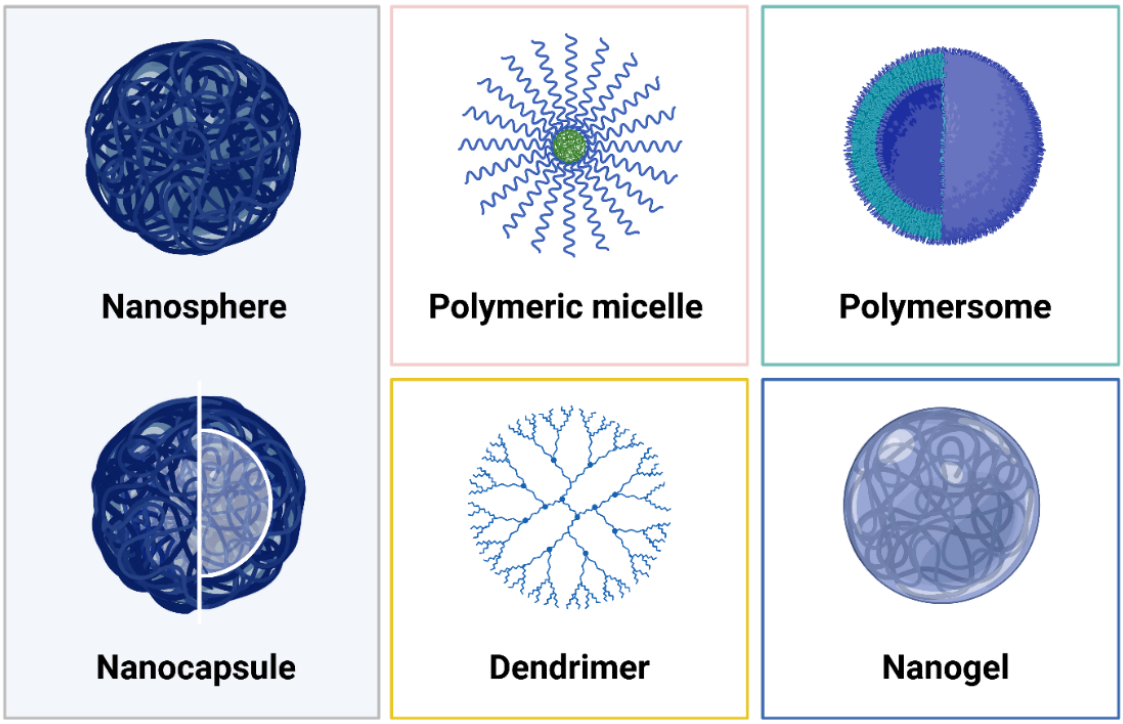


Figure 2. Classification of polymeric NPs according to structure.

1.4.2 Crosslinked Polymeric Nanoparticles

Crosslinked polymers consist of multiple linear polymer chains that are interconnected at several points, resulting in a three-dimensional polymer network (Figure 3).[84,85] This network can be considered a single macromolecule, primarily when the interconnections between the chains are of a covalent nature. Whilst these polymeric networks are insoluble in liquids, they can be able to swell in suitable solvents yielding gels.

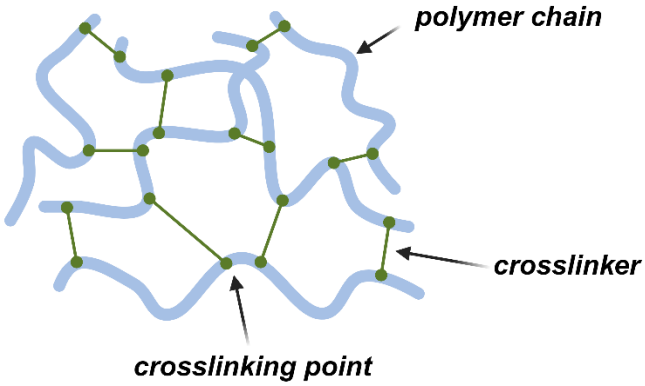


Figure 3. Structure of a generic crosslinked polymer.

Polymeric NPs can contain non-crosslinked and covalently crosslinked polymers resulting in profound differences in the structural and encapsulation stability of the drug delivery system. For example, polymeric micelles derive from the dynamic self-assembly of amphiphilic block copolymers in water and maintain their structure due to hydrophobic interactions. The structural and encapsulation stability of these systems can be severely challenged by dilution *in vivo* due to the relatively weak formation forces, resulting in dissociation into unimers and premature drug release.[86,87] The crosslinked analogues of such micellar NPs have been shown to have increased stability upon dilution and heightened resistance to deformation under shear forces.[88,89] Similarly, crosslinking of polymersomes leads to an increase in carrier stability and enables the modulation of properties such as permeability of the carrier's membrane and payload release.[90–93] Nanogels, which are by definition crosslinked polymeric NPs, maintain their structural integrity due to covalent crosslinking or non-covalent interactions defined as physical crosslinking. It has been proposed that covalently crosslinked NGs could present higher stability *in vivo* and lessened premature leakage of the drug payload, compared to non-covalently crosslinked NGs.[94] Moreover, the density of the crosslinking was shown to influence the degree of payload leakage from such systems.[95]

1.4.3 Biocompatibility and Degradation of Polymeric Drug Delivery Systems

Polymer degradation and biocompatibility are some of the key parameters that influence the design of polymeric NPs for therapeutic applications.[64] Particularly, these are of crucial importance for polymers purposed for parenteral administration.[96,97] Polymer biocompatibility is defined as the ability of the polymer to be in contact with a living system without producing adverse effects.[13] Polymer degradation denotes the process of polymer cleavage and molar mass decrease which, in the most ideal scenario, allows for the total breakdown of the polymeric carrier to non-toxic byproducts that can be easily eliminated from the body. [13,64,96] Polymer erosion is a term related to degradation which is often used interchangeably but should be limited to describing the degradation which occurs on the surface of the material and progresses into the bulk.[13] For clarity, expressions such as “surface erosion” and “bulk erosion” will be denoted with the term degradation throughout this work. Whilst polymeric NPs based on non-degradable polymers such as polyacrylates and poly(methyl methacrylate) have been reported, degradable polymers remain the preferred modality for drug delivery applications.[64,98,99]

Classical degradable polymers contain hydrolytically or proteolytically labile bonds within their structure.[96] Known hydrolytically labile moieties include carbonates, esters, carbamates, orthoesters, and amides, which present differential rates of hydrolysis. Whilst the hydrolysis rate of polymers containing these moieties will depend on the specific polymer morphology and the nature of the substituents present within the structure, an approximation of the hydrolysis rates of these linkages under physiological conditions has been proposed by Gombotz *et al*. (Figure 4).[100]

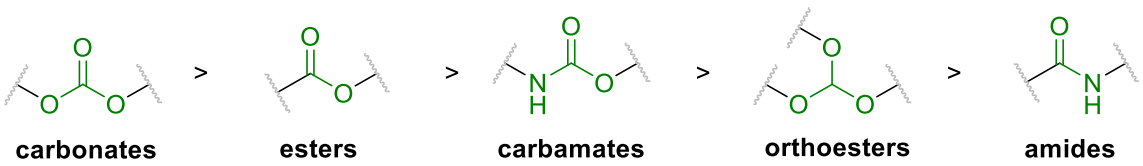


Figure 4. Approximation of hydrolysis rates of polymers containing carbonates, esters, carbamates, orthoesters, and amides based on the analysis of low-MW compounds containing these chemical motifs.[100]

Among these, degradable polymers bearing the ester chemical motif such as the aliphatic polyesters poly(lactic acid) (PLA), poly(lactic-*co*-glycolic acid) (PLGA) and poly(ε-caprolactone) (PCL) have received unprecedented attention within the biomedical field and are approved by healthcare regulatory bodies.[101,102] Moreover, PLA and PLGA have the potential to ultimately degrade to metabolisable molecules which are then cleared by the body's natural homeostatic mechanisms.[103]

Unlike classical degradable polymers such as PLA and PLGA, the degradation of polymeric NPs based on non-degradable polymers can be achieved *via* the introduction of polymer crosslinks containing labile bonds. For example, polyacrylamide NPs crosslinked *via* ester-containing crosslinkers have been shown to degrade to short water-soluble fragments which can potentially be eliminated *via* the renal pathway.[104,105]

1.4.4 Mechanisms of Drug Release from Degradable Polymers

The process of drug release from polymers can be defined as the migration of the drug from its initial position within a polymer to the polymer's outer surface and subsequently to the surrounding environment.[3] The overall process of drug release from degradable polymeric systems such as PLGA will be affected by a combination of factors such as the properties of the DDS (size, porosity, shape), the composition of the external environment (pH, temperature, osmolality, presence of enzymes) and the properties of the drug (solubility, stability, charge, size).[64,106]

The four essential related mechanisms of drug release from polymeric DDSs are i) diffusion through water-filled pores, ii) diffusion through the polymer, iii) osmotic pumping, and iv) degradation without drug transport (Figure 5).[106]

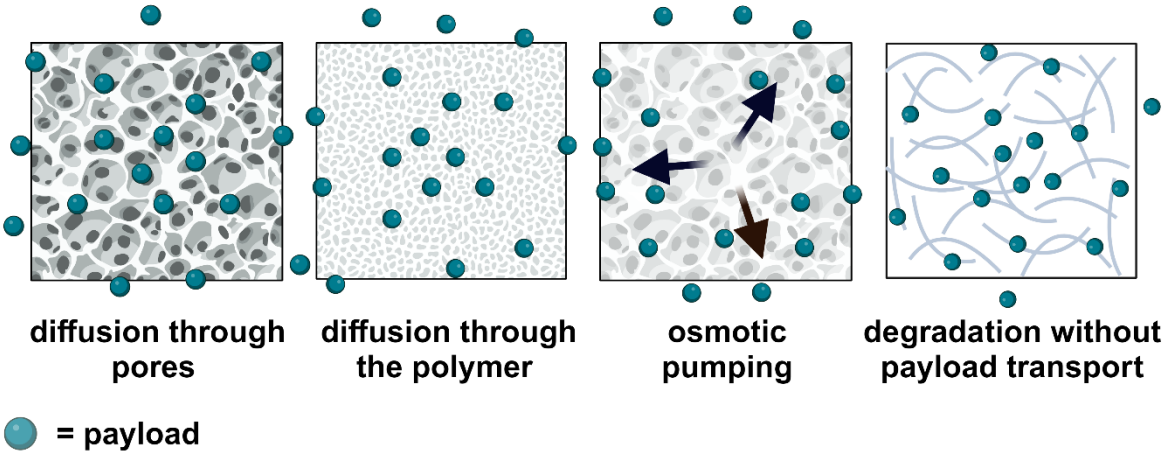


Figure 5. Mechanisms of drug release from polymeric drug delivery systems classified by the modality of release as proposed by Fredenberg *et al*.[106]

Generally, drugs are released from degradable polymeric DDSs such as PLGA *via* diffusion through water-filled pores, where diffusion is defined as the random movements of the drug, driven by the chemical potential gradient.[106] Pore-forming processes such as polymer degradation and swelling are therefore expected to increase the rate of drug release from these systems.

Contrary to classical degradable polymers such as PLGA, stimuli-responsive degradable polymers can undergo a rapid degradation *via* exposure to a particular stimulus resulting in the triggered release of the encapsulated payload in specific biological environments (see 1.6).

1.5 Poly(lactic-co-glycolic acid) (PLGA) Nanoparticles

1.5.1 Poly(α-hydroxy acids)

Poly(glycolic acid) (PGA), poly(lactic acid) (PLA), and poly(lactic-*co*-glycolic acid) (PLGA) are fundamentally polymers of α-hydroxy acids and have been extensively investigated as biomaterials (Figure 6).

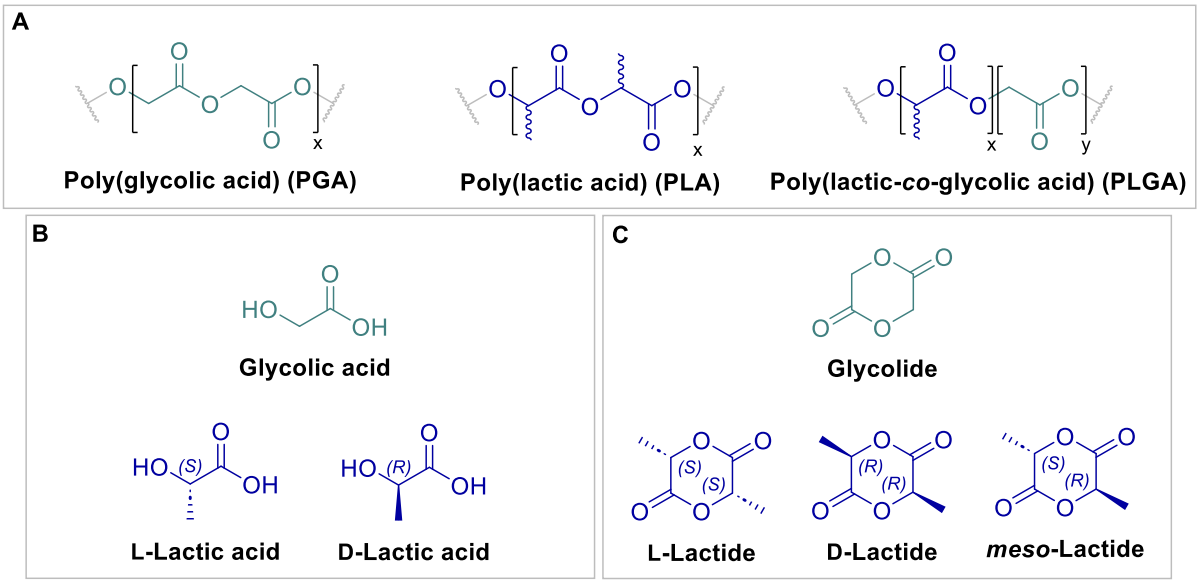


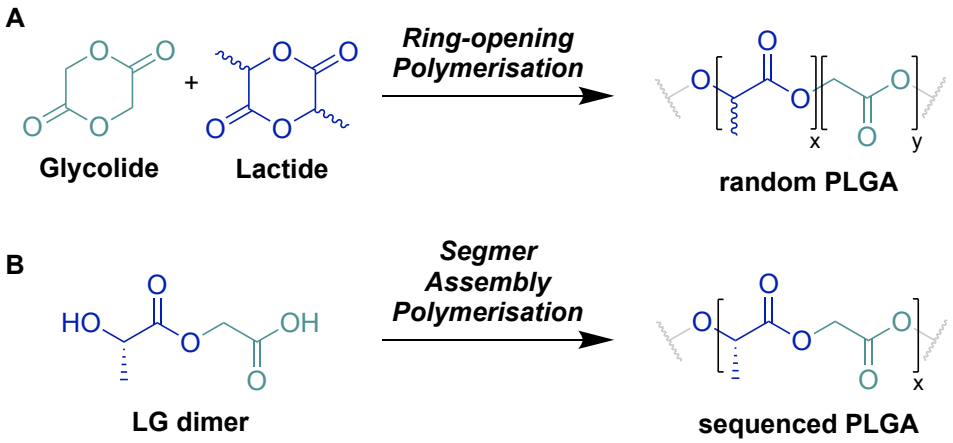
Figure 6. A) Structure of poly(α-hydroxy acids) PGA, PLA, and PLGA (stereochemistry of the lactate unit not shown), B) structure of glycolic and lactic acid, and C) structure of cyclic dimers of glycolic and lactic acid.

PGA can be obtained from the ring-opening polymerisation of glycolide and has been used to fabricate the first synthetic absorbable sutures by Frazza and Schmitt in the 1970s.[107] PGA is highly crystalline, has very low solubility in most organic solvents, and undergoes significant mass loss within 6-12 months due to hydrolytic degradation.[108–110] PLA is traditionally synthesised by ring-opening polymerisation (ROP) of lactide, the cyclic dimer of lactic acid that can be present as the *SS* isomer (L-lactide), *RR* isomer (D-lactide), and *RS* isomer (*meso*-lactide).[102] L-lactide can be prepared from the naturally occurring L-lactic acid, and its stereo-pure homopolymer (PLLA) is considered crystalline. [109] ROP of racemic lactide can yield atactic polymers (PDLLA) which are essentially amorphous and thus more permeable leading to a higher susceptibility to hydrolysis. Additionally, ROP of racemic lactide can also afford isotactic stereoblock polymers which can be crystalline.[111] Compared to PGA, PLAs

generally present slower hydrolysis rates due to the presence of the methyl groups, resulting in complete degradation times that range from months to decades.[102,112,113]

Given the different susceptibility to hydrolysis of PGA and PLA, the copolymers of racemic or L-lactide and glycolide (PLGA) have been investigated with the purpose of expanding the range of biomedical applications of poly(α-hydroxy acids) by accessing tailored degradation times.[114–117] Compared to PGA and PLA, most PLGA compositions display enhanced hydrolytic susceptibility and are amorphous. Particularly, the highest susceptibility to hydrolytic degradation was found for the 50:50 lactate:glycolate PLGA composition.[118–120]

PLGA is traditionally synthesised *via* ROP of glycolide and racemic or L-lactide yielding random copolymers which are often defined as "blocky" or "gradient" due to the differential reactivity of the two lactones.[121,122] Seminal work by Meyer *et al.* established a synthetic methodology that allows access to sequenced PLGA enabling a high level of control over the monomer sequence, lactate stereochemistry, and tacticity of the polymer.[121,123–127] This approach consists of the polycondensation of discrete low-MW compounds such as dimers of glycolic and lactic acid to yield precisely sequenced PLGA enabling access to several sequence patterns and was named segmer assembly polymerisation (Scheme 1). The relationship between sequence and PLGA properties is further discussed in section 1.5.2.



Scheme 1. A) Ring-opening polymerisation of glycolide and generic lactide yielding random PLGA and B) segmer assembly polymerisation of an LG dimer yielding sequenced PLGA. Adapted from Meyer et al.[124]

1.5.2 PLGA as a Versatile Degradable Polymer

PLGA is an FDA-approved copolymer of lactic and glycolic acid belonging to the family of poly(α-hydroxy acids) alongside PLA, a polymer originally developed for use in medical applications such as degradable sutures.[128] PLGA is biocompatible, and the products of its complete degradation can undergo full elimination from the body. Particularly, L-lactic acid is metabolised to water and carbon dioxide *via* the Krebs cycle, whilst glycolic acid undergoes direct renal elimination or further metabolism.

As a polymer, PLGA is amenable to substantial re-design allowing access to specific properties related to solubility, thermal stability, mechanical properties, degradation, and biocompatibility.[129] In the context of drug delivery applications, the study of the degradation aspects of PLGA received unprecedented attention due to its direct influence on drug release and biocompatibility parameters.

PLGA degrades *in vitro* and *in vivo* through ester hydrolysis releasing acidic oligomers and monomers which autocatalyse further PLGA degradation.[130] Whilst the involvement of enzymatic hydrolysis of PLGA *in vivo* has been postulated due to (i) discrepancies with *in vitro* degradation rates and (ii) enzymatic degradations detected *in vitro*, this modality of PLGA degradation *in vivo* is still an ongoing object of debate.[131,132]

The hydrolytic degradation of PLGA materials has been proposed to be a stepwise process comprising of (i) an initial hydration phase seeing water penetration into the polymer matrix, (ii) initial degradation starting in the hydrated regions and resulting in a decrease of the polymer MW, (iii) further degradation that leads to loss of the structural integrity and mass loss, and (iv) the hydrolysis of smaller polymer fragments yielding water-soluble molecules.[133] Initial investigations suggested that PLGA degradation is a process occurring homogenously throughout PLGA-based materials however, nowadays PLGA is considered a “bulk degrading” polymer with the core of relatively large PLGA-based DDSs degrading more rapidly than the surface both *in vitro* and *in vivo*.[134] This phenomenon has been explained in terms of the autocatalytic effect of oligomers trapped in the core of the device which cannot percolate into the surrounding medium as easily as those formed on the surface.[135]

The rate of degradation of PLGA-based devices is influenced by many complex factors including polymer composition, crystallinity, size, and the characteristics of the environment in which degradation takes place.[103,136] For example, research by Miller, Brady and Curtright was the first to establish the existence of differential degradation rates of poly(α-hydroxy acids) containing different proportions of lactate and glycolate units.[118] Nowadays, it is generally recognised that a higher glycolate content in PLGA induces faster degradation by increasing the hydrophilicity of the polymer.[133,137] The nature of the polymer end-group has also been proposed as a critical factor influencing the rate of degradation. For instance, uncapped PLGA having a carboxylic acid moiety on the polymer terminus was shown to degrade faster than ester-capped PLGA.[138] The size of PLGA-based materials also influences the degradation rate with thicker PLGA films degrading faster than thinner ones regardless of an identical composition, possibly due to a stronger autocatalytic effect.[139]

Besides these factors, work conducted by Meyer and collaborators established a strong correlation between monomer sequence and stereochemistry with a range of PLGA properties including degradation.[121,124,126,127,140,141] Swelling, degradation, and drug release from PLGA have been found to be influenced by monomer sequence.[121] Particularly, since the linkages between two adjacent glycolic units are more susceptible to hydrolysis than the linkages between lactic-glycolic and lactic-lactic units, the ability to control the monomer sequence of PLGA can enable the fine-tuning of the polymer's degradation rates with potential implications for PLGA-based drug delivery applications.[142] For instance, alternating PLGA which bears no glycolic-glycolic linkages degrades more slowly and exhibits a more sustained drug release than the random PLGA polymer with the same ratio of lactic and glycolic units.[124]

Additionally, the crosslinking of PLGA to form polymer networks was proposed as a strategy to improve the stability of PLGA-based materials. Specifically, macroscopic crosslinked polymeric networks (gels) containing the PLGA chemical motif have demonstrated improved properties over non-crosslinked analogues. For example, Agarwal and Eger reported on PLGA networks with dynamic covalent bonds achieved *via* crosslinking of hydroxy-terminated star-shaped PLGA with 4,4′-methylene diphenyl diisocyanate resulting in PLGA-based polymer networks with enhanced thermomechanical properties.[143] Another group reported how the crosslinking of

PLGA *via* electron beam radiation in the presence of pentaerythritol tetra-acrylate was able to induce enhanced mechanical properties and reduce the rates of hydrolytic degradation.[144]

A further example involves PLGA–PEG–PLGA macromonomers (M_n > 5000 g/mol) terminated by α,ω-itaconyl groups crosslinked via polymerisation in the presence of the photoinitator camphorquinone to give a hydrogel network (Figure 7). Importantly, it was found that the amount of itaconic acid functionalisation and crosslinking duration showed a positive correlation with hydrolytic stability and the lifetime of the hydrogel.[145]. Similarly, the macromonomer was crosslinked using the photoinitiator lithium phenyl-2,4,6-trimethylbenzoylphosphinate giving a covalently crosslinked gel presenting long-lasting stability, which was markedly superior to the non-covalently crosslinked gel obtained by thermogelation of the macromonomer.[146]

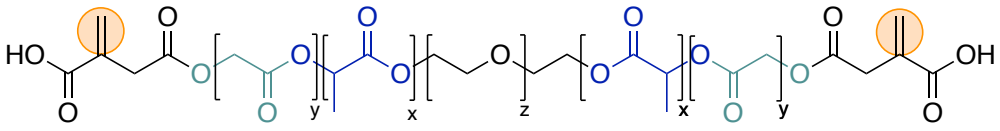


Figure 7. α,ω-itaconyl terminated PLGA-PEG-PLGA macromonomers yield highly stable hydrogel networks upon radical polymerisation of alkenes highlighted in orange.[145]

1.5.3 PLGA for Drug Delivery

As a drug delivery polymer, PLGA can enable the sustained release of therapeutics from long-acting formulations facilitating reduced dosing frequencies, decreased incidence of side effects, maintenance of stable plasma concentrations of therapeutics and improved patient compliance.[147] More than 60 drug products based on PLGA having various shapes and sizes are present on the market including implants, microparticles, and an injectable *in situ* forming implant (Table 2).[148]

Product	Therapeutic substance	PLGA carrier	Indication	Administration route
Decapeptyl®	triptorelin	MP	prostate cancer	IM
Lupron Depot®	leuprolide acetate	MP	prostate cancer endometriosis	IM
Nutropin Depot®	somatropin	MP	growth failure	SC
Sandostatin® LAR	octreotide acetate	MP	acromegaly	IM
Somatuline® LA	lanreotide acetate	MP	acromegaly	IM
Trelstar™ Depot	triptorelin pamoate	MP	prostate cancer	IM
Vivitrol®	naltrexone	MP	alcohol dependence opioid dependence	IM
Risperdal® Consta™	risperidone	MP	schizophrenia	IM
Zoladex®	goserelin acetate	implant	prostate cancer endometriosis	SC
Ozurdex®	dexamethasone	implant	macular oedema	intravitreal
Durysta™	bimatoprost	Implant	open-angle glaucoma	intracameral
Eligard®	leuprolide acetate	*in situ* forming implant	prostate cancer	SC

Table 2. Examples of approved PLGA-based microparticles and implants (2021). MP = microparticle, IM = intramuscular administration, SC = subcutaneous administration.

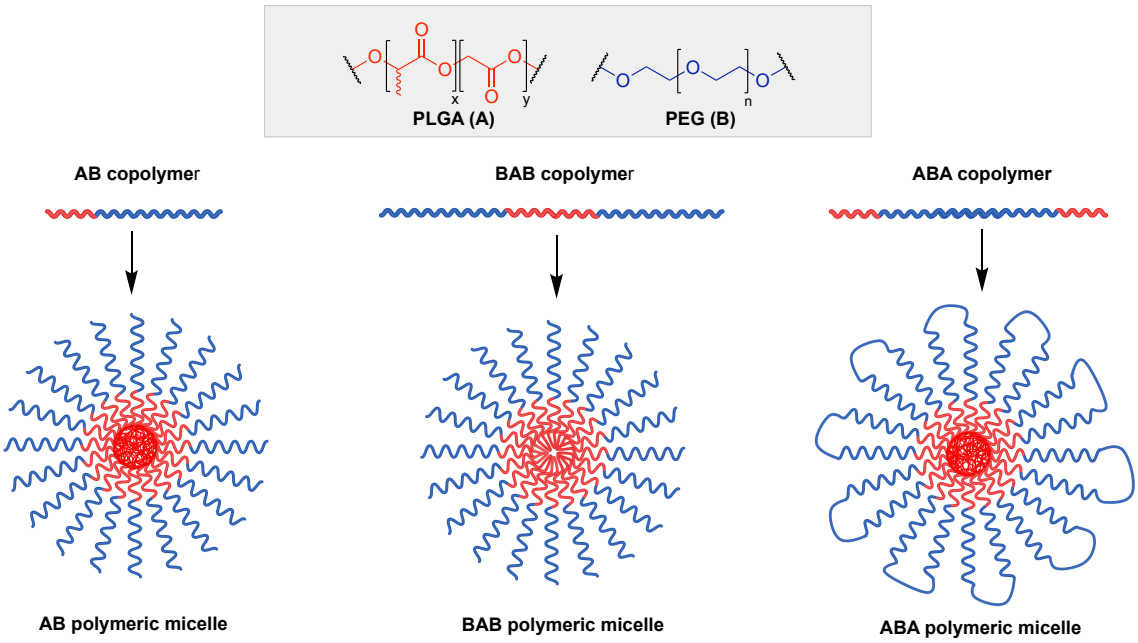
1.5.4 PEGylated PLGA

PEG is a biocompatible hydrophilic polymer of ethylene glycol which can impart "stealth" properties to therapeutics and drug carriers, enabling prolonged blood circulation times.[149] Nowadays, PEG is an integral part of numerous pharmaceutical products approved by the FDA and EMA, including NPs such as Doxil® and Sars-CoV-2 mRNA vaccines.[150,151]

The term "stealth effect" generally describes the masking of non-specific interactions of carriers within the body, e.g. interaction with blood components leading to complement activation and ultimately resulting in NP clearance from the blood compartment.[149] The main mechanism responsible for this effect is the formation of a conformational cloud created by hydrophilic polymers such as PEG grafted on the surface of NPs which prevents interactions between NPs and macromolecules.[152] More specifically, the existence of a flexible polymeric shell can create a strong entropic barrier which repels close interactions with other particles and macromolecules by precluding contacts occurring within the attractive van der Waals region of NP cores.[153] As a result of this, the PEGylated NPs can present enhanced colloidal stability and prolonged circulation times.

PLGA-based drug delivery systems contain PLGA and/or its block copolymers with poly(ethylene glycol) (PEG).[154] Some of the most common forms of PLGA-PEG copolymers investigated for drug delivery are diblock copolymers and triblock copolymers of the ABA type (PLGA-PEG-PLGA) and the BAB type (PEG-PLGA-PEG).[155–159] These PEGylated copolymers are synthetically accessible via ROP and/or coupling reactions, depending on the desired type of block copolymer. For example, PLGA-PEG can be synthesised by ROP of lactide and glycolide in the presence of a methoxy-terminated PEG alcohol and stannous octoate.[155] Alternatively, PLGA-PEG can also be prepared via conjugation of activated PLGA (e.g. PLGA-NHS) with amine-terminated PEG.[156] On the other hand, PLGA-PEG-PLGA copolymers (ABA type) can be prepared via ROP of lactide and glycolide in the presence of a PEG dialcohol.[160] Finally, PEG-PLGA-PEG (BAB type) can be synthesised via coupling reactions involving the diblock copolymer PLGA-PEG and a methoxy-terminated PEG alcohol to afford the PEGylated triblock copolymer.[159]

The PLGA-PEG block copolymers discussed above are known to self-assemble in water to yield micelles with a PLGA core and a hydrophilic PEGylated shell (Scheme 2).[160] The resulting micelles can be further processed to form gels which hold great potential for medical applications.



Scheme 2. Types of polymeric micelles formed from the self-assembly of PLGA-PEG block copolymers in water. The BAB copolymer assumes a conformation resembling a "hairpin".

1.5.5 PLGA-based Nanoparticles

Therapeutic NPs containing PLGA, and its copolymers are among the most investigated polymeric NPs and are featured in countless reports.[161–170] Small molecules, peptides, enzymes, and nucleic acids have been encapsulated within PLGA-based NPs, demonstrating a substantial level of efficacy in animal models (Table 3). For instance, Farokhzad *et al*. used Collagen IV-targeted PLGA-PEG NPs containing the anti-inflammatory peptide Ac2-26 for the treatment of chronic, advanced atherosclerosis in mice.[171] The treatment with the NPs was able to induce a marked improvement of pre-existing atherosclerotic lesions in mice including the stabilisation of the lesions, suppression of oxidative stress, and a decrease in plaque necrosis.

PLGA-PEG NPs, functionalised with A10 2'-fluoropyrimidine RNA aptamers capable of recognising the prostate-specific membrane antigen, and loaded with the antineoplastic drug docetaxel were shown to be able to induce complete tumour reduction in five of seven xenograft mice via a single intratumoral injection.[172] Moreover, the survival upon 109 days of study was 100% for the group treated with NPs, compared to 14% for the group treated with free docetaxel.

Besides showing potential for the amelioration of existing therapies and the establishment of completely new treatments, the use of PLGA-based NPs has demonstrated the ability to enable the delivery of therapeutics across complex biological barriers. For instance, Del Grosso *et al*. demonstrated the delivery of therapeutic proteins into the brain of a murine model of lysosomal storage disease using PLGA-based NPs functionalised with brain-targeting peptides.[173] Moreover, Gan *et al*. reported that NPs based on PLGA and PLGA-PEG, loaded with insulin and modified with a cell-penetrating peptide and a liver-targeting moiety, exhibited effective intestinal absorption and hepatic deposition of insulin upon oral administration *in vivo*.

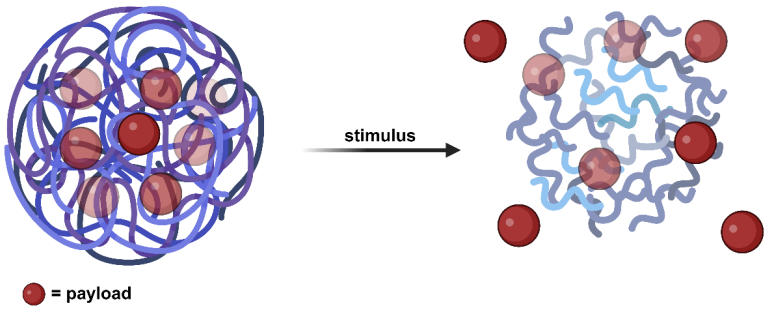
PLGA form	Therapeutic substance	Therapeutic aim	Ref
PLGA	doxorubicin-triphenylphosphonium	cancer treatment	[174]
PLGA	siRNA	intravaginal gene silencing	[175]
PLGA	crosslinked galactosylceramidase	enzyme replacement therapy	[173]
PLGA-PEG	Ac2-26	atherosclerosis	[171]
PLGA-PEG	galantamine	brain drug delivery	[176]
PLGA-PEG	docetaxel	cancer treatment	[172]
PLGA and PLGA-PEG	insulin	oral insulin therapy	[177]

Table 3. Selected examples of pre-clinical polymeric NPs containing PLGA and PLGA-PEG with reported efficacy *in vivo*.

Despite the remarkable clinical success of PLGA as the archetypal degradable polymer for manufacturing medicinal implants and microparticles, NPs based on PLGA are yet to be clinically approved. Factors such as difficulties in manufacturing scale-up, poor loading for certain therapeutic payloads, high initial burst release, generation of acidic products upon polymer degradation, and premature clearance from the bloodstream have been proposed as potential obstacles to clinical translation.[124,154]

1.6 Stimuli-Responsive Polymeric NPs

The ability to selectively induce physicochemical modifications of polymeric carriers can enable a high level of control over the (i) site and/or (ii) rate of payload release from these delivery systems. Stimuli-responsive polymeric NPs can undergo processes such as polymer degradation, shedding of surface layers, or charge switching upon interaction with a particular stimulus.[64] These processes may in turn evoke what is in fact a triggered or "on-demand" release of a therapeutic payload encapsulated within stimuli-responsive polymeric NPs (Scheme 3).[178] The synthetic versatility of polymers as drug delivery platforms allows the incorporation of a broad spectrum of stimuli-responsive chemical motifs which can be synthetically diversified to enable fine-tuning of their reactivity and thus enable a high level of precise control over payload release.[179]



Scheme 3. Schematic of the disintegration of a stimuli-responsive polymeric NP containing a therapeutic payload upon interaction with a stimulus, resulting in the triggered release of the payload.

Polymeric NPs which are responsive to exogenous stimuli such as heat, ultrasounds, and light have been reported.[180–182] Significant work is being carried out within the field of polymeric NPs which can respond to endogenous stimuli such as acidic microenvironments, reducing agents, oxidants, and disease-specific markers leading

to drug delivery systems which are able to selectively release their payload in specific biological milieus.[183–189]

For instance, tumour tissues have a lower extracellular pH (pH 6.2 – 6.9) than blood and healthy tissues and thus acid-labile polymeric NPs can be exploited to release elevated amounts of the therapeutic payload selectively in these acidic microenvironments.[190–193] Moreover, endosomes and lysosomes present low pH (pH ~4.0 – 6.0) and hence acid-labile polymeric NPs can operate a triggered payload release in these subcellular compartments, enabling efficient intracellular delivery.[194–196]

The presence of specific enzymes can act as a highly selective stimulus for responsive NPs as enzymatic activity and/or enzyme concentrations can be upregulated in several pathologies including cancer and inflammation.[197] For instance, polymer-drug conjugates containing enzyme-cleavable chemical motifs such as the amino acid sequence Gly-Phe-Leu-Gly can be selectively degraded in the lysosome by cathepsin B, a protease overexpressed in cancer cells, releasing the therapeutic payload.[198]

Redox-responsive DDSs are receiving unprecedented attention within the medical field as they can stably encapsulate the therapeutic payload in circulation and healthy tissues, whilst releasing it in the reducing intracellular environments, tumours, and inflamed tissues.[199,200] Polymers containing the chalcogens sulphur and selenium are recognised as attractive redox-responsive polymeric materials for drug delivery as many have shown reactivity towards reducing agents such as glutathione and oxidants such as reactive oxygen species (ROS).[201]

1.6.1 Disulphide-containing Nanoparticles

The tripeptide glutathione (GSH) is the most abundant low-MW thiol in animal cells having an intracellular concentration of 2-10 mM (Figure 8A).[202,203] Conversely, the concentration of GSH in extracellular fluids and circulation is 100-1000 times lower (2-20 μM). GSH and its oxidised form glutathione disulphide (GSSG) constitute the major redox couple in animal cells with the elevated intracellular concentration of the reduced form GSH being maintained by NADPH and glutathione reductase. Additionally, GSH can be even more concentrated in certain tumour tissues, including multi-drug resistant ones.[200,204]

Given the asymmetric localisation of highly concentrated glutathione, polymers capable of undergoing degradation upon exposure to elevated GSH concentrations are desirable carriers for intracellular and cancer-targeted drug delivery.[205,206] The disulphide chemical motif has assumed a central position in this context as these moieties can be reduced to thiols *via* thiol-disulphide exchange reactions with GSH, resulting in net lysis of the S-S bond (Figure 8B).[207–209] In its essential form, the thiol-disulphide exchange reaction proceeds *via* an S_N2 mechanism involving an attack of the thiolate anion acting as the nucleophile to the sulphur atom of the disulphide to form a new S-S bond.[210,211]

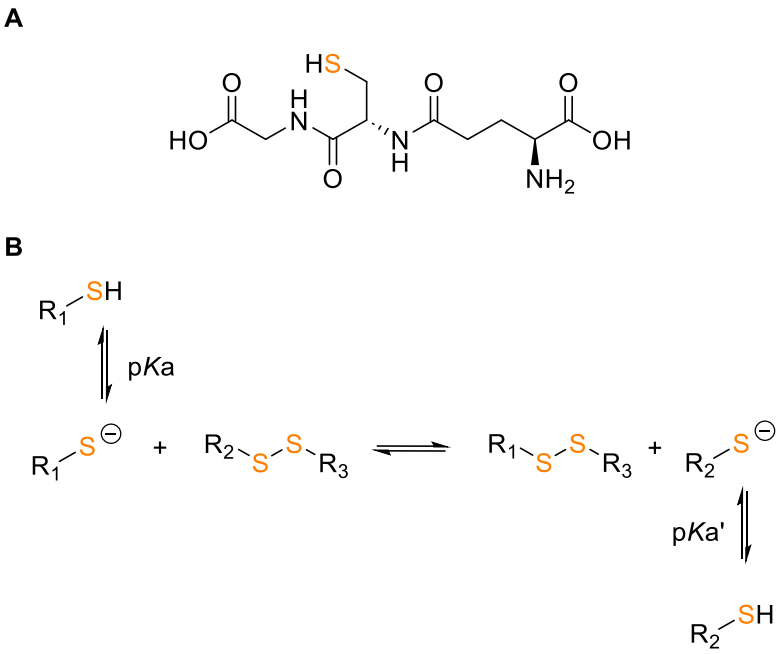
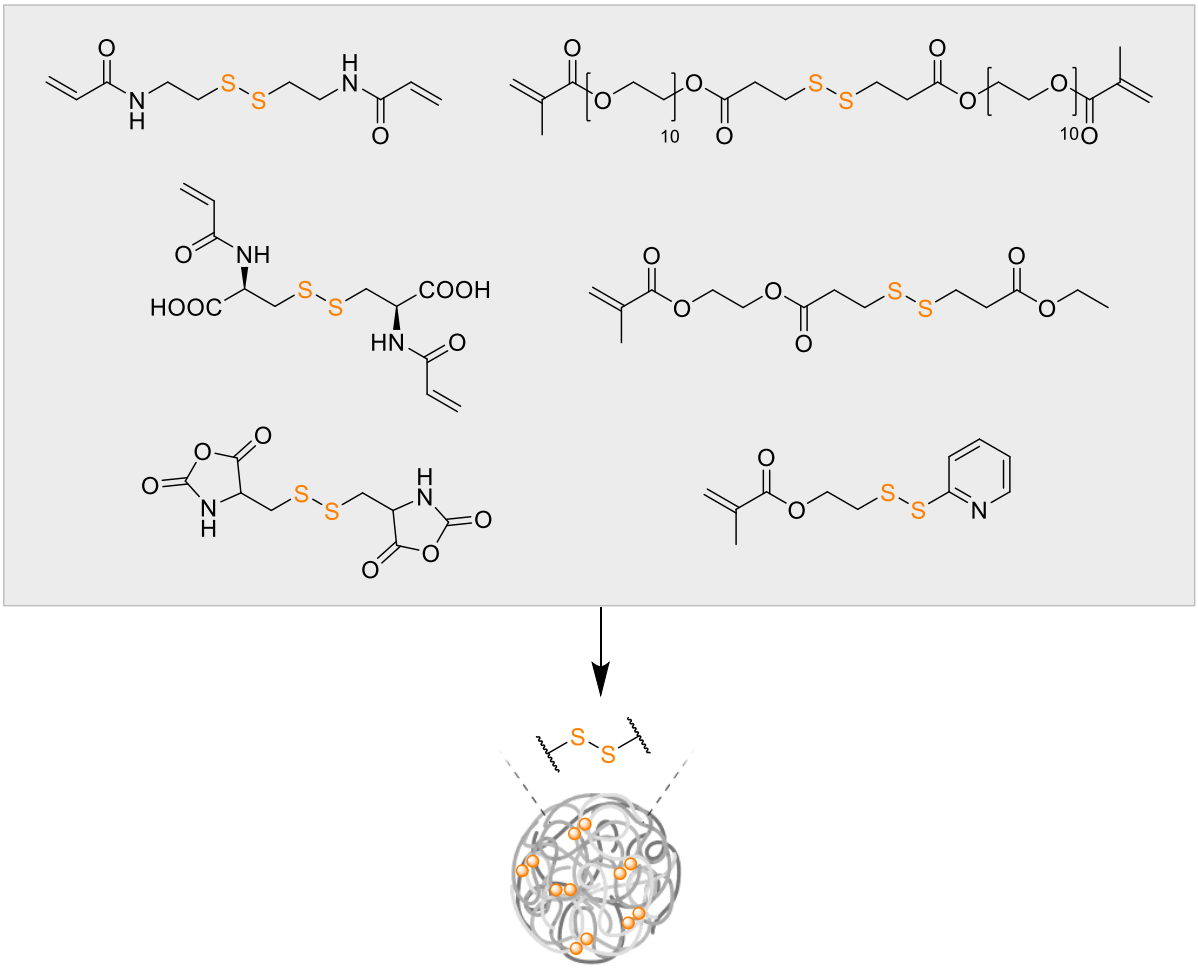


Figure 8. A) chemical structure of glutathione, B) mechanism of the disulphide exchange reaction.

Disulphides are a common redox-responsive moiety in polymeric NPs due to facile synthetic accessibility, natural presence in biological systems, and well-established responsiveness to biologically relevant concentrations of GSH.[212] Besides the responsiveness to glutathione alone, disulphides embedded into polymeric NPs are hypothesised to facilitate cellular uptake and endosomal escape via covalent interaction with membrane thiols which might potentially strain the packing of endosomal membranes.[213]

Disulphide-containing crosslinkers are commonly reported building blocks for redox-responsive polymeric NPs.[214–220] Commercially available cystamine, cystine, and 3,3'-dithiopropionic acid are versatile starting materials from which a range of polymerisable disulphides can be prepared and subsequently polymerised into NPs (Scheme 4).

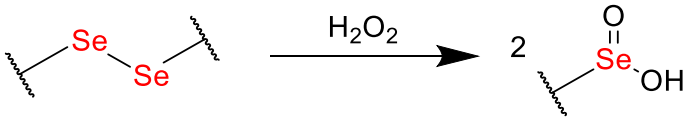


Scheme 4. Polymerisable building blocks for the synthesis of disulphide-containing polymeric NPs.

Disulphide-containing polymeric NPs based on PEG, oligo(ethylene glycol), chitosan, poly(*N*-isopropylacrylamide), poly(acrylic acid), carboxymethyl cellulose, hyperbranched polyglycerol, and poly(amino acids) have been reported for the encapsulation of small molecules such as doxorubicin.[215,216,218,220–226]

1.6.2 Diselenide-containing Nanoparticles

The Se-Se bond has a lower bond energy than the S-S bond (172 kJ mol^{-1} *vs* 240 kJ mol^{-1}) making diselenides generally more responsive to mild stimuli than disulphide analogues.[227–229] Diselenide-containing polymeric DDSs such as hydrogels and micelles have been described as dually responsive systems which can undergo degradation and payload release by the action of reducing agents such as glutathione or dithiothreitol, and oxidants such as the reactive oxygen species (ROS) such as hydrogen peroxide and singlet oxygen.[230–233] Whilst ROS assume a physiologically significant role which is dependent on their concentration, localisation, and permanence in biological systems, pathological states such as cancer, inflammation, atherosclerosis, and ageing are characterised by ROS overproduction.[234–237] Diselenides embedded into polymeric NPs have been proposed to cleave upon treatment with hydrogen peroxide and related ROS to yield seleninic acids (Scheme 5). [229,231–233,238,239]



Scheme 5. Oxidation of diselenides to two equivalents of seleninic acids by hydrogen peroxide resulting in cleavage of the Se-Se bond.

Diselenide-containing polymeric NPs based on PEG, poly(acrylic acid), and polyzwitterions encapsulating small molecules such as doxorubicin and Nile red have been reported.[229,240–244]

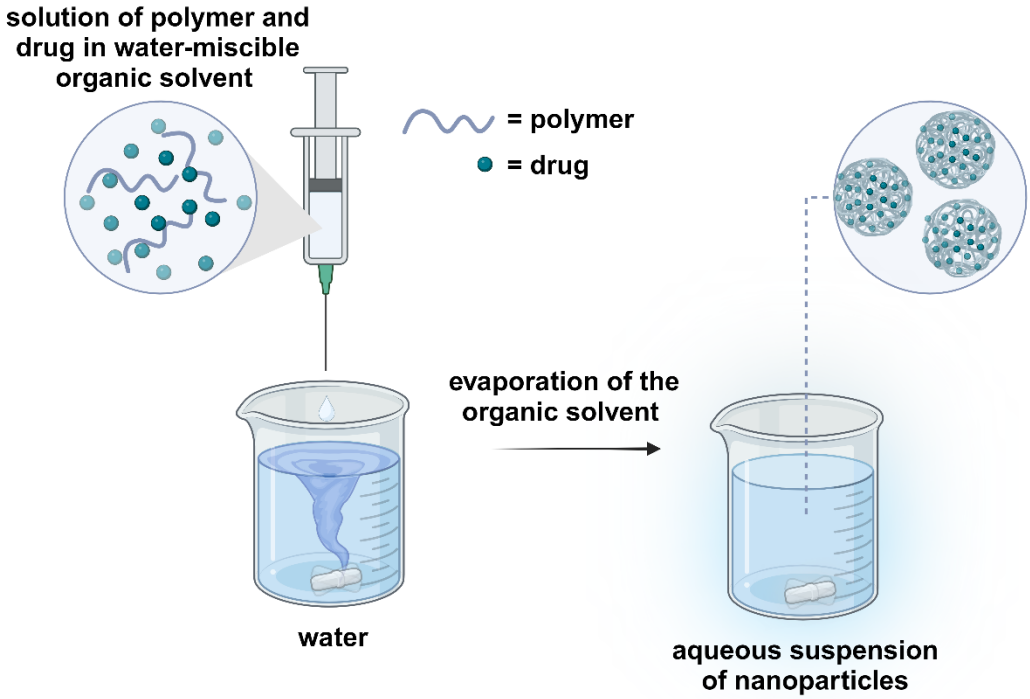
1.7 Preparation of Polymeric Nanoparticles

Polymeric NPs for drug delivery are prepared by the physical manipulation of polymers and chemical crosslinking of polymers or synthesised *via* the polymerisation of smaller building blocks such as monomers and crosslinkers. Examples of strategies for the preparation of polymeric NPs relevant to this work are discussed in the following sections.

1.7.1 Nanoprecipitation

Nanoprecipitation is a method for the preparation of polymeric NPs patented in 1988 and published the following year by Fessi *et al*.[245] In its initially reported form the nanoprecipitation methodology was referred to as "nanocapsule formation by interfacial polymer deposition following solvent displacement". The nanoprecipitation methodology and its many subsequent iterations assumed a central position for the preparation of sub-micron polymeric particles with narrow size distributions, mainly due to its simplicity of execution, process scalability, good reproducibility, and safety.[246,247]

In the most essential form, the nanoprecipitation process consists of the addition of a water-miscible organic solvent containing a hydrophobic polymer and the drug of interest to water (non-solvent) under stirring, followed by the elimination of the organic solvent by stirring at room temperature (rt) or under reduced pressure (Scheme 6). This process results in an aqueous suspension of polymeric NPs which can be subjected to further ultracentrifugation or lyophilisation to allow the isolation of NPs in their solid form. As a common method variation, stabilisers such as polyvinyl alcohol (PVA) or amphiphilic block copolymers (Poloxamer/Pluronic) can be added to the aqueous phase to stabilize the NPs against aggregation.[248]



Scheme 6. Schematic of the nanoprecipitation method for the preparation of drug-loaded polymeric NPs.

The rationale for the formation of NPs during the nanoprecipitation process has been proposed by Ganachaud and Katz who invoked the "Ouzo effect", a spontaneous emulsification process in which the mixing of a solution with a non-solvent induces a supersaturation of the solute, which ultimately leads to phase separation yielding a dispersion of droplets.[249,250] The effect is visible in alcoholic beverages containing water-insoluble oils which become cloudy upon dilution with water due to the formation of light-scattering oil droplets. By analogy, it was hypothesised that hydrophobic small molecules, lipids, and polymers behave similarly to oil droplets and give rise to NP dispersions under these conditions.[251] Moreover, if the initial polymer solution contains oil, the products of the nanoprecipitation method are polymeric nanocapsules containing an oily core, as originally reported by Fessi.[245,252] Polymers amenable to nanoprecipitation include PLA[253], PLGA[254], PLGA-PEG[156], PCL[255], polystyrene (PS)[256], and poly(methylmethacrylate) (PMMA)[257].

Due to the configuration of the method, nanoprecipitation was established as a method for the encapsulation of hydrophobic payloads which can easily be dissolved in the water-miscible organic solvent. Whilst the encapsulation of hydrophilic drugs has initially been considered challenging due to low loading efficiencies resulting from drug migration into the aqueous phase, the optimisation of the nanoprecipitation parameters such as modifications of the pH of the aqueous phase and an appropriate selection of the drug form are able to alleviate this shortcoming.[247,258,259] Examples of potentially therapeutic NPs prepared *via* the nanoprecipitation method are presented in Table 4.

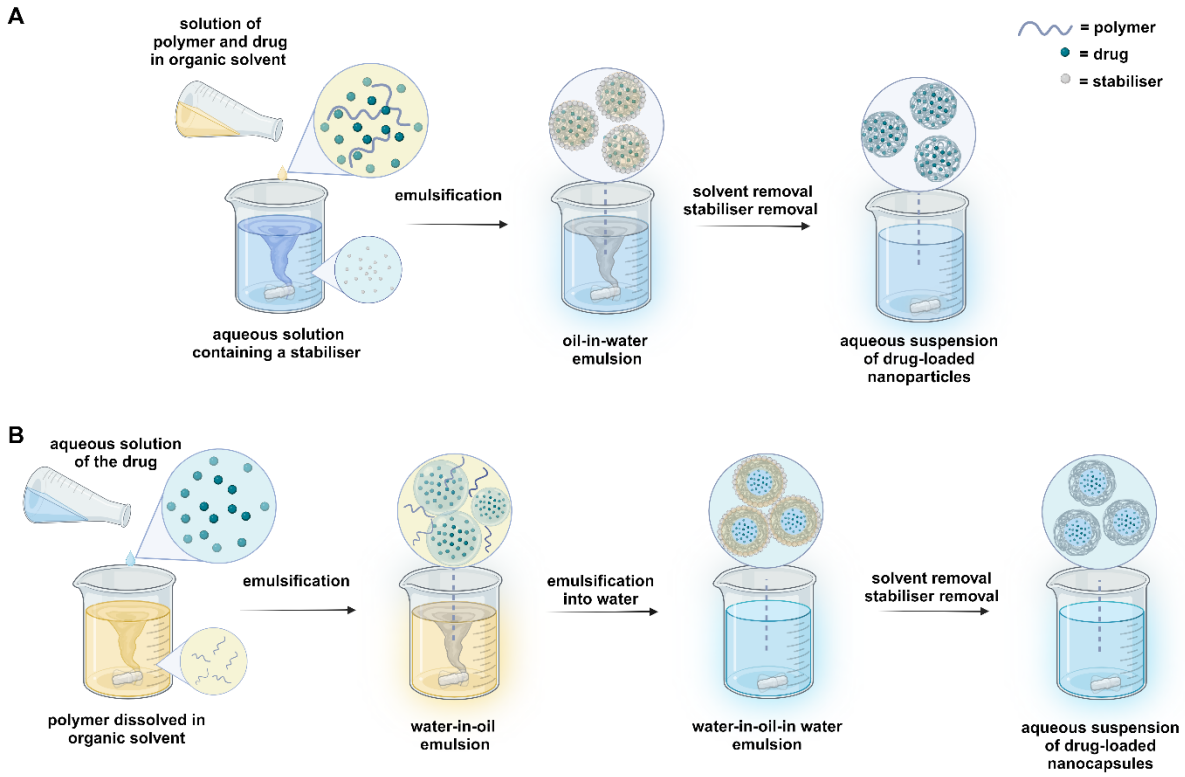
Polymer	**Solvent**	**Stabiliser**	**Therapeutic substance**	**NP size (nm)**	**Potential therapeutic use**	**Ref**
PLA-PEG	MeCN	-	paclitaxel	83.4	cancer	[260]
PLGA-PEG	MeCN	-	Ac2-26	<90	atherosclerosis	[171]
PCL	acetone	Pluronic F68	isradipine	197.5	hypertension	[261]
PLGA	DMF	PVA	cisplatin	126	cancer	[262]
PLGA	acetone	Poloxamer 188	paclitaxel	≤160	cancer	[161]
mPEG-PCL	acetone	-	docetaxel	~70	cancer	[263]
PLGA	DMSO or DMSO:acetone	various stabilisers	amphotericin B	≤153	fungal infections	[264]

Table 4. Selected examples of nanoprecipitation-based methodologies for the preparation of drug-loaded polymeric NPs.

1.7.2 Emulsion-based Methods

Drug-loaded polymeric NPs are achievable *via* emulsions containing a hydrophobic polymer. Typically, a solution of the polymer and drug in a volatile organic solvent such as dichloromethane is emulsified into an aqueous phase containing a stabiliser such as polyvinyl alcohol (PVA) (Scheme 7A).[265] This mixture gives a water-in-oil emulsion *via* exposure to a source of high energy such as an ultrasonicator, homogeniser or colloid mill.[266] The subsequent elimination of the organic solvent induces the precipitation of the polymer yielding an aqueous suspension of polymeric NPs. The obtained NPs can then be isolated by centrifugation and washed with water to remove the stabiliser.[267]

The application of water-in-oil emulsion methods is typically limited to the encapsulation of hydrophobic substances due to the diffusion and partitioning of hydrophilic substances into the aqueous phase.[266] To overcome this limitation, the double emulsion method can be adopted (Scheme 7B). This method requires the preparation of a water-in-oil emulsion containing the hydrophilic payload in the aqueous phase. The water-in-oil emulsion is then emulsified into a secondary aqueous phase containing a stabiliser to give a water-in-oil-in-water double emulsion. The removal of the organic solvent from the system induces the precipitation of the hydrophobic polymer yielding polymeric nanocapsules containing the hydrophilic payload within their cores.



Scheme 7. Schematic of A) emulsion method and B) double emulsion method for the preparation of drug-loaded polymeric NPs.

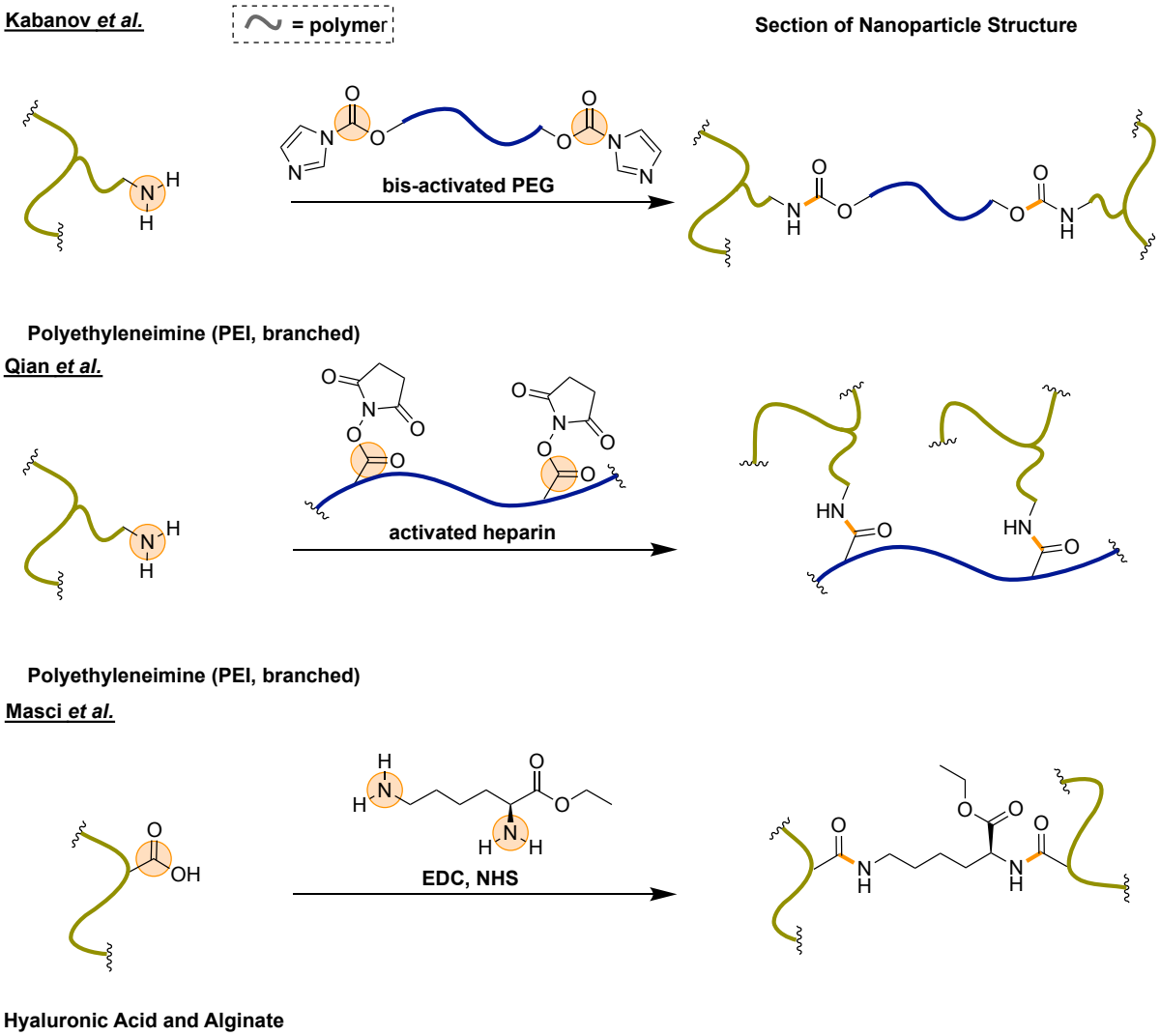
A list of examples of typical emulsion and double emulsion compositions employed for the preparation of polymeric NPs encapsulating small-molecule drugs such as loperamide and proteins such as bovine serum albumin (BSA) is given in Table 5.

Polymer	Emulsion	Stabiliser	Payload	Reported NP size (nm)	Ref
PLGA	CH_2Cl_2/H_2O	PVA	cyclosporine	≤223	[268]
PLGA-PEG	CH_2Cl_2/H_2O	PVA	cyclosporine	≤212	[268]
PLA	CH_2Cl_2/H_2O	PVA	loperamide	≤264	[269]
PLGA	propylene glycol:CH_2Cl_2/H_2O	PVA	rutin	252	[270]
PLGA	$H_2O/CH_2Cl_2/H_2O$	PVA	propranolol HCl	<280	[271]
PCL	$H_2O/CH_2Cl_2/H_2O$	PVA	propranolol HCl	<280	[271]
ethylcellulose	$H_2O/CH_2Cl_2/H_2O$	PVA	propranolol HCl	<280	[271]
PLGA	H_2O/CH_2Cl_2:acetone/H_2O	Pluronic F68, PVA	BSA	-	[267]
PLGA	$H_2O/CH_2Cl_2/H_2O$	PVA	BSA	≤278	[272]
PCL	$H_2O/CH_2Cl_2/H_2O$	PVA	BSA	≤308	[272]

Table 5. Selected examples of drug-loaded polymeric NPs prepared from polymers via emulsion-based methods.

1.7.3 Crosslinking of Polymers

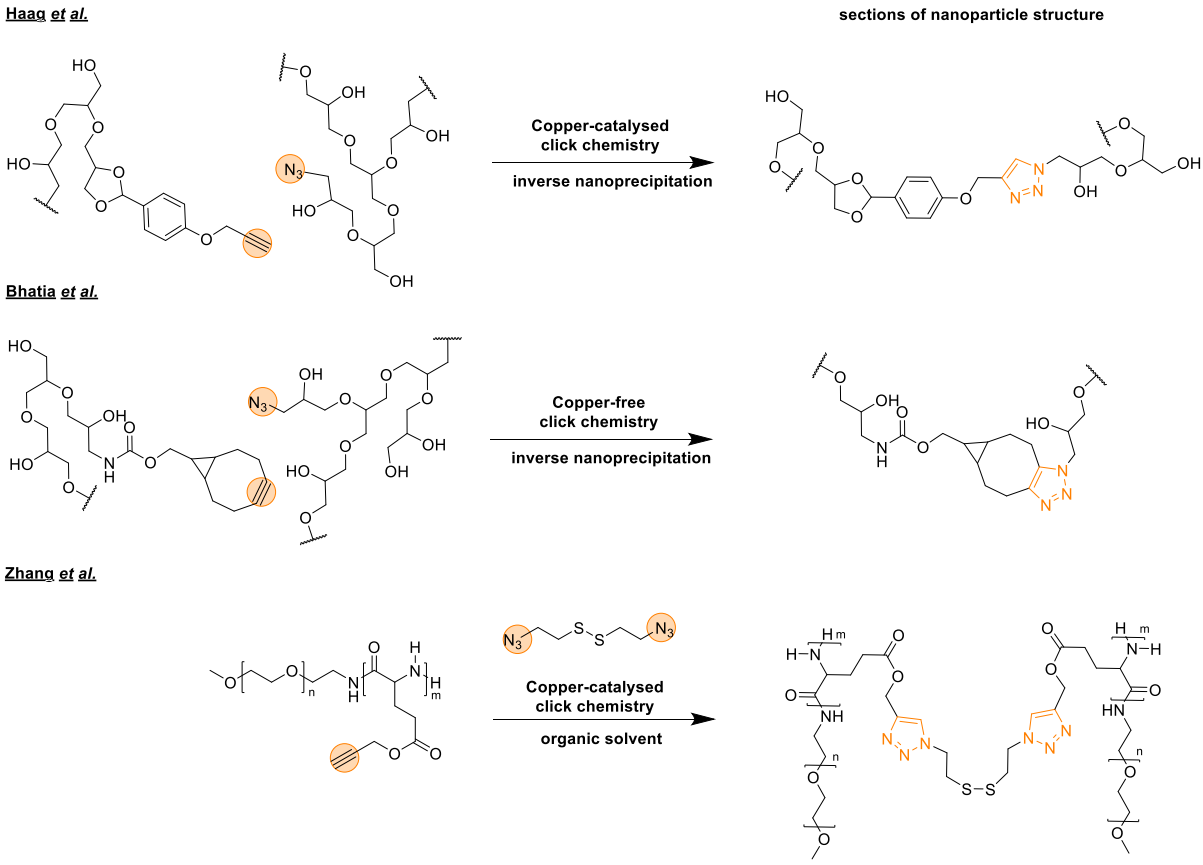
Polymers bearing reactive moieties such as amines and carboxylic acids can be crosslinked to afford crosslinked polymeric NPs (Scheme 8). For example, Kabanov *et al.* crosslinked polyethyleneimine (PEI) with bis-activated PEG under emulsion conditions to obtain carbamate-crosslinked polymeric NPs termed nanogels and ulitised them to encapsulate antisense oligonucleotides and cytotoxic drugs.[273,274] Similarly, Qian *et al.* crosslinked PEI with heparin activated as *N*-hydroxysuccinimide *via* amide-bond formation to obtain crosslinked polymeric NPs for the encapsulation of plasmids.[275] Masci *et al.* reported on the crosslinking of alginate and hyaluronic acid with the diamine L-lysine ethyl ester within polyion complex micelles which served as nanoreactors enabling fully aqueous crosslinking reaction conditions.[276]



Scheme 8. Preparation of crosslinked polymeric NPs via crosslinking of reactive polymers.[273–277]

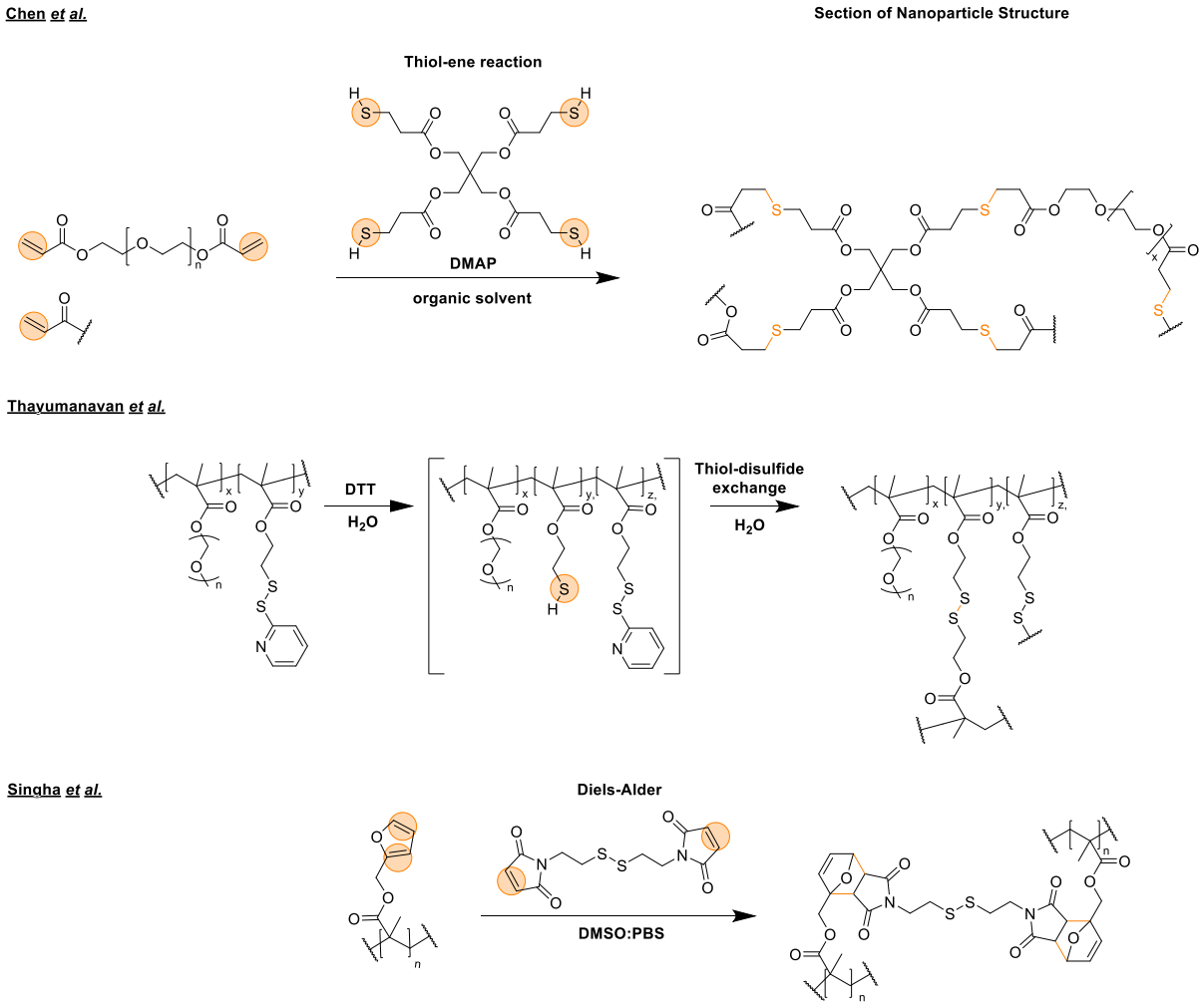
Crosslinked polymeric NPs have also been prepared from tailored synthetic polymers by means of click chemistry (Scheme 9). For example, Haag *et al.* crosslinked azide- and alkyne-modified polyglycerol *via* copper-catalysed azide-alkyne cycloaddition under inverse nanoprecipitation of aqueous solutions into acetone with simultaneous encapsulation of the enzyme asparaginase.[278] Zhang *et al.* used click chemistry to crosslink the propargylated block copolymer methoxy poly(ethylene glycol)-*b*-poly(γ-propargyl-L-glutamate) with 2-azidoethyl disulphide in DMF to obtain crosslinked polymeric NPs with covalently-loaded doxorubicin.[279] Similarly, Stansbury *et al.* prepared polymeric NPs by core-crosslinking of polymeric micelles deriving from the assembly of amphiphilic block copolymers containing azides with propargyl ether via CuACC.[280] Bhatia *et al.* used copper-free click chemistry in inverse nanoprecipitation of azide- and cyclooctyne-functionalised polyglycerols to prepare polymeric NPs which

can adapt onto the surface of influenza A viruses and inhibit binding and cell infection.[281]



Scheme 9. Preparation of crosslinked polymeric NPs via click chemistry.[278,279,281]

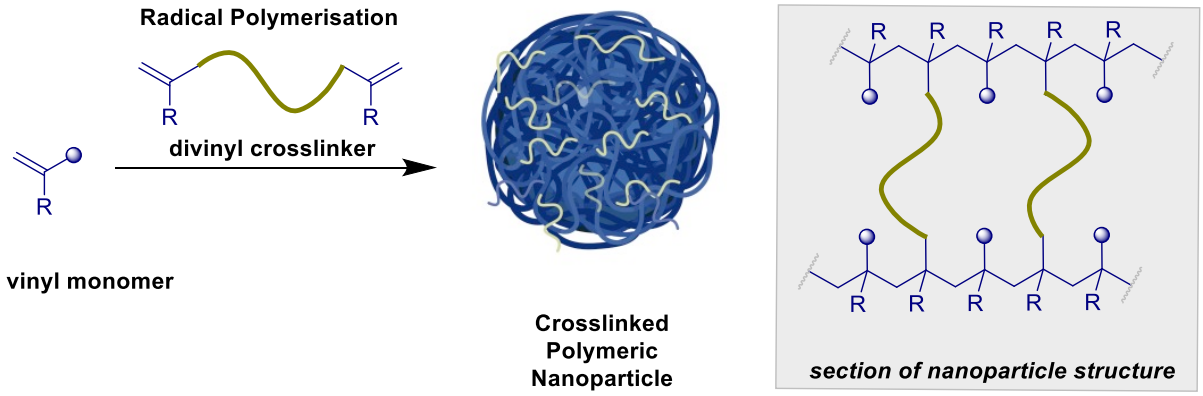
Crosslinked polymeric NPs can also be prepared via chemistries such as thiol-ene reactions, thiol-disulphide exchange, and Diels-Alder chemistry (Scheme 10). For instance, Chen *et al.* prepared polymeric NPs via DMAP-catalysed thiol-ene reaction of acrylated polymers and the tetrathiol pentaerythritol tetra(3-mercaptoprionate) for the encapsulation of insulin.[282] Polymers having pendant thiol and disulphide groups can be crosslinked to form polymeric NPs via thiol-disulphide reactions.[212] Thayumanavan *et al.* prepared crosslinked polymeric NPs from copolymers bearing pyridyldisulphide units and are able to form nanoaggregates in solution.[223] The substoichiometric reduction of the disulphide units with DTT exposes thiols which then react with remaining disulphides *via* thiol-disulphide exchange reactions to yield disulphide crosslinked polymeric NPs. Singha *et al.* prepared polymeric NPs by crosslinking a furane-containing amphiphilic copolymer with dithiobismaleimidoethane for the encapsulation of doxorubicin.[283]



Scheme 10. Preparation of crosslinked polymeric NPs via crosslinking of thiol- and furane-functionalised polymers.[223,282,283]

1.7.4 Radical Polymerisation of Monomers

The radical polymerisation of monomers and simultaneous NP formation allows for a high degree of NP design and in doing so enables the tailoring of NP properties.[284] In principle, crosslinked polymeric NPs are achievable *via* the radical crosslinking copolymerisation of vinyls with divinyl crosslinkers (Scheme 11). Reported synthetic procedures for the synthesis of polymeric NPs from monomers include both conventional and living radical polymerisations which can be conducted in solution, miniemulsion, microemulsion, or within liposomal "nanoreactors".[285]

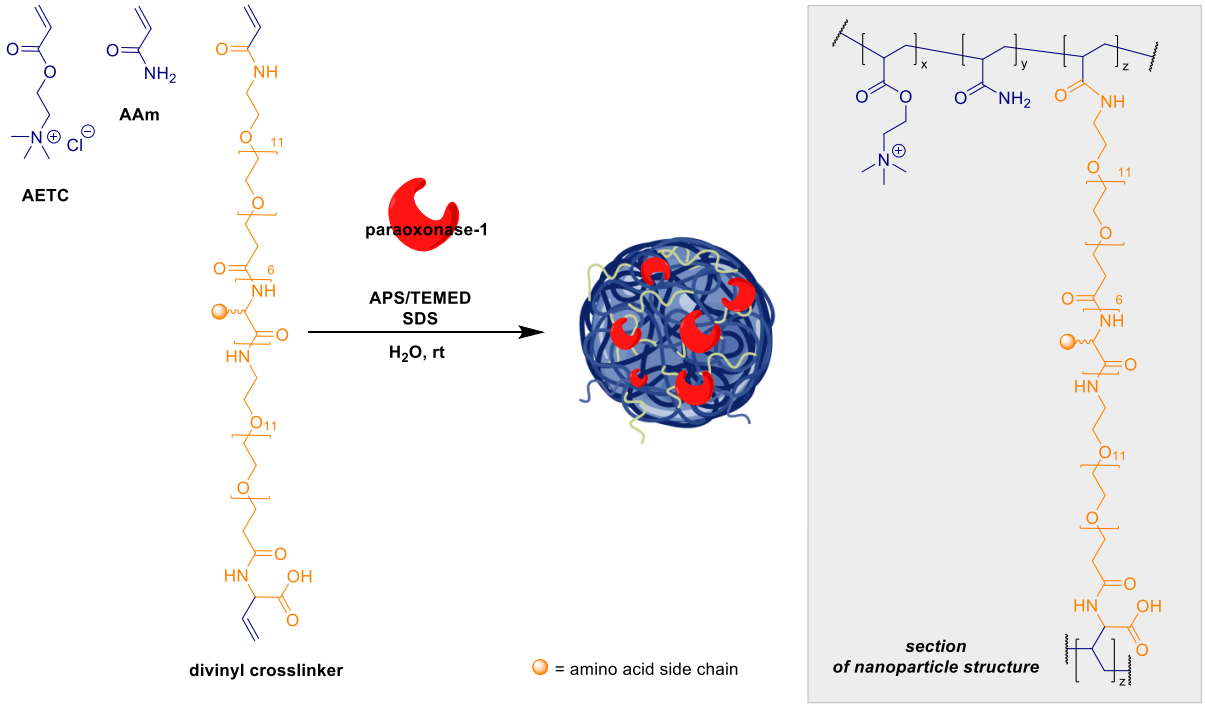


Scheme 11. General scheme for the radical crosslinking copolymerisation of vinyl monomers with a divinyl crosslinker to give a crosslinked polymeric NP with internal structure presented in the grey box.

1.7.4.1 Solution Polymerisations

Radical crosslinking copolymerisations of vinyls initiated by benzoyl peroxide or AIBN in organic solvents such as ketones, DMF, and DMSO have been reported to yield crosslinked polymeric NPs and microparticles.[286–288] Radical polymerisations in aqueous solution are more desirable for biomedical applications and fully aqueous approaches of crosslinking copolymerisations of monomers such as acrylamide using biomacromolecular templates for NP synthesis have been reported.[289–293] These methodologies rely either on the non-covalent interactions of monomers with proteins causing enrichment of polymerisable monomers in the protein surrounding, or the covalent modification of proteins with vinyl groups which act as handles for the "directed" polymerisation of monomers. Protein-templated polymerisations are usually initiated by the APS/TEMED system at room temperature and yield crosslinked

polymeric NPs containing protein payloads. For instance, Kamaly *et al.* reported crosslinked polymeric NPs encapsulating the enzyme paraoxonase-1 (Scheme 12).[294] This type of protein-templated polymerisation exploits the electrostatic interaction of the negatively charged protein with a cationic monomer (AETC) to allow the simultaneous crosslinking copolymerisation and protein encapsulation, which occurs with the conservation of enzymatic activity.



Scheme 12. Protein-templated radical crosslinking copolymerisation yielding crosslinked polymeric NPs loaded with paraoxonase-1 as reported by Kamaly *et al*. AETC = [2-(acryloyloxy)ethyl]trimethylammonium chloride, AAm = acrylamide, APS = ammonium persulfate, TEMED = tetramethylethylenediamine, SDS= sodium dodecyl sulfate.[294]

1.7.4.2 Miniemulsion Polymerisation

Miniemulsions are thermodynamically unstable liquid/liquid dispersions containing small droplets (30-500 nm) of the internal phase having narrow size distributions which can be kinetically stabilised to give long-term stable systems.[295–297] In miniemulsions, the small size of the dispersed droplets can be achieved via ultrasonication or high-pressure homogenization.[298] Polymerisable miniemulsions can be formulated to

favour polymerisation reactions within the single dispersed droplets, resulting in particles having an identical size as the droplet they originated from.[299–301] Water-in-oil miniemulsions are formulated to polymerise hydrophilic monomers with the system being stabilised by non-ionic surfactants such as Span 80 or non-ionic block copolymers.[295]

The common water-in-oil miniemulsion procedure consists of the emulsification of an aqueous solution of monomers into a solution of the surfactant in an organic solvent, followed by application of energy to give small, dispersed droplets. The polymerisation can be initiated by either water-soluble initiators such as KPS or oil-soluble initiators such as AIBN. The choice of the initiator has the potential to influence the nucleation locus with water-soluble initiators potentially favouring nucleation within the dispersed droplets.[297] Selected examples of radical polymerisations in miniemulsions yielding crosslinked polymeric NPs are presented in Table 6.

monomer	**crosslinker**	**surfactant**	**internal/external phase**	**initiator**	**ref**
hydroxyethyl acrylate or acrylamide or acrylic acid	diethylene glycol diacrylate	Span 80 or KLE3729	H_2O/cyclohexane or H_2O/hexadecane	PEGA200 or AIBN	295
N-vinylcaprolactam	*N*,*N*'-methyelenbisacrylamide	Span 80	H_2O/hexadecane	KPS	300
acrylamide	methacrylated dextran	Lubrizol U	H_2O/cyclohexane	V-59 or V-70 or VA-044	302
N-acryloyl-L-glutamic acid	*N*,*N*'-methyelenbisacrylamide	PGR	H_2O/cyclohexane	KPS or AIBN	303

Table 6. Examples of crosslinked polymeric NPs synthesised by radical miniemulsion polymerisation.

1.7.4.3 Microemulsion Polymerisation

Microemulsions are thermodynamically stable dispersions of two immiscible liquids stabilised by surfactants and formed spontaneously at specific component concentrations.[304] The concentration of surfactants required to formulate a microemulsion is substantially higher compared to classical emulsions and can amount to ~10 wt%.[305] Since the surfactant is present in a higher concentration than its critical micellar concentration in a given solvent, microemulsions are considered dispersed systems composed of micelles swollen with the internal phase.

Conventional radical polymerisation of acrylamide in water-in-oil microemulsions is a thoroughly investigated system and its comparison with miniemulsion polymerisations revealed substantial differences between the two systems.[305,306] Particularly, the size of the obtained particles is often larger than the "parent" swollen micelles and the final number of particles obtained is often 2-3 times smaller than the number micelles initially present in the system, indicating the existence of processes such as "sticky" collision of micelles and diffusion of monomers from "reservoir" to polymerising micelles *via* the external phase.

Polymerisations in water-in-oil microemulsions can be initiated with both water-soluble initiators such as KPS and oil-soluble initiators such as AIBN, with KPS initiating the polymerisation within the swollen micelles, and AIBN initiating the polymerisation at the oil-water interface *via* interaction with monomers such as acrylamide, which can exhibit a co-surfactant-like behaviour by insertion between the surfactant molecules.[307] Regardless of the chemical nature of the initiator and the intrinsic dynamic nature of microemulsions as polymerising systems, studies have shown that all of the monomeric payload is eventually consumed.[308]

A typical microemulsion polymerisation of hydrophilic monomers consists of the dissolution of an aqueous solution of monomers into an organic solvent containing a surfactant such as Aerosol OT with the initiator present in one of the two phases, depending on its solubility.[306] A list of examples of microemulsion polymerisation compositions employed for the synthesis of crosslinked polymeric NPs is given in Table 7.

monomer	crosslinker	surfactant	internal/external phase	initiator	ref
acrylamide	*N*,*N*'-methyelenbisacrylamide	Aerosol OT	H_2O/toluene	AIBN	[309]
acrylamide	*N*,*N*'-methyelenbisacrylamide	Aerosol OT	monomers/hexane	APS:TEMED	[310]
N-vinylformamide	BDEP	Span 80/Tween 80	H_2O/hexane	VAZO-52	[311]
2-acrylamido-2-methyl-1-propanesulfonic acid	*N*,*N*'-methyelenbisacrylamide	Span 80/Tween 80	H_2O/toluene	AIBN	[312]
2-hydroxyethyl acrylate 2-acryloxyethyltrime-thylammonium chloride	PEG diacrylate	Laureth-3	H_2O/heptane	Trigonox EHP	[312]

Table 7. Selected examples of crosslinked polymeric NPs prepared via radical microemulsion polymerisation. BDEP = 2-Bis[2,2′-di(N-vinylformamido)ethoxy]propane.

1.7.4.4 Precipitation and Dispersion Polymerisation

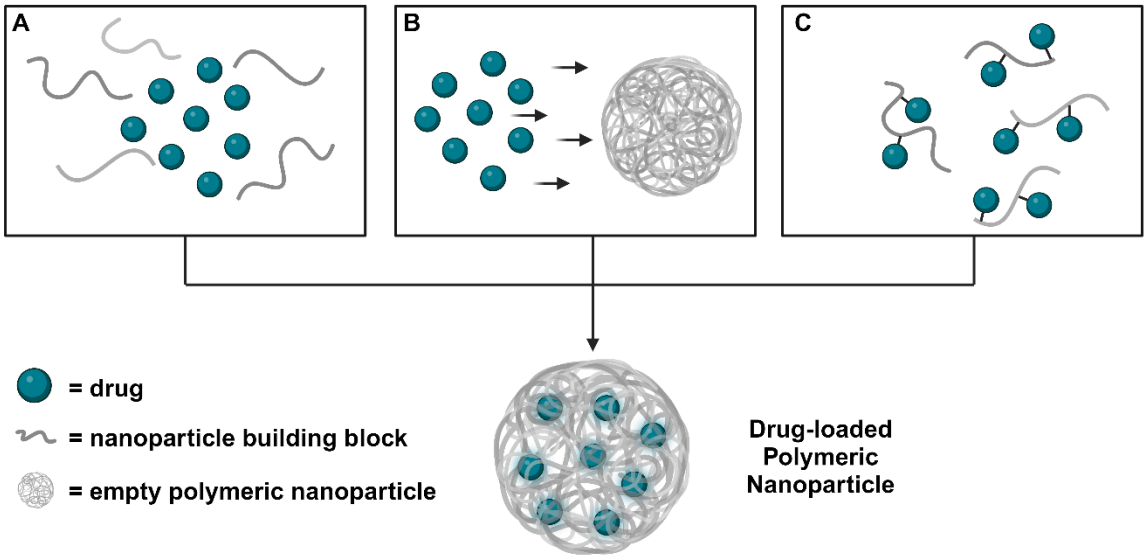
The precipitation polymerisation method is essentially a solution polymerisation in which the reaction components (e.g. monomers and initiator) are freely soluble in the reaction solvent whilst the polymer is insoluble and thus precipitates.[313,314] The method is typically used to synthesise particles based on thermoresponsive polymers presenting a lower critical solution temperature (LCST) in water and thus suffer a hydrophilic to hydrophobic transition at high temperatures.[315]

A lack of particle stabilisation which can manifest as particle coagulation is sometimes observed in precipitation polymerisations resulting in particles having an irregular shape and non-uniform size distribution.[316] To circumvent this, a stabiliser is often

added to the polymerisation mixture which can induce the formation of better stabilized, smaller NPs *via* a process named dispersion polymerisation.[314] The stabiliser used is most often a non-ionic polymer capable of adsorption to the surface of the formed particles.

1.8 Payload Loading Methods

Therapeutic substances can be (i) encapsulated within polymeric NPs during the nanoparticle formation process, (ii) encapsulated *via* contact with fully formed NPs, or (iii) covalently attached to the NP (Scheme 13).



Scheme 13. Drug loading methods for polymeric nanoparticles. A) simultaneous nanoparticle formation and drug encapsulation, B) drug loading by contacting the drug with empty polymeric nanoparticles, and C) covalent drug loading via drug-polymer conjugates.

NP preparation methods such as nanoprecipitation and emulsification/solvent evaporation allow the simultaneous encapsulation of hydrophobic substances and NP formation. Similarly, protein-templated polymerisations allow the simultaneous NP formation and encapsulation of the protein payload which may proceed with the preservation of payload functionality.[293]

On the other hand, Lyon *et al.* presented the “breathing in method” in which lyophilised nanogels are contacted with a concentrated aqueous solution of biomacromolecules such as siRNA allowing the nanoparticles to swell, and thus incorporate most of the

aqueous phase containing the payload.[317] Similarly, Pakulska *et al.* loaded proteins onto PLGA NPs by contacting the forming NPs with an aqueous solution of the protein, resulting in their electrostatic adsorption to the NPs and controlled release.[318]

Small-molecule drugs can be covalently encapsulated within polymeric NP *via* drug-polymer conjugates.[319–322] Besides providing high drug loadings, this method can enable the triggered drug release *via* selective cleavage of the bonds connecting the polymer and the drug.

1.9 Thesis Synopsis

This project has aimed to design, synthesise, and analyse novel crosslinked polymeric NPs containing chemical motifs inspired by the chemistry of degradable polymers. The chapters of this thesis describe the investigation of underexplored nano-chemical space performed with the intent of developing unprecedented NP platforms as novel design options for NP-based drug delivery.

Chapter 2 describes the synthesis of novel polymerisable oligoesters named oligolactoglycolic acid dimethacrylates (OLGADMAs) as essential NP building blocks used in this work.

Chapter 3 describes the polymerisation of OLGADMAs into PLGA-inspired crosslinked polymeric NPs via an unprecedented nanoprecipitation-based methodology and explores the *in vitro* stability of a library of NPs performed via a comparative study against NPs based on PLGA, PLGA-PEG, and sequenced PLGA. The chapter concludes with a preliminary estimation of the *in vitro* biocompatibility and the cellular internalisation of the prepared NPs.

Chapter 4 describes the application of PLGA-inspired crosslinked NPs for the encapsulation of hydrophobic drugs, and the analysis of a library of drug-loaded NPs in terms of drug release, colloidal stability in biological media, stability upon storage at room temperature, and effect on cell viability *in vitro*.

Chapter 5 describes the synthesis of a novel disulphide-containing polymerisable monomer designed around the concepts of glutathione-responsive chemistry and oligolactoglycolic acid dimethacrylates. The section concludes with the synthesis and analysis of disulphide-containing NPs, and a preliminary study focusing on the *in vitro* stability of these NPs in the presence of glutathione. Furthermore, the chapter describes the initial synthetic efforts towards developing diselenide-containing crosslinked polymeric NPs.

Chapter 6 summarises the main findings and provides future directions aimed towards the further development of the project.

Chapter 2: Design and Synthesis of Oligolactoglycolic Acid Dimethacrylates

2.1 Introduction

The absence of clinically approved PLGA NPs is suggestive of the pressing need for the optimisation of PLGA-based NPs for drug delivery applications. At present, the landscape of investigational PLGA nanomedicines is heavily dominated by non-sequenced, linear PLGA and its block copolymers with PEG. As discussed in Chapter 1, PLGA crosslinking and PLGA sequencing have been separately proposed as strategies that allow for increased stability of PLGA materials and potential advantages of sequenced and crosslinked PLGA in the context of biomedical applications have been hypothesised.

Covalently crosslinked NP modalities featuring the PLGA chemical motif remain somewhat underexplored, with reported examples containing random PLGA obtained by ROP. For instance, Zhong *et al.* reported on crosslinked polymeric NPs based on lipoyl ester terminated star PLGA which was crosslinked by treatment with dithiothreitol (DTT) to obtain a disulphide crosslinked NP core (Figure 9A). The resulting disulphide-crosslinked NPs demonstrated marked advantages over counterparts comprising linear PLGA including increased stability, reduced drug leakage, and reduction-triggered payload release imparted by the disulphide-crosslinked structure.[323,324] Alternatively, Lu *et al.* reported on the photo-crosslinking of micelles formed from PLGA-PEG functionalised with poly(propylene fumarate) in the presence of the UV initiator Igracure 2959 to obtain crosslinked NPs for cancer-targeted imaging and drug delivery (Figure 9B).[325]

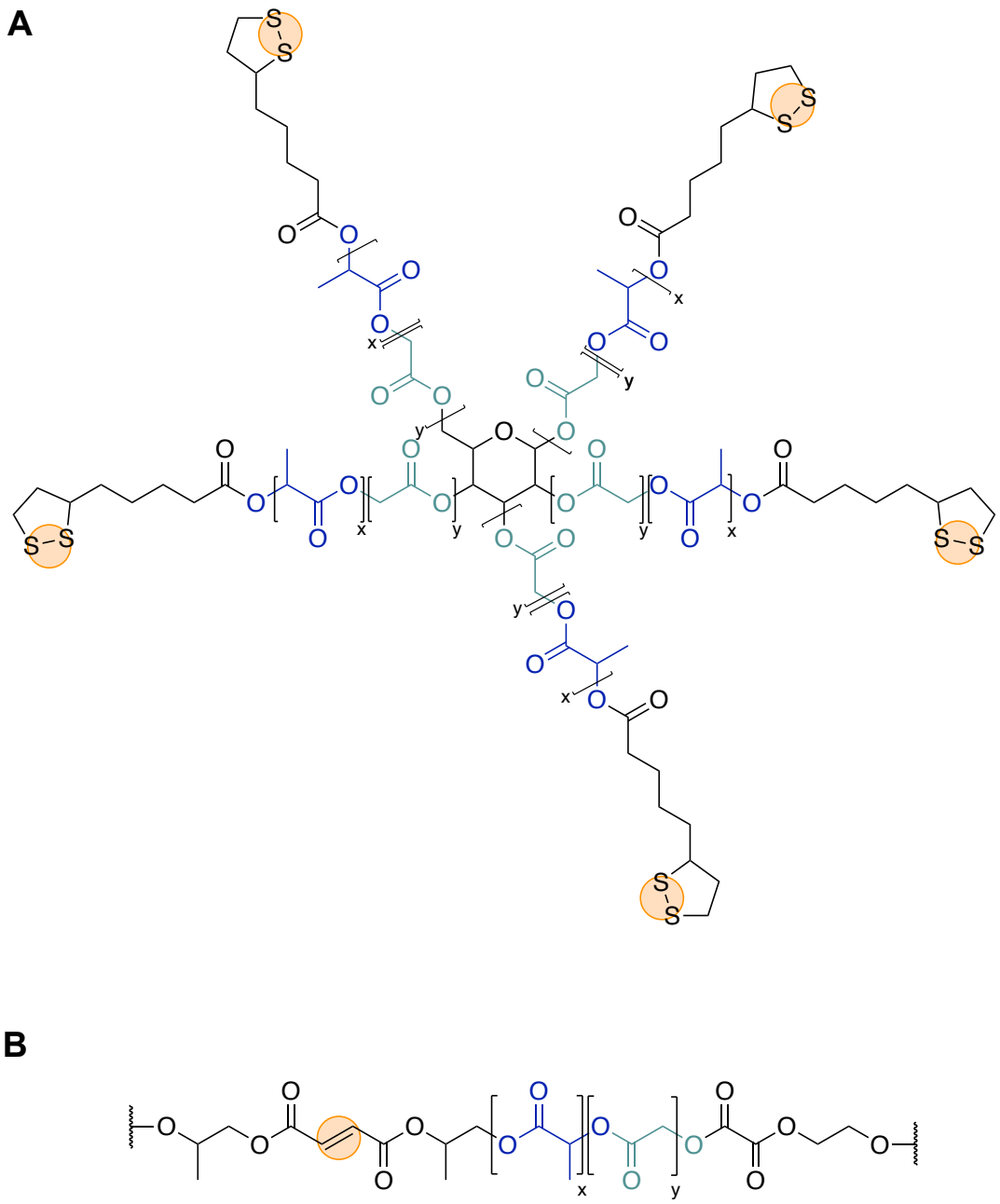
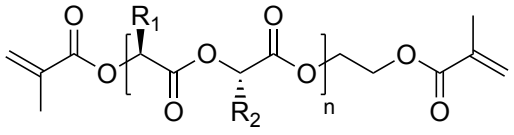


Figure 9. Examples of functionalised polymers containing the PLGA chemical motif that can yield PLGA-based crosslinked NPs via A) thiol-disulphide exchange involving disulphides highlighted in orange, and B) radical polymerisation of alkenes highlighted in orange.

On the other hand, the effect of the PLGA sequence on the *in vitro* properties related to degradation and payload release from PLGA has been demonstrated by the Meyer group. For instance, microparticles prepared from sequenced PLGA were shown to exhibit slower degradation rates, a more sustained release of the payload with a more gradual burst release, and lower amounts of percolating acids, compared to

microparticles prepared using random PLGA.[127,141] Moreover, the differences in the behaviour of sequenced and random PLGA were subsequently confirmed *in vivo*, with sequenced PLGA inducing a lower granulomatous foreign-body reaction than the random PLGA analogue.[127]

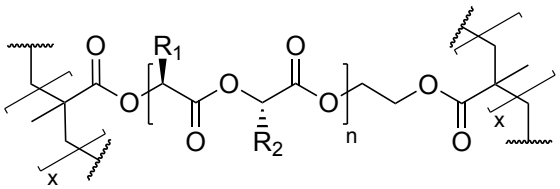
Building on the prior works presented above, a novel class of NPs designed around the concepts of sequenced PLGA chemistry and crosslinked polymers was targeted in this work. These NPs have been envisaged as synthetically accessible *via* the radical polymerisation of precisely sequenced, polymerisable oligoesters named oligolactoglycolic acid dimethacrylates (OLGADMAs) having the general chemical structure shown in Figure 10.



R_1, R_2 = H or CH_3 with $R_1 \neq R_2$
n = 2, 3 or 4

Figure 10. General chemical structure of oligolactoglycolic acid dimethacrylates (OLGADMAs).

It was envisaged that the structure of NPs resulting from the radical polymerisation of these OLGADMAs would comprise a polymethacrylate backbone and sequenced oligoesters, yielding what is *de facto* a sequenced poly(oligoester) NP having a highly crosslinked structure (Figure 11). Moreover, the presence of methacrylate moieties within the structure of OLGADMAs was envisaged as a means for the diversification of the composition of the resulting NPs achievable via the copolymerisation of OLGADMAs with additional polymerisable building blocks such as PEGylated or stimuli-responsive monomers.



R_1, R_2 = H or CH_3 with $R_1 \neq R_2$
n = 2, 3 or 4

Figure 11. Proposed structure of a section of crosslinked polymeric NPs resulting from the radical polymerisation of OLGADMAs.

2.2 Design of OLGADMAs and Naming Conventions

OLGADMAs with eight types of oligoester cores having lactate/glycolate ratios equal to 1 were synthesised in this work (Figure 12). These compounds were classified as tetramers (**4**), hexamers (**6**), and octamers (**8**) based on the number of lactate and glycolate units present within their structures. Additionally, the prepared OLGADMAs were further classified into alternating (**A**) or block (**B**) compounds based on the presence or absence of adjacent lactate or glycolate units. Given this, OLGADMAs prepared in this work will be abbreviated via a code consisting of the number of acid units, followed by the type of sequence present in the compound. Further suffixes **a** and **b** will be included for tetramer OLGADMAs, as these compounds have been prepared in both sequence directions relative to the asymmetrical end groups.

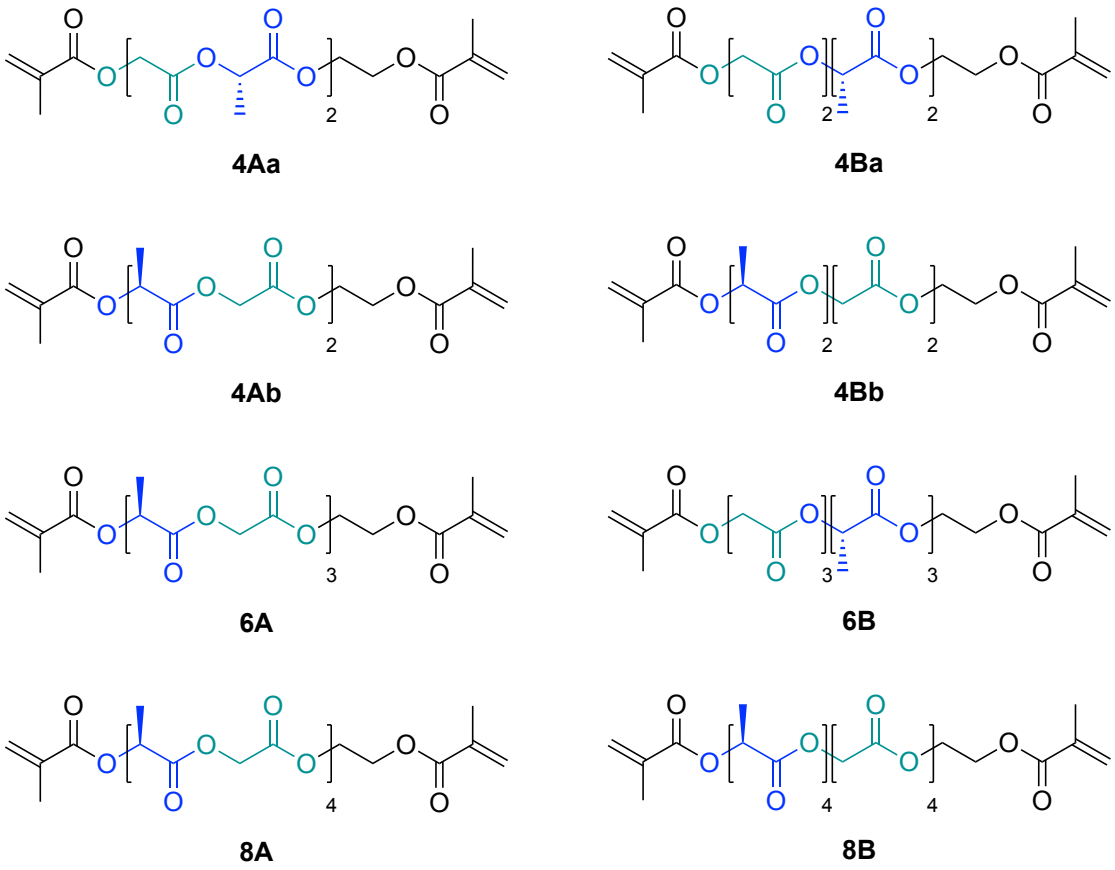


Figure 12. Chemical structures of OLGADMAs synthesised in this work alongside compound code.

2.3 Synthesis of OLGADMAs

OLGADMAs presented in this work were synthesised from protected monomers **1**-**4,** using lactic acid derivatives having the (*S*) absolute configuration (Figure 13). The non-methacrylate monomers were assembled into orthogonally protected oligoesters by means of ester formation reactions and selective deprotections via catalytic hydrogenation and silyl ether cleavage using procedures reported by Meyer *et al*. with some modifications.[326,327]

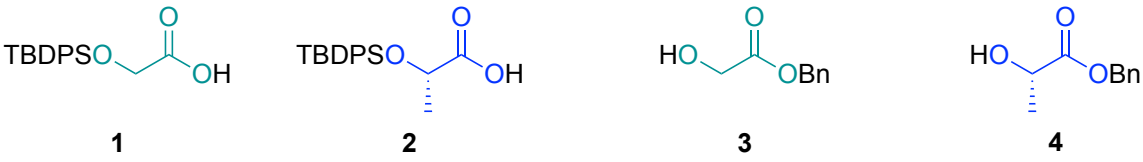
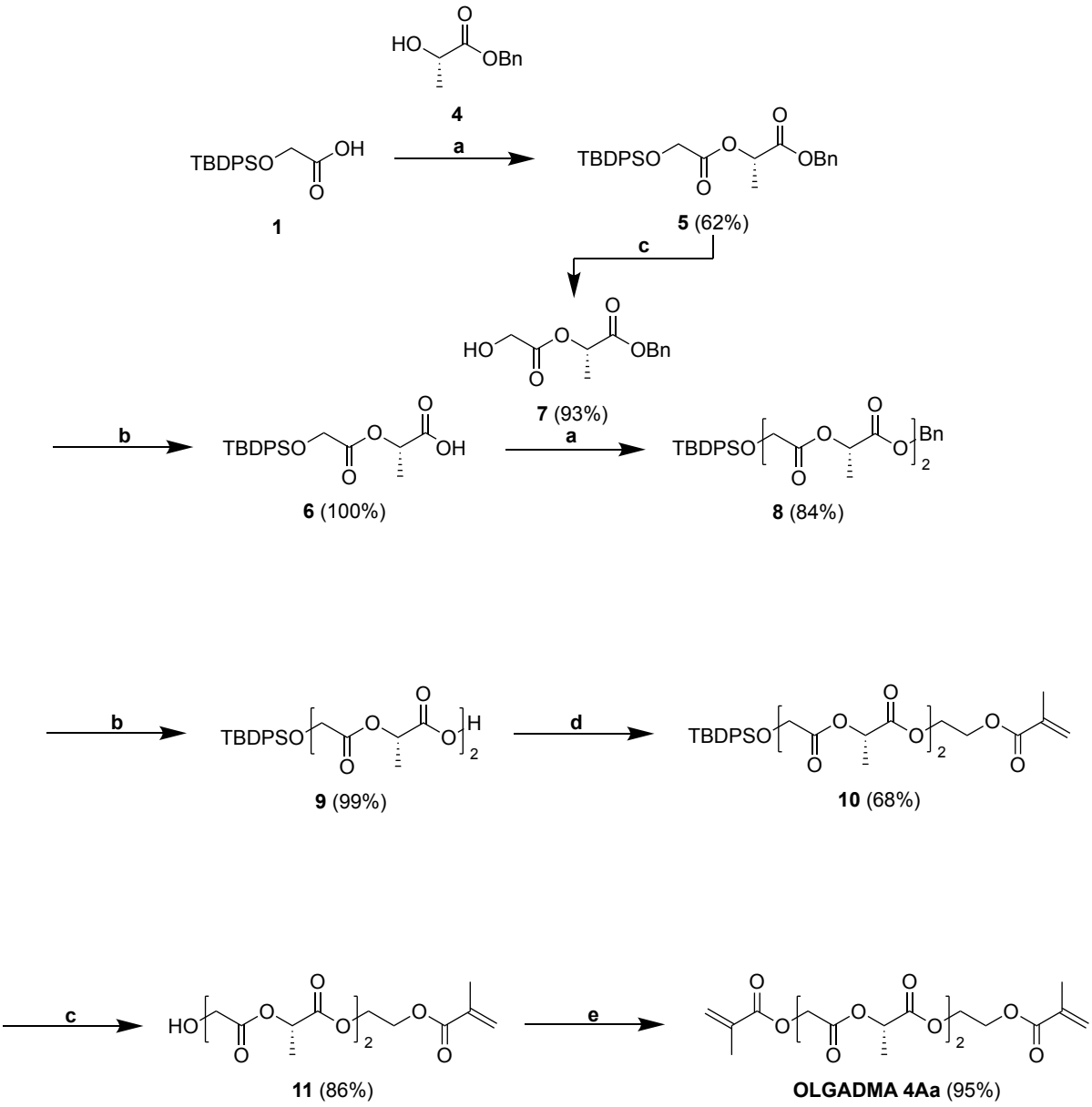


Figure 13. Protected monomers 1-4 as starting materials for the synthesis of OLGADMAs.

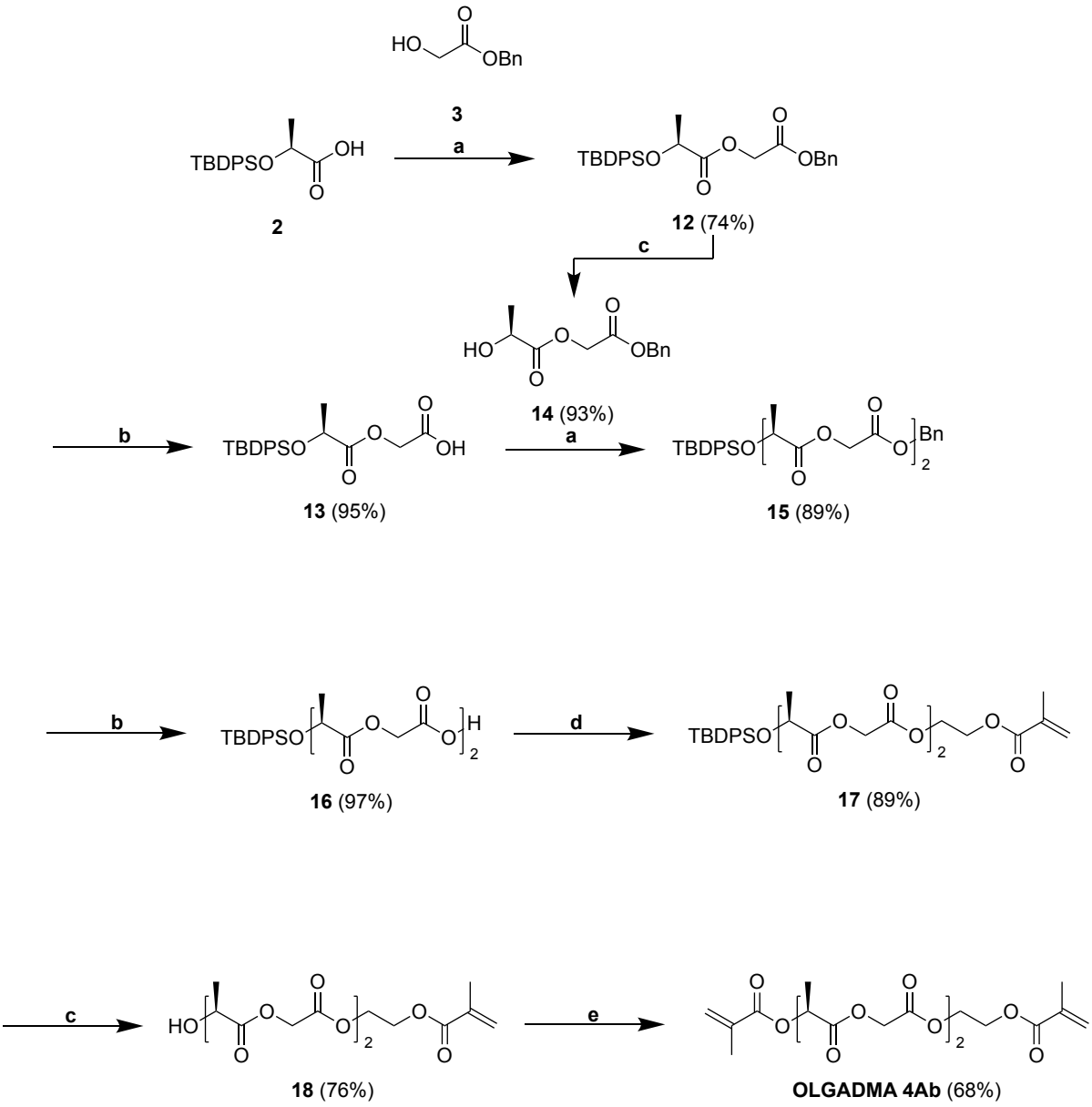
Once the desired orthogonally diprotected oligoesters were prepared, these were derivatised to dimethacrylates through a four-step procedure involving hydroxyethyl methacrylate (HEMA) and methacryloyl chloride as methacrylating agents.

Eight types of OLGADMAs were prepared according to Scheme 14-21. For example, **OLGADMA 4Aa** was prepared via the stepwise synthetic procedure presented in Scheme 14. The coupling of TBDPS-protected glycolic acid **1** and benzyl (*S*)-lactate **4** was carried out to afford diprotected dimer **5**. Dimer **5** was then subjected to debenzylation via catalytic hydrogenation with Pd/C under H_2 gas atmosphere to afford acid **6**, and silyl ether cleavage with buffered TBAF to afford alcohol **7**. The coupling of acid **6** and alcohol **7** yielded diprotected tetramer **8** which was then subjected to debenzylation to afford acid **9**. The derivatisation of acid **9** with HEMA afforded methacrylate **10** which was then subjected to silyl ether cleavage with TBAF to afford alcohol **11**. The treatment of alcohol **11** with methacryloyl chloride in the presence of a base allowed the isolation of the desired **OLGADMA 4Aa**.

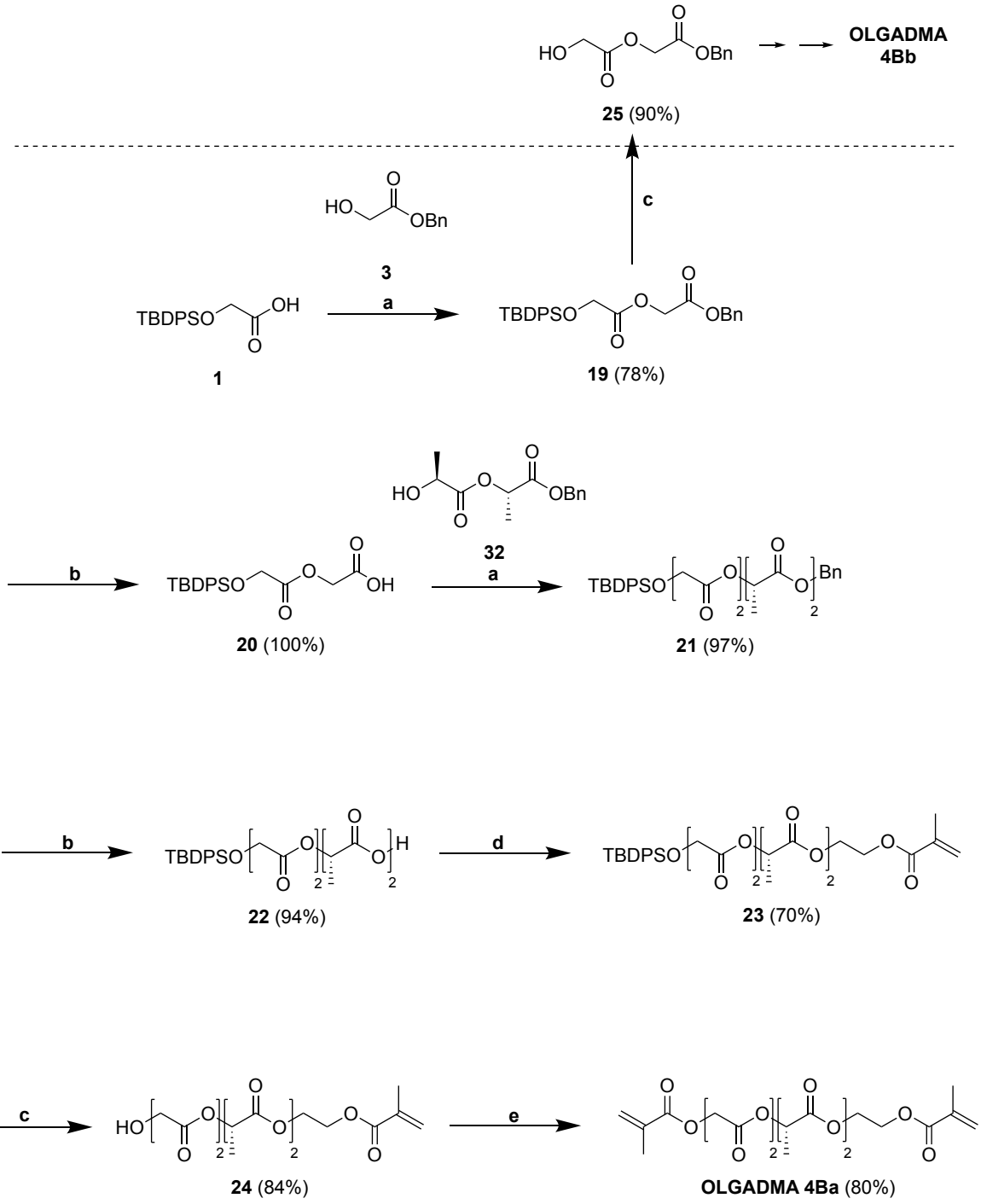
Generally, the formation of ester bonds using carbodiimide chemistry resulted in yields ranging from 20% to 97%, depending on the specific example. Debenzylation via catalytic hydrogenation led to the isolation of acids with yields ranging from 90% to 100%. Silyl ether cleavage was achieved with yields between 60% and 93%. Coupling reactions involving HEMA afforded the desired methacrylates with yields ranging from 58% to 89%. Methacrylations of alcohols with methacryloyl chloride proceeded with yields ranging from 30% to 95% to afford the desired **OLGADMA**s which were isolated as water-insoluble oils. The overall yields and the amounts of isolated OLGADMAs prepared in this work are presented in 7.2.1.



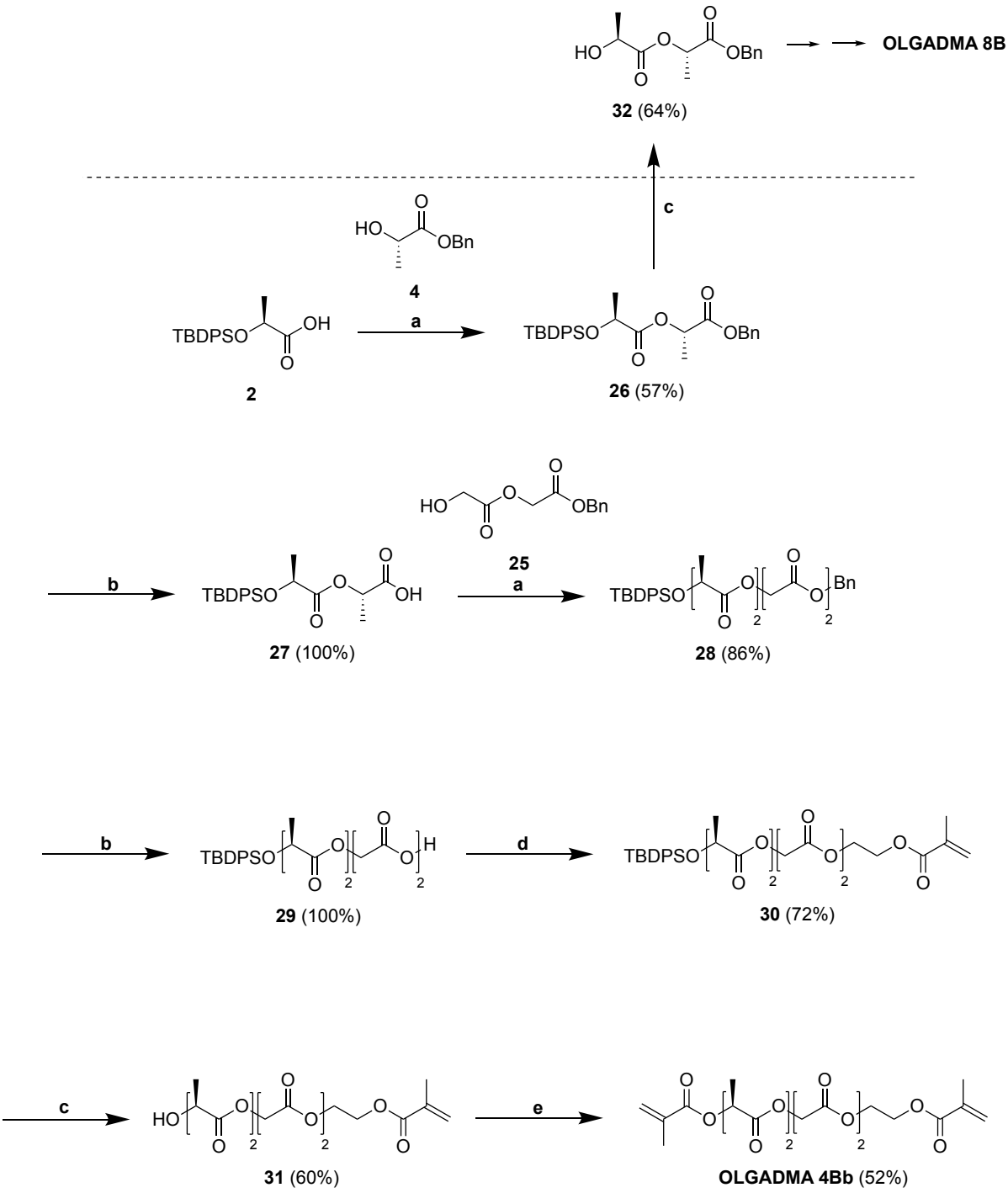
Scheme 14. Synthesis of **OLGADMA 4Aa**. a) alcohol (1.2 equiv), EDC HCl (1.3 equiv), DMAP (0.5 equiv), CH_2Cl_2, rt; b) H_2, Pd/C (5 wt.%), EtOAc, rt; c) TBAF (1.5 equiv), AcOH (3 equiv), THF, 0 °C to rt; d) HEMA (1.3 equiv), DMAP (0.5 equiv), CH_2Cl_2, rt; e) methacryloyl chloride (2 equiv), TEA (4 equiv), CH_2Cl_2, 0 °C to rt.



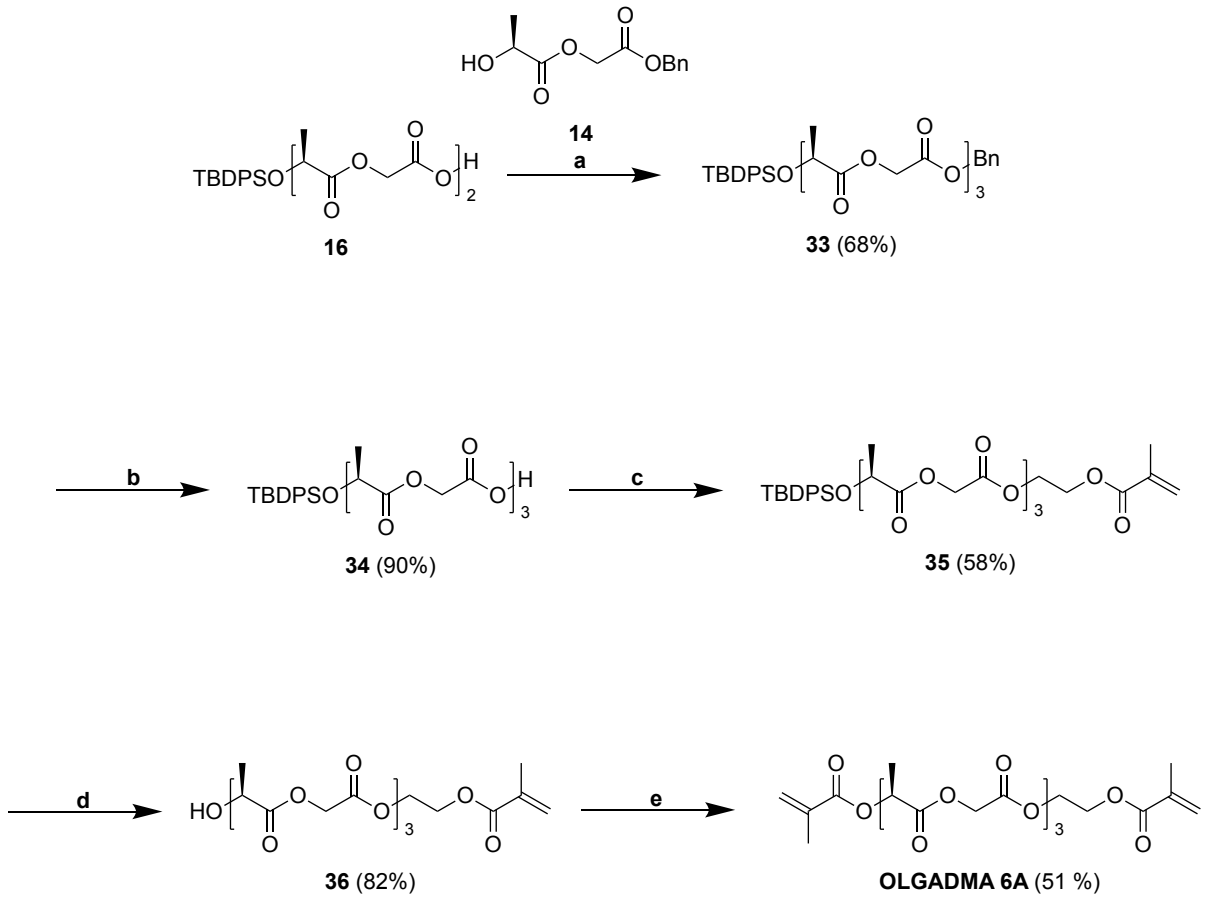
Scheme 15. Synthesis of **OLGADMA 4Ab**. a) alcohol (1.2 equiv), EDC HCl (1.3 equiv), DMAP (0.5 equiv), CH_2Cl_2, rt; b) H_2, Pd/C (5 wt.%), EtOAc, rt; c) TBAF (1.5 equiv), AcOH (3 equiv), THF, 0 °C to rt; d) HEMA (1.3 equiv), DMAP (0.5 equiv), CH_2Cl_2, rt; e) methacryloyl chloride (2 equiv), TEA (4 equiv), CH_2Cl_2, 0 °C to rt. *Yicheng Wang is acknowledged for her help with the scale-up of **OLGADMA 4Ab**.



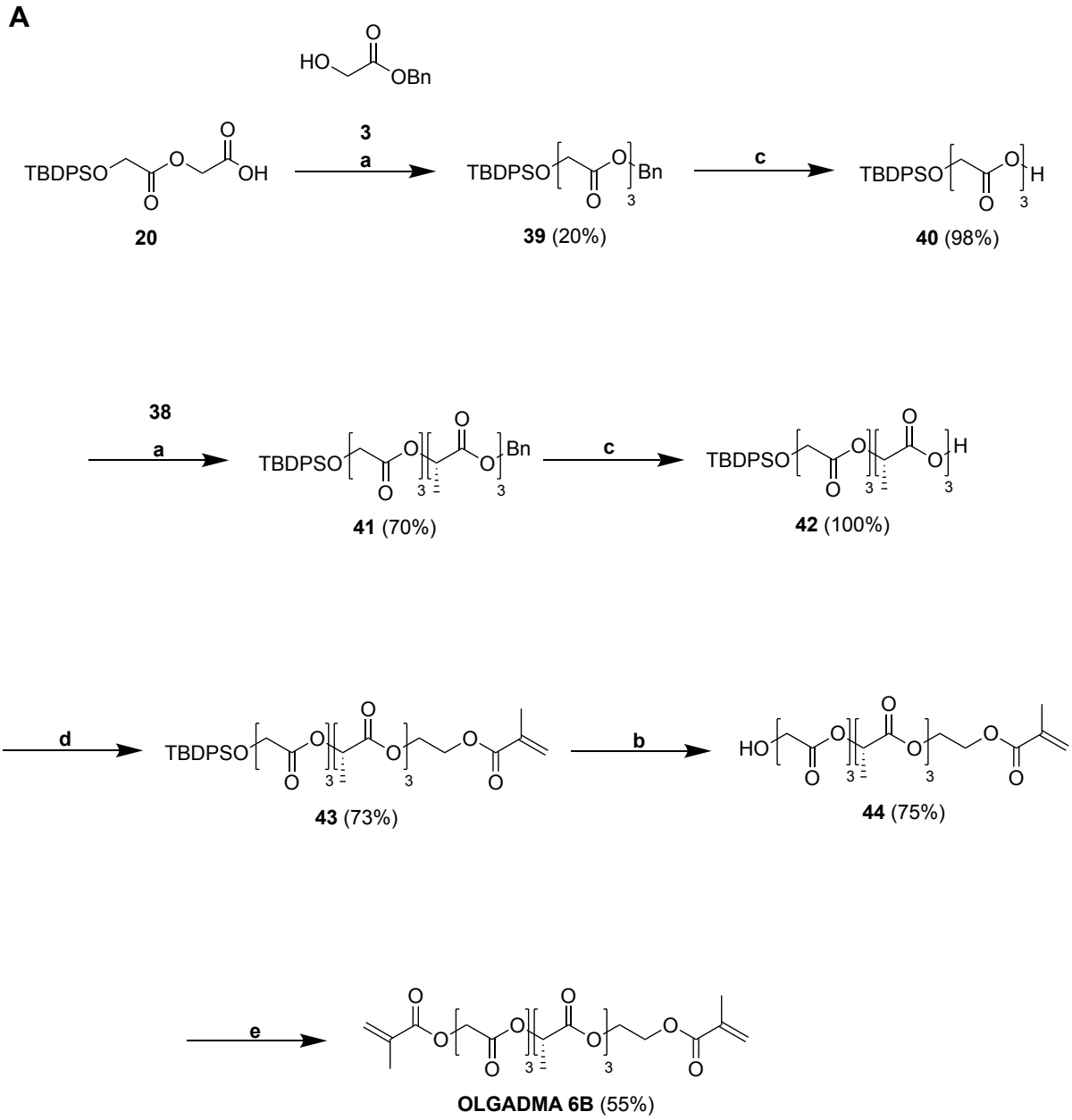
Scheme 16. Synthesis of **OLGADMA 4Ba**. a) alcohol (1.2 equiv), EDC HCl (1.3 equiv), DMAP (0.5 equiv), CH_2Cl_2, rt; b) H_2, Pd/C (5 wt.%), EtOAc, rt; c) TBAF (1.5 equiv), AcOH (3 equiv), THF, 0 °C to rt; d) HEMA (1.3 equiv), DMAP (0.5 equiv), CH_2Cl_2, rt; e) methacryloyl chloride (2 equiv), TEA (4 equiv), CH_2Cl_2, 0 °C to rt.



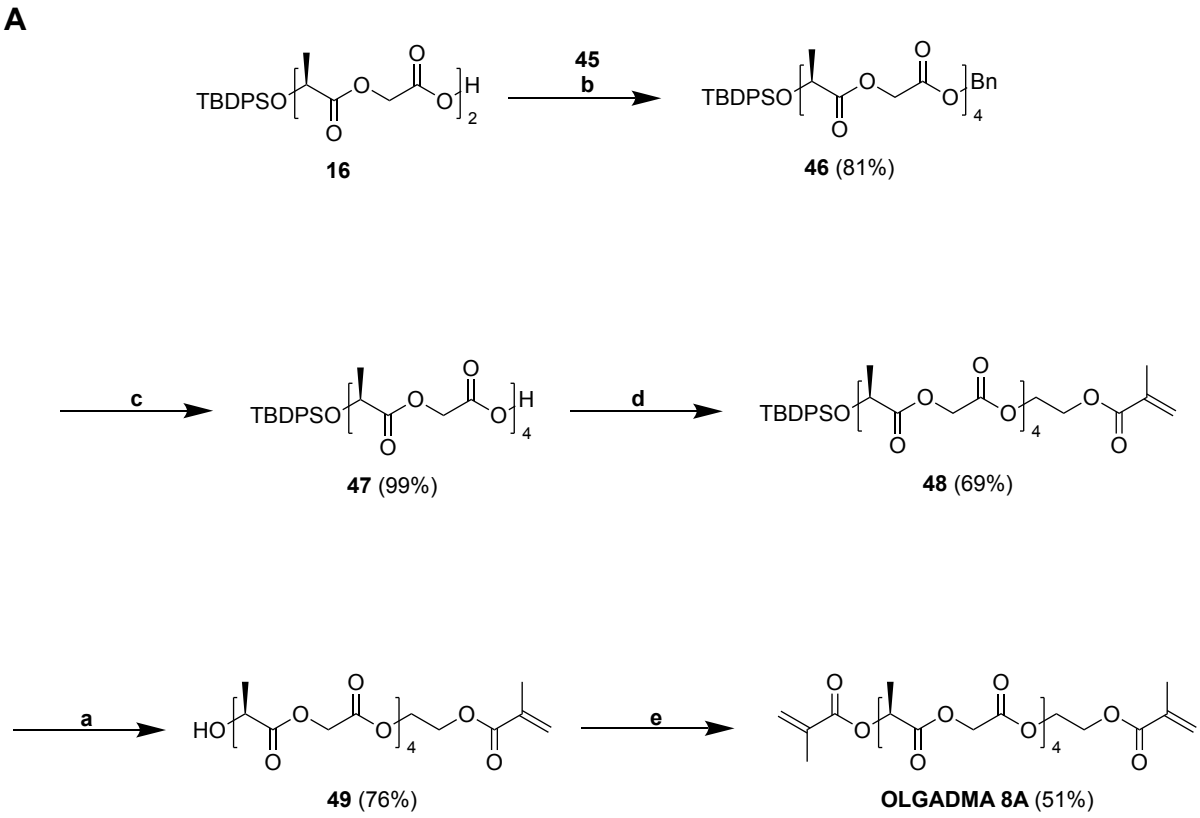
Scheme 17. Synthesis of **OLGADMA 4Bb**. a) alcohol (1.2 equiv), EDC HCl (1.3 equiv), DMAP (0.5 equiv), CH_2Cl_2, rt; b) H_2, Pd/C (5 wt%), EtOAc, rt; c) TBAF (1.5 equiv), AcOH (3 equiv), THF, 0 °C to rt; d) HEMA (1.3 equiv), DMAP (0.5 equiv), CH_2Cl_2, rt; e) methacryloyl chloride (2 equiv), TEA (4 equiv), CH_2Cl_2, 0 °C to rt.



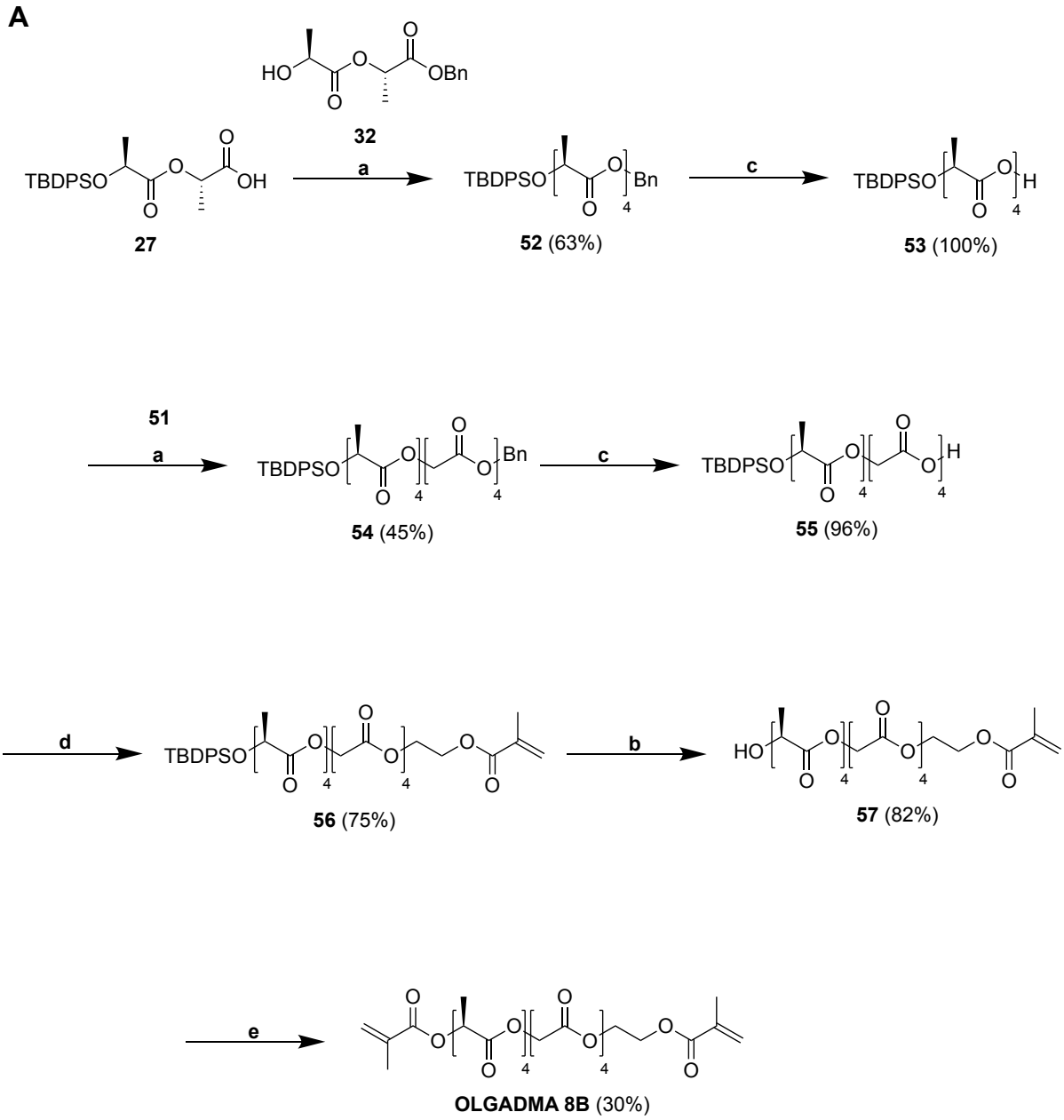
Scheme 18. Synthesis of **OLGADMA 6A**. a) alcohol (1.2 equiv), EDC HCl (1.3 equiv), DMAP (0.5 equiv), CH_2Cl_2, rt; b) H_2, Pd/C (5 wt.%), EtOAc, rt; c) HEMA (1.3 equiv), DMAP (0.5 equiv), CH_2Cl_2, rt; d) TBAF (1.5 equiv), AcOH (3 equiv), THF, 0 °C to rt; e) methacryloyl chloride (2 equiv), TEA (4 equiv), CH_2Cl_2, 0 °C to rt.



Scheme 19. Synthesis of A) **OLGADMA 6B**, and B) **38**. a) alcohol (1.2 equiv), EDC HCl (1.3 equiv), DMAP (0.5 equiv), CH_2Cl_2, rt; b) TBAF (1.5 equiv), AcOH (3 equiv), THF, 0 °C to rt; c) H_2, Pd/C (5 wt.%), EtOAc, rt; d) HEMA (1.3 equiv), DMAP (0.5 equiv), CH_2Cl_2, rt; e) methacryloyl chloride (2 equiv), TEA (4 equiv), CH_2Cl_2, 0 °C to rt.



Scheme 20. Synthesis of A) **OLGADMA 8A**, and B) **45**. a) TBAF (1.5 equiv), AcOH (3 equiv), THF, 0 °C to rt; b) alcohol (1.2 equiv), EDC HCl (1.3 equiv), DMAP (0.5 equiv), CH_2Cl_2, rt; c) H_2, Pd/C (5 wt.%), EtOAc, rt; d) HEMA (1.3 equiv), DMAP (0.5 equiv), CH_2Cl_2, rt; e) methacryloyl chloride (2 equiv), TEA (4 equiv), CH_2Cl_2, 0 °C to rt.



Scheme 21. Synthesis of A) **OLGADMA 8B**, and B) **51**. a) alcohol (1.2 equiv), EDC HCl (1.3 equiv), DMAP (0.5 equiv), CH_2Cl_2, rt; b) TBAF (1.5 equiv), AcOH (3 equiv), THF, 0 °C to rt; c) H_2, Pd/C (5 wt.%), EtOAc, rt; d) HEMA (1.3 equiv), DMAP (0.5 equiv), CH_2Cl_2, rt; e) methacryloyl chloride (2 equiv), TEA (4 equiv), CH_2Cl_2, 0 °C to rt.

2.4 General Considerations Concerning OLGA-based Nanoparticles

Given the structure and composition of OLGADMAs as fundamental building blocks used in this work, it was postulated that the NPs resulting from their polymerisation (OLGA-based NPs) would exhibit:

(i) elevated physical and chemical stability due to covalent crosslinking and ester sequencing,

(ii) potential for drug encapsulation and drug release tunability due to the design flexibility related to oligoester sequence and length, and the intrinsic synthetic flexibility of the radical polymerisation platform which may enable the diversification of the NP composition via copolymerisation with additional monomers in a single synthetic step,

(iii) improved synthetic and functional reproducibility due to the discreet structural nature of OLGADMAs as well-defined molecules in contrast to starting materials with intrinsically variable MW and sequence such as random PLGA polymers,

(iv) degradability *in vivo* due to the high ester content, yielding shorter water-soluble fragments upon hydrolytic degradation.

2.5 Chapter Summary

A novel class of divinyl compounds named oligolactoglycolic acid dimethacrylates (OLGADMAs) was designed around the concepts of sequenced PLGA and polymerisable monomers. A library of eight OLGADMAs was successfully prepared from orthogonally diprotected precursor molecules via stepwise synthesis. The methodology allowed to access OLGADMAs comprising precise alternating and block sequences, having chain lengths of four, six, and eight lactic and glycolic units, incorporated within the structure in a 1:1 ratio. The compounds were isolated as water-insoluble oils and were envisaged as potentially valuable building blocks for the synthesis of crosslinked polymeric NPs via radical polymerisation reactions.

The following chapter details the development of a synthetic methodology for the polymerisation of OLGADMAs, the synthesis of oligolactoglycolic acid-based NPs, and the analysis of the NPs in terms of stability in water at a physiological temperature, the effect on cell viability *in vitro*, and the evaluation of the cellular uptake.

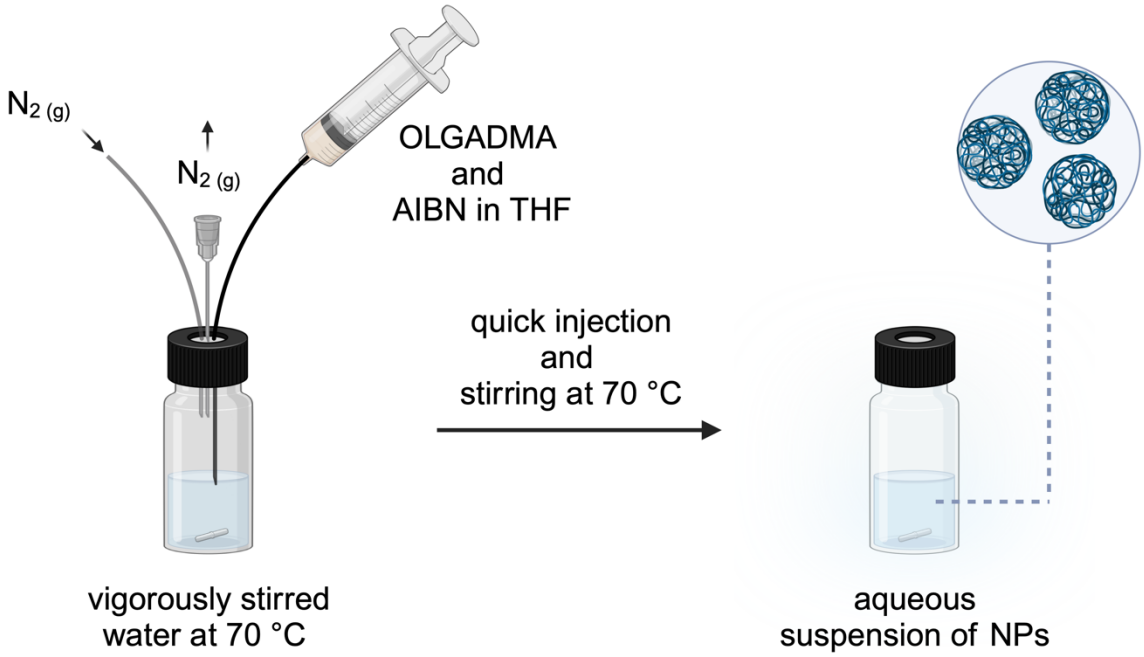
Chapter 3: Synthesis and Analysis of OLGA-based Nanoparticles

3.1 Introduction

Having successfully synthesised a library of OLGADMAs, attempts to polymerise these compounds to afford crosslinked polymeric NPs were undertaken via solution polymerisations in the presence of the radical initiator AIBN. In this context, experiments involving **OLGADMA 4Aa** performed in acetonitrile, *N*,*N*-dimethylformamide, and dimethylsulfoxide were found unable to provide the desired NPs, suggesting the necessity for a synthetic methodology which is able to grant a certain level of templating conditions, such as those achieved with emulsion-based polymerisations, to achieve the formation of NPs.

Given the poor aqueous solubility of OLGADMAs, it was hypothesised that these compounds could be successfully dispersed in water via a procedure analogous to the nanoprecipitation methodology. The resulting dispersion of oil droplets in water could then undergo radical polymerisation in the presence of a radical initiator, affording an aqueous suspension of polymeric NPs.

In this context, a procedure was sought that could enable the activation of the radical initiator and removal of the water-miscible organic solvent from the reaction system. Ultimately, the rapid injection of a THF solution of OLGADMAs, or their mixtures with PEGylated monomers, and AIBN into vigorously stirred water at 70 °C and under an inert atmosphere proved successful in providing polymeric NPs (Scheme 22). The novel polymerisation methodology was termed nanoprecipitation polymerisation.



Scheme 22. General procedure for the nanoprecipitation polymerisation of OLGADMAs. To achieve drug encapsulation, the THF solution containing OLGADMA and AIBN can be used to solubilise the drug.

General considerations regarding the nanoprecipitation polymerisation methodology are presented below:

(i) Polymeric NPs were prepared from OLGAMDAs and mixtures of OLGADMAs and several PEG-containing monomers in a 1:1 ratio by weight.

(ii) The reaction duration at 70 °C was kept at 30 min in the initial stages of the study, whilst being subsequently limited to 15 min after optimal reaction conditions had been identified.

(iii) THF was chosen as the water-miscible organic solvent as it can solubilise the reaction components and has a boiling point of 66 °C which was thought to lead to a rapid evaporation of the organic solvent upon contact with water at 70 °C.

(iv) AIBN was chosen as an oil-soluble initiator with its concentration fixed at 20 wt% of the total reactants. Furthermore, the effect of alternative AIBN concentrations is discussed in section 3.2.4, and the use of the water-soluble initiator V-50 is discussed in section 3.9.

(v) The reactions were conducted under a N_2 gas atmosphere and were quenched by cooling the reaction mixture in an ice bath and exposure to air.

(vi) Repetitive centrifugal filtration, achieved within centrifugal filter units (30 kDa MWCO or 100kDa MWCO) was chosen as the optimal NP purification method as it allowed for the separation of water-soluble impurities by filtration, and the removal of water-insoluble impurities by sedimentation on the bottom of the filter.

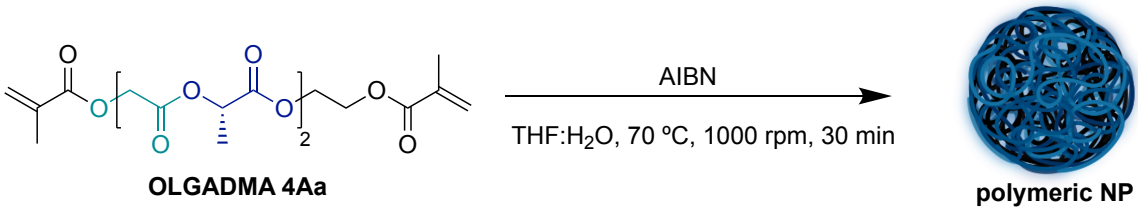
The main advantages of this technique are reflected in its ability to yield sub-micron polymeric particles rapidly (e.g. within 15 minutes), without sonication requirements, and in the absence of stabilisers such as surfactants. The configuration of the method enables processes such as monomer polymerisation, drug encapsulation, and NP functionalisation (e.g. PEGylation) to occur simultaneously, in one pot. Furthermore, due to its simplicity, a facile translation of the nanoprecipitation polymerisation technique towards automated methods for the preparation of polymeric NPs in a flexible and modular fashion can be envisaged.

The following section outlines key experiments performed to establish and analyse the nanoprecipitation polymerisation methodology and the resulting NPs.

3.2 Initial Work Towards OLGA-based NPs

3.2.1 Nanoprecipitation Polymerisation of **OLGADMA 4Aa**

Initial studies aimed to confirm the polymerisation reaction of OLGADMAs under nanoprecipitation polymerisation conditions. For this purpose, the analysis of an aqueous suspension of particles obtained by subjecting **OLGADMA 4Aa** to 30 min of reaction conditions was performed (Scheme 23). The key findings are exemplified via comparison against a control experiment performed in the absence of AIBN.



OLGADMA 4Aa **polymeric NP**

Scheme 23. Nanoprecipitation polymerisation of **OLGADMA 4Aa**. **OLGADMA 4Aa** (80 wt%), AIBN (20 wt%), THF:H_2O (1:3).

Firstly, given the absence of a surfactant in the mixture, it was postulated that large droplets of **OLGADMA 4Aa** would form by coalescence over the course of the experiment if the formation of colloidally stable NPs did not occur. Indeed, the DLS (dynamic light scattering) analysis of the crude mixture confirmed the presence of sub-micron particles in the reaction mixture, and drastically larger particles (>1 μm) in the control sample (Figure 14).

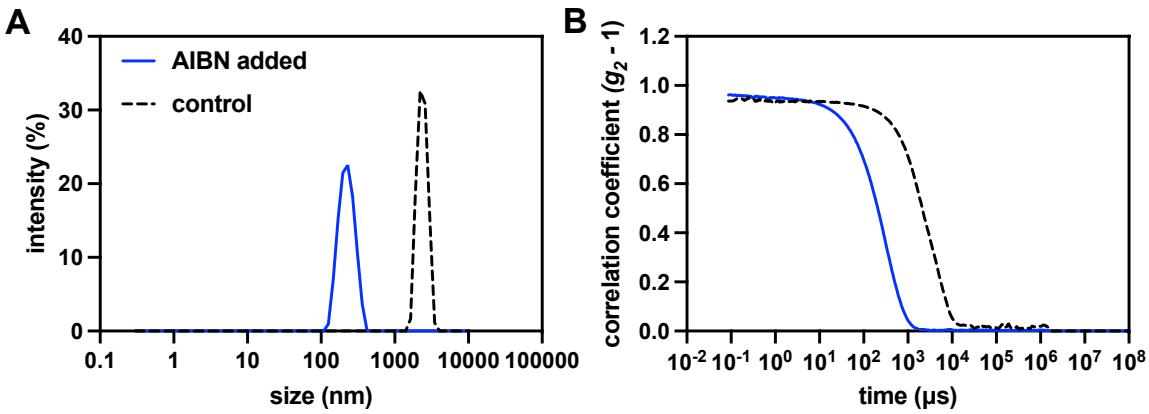


Figure 14. DLS analysis of the crude reaction mixture resulting from the nanoprecipitation polymerisation reaction of **OLGADMA 4Aa**, and the control experiment (with no AIBN added) as measured by DLS. A) Intensity-weighted size distributions, and B) correlogram.

The lyophilisation of the reaction mixture yielded a white powder, whilst the control sample afforded an oil. At this point, ^{1}H NMR spectroscopic analysis was attempted to characterise the samples. The control sample dissolved readily in deuterated DMSO, whilst the AIBN-treated sample was insoluble and formed a cloudy suspension. As expected, the ^{1}H NMR analysis of these materials revealed the presence of **OLGADMA 4Aa** in the control sample. Conversely, **OLGADMA 4Aa** could not be detected in the sample obtained from the reaction mixture involving AIBN, suggesting that polymeric NPs were obtained.

At this point, the reaction sample in powder form was analysed via FTIR spectroscopy which revealed differences with the spectrum of the starting material **OLGADMA 4Aa**. In this context, the vibrational bands in the carbonyl stretch region were identified as particularly diagnostic (Figure 15). Specifically, the two distinct vibrational bands at 1751 cm^{-1} and 1722 cm^{-1}, attributed to α,β-saturated (lactate/glycolate) and α,β-unsaturated carbonyls (methacrylates) visible in the spectrum of **OLGADMA 4Aa** coalesced into a broad vibrational band at 1744 cm^{-1} in the spectrum of the reaction sample. This observation was considered consistent with the successful polymerisation of the methacrylate moieties, and the formation of a polymethacrylate backbone.

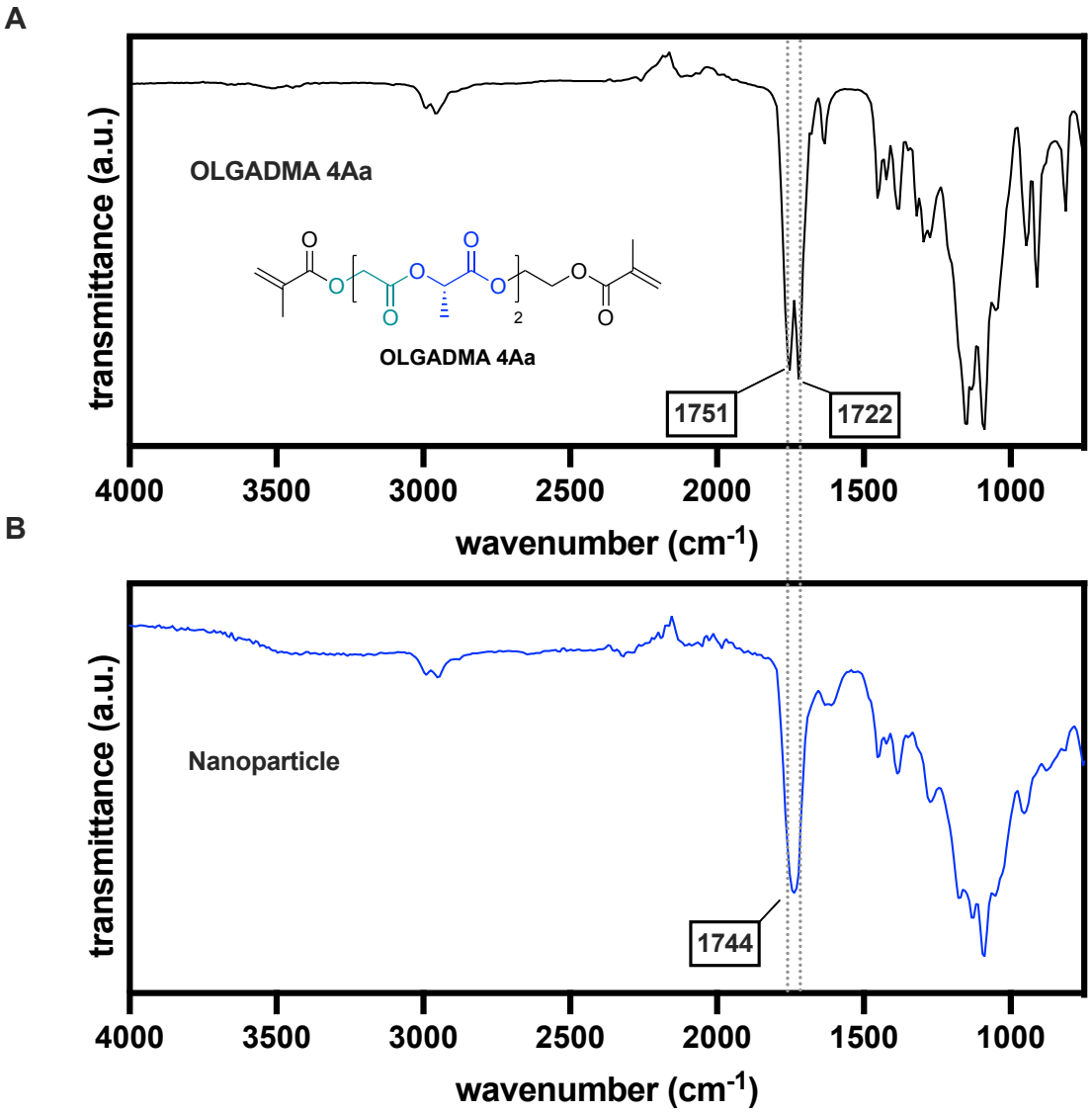


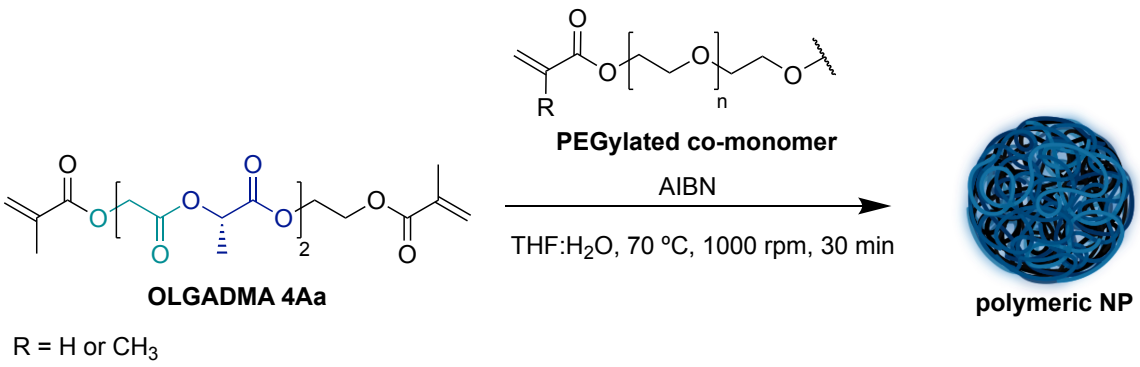
Figure 15. ATR FTIR spectra of A) **OLGADMA 4Aa**, and B) sample obtained from the nanoprecipitation polymerisation reaction of **OLGADMA 4Aa**.

Taken altogether, the analysis detailed above allowed us to confirm the conversion of **OLGADMA 4Aa** during the nanoprecipitation polymerisation reaction, and the formation of NPs, whilst establishing FTIR spectroscopy as a useful technique for the direct characterisation of the resulting NPs. Moreover, the prepared NPs were found to be insoluble in deuterium oxide, deuterated DMSO, and $CDCl_3$. Therefore, it was hypothesised that polymerised **OLGADMA 4Aa** was highly crosslinked and could thus exhibit limited solvation and mobility in the tested solvents, making the direct observation of the NPs by solution NMR spectroscopy unsuitable at practical concentrations.

The following section discusses the nanoprecipitation polymerisation reaction of **OLGADMA 4Aa** conducted in the presence of PEGylated monomers.

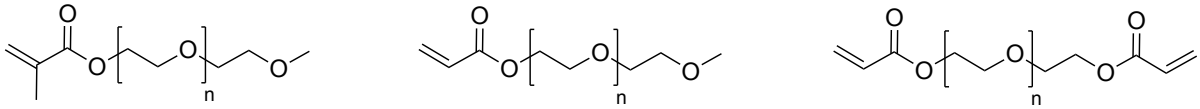
3.2.2 Nanoprecipitation Polymerisation of **OLGADMA 4Aa** in the Presence of PEGylated Monomers

Since NP PEGylation is known to improve the colloidal stability of NPs and increase NP hydrophilicity, it was deemed of interest to ascertain whether it was possible to introduce the biocompatible PEG chemical motif into the structure of polymeric NPs prepared from OLGADMAs. For this purpose, the nanoprecipitation polymerisation of mixtures of **OLGADMA 4Aa** and PEG-containing acrylates and methacrylates was attempted according to Scheme 24.



Scheme 24. Nanoprecipitation polymerisation of **OLGADMA 4Aa** in the presence of a generic PEGylated monomer. **OLGADMA 4Aa** (40 wt%), PEGylated monomer (40 wt%), AIBN (20 wt%), THF: H_2O (1:3).

A screening of monomer combinations allowed for the preparation of three types of PEG-containing NPs via the nanoprecipitation polymerisation of **OLGADMA 4Aa** conducted in the presence of poly(ethylene glycol) methyl ether methacrylate M_n 500 (mPEGMA500), poly(ethylene glycol) methyl ether acrylate M_n 1000 (mPEGA1000), and poly(ethylene glycol) diacrylate M_n 700 (PEGDA700) as PEGylated monomers (Figure 16).



mPEGMA500 **mPEGA1000** **PEGDA700**

Figure 16. Chemical structure of PEGylated monomers mPEGMA500, mPEGA1000, and PEGDA700.

The resulting suspensions were extensively purified via centrifugal filtration (100 kDa MWCO) to ensure the complete removal of the unreacted PEGylated monomer eventually present. The purified samples prepared using mPEGMA500 and mPEGA1000 contained large particles (> 1μm) detected by DLS analysis and were subjected to a further purification step using syringe filtration (5.0 μm). Conversely, the sample obtained from the reaction of **OLGADMA 4Aa** and PEGDA700 yielded a suspension in which large particles were undetectable, as confirmed by visual inspection and DLS analysis.

The purified suspensions were analysed by DLS, and ELS, and subsequently lyophilised to determine the yield of the reactions. A list of the measured parameters, compared to those of NPs prepared from **OLGADMA 4Aa** in the absence of PEGylated monomers, is presented in Table 8.

PEGylated monomer	z-average (nm ± SD)	PI ± SD	ζ-potential (mV ± SD)	Estimated NP Yield* (%)
-	217.7 ± 3.3	0.02 ± 0.02	-20.0 ± 0.7	21
mPEGMA500	400.3 ± 8.1	0.18 ± 0.01	-51.68 ± 0.82	10
mPEGA1000	199.7 ± 1.1	0.08 ± 0.02	-45.99 ± 1.05	3
PEGDA700	190.3 ± 0.2	0.09 ± 0.01	-40.87 ± 0.15	31

Table 8. DLS and ELS analysis of NPs prepared from the nanoprecipitation polymerisation of **OLGADMA 4Aa**, and its mixtures with PEGylated monomers: mPEGMA500, mPEGA1000, and PEGDA700 (1:1 by weight). *Calculated as the ratio of the mass of powders obtained by the lyophilisation of NP suspensions and the mass of the total monomer feed, expressed as a percentage.

The NPs prepared in the presence of mPEGA1000 and PEGDA700 presented sizes comparable to non-PEGylated NPs, and a relatively low PI (polydispersity index) (≤ 0.1). In comparison, the size distribution of particles prepared in the presence of mPEGMA500 was broader, with inseparable particles larger than 1 μm detected by DLS (Figure 17).

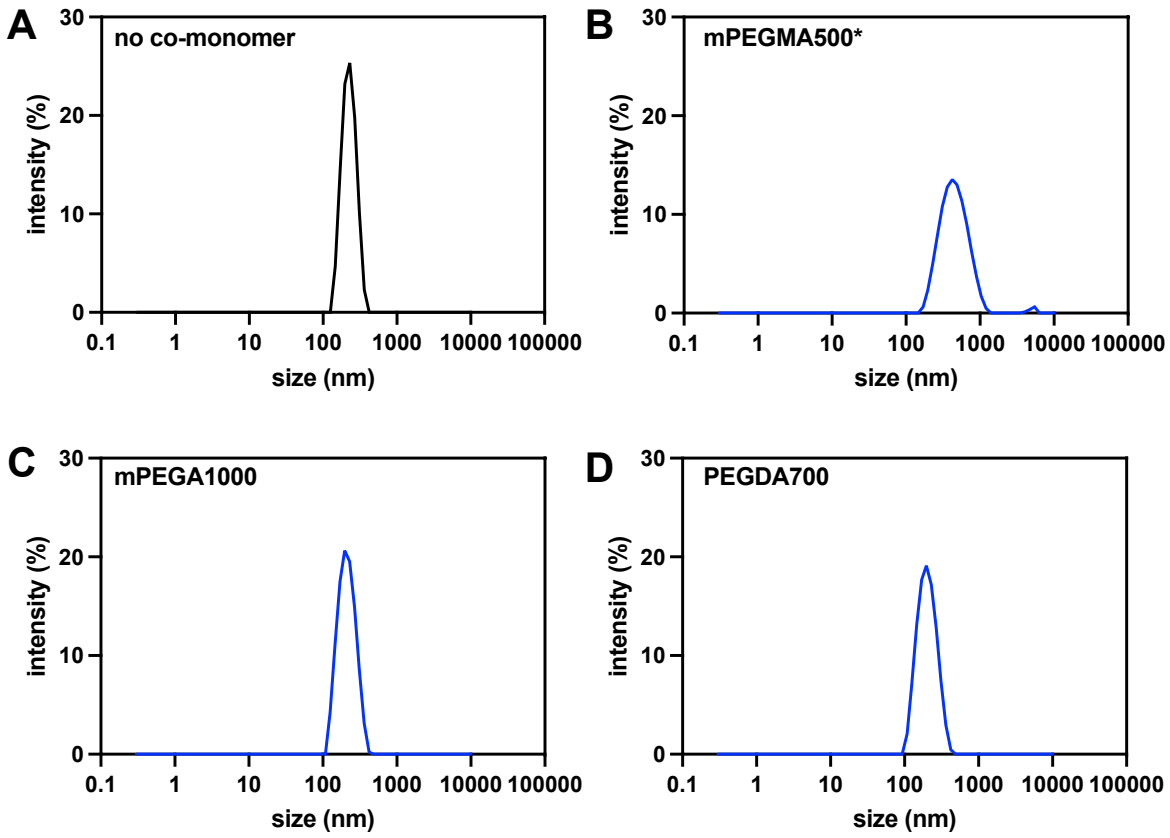


Figure 17. Intensity-weighted size distribution of NPs prepared from A) **OLGADMA 4Aa**, and B-D) mixtures of **OLGADMA 4Aa** and PEGylated monomers (1:1 by weight). *Particles larger than 1 μm detected by DLS.

The ζ-potential of PEG-containing NPs measured by ELS (electrophoretic light scattering) was substantially more negative than that of NPs prepared in the absence of PEGylated monomers. Given the absence of ionisable groups in the starting materials, a certain degree of hydrolysis of one or more types of ester bonds occurring during the reaction and exposing carboxylic acids has been invoked to rationalise this observation.

The estimation of the NP yields revealed substantial differences among the three examples listed in Table 8, with the reaction involving PEGDA700 yielding the highest quantity of solids upon lyophilisation. Conversely, the reaction involving mPEGA1000 was the lowest-yielding reaction, followed by the reaction involving mPEGMA500.

The lyophilisation of the NP suspensions afforded white powders which were subjected to spectroscopic analysis. Comparatively to observations presented in the previous section, the NPs prepared in the presence of PEGylated monomers formed a slightly cloudy suspension in deuterated DMSO. The analysis of the ^{1}H NMR spectra revealed the absence of resonances belonging to **OLGADMA 4Aa**. However, unlike the NPs prepared from **OLGADMA 4Aa** alone**,** the ^{1}H NMR spectra of NPs prepared in the presence of PEGylated monomers presented a broad signal of low intensity around δ 3.50 ppm which was attributed to methylene protons of the PEG units (Figure 18). The observation of these resonances could be explained by the existence of mobile and well-solvated PEG-containing segments, possibly residing on the surface of the NPs, such as those observed in the ^{1}H NMR spectra of PLGA-PEG NPs measured in deuterium oxide.[328]

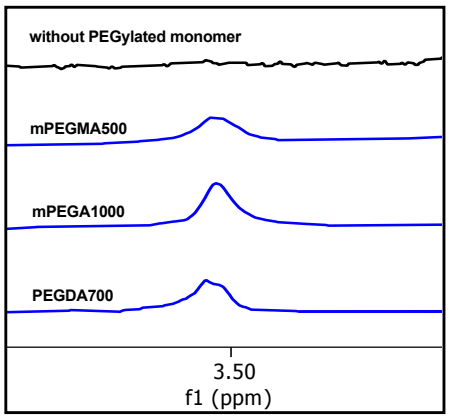


Figure 18. Stacked sections of ^{1}H NMR (400 MHz, $(CD_3)_2SO$) spectra of the powders obtained from purified NPs prepared via nanoprecipitation polymerisation of **OLGADMA 4Aa** (without PEGylated monomer), and mixtures of **OLGADMA 4Aa** and mPEGMA500, mPEGA1000, and mPEGMA500, mPEGA1000, and PEGDA700 (1:1 ratio by weight).

The FTIR spectroscopy analysis of the NPs in powder form was performed to confirm whether the polymerisation reaction took place. As exemplified by the spectrum of NPs

prepared in the presence of PEGDA700, a single vibrational band was observed at 1744 cm^{-1} (Figure 19), whilst **OLGADMA 4Aa** and a physical mixture of **OLGADMA 4Aa** and **PEGDA700** show two distinct vibrational bands in the carbonyl stretch region of the spectra. Given this, the successful polymerisation of the vinyl moieties of the starting materials was confirmed. The identical conclusion was inferred upon examination of the FTIR spectra of the NPs prepared in the presence of mPEGMA500, and mPEGA1000.

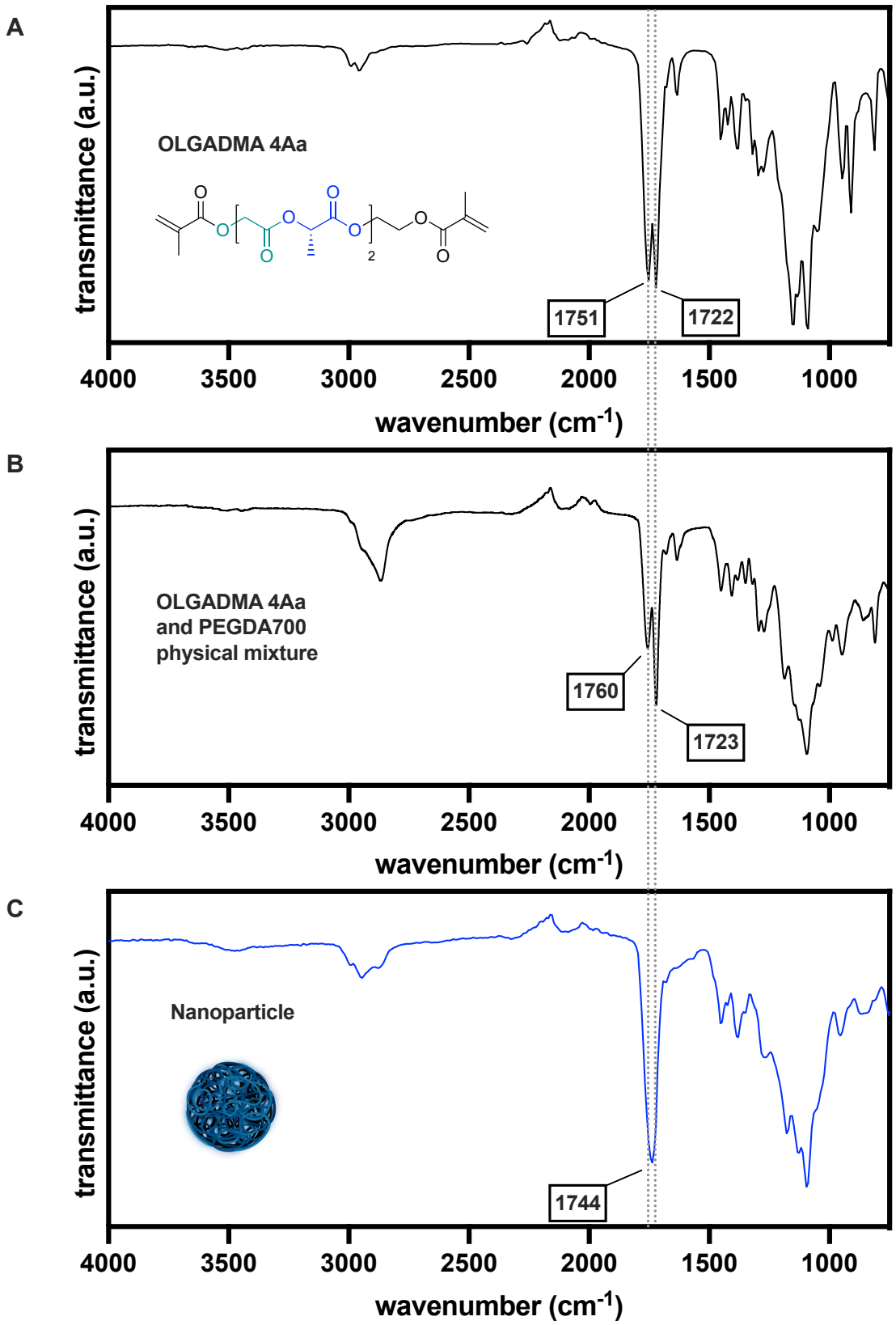


Figure 19. ATR FTIR spectra of A) **OLGADMA 4Aa**, B) a physical mixture of **OLGADMA 4Aa** and PEGDA700 (1:1 w/w mixture), and C) NPs prepared using **OLGADMA 4Aa** and PEGDA700 (1:1 ratio by weight). Vibrational bands related to carbonyl stretching are labelled.

Furthermore, the comparison of the FTIR spectra of NPs prepared in the absence and in the presence of PEGylated monomers revealed differences in the C-H stretching region as shown in Figure 20. Particularly, an overlap of three major vibrational bands could be observed for NPs prepared in the presence of PEGylated monomers, whilst two major vibrational bands were visible in the C-H stretching regions of the NPs prepared in the absence of PEGylated monomers.

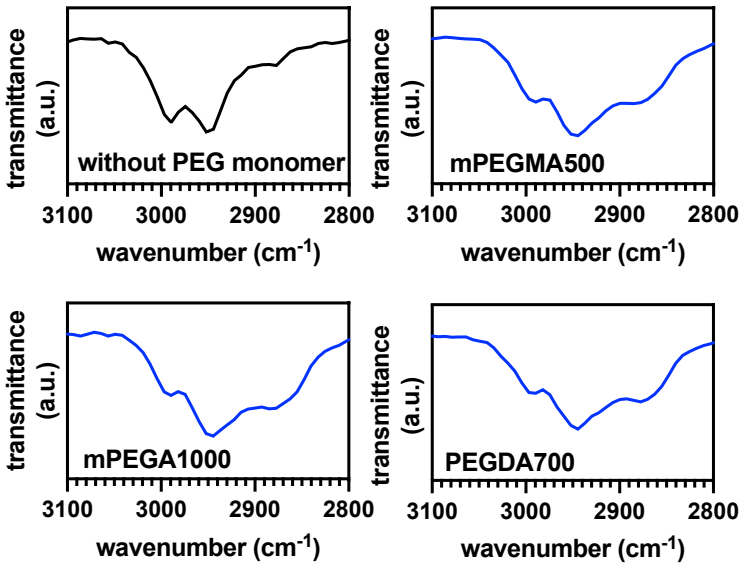


Figure 20. C-H stretching region of ATR-FTIR spectra of NPs prepared via the nanoprecipitation polymerisation of **OLGADMA 4Aa** (without PEGylated monomer) and mixtures of **OLGADMA 4Aa** with mPEGMA500, mPEGA1000, and PEGDA700 (1:1 ratio by weight).

The experiments detailed above enabled synthetic access to OLGA-based NPs containing the PEG chemical motif and established PEGDA700 as a PEGylated monomer capable of yielding the suspension of NPs with the highest concentration of NPs having a size and PI within the desirable range. Moreover, the NPs prepared in the presence of PEGDA700 exhibited a marked advantage over NPs prepared from **OLGADMA 4Aa** alone in terms of the estimated NP yield of drug-loaded OLGA-based NPs, as further discussed in 4.2.2. Given these observations, the synthesis of OLGA-based NPs conducted employing OLGADMAs in the presence of PEGDA700 were explored further to ultimately constitute the standard monomer composition of OLGA-based NPs presented in this work.

3.2.3 Influence of the Reaction Duration on the Size of OLGA-based Nanoparticles

Early observations of the nanoprecipitation reaction involving **OLGADMA 4Aa** and PEGDA700 mixtures revealed substantial discrepancies in the size of the obtained NPs which appeared related to the duration of the reaction. To rationalise these findings, the nanoprecipitation polymerisation reaction was studied *via* the DLS, ELS, and ^{1}H NMR spectroscopy analysis of the crude reaction mixture over time.

The DLS analysis of the crude reaction mixture over 240 min under typical reaction conditions revealed a gradual, time-dependent increase in the size of the NPs (Figure 21). On the other hand, the PI and ζ-potential values remained relatively stable with the latter having negative values. The ^{1}H NMR spectroscopy analysis revealed that the polymerisation is a rapid process, as evidenced by the absence of detectable reactants after 15 minutes of reaction (Figure 22). For comparison, the resonances belonging to **OLGADMA 4Aa** and PEGDA700 can be observed in the ^{1}H NMR spectrum of the control experiment conducted at the identical concentration of starting materials and in the absence of AIBN. Specifically, resonances such as those attributed to vinylic protons of the reactants (δ 5.60-6.40 ppm), the two quartets belonging to the methine protons of the lactate units of **OLGADMA 4Aa** (δ 5.05-5.25 ppm), the diastereotopic methylene protons of the glycolate units of **OLGADMA 4Aa** (δ 4.75-4.95 ppm), the protons of the ethylene glycol unit of **OLGADMA 4Aa** (δ 4.27-4.40 ppm), and the protons of the ethylene glycol units of PEGDA700 (δ 3.45-4.25 ppm) are detectable by ^{1}H NMR spectroscopy when AIBN is omitted from the standard nanoprecipitation polymerisation protocol, as seen in Figure 22.

Furthermore, the examination of the ^{1}H NMR spectra of the aliquots of the crude reaction mixture revealed the presence of hypothetical PEG-containing species manifesting their presence in the solution over time, as evidenced by resonances of increasing integration visible at δ 3.51 ppm which could be attributed to protons of the oxyethylene units of PEG. At this point, the hydrolysis of polymer segments deriving from the polymerisation of PEGDA700 was hypothesised. To further support this hypothesis, species agreeable with the structure of PEG alcohols were isolated from the crude mixtures upon the removal of the formed NPs.

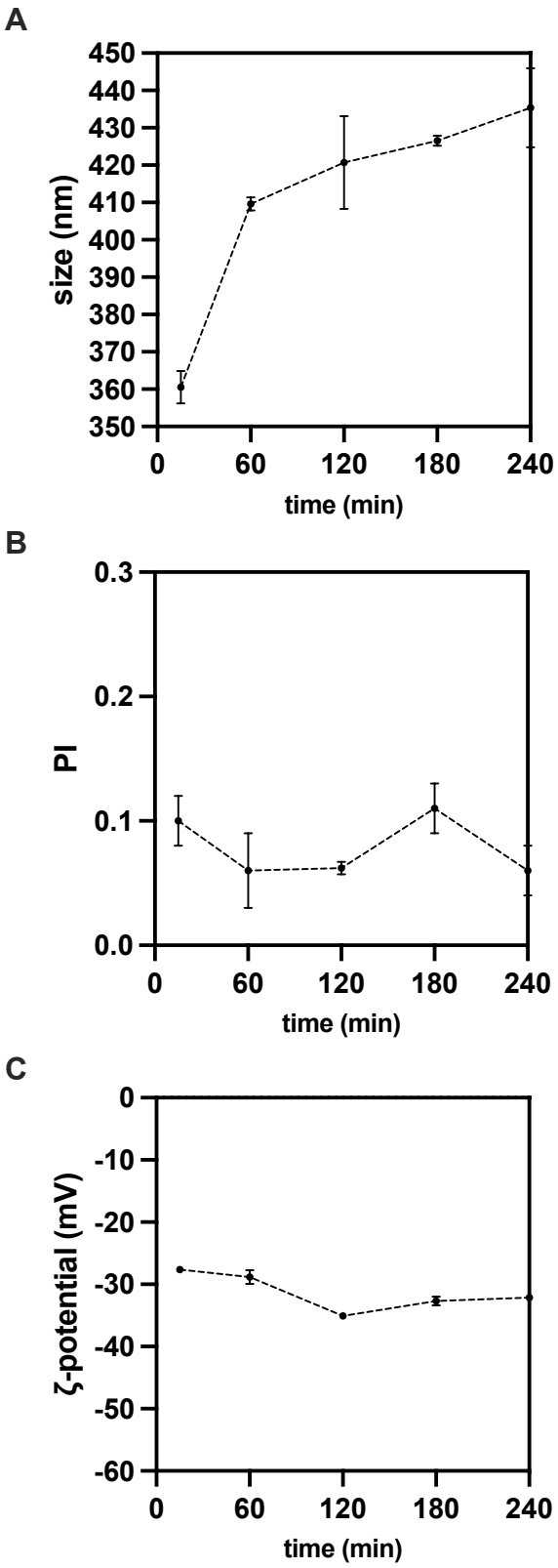


Figure 21. DLS and ELS analysis of the nanoprecipitation polymerisation of **OLGADMA 4Aa** in the presence of PEGDA700 (crude reaction mixture) over a period of 240 min. A) evolution of NP size expressed as z-average, B) evolution of the PI, and C) evolution of the ζ-potential.

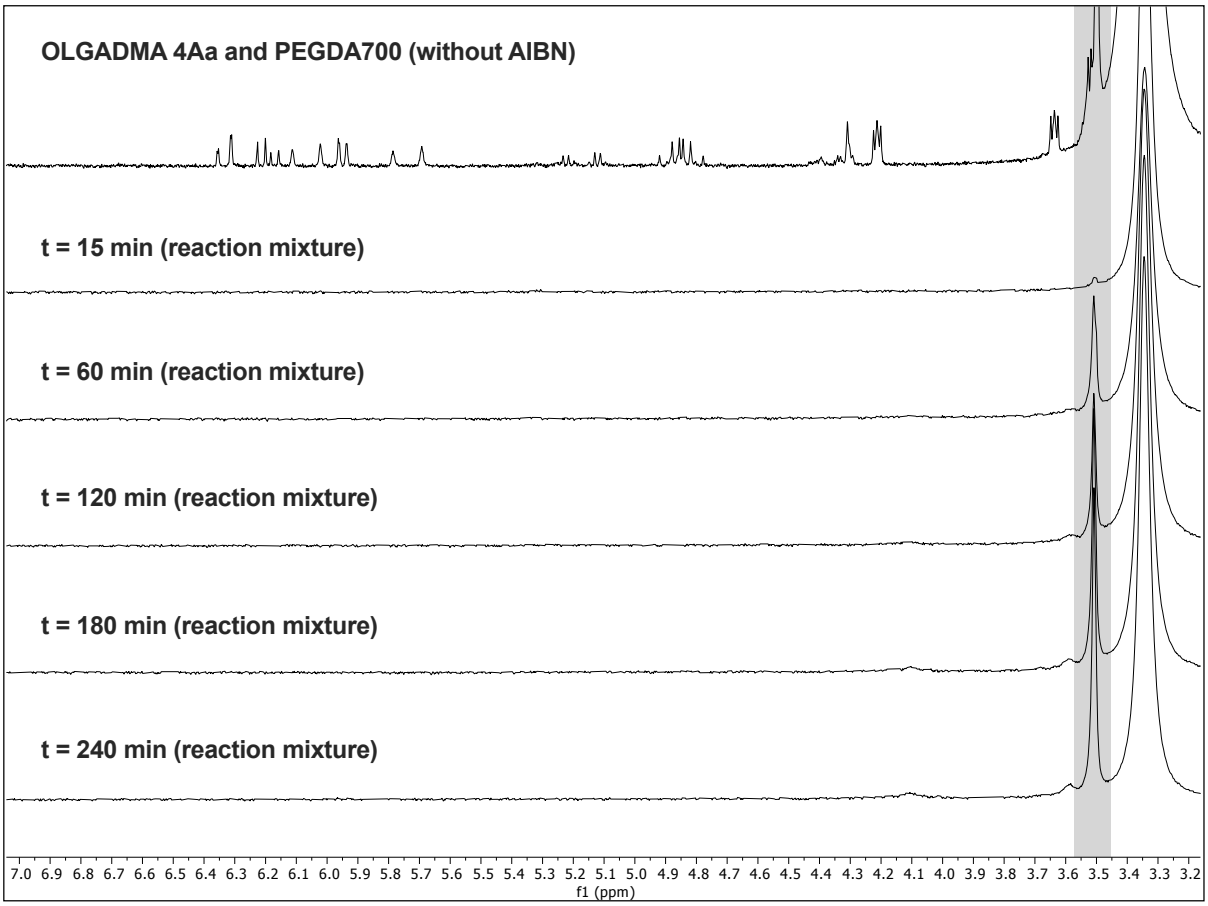


Figure 22. Stacked sections of the ^{1}H NMR (400 MHz, $(CD_3)_2SO$) spectra of a mixture of **OLGADMA 4Aa** and PEGDA700 at typical reaction concentrations (without AIBN), and aliquots of the nanoprecipitation polymerisation crude reaction mixture sampled at differ different time points. The resonances attributed to protons of the ethylene units of PEG are highlighted in grey. The H_2O resonance is visible at δ 3.33 ppm.

Taken altogether, the observations presented above could imply an initial phase of rapid polymerisation and NP formation succeeded by a phase of homogeneous NP swelling, presumably driven by ester hydrolysis occurring during longer reaction durations at 70 °C. In this setting, ester groups such as those deriving from polymerised PEGDA700 could undergo hydrolysis releasing PEGylated alcohols which are soluble and thus become detectable by solution NMR spectroscopy of the crude mixture. Due to these observations, the duration of nanoprecipitation polymerisation experiments was deliberately confined to a 15-minute window across all further investigations presented in this work.

3.2.4 Influence of the AIBN Concentration on the Size and the Yield of the Nanoparticles

To study the potential effects of AIBN concentration on the size and the yield of NPs resulting from nanoprecipitation polymerisation, experiments involving **OLGADMA 4Aa** and PEGDA700 were conducted in the presence of 0.2 wt%, 2.0 wt%, and 20.0 wt% of AIBN maintaining the 15 min reaction window. The NPs were then subjected to the standard purification protocol and diluted to a constant volume. The analysis of the size of the obtained NPs was performed using a combination of DLS and multi-angle dynamic light scattering (MADLS®). The concentration of AIBN influenced both the NP size and the estimated yield of the reaction. Particularly, all three AIBN concentrations allowed the detection of sub-micrometre particles via MADLS® analysis (Figure 23).

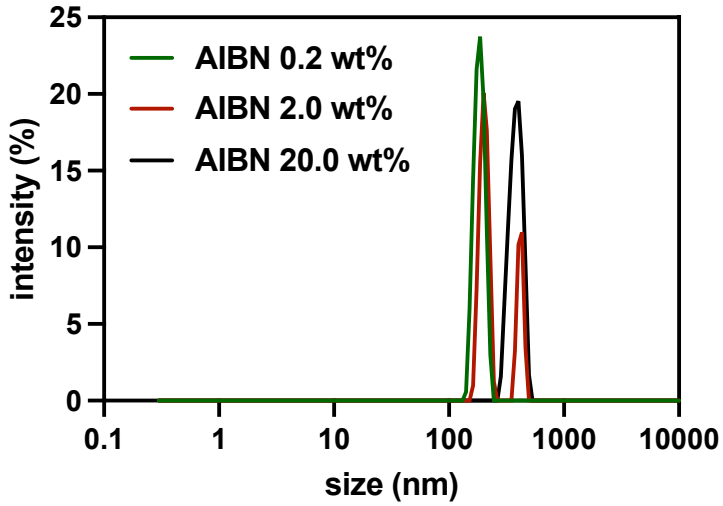


Figure 23. MADLS® analysis of particles prepared in the presence of 0.2 wt%, 2.0 wt%, and 20.0 wt% of AIBN.

The reaction involving 0.2 wt% of AIBN yielded the smallest NPs which were isolated as suspensions having large particle contaminants not suitable for DLS analysis. The reaction conducted in the presence of 2.0 wt% of AIBN afforded a mixture of two size populations as revealed by MADLS® analysis. The analysis of NPs obtained in the presence of 20.0 wt% of AIBN afforded the largest NPs, isolated as a single size-population of NPs and presenting no large-particle contaminants detectable by visual inspection and DLS.

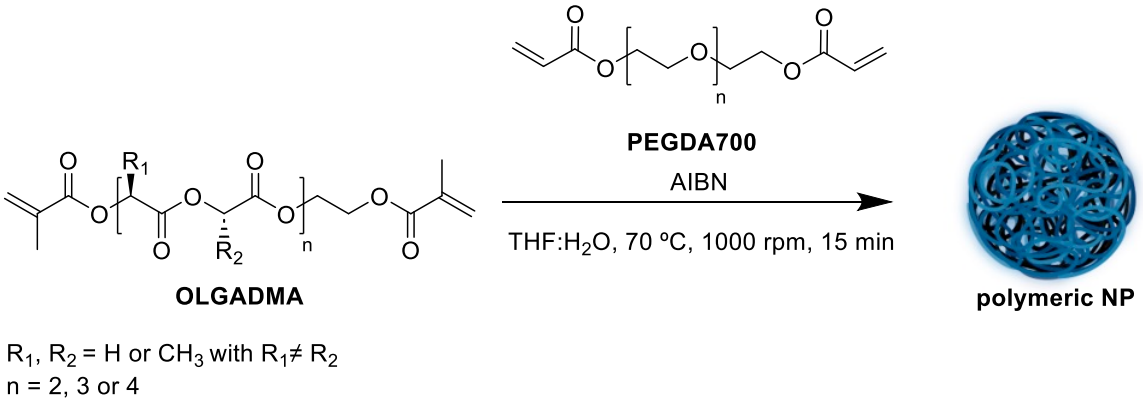
Moreover, the estimation of the NP yield of the experiments calculated from the mass of the powders obtained by lyophilisation of the purified NP suspensions revealed the reaction performed in the presence of 20.0 wt% AIBN was the highest-yielding one (Table 9). Conversely, the reactions performed in the presence of 0.2 wt% and 2.0 wt% of AIBN yielded a negligible quantity of powders which suggested yields of <1%. Given the observation presented above, AIBN was used at a fixed concentration of 20 wt% in studies presented in this work.

AIBN Concentration (wt%)	**Estimated Yield* (%)**
0.2	<1
2.0	<1
20.0	30

Table 9. Estimated yields of nanoprecipitation polymerisation reactions involving **OLGADMA 4Aa** and PEGDA700, conducted in the presence of 0.2 wt%, 2.0 wt%, and 20.0 wt% of AIBN. *Calculated as the ratio of the mass of the powders obtained via lyophilisation of NP suspensions and the total monomer feed, expressed as a percentage.

3.3 Standard Nanoprecipitation Polymerisation Conditions and Naming Conventions

The studies outlined in the previous sections allowed for the establishment of the standard nanoprecipitation polymerisation conditions used for synthesising OLGA-based NPs which were employed throughout the rest of this work (Scheme 25). The resulting crude reaction mixtures were purified via repetitive centrifugal filtration prior to being subjected to DLS, ELS, and FTIR spectroscopy analysis.



Scheme 25. Standard conditions for the nanoprecipitation polymerisation of a generic OLGADMA. OLGADMA (40 wt%), PEGDA700 (40 wt%), AIBN (20 wt%), THF:H_2O (1:3).

The OLGA-based NPs synthesised using standard nanoprecipitation polymerisation conditions are designated with **NP** followed by the alphanumeric code of the OLGADMA employed for the synthesis. For instance, **NP4Aa** denotes NPs prepared from **OLGADMA 4Aa** under standard reaction conditions.

3.4 Synthesis and Analysis of NP4Aa

NP4Aa have been synthesised *via* nanoprecipitation polymerisation of **OLGADMA 4Aa** under standard conditions. The experiment yielded a stable aqueous NP suspension which was obtained without the need for further sample manipulation such as sonication or filtration. **NP4Aa** were analysed by DLS, ELS, and TEM (Figure 24). The DLS analysis revealed the presence of submicron particles with a z-average of 227.9 ± 2.0 nm, alongside a PI of 0.13 ± 0.02. The ζ-potential of **NP4Aa** in deionised water was negative, with a value of -41.86 ± 1.42 mV. The TEM analysis of the sample revealed the presence of spherical NPs comprising a dense core and a sparser periphery showing a dotted pattern visible under higher magnifications.

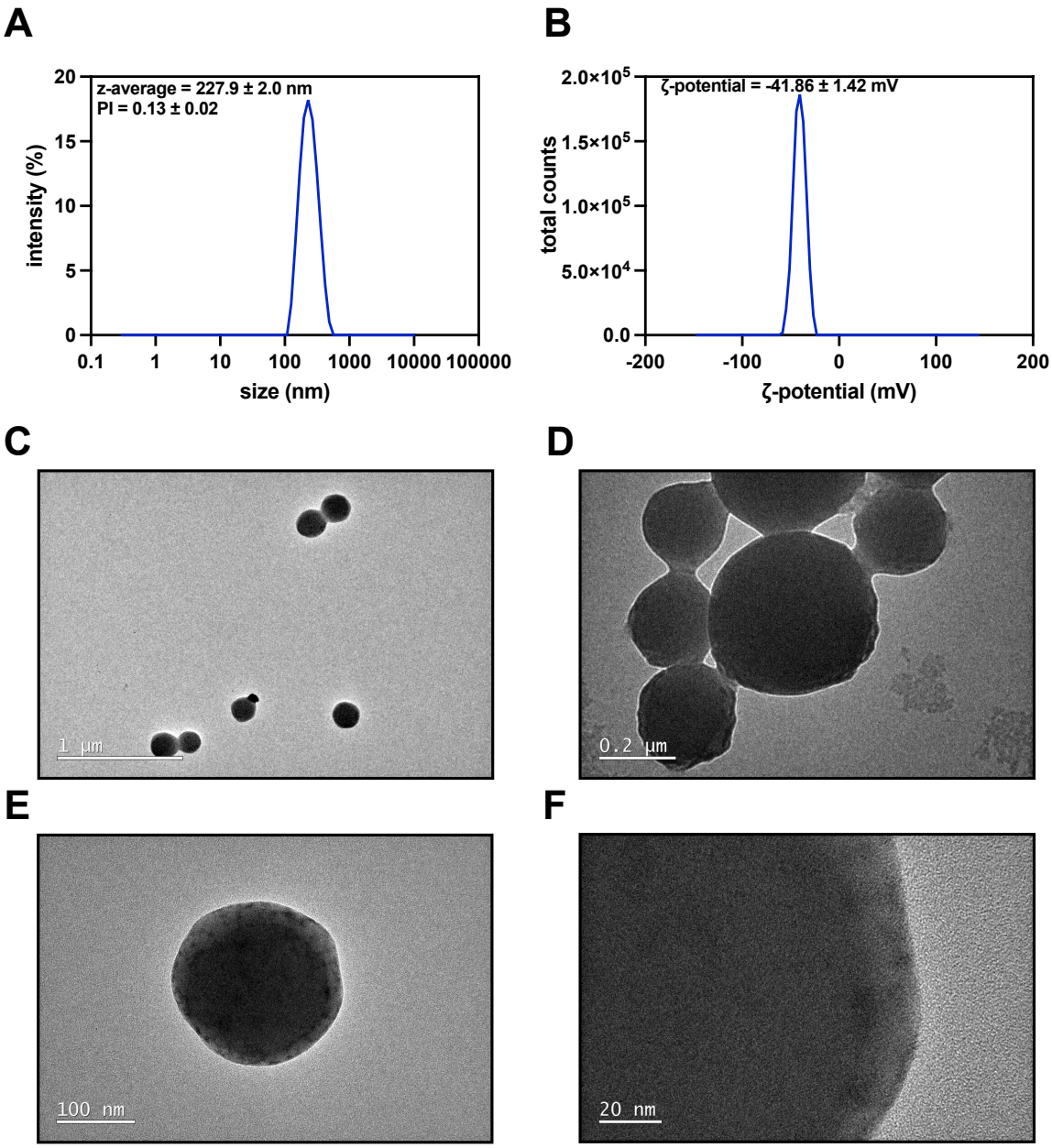


Figure 24. DLS, ELS, and TEM analysis of **NP4Aa**. A) Intensity-weighted size distribution, B) ζ-potential distribution, C) TEM micrograph (8000×, scale bar = 1 µm), D) TEM micrograph (25 000×, scale bar = 0.2 µm), E) TEM micrograph (50 000×, scale bar = 100 nm), and F) TEM micrograph (200 000×, scale bar = 20 nm).

The FTIR analysis of **NP4Aa** NPs in powder form revealed the presence of a single and relatively broad vibrational band at 1740 cm^{-1}, consistent with a sample comprising aliphatic esters (Figure 25). Moreover, intense nitrile vibration bands deriving from residual AIBN could not be detected by FTIR.

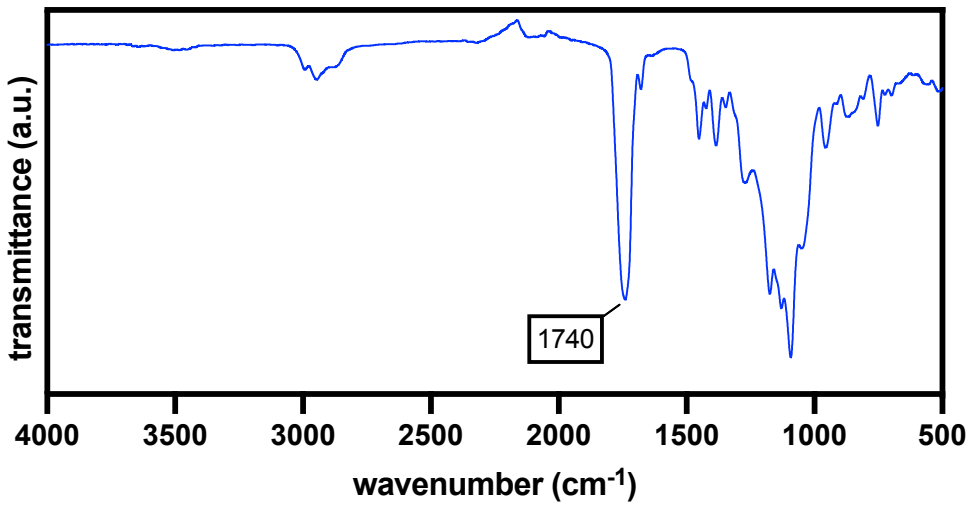


Figure 25. ATR FTIR spectrum of **NP4Aa**. A single vibrational band attributed to the ester C=O stretch is visible at 1740 cm^{-1}.

3.5 Synthesis and Analysis of a Library of OLGA-based NPs

The synthesis of a library of polymeric NPs based on OLGADMAs described in Chapter 2 was attempted using standard nanoprecipitation polymerisation conditions followed by a purification step via centrifugal filtration. Stable NP suspensions were obtained from six OLGADMAs and are listed in Table 10. Large particles detectable by visual inspection and DLS were absent in four NP suspensions, whilst suspensions of **NP6B** and **NP8B** required a further syringe filtration step to remove these particles. Suspension **NP6A** presented the highest concentration of solids, whilst **NP6B** was the most diluted.

NP suspension	Filtration required*	Estimated Yield* (%)
NP4Aa	No	31
NP4Ab	No	25
NP4Bb	No	31
NP6A	No	33
NP6B	Yes	3
NP8B	Yes	6

Table 10. List of OLGA-based NPs prepared in this work alongside the estimated NP yield. *Calculated as the ratio of the mass of the powders obtained by lyophilisation of NP suspensions and the total monomer feed, expressed as a percentage.

The reaction involving **OLGADMA 4Ba** and **OLGADMA 8A** failed to yield the desired NP suspensions. Whilst polymerisation did occur in these experiments, as confirmed by FTIR spectroscopic analysis, the isolated materials were consistently macroscopic solids and could not be successfully re-suspended in water by sonication. Furthermore, the filtration of these samples through syringe filters (pore size 5.0 μm), followed by lyophilisation of the obtained liquids yielded a negligible quantity of powders which suggested the lack of colloidally stable NPs in these samples.

To explain the observed differences in the ability of structurally diverse OLGADMAs to yield NPs, future work related to this chapter could focus on investigating the behaviour of OLGADMAs in solution, for example via diffusion-ordered NMR spectroscopy (DOSY NMR). This type of analysis may provide information regarding the existence of preferred arrangements of OLGADMA molecules in solution, which were identified as a possible cause of the differential outcomes of nanoprecipitation polymerisation experiments.

The prepared OLGA-based NPs were subjected to DLS and ELS analysis for the determination of the size, PI, and ζ-potential (Table 11).

Nanoparticle	z-average (nm ± SD)	PI ± SD	ζ-potential (mV ± SD)
NP4Aa	227.9 ± 2.0	0.13 ± 0.02	-41.9 ± 1.4
NP4Ab	235.8 ± 0.7	0.12 ± 0.01	-51.6 ± 1.0
NP4Bb	366.0 ± 6.2	0.13 ± 0.02	-47.0 ± 0.7
NP6A	240.3 ± 5.1	0.18 ± 0.03	-39.1 ± 0.4
NP6B	171.70 ± 2.25	0.31 ± 0.01	-36.9 ± 0.5
NP8B	188.4 ± 3.8	0.23 ± 0.04	-45.8 ± 0.5

Table 11. DLS and ELS analysis of a library of OLGA-based NPs.

The prepared NPs exhibited sizes between 171.70 ± 2.25 and 366.0 ± 6.2 nm with PI values ranging from 0.12 – 0.31. The ζ-potential in deionised water was negative for all prepared NPs and ranged between -36.9 ± 0.5 mV and -51.6 ± 1.0 mV.

Following the successful synthesis of a library of six types of OLGA-based NPs presented above, the analysis of the stability of these NPs in aqueous environments at 37 °C was performed and compared to that of PLGA-based NPs as an ester-based class of polymeric NPs which is well-established within the drug delivery context. The main findings are summarised in the following sections.

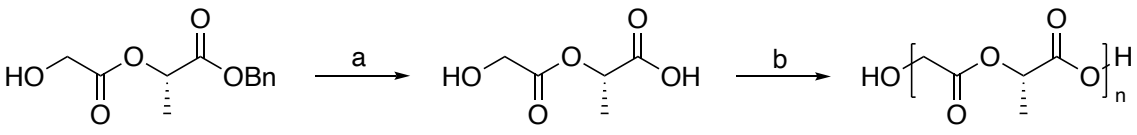
3.6 Comparative Stability Study of OLGA-based and PLGA-based Nanoparticles

As mentioned in Chapter 2, OLGA-based NPs were expected to exhibit elevated stability in aqueous environments due to the crosslinked structure and the presence of sequenced oligoesters. To test this hypothesis, the stability of the prepared OLGA-based NPs was assessed via incubation of aqueous NP suspensions at the physiological temperature of 37 °C followed by the determination of the NP size, PI, ζ-potential, and pH of the suspensions over 5 weeks. The results were compared against the identical analysis of PLGA-based NPs prepared from three types of PLGA polymers. Specifically, these included a non-sequenced form of PLGA, a sequenced form of PLGA, and a PEGylated form of PLGA which share chemical composition similarities with OLGA-based NPs and were hypothesised to yield NPs which cover a range of different stabilities under the experimental conditions detailed above. The study described in the following section is inspired by the work of Feijen *et al.* who reported on a comparative exploration of the degradation of NPs based on PLA, PLGA, and PLGA-PEG over weeks of NP incubation at 37 °C within an aqueous buffer.[329] Notably, the investigation of the stability of ester-based materials over prolonged periods at the physiological temperature may be considered of limited relevance for the characterisation of non-depot drug delivery systems. However, this type of *in vitro* study was envisaged to offer a preliminary insight into the general physicochemical stability of OLGA-based NPs as completely novel nanomaterials. Future work will focus on evaluating the stability of OLGA-based NPs *in vivo*, which may be possible via FRET (Förster Resonance Energy Transfer)-based investigations such as those reported for PLGA NPs by Tagit *et al*.[330]

3.6.1 Preparation and Analysis of PLGA-based NPs

The PLGA-based NPs required for the comparative stability study were prepared from three types of PLGA polymers using conditions that mirrored the nanoprecipitation polymerisation reaction conducted in the absence of AIBN. For this purpose, **PLGA** (Resomer® RG 504 H, acid terminated, L:G 50:50, M_w 38,000-54,000 Da) and **PLGA-PEG** (PLGA-PEG-COOH, acid terminated, L:G 50:50, M_n 50,000-5,000 Da) were obtained from commercial sources. Alternating PLGA (**PLGA alt**) (sequenced, acid-terminated, L:G 50:50, M_w 7158 Da) was synthesised from compound **7** over two

steps, according to procedures reported by Stayshich and Meyer (Scheme 26).[326] Shortly, alcohol **7** was subjected to debenzylation via catalytic hydrogenation to afford compound **58**. In the following step, the polycondensation of **58** conducted in the presence of DCC and DMAP afforded the desired **PLGA alt**.



7 **58** **PLGA alt**

Scheme 26. Synthesis of alternating PLGA (**PLGA alt**) as reported by Stayshich and Meyer.[326] a) H_2, Pd/C (5 wt%), EtOAc, rt, b) DCC (1.5 equiv), DMAP (0.08 equiv), CH_2Cl_2, 0 °C to rt.

The PLGA-based NPs prepared from **PLGA**, **PLGA alt** and **PLGA-PEG** are designated with **NP-PLGA**, **NP-PLGA alt**, and **NP-PLGA-PEG** respectively (Table 12). The preparation of **NP-PLGA** and **NP-PLGA alt** yielded suspensions containing large particles detectable by DLS and required further purification via syringe filtration, whilst **NP-PLGA-PEG** was isolated directly as a homogeneous NP suspension. Expectedly, **NP-PLGA-PEG** was obtained as the most concentrated suspension, whilst **PLGA alt** yielded the suspension with the lowest quantity of solids.

Type of PLGA polymer	Nanoparticle	Filtration required (5.0 μm)	Estimated Yield* (%)
PLGA	**NP-PLGA**	Yes	25
PLGA alt	**NP-PLGA alt**	Yes	8
PLGA-PEG	**NP-PLGA-PEG**	No	83

Table 12. Polymer composition of PLGA-based NPs prepared in this work alongside yield estimates. *Calculated as the ratio of the mass of the powders obtained by lyophilisation of NP suspensions and the mass of the total polymer feed, expressed as a percentage.

The sizes of the prepared PLGA-based NPs were all <150 nm with PI values <0.3, as determined by DLS. The ζ-potential of PLGA-based NPs was negative in deionised water with values below -30 mV. **NP-PLGA-PEG** presented the smallest size, lowest PI, and the most negative ζ-potential among the three examples.

PLGA-based NP	z-average (nm ± SD)	PI ± SD	ζ-potential (mV ± SD)
NP-PLGA	123.6 ± 1.8	0.130 ± 0.005	-35.8 ± 2.4
NP-PLGA alt	136.8 ± 1.2	0.24 ± 0.03	-31.3 ± 1.3
NP-PLGA-PEG	68.0 ± 0.4	0.120 ± 0.003	-50.8 ± 2.3

Table 13. List of PLGA-based NPs prepared in this work alongside NP size expressed as *z*-average, PI, and ζ-potential measured in deionised water.

3.6.2 Size Stability at 37 °C

The DLS analysis of PLGA-based NPs demonstrated that **NP-PLGA** and **NP-PLGA alt** exhibit elevated size stability under experimental conditions outlined at the beginning of this section (Figure 26). This finding was substantiated by consistently stable z-average and PI values detected throughout the study. Conversely, **NP-PLGA-PEG** manifested a progressive increase in size, ultimately increasing 10-fold by the end of the study. Particularly, the size of **NP-PLGA-PEG** doubled after two weeks under experimental conditions after which, a faster increase in size and PI, suggestive of NP aggregation, was detected. These observations were congruent with earlier reports on the differences in the size-stability of PLGA and PLGA-PEG NPs *in vitro*.[329]

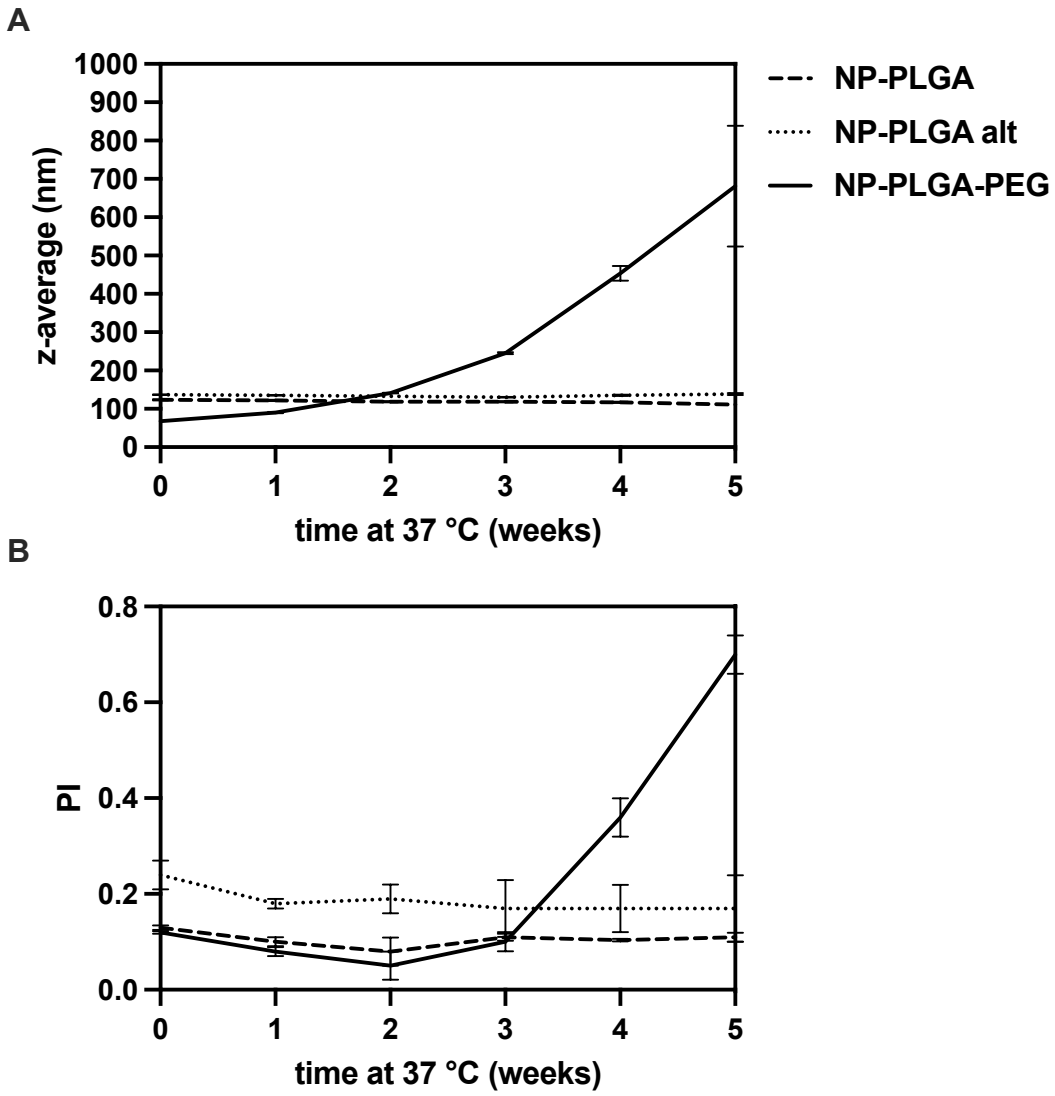


Figure 26. DLS analysis of PLGA-based NPs performed over 5 weeks of incubation in water at a temperature of 37 °C. A) NP size expressed as z-average, and B) polydispersity index (PI).

In comparison, five out of six OLGA-based NPs showed good size stability, with only limited size variations detected throughout the study (Figure 27). Specifically, **NP4Aa** and **NP4Ab** showcased size variations within a narrow window of <10 nm, whilst the size variations of **NP4Bb**, **NP6A**, and **NP8B** did not exceed 30 nm. Moreover, the PI values remained ≤0.2, with only a slight increase above this value detected for **NP8B** after five weeks at 37 °C (Figure 27B). Exceptionally, **NP6B** displayed sudden colloidal instability which manifested via the formation of a precipitate within the first week of the study and was therefore discarded from further assessments. Taken altogether, five types of OLGA-based NPs displayed size stability similar to that of NPs prepared

from **PLGA** and **PLGA alt**, regardless of the similarities in chemical composition to the markedly less size-stable **NP-PLGA-PEG**.

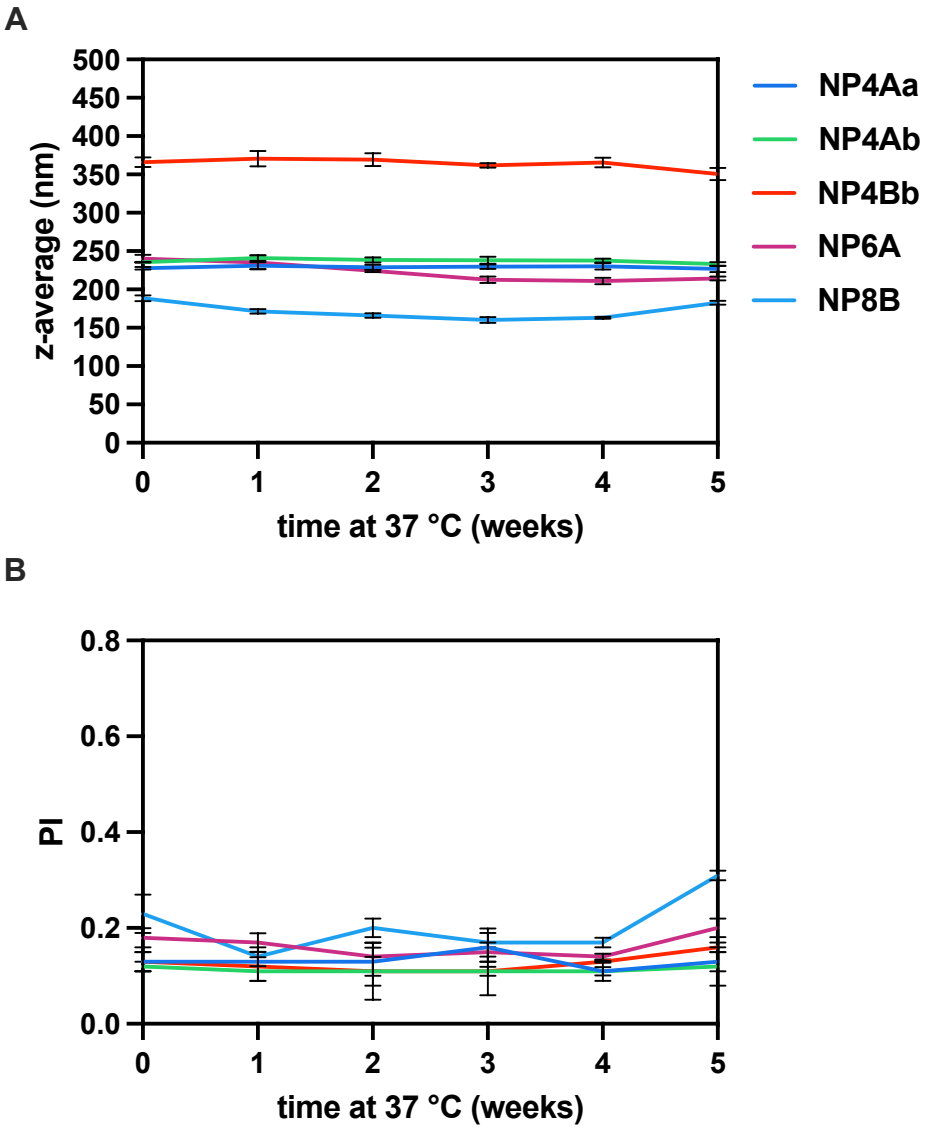


Figure 27. DLS analysis of OLGA-based NPs performed over 5 weeks of incubation in water at a temperature of 37 °C. A) NP size expressed as z-average and B) polydispersity index (PI).

3.6.3 ζ-potential Stability at 37 °C

The examination of the ζ-potential of PLGA-based via ELS showed variability with **NP-PLGA** and **NP-PLGA alt** with values remaining within the -31.29 ± 1.28 mV and -42.15 ± 1.31 mV window (Figure 28A). On the other hand, **NP-PLGA-PEG** exhibited a clear trend towards progressively less negative ζ-potential values which evolved from -50.84 ± 2.30 mV to -18.75 ± 0.54 mV**.** The ζ-potential of OLGA-based NPs showed similar behaviour to that of **NP-PLGA** and **NP-PLGA alt**, with variable values remaining within the -27.55 ± 3.80 mV and -55.63 ± 1.93 mV window (Figure 28B). Moreover, a clear trend towards less negative ζ-potential values, such as observed with **NP-PLGA-PEG**, was not evident with OLGA-based NPs.

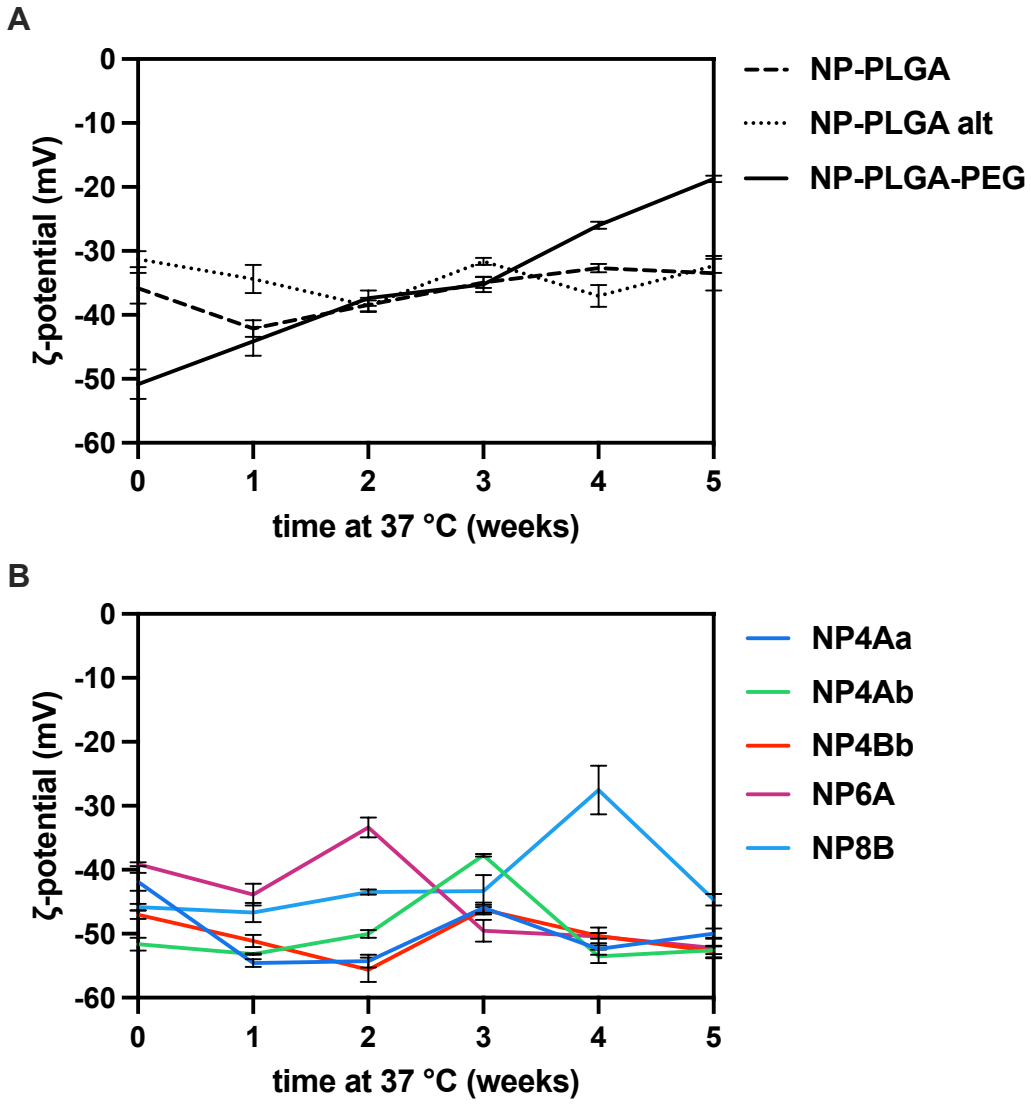


Figure 28. PI of A) OLGA-based NPs, and B) PLGA-based NPs subjected to incubation at a temperature of 37 °C over a period of 5 weeks.

3.6.4 pH Stability at 37 °C

The pH analysis revealed the freshly prepared suspensions of PLGA-based NPs displayed an acidic pH ranging from 4.09 for **NP-PLGA-PEG** to 6.07 for **NP-PLGA alt** (Figure 29A). A gradual progression towards more acidic values was detected with PLGA-based NPs over the course of the study. The suspension subjected to 5 weeks of experimental conditions containing **NP-PLGA-PEG** was the most acidic (pH 2.44), followed by **NP-PLGA** (pH 3.14), and **NP-PLGA alt** (pH 4.29). These results may be reflective of the hydrolytic stability of the different PLGA forms under experimental conditions and are congruent with previously reported properties of MPs and NPs prepared from these polymers. Analogously to PLGA-based NPs, the pH of freshly prepared OLGA-based NPs was acidic ranging from pH 4.17 to pH 5.00 (Figure 29B). However, contrary to PLGA-based NPs the trend of progressive acidification of the suspension containing OLGA-based NPs was not observed. Particularly, the pH of the examined NP suspensions demonstrated a slight variability throughout the study with the pH values at all time points remaining within a relatively narrow window of approximately 1.5 pH units. These findings could potentially be explained by the increased hydrolytic stability of the NPs deriving from the presence of sequenced oligoesters and/or the absence of free carboxylic acids in the NP building blocks, which are known to catalyse the hydrolysis of ester-containing polymers.

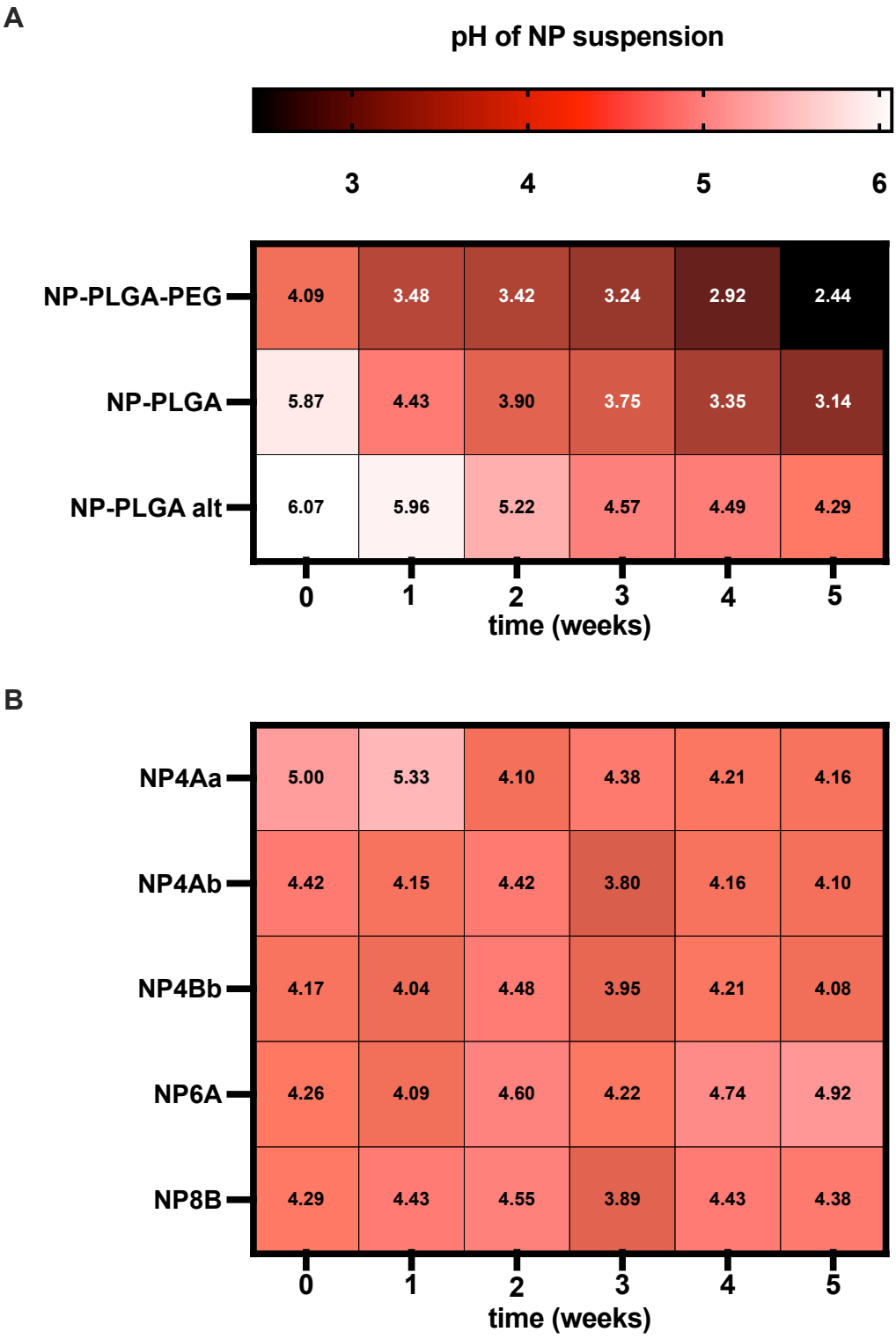


Figure 29. pH of aqueous NP suspensions subjected to incubation at a temperature of 37 °C over a period of 5 weeks. A) PLGA-based NPs, and B) OLGA-based NPs.

3.6.5 Analysis of the Stability of **NP4Aa**, **NP4Ab**, and **NP4Bb** via FTIR Spectroscopy

To detect possible changes in the chemical composition of OLGA-based NPs, NPs synthesised from tetramer OLGADMAs were further analysed via FTIR spectroscopy at weekly intervals (Figure 30). Whilst the FTIR spectra of **NP4Ab** remained relatively unchanged throughout the study, changes in the FTIR spectra were detected with **NP4Aa** and **NP4Bb**. Particularly, the presence of a broad vibration band was observed in the OH stretch region of **NP4Aa** after 5 weeks at 37 °C, alongside the appearance of new vibrational bands in the fingerprint region. Similarly, the FTIR spectrum of **NP4Bb** recorded after 5 weeks under experimental conditions showed similar changes of a lesser degree. Whilst these observations can be suggestive of ester hydrolysis occurring after 4 weeks at 37 °C, the size stability of NPs appears to be maintained as discussed above.

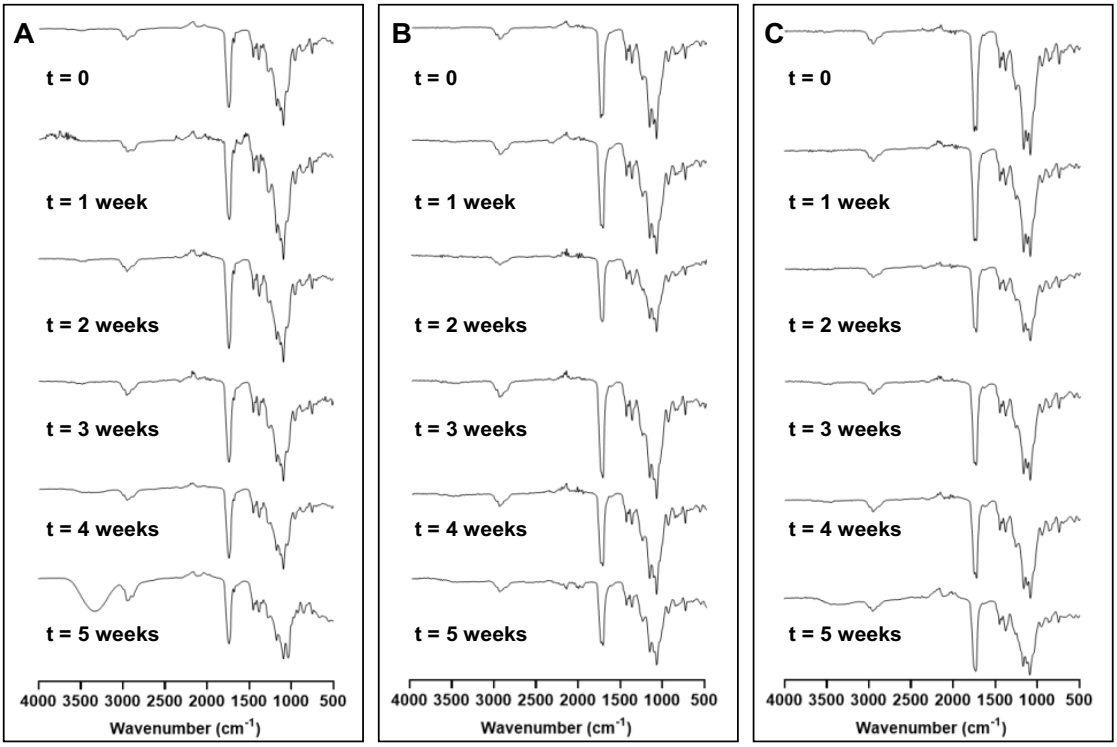


Figure 30. ATR FTIR spectra of NPs prepared from tetramer OLGADMAs subjected to incubation at a temperature of 37 °C, recorded over a period of 5 weeks. A) **NP4Aa**, B) **NP4Ab**, and C) **NP4Bb**.

3.7 Effect of NP4Aa, NP4Ab, and NP4Bb on Cell Viability In Vitro

To evaluate the potential cytotoxic effects of OLGADMA-based NPs, viability assessments on HeLa cells following 24 and 48 hours of exposure to aqueous NP suspensions containing different concentrations of **NP4Aa**, **NP4Ab**, and **NP4Bb** were performed (Figure 31). To this end, the Cell counting Kit-8 (CCK-8) assay was used to quantify cell viability upon 24 h and 48 h hours of treatment with the NPs. Notably, after incubating HeLa cells with NP suspensions for 24 hours, the standardised cell viability exceeded 80% across the tested NP types and concentrations. Furthermore, no significant decline in cell viability could be detected following a 48-hour incubation period with NP suspensions.

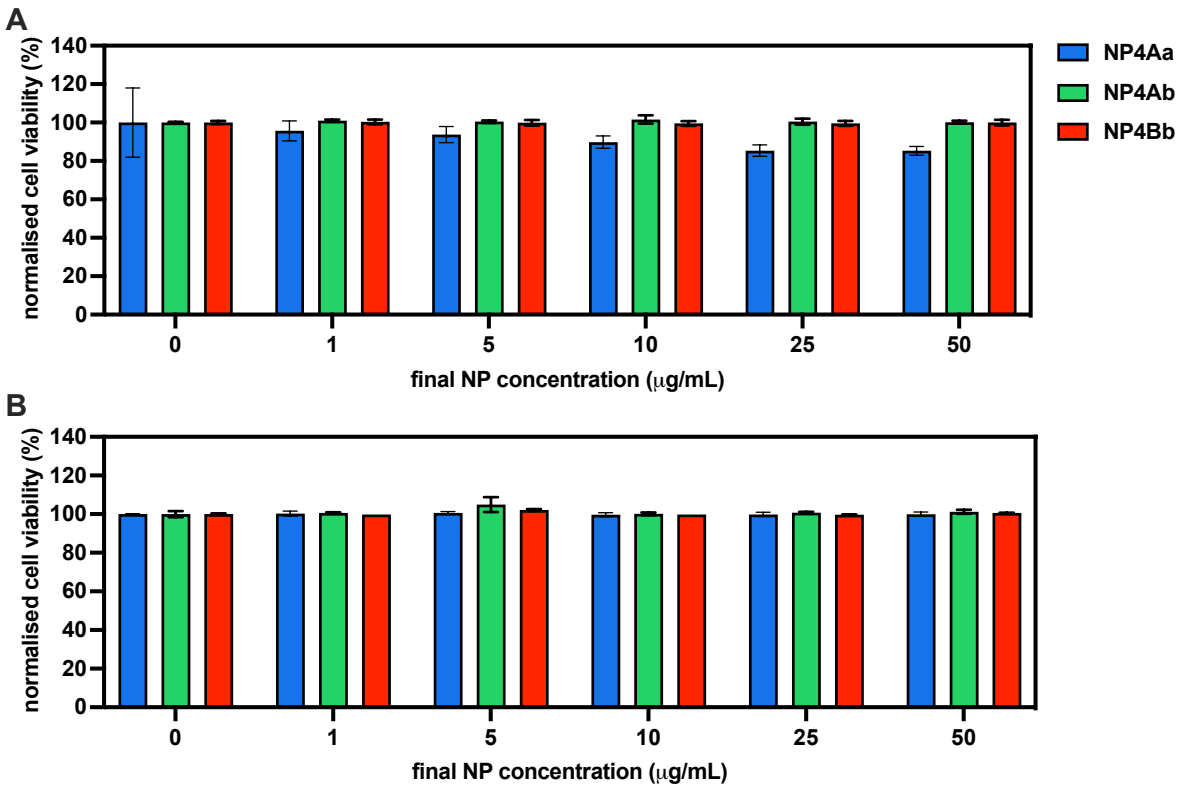


Figure 31. Normalised HeLa cell viability upon treatment with aqueous suspensions of **NP4Aa**, **NP4Ab**, and **NP4Bb** containing 0.01 – 0.5 mg/mL of NPs over a period of A) 24 h, and B) 48 h.

3.8 Cellular Uptake of Fluorescent NP4Aa

Having verified the effect of **NP4Aa**, **NP4Ab**, and **NP4Bb** on cell viability in vitro, it was considered noteworthy to explore the capacity of these NPs to be internalised by cells. To this end, fluorescent **NP4Aa** were synthesised utilising a modified nanoprecipitation polymerisation protocol comprising the monomer fluorescein O-methacrylate. The prepared fluorescent NPs had a size of 272.0 ± 6.6 nm expressed as z-average, alongside a PI of 0.20 ± 0.06. The ζ-potential of the fluorescent NPs measured in deionised water was negative with a value of -27.7 ± 1.2 mV.

To verify the cellular uptake of OLGADMA-based NPs, HeLa cells were incubated with fluorescent **NP4Aa** to achieve NP concentrations of 40, 60, and 100 μg/mL. Following 6 h of treatment with fluorescent NPs, confocal microscopy analysis revealed efficient cellular internalisation of NPs, which occurred with a highly uniform distribution for the tested NP concentrations (Figures 32-34). The NPs exhibited accumulation in the perinuclear region of HeLa cells and displayed a relative colocalisation with Lysotracker Red, a fluorescent dye capable of staining acidic subcellular compartments such as late endosomes and lysosomes. The confocal microscopy analysis outlined above was conducted in collaboration with Rupali Dabas.

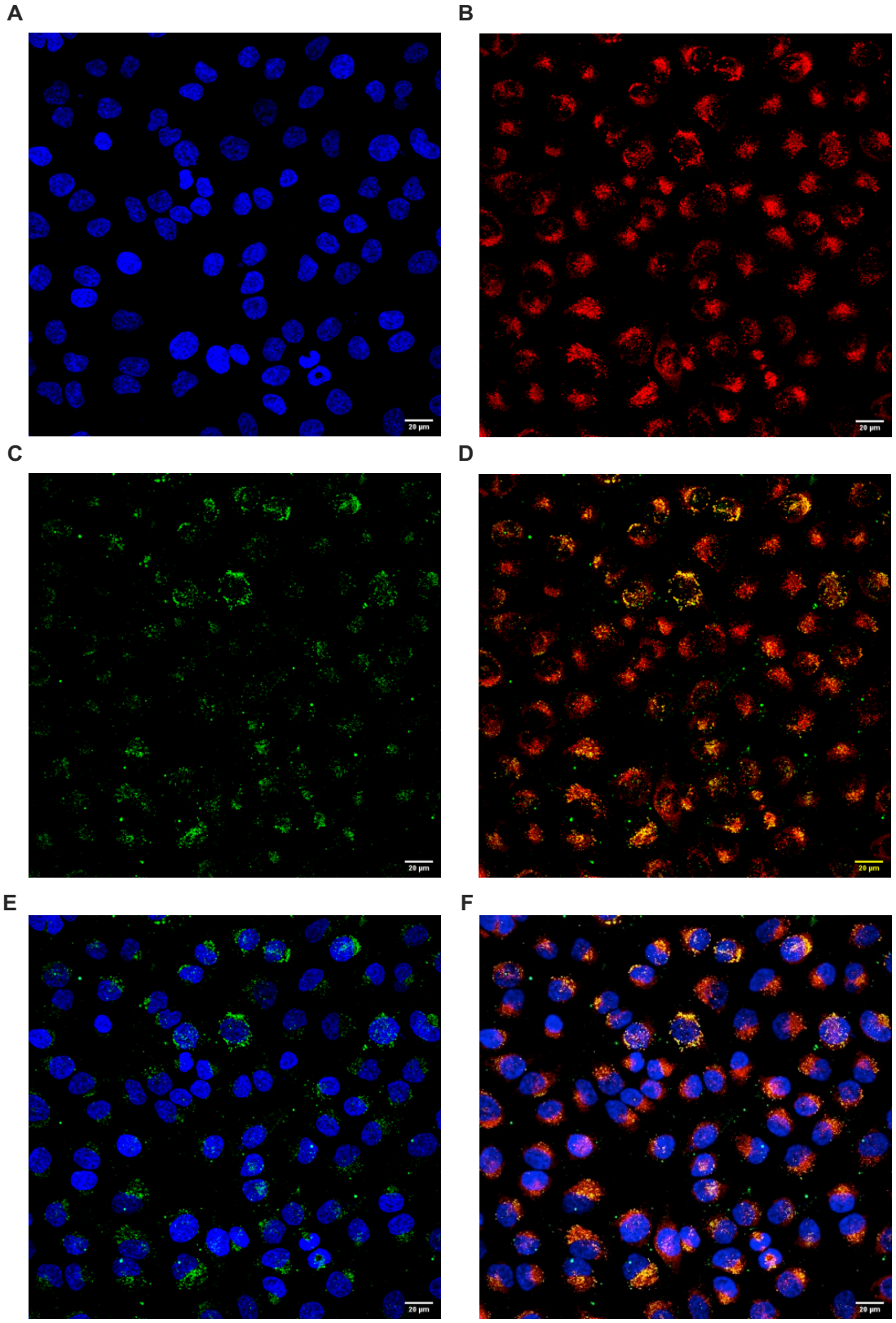


Figure 32. Confocal microscopy images of HeLa cells treated with fluorescent **NP4Aa** at a final concentration of 40 μg/mL over 6 h (40×, scale bar = 20 μm). A) Hoechst staining, B) Lysotracker Red staining, C) fluorescent **NP4Aa**, D) Lysotracker Red and fluorescent **NP4Aa** merged, E) Hoechst and fluorescent **NP4Aa** merged, F) Hoechst, Lysotracker Red, and fluorescent **NP4Aa** merged.

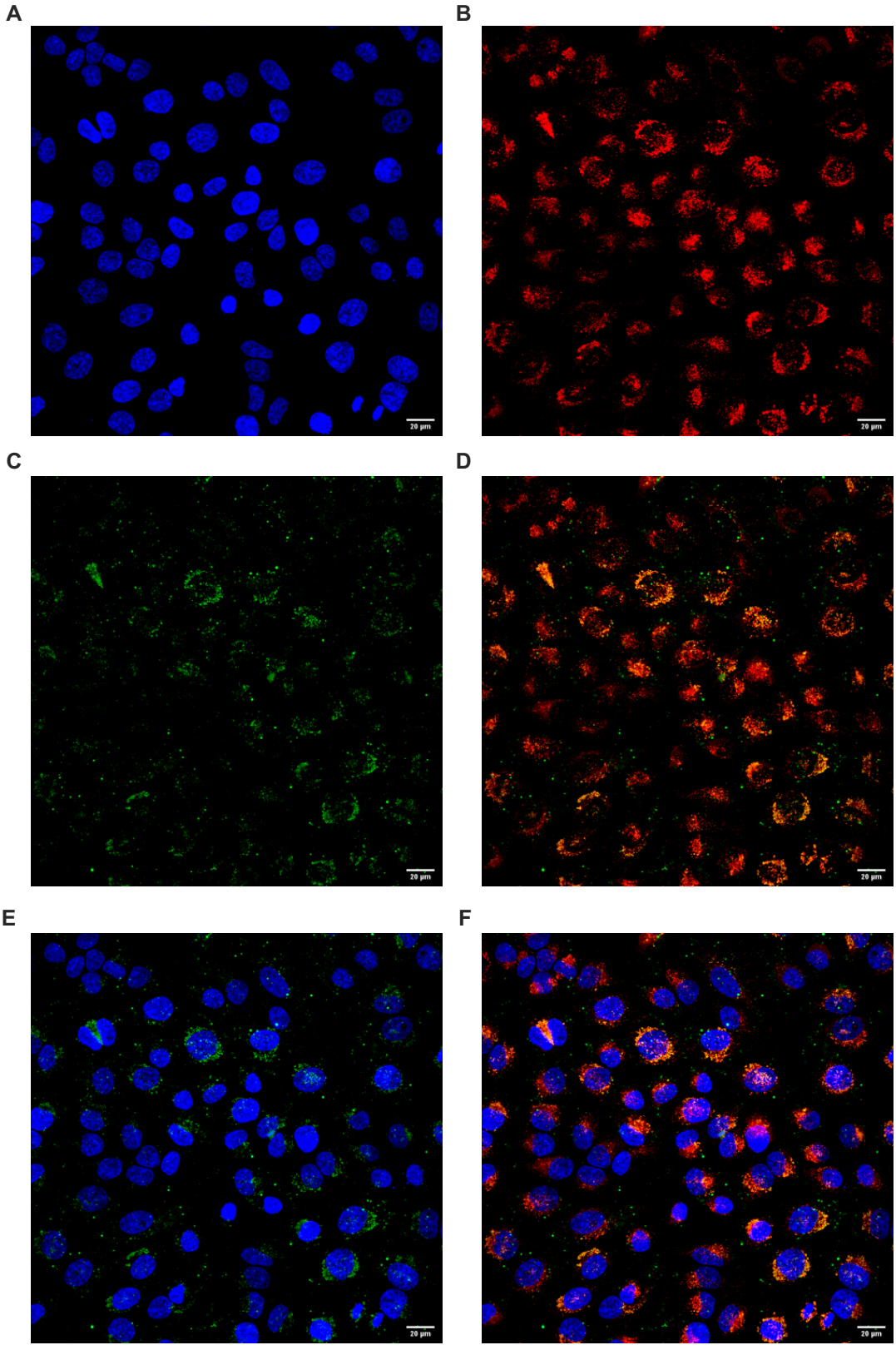


Figure 33. Confocal microscopy images of HeLa cells treated with fluorescent **NP4Aa** at a final concentration of 60 μg/mL over 6 h (40×, scale bar = 20 μm). A) Hoechst staining, B) Lysotracker Red staining, C) fluorescent **NP4Aa**, D) Lysotracker Red and fluorescent **NP4Aa** merged, E) Hoechst and fluorescent **NP4Aa** merged, F) Hoechst, Lysotracker Red, and fluorescent **NP4Aa** merged.

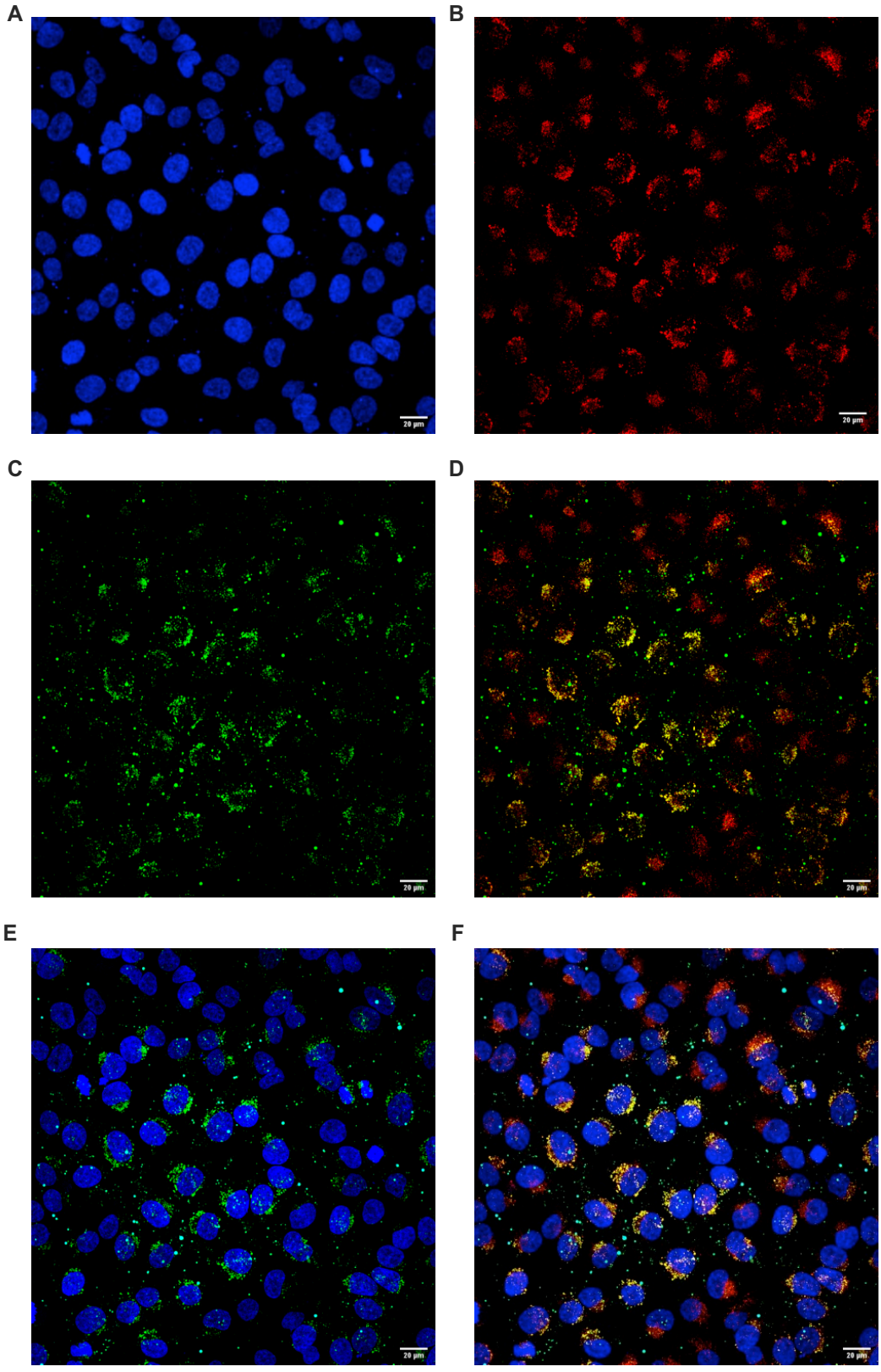
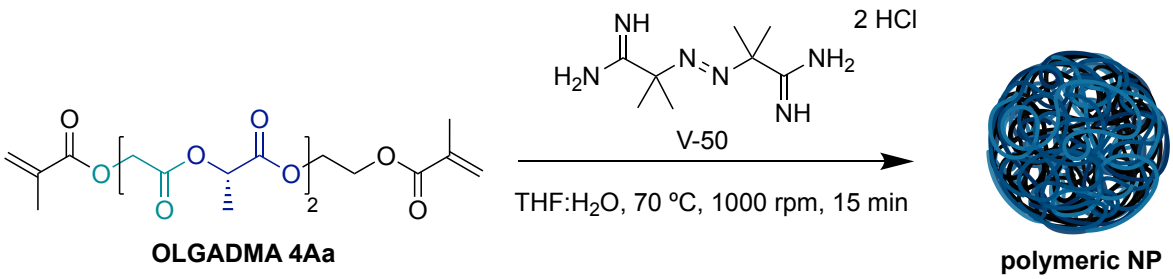


Figure 34. Confocal microscopy images of HeLa cells treated with fluorescent **NP4Aa** at a final concentration of 100 μg/mL over 6 h (40×, scale bar = 20 μm). A) Hoechst staining, B) Lysotracker Red staining, C) fluorescent **NP4Aa**, D) Lysotracker Red and fluorescent **NP4Aa** merged, E) Hoechst and fluorescent **NP4Aa** merged, F) Hoechst, Lysotracker Red, and fluorescent **NP4Aa** merged.

3.9 Nanoprecipitation Polymerisation of OLGADMA 4Aa in the Presence of the Water-Soluble Initiator V-50

Whilst the presence of residual AIBN could not be detected *via* FTIR analysis of the NPs prepared in this work, there was an interest in investigating the possibility of polymerising the NPs in the presence of a water-soluble initiator. Specifically, it was hypothesised that a water-soluble initiator would present a low propensity to partition itself within OLGADMA droplets during the nanoprecipitation polymerisation process and would undergo a more facile elimination from the crude reaction mixtures through repeated aqueous washes during the NP purification step via centrifugal filtration.

To achieve this, **OLGADMA 4Aa** was subjected to a modified nanoprecipitation polymerisation protocol involving the injection of the monomer in THF into a vigorously stirred aqueous solution of 2,2′-azobis(2-methylpropionamidine) dihydrochloride (V-50) at a temperature of 70 °C (Scheme 27). The obtained particle suspension was subjected to the standard purification protocol to yield an aqueous suspension of polymeric NPs.



Scheme 27. Nanoprecipitation polymerisation of **OLGADMA 4Aa** in the presence of the water-soluble initiator V-50. **OLGADMA 4Aa** (80 wt%), V-50 (20 wt%), THF:H_2O (1:3).

The DLS analysis of the obtained suspension revealed the presence of sub-micrometre particles with a z-average of 395.0 ± 6.9 nm and a PI of 0.17 ± 0.03 (Figure 35A). In contrast to NPs prepared in the presence of AIBN, the NPs synthesised with V-50 exhibited a positive ζ-potential of 13.0 ± 3.3 mV in deionised water (Figure 35B). This phenomenon could be explained by the existence of surface cations originating from polymer chains directly initiated by V-50 radicals, which carry positive charges.

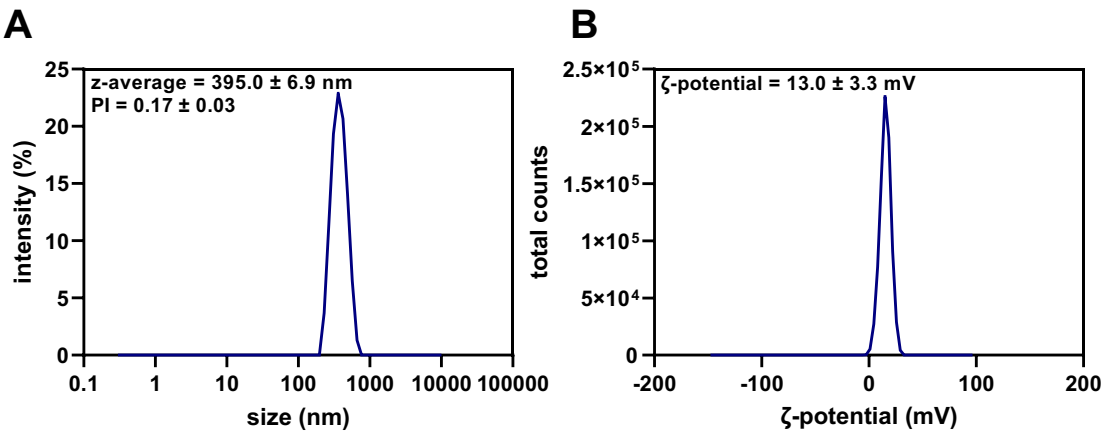


Figure 35. DLS and ELS analysis of NPs prepared via the nanoprecipitation polymerisation of **OLGADMA 4Aa** in the presence of the V-50 initiator. A) Intensity-weighted size distribution, and B) ζ-potential distribution.

Comparable to NPs synthesised in the presence of AIBN, the FTIR analysis of NPs prepared in the presence of V-50 revealed a single vibration band at 1743 cm^{-1} which was considered congruent with the successful polymerisation of **OLGADMA 4Aa** (Figure 36).

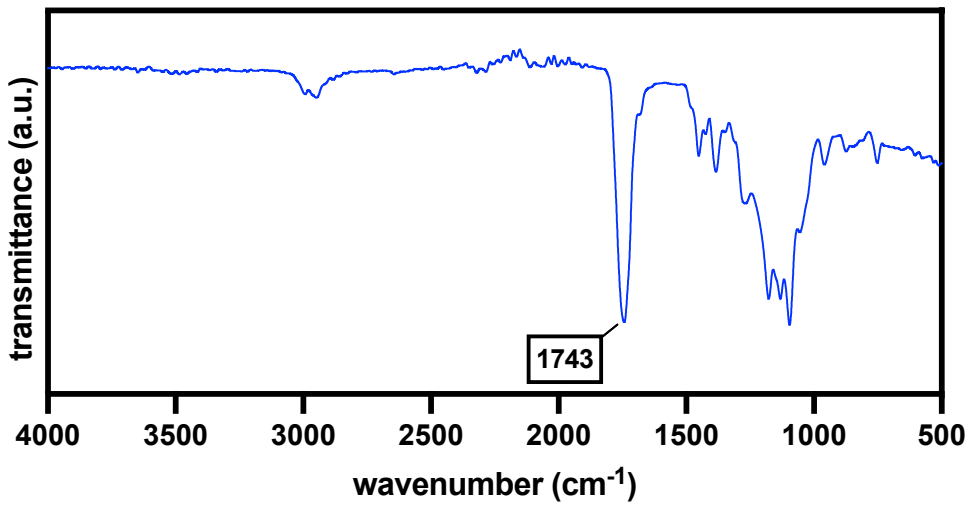


Figure 36. ATR FTIR of NPs prepared via nanoprecipitation of **OLGADMA 4Aa** in the presence of the V-50 initiator.

Given the result outlined above, it was hypothesised that **OLGADMA 4Aa** could be polymerised to form polymeric NPs by the action of radicals formed in the aqueous phase of the nanoprecipitation polymerisation reaction.

3.10 Chapter Summary

A library of polymerisable oligoesters named oligolactoglycolic acid dimethacrylates (OLGADMAs) was prepared *via* a multi-step synthetic strategy. A unique methodology termed 'nanoprecipitation polymerisation' was developed to polymerise OLGADMAs into polymeric NPs in the presence of AIBN. The methodology is surfactant-free and allows for the copolymerisation of OLGADMAs with PEGylated monomers such as PEGDA700 yielding stable NPs within 15 minutes of reaction. Structurally diverse OLGADMAs demonstrated differential outcomes under nanoprecipitation polymerisation conditions, revealing the existence of OLGADMAs that favour the formation of stable NPs over macroscopic solids.

OLGA-based NPs maintained a good level of size stability in an aqueous environment at the physiological temperature of 37 °C for at least five weeks. Moreover, aqueous suspensions of OLGA-based NPs retain the pH within a narrow window over 5 weeks at 37 °C, whilst PLGA-based NPs showcase gradual acidification. Despite being PEGylated, the size-stability of OLGA-based NPs at 37 °C was found to be similar to that of NPs prepared from PLGA and sequenced PLGA, whilst being markedly more stable than NPs prepared from PLGA-PEG.

OLGA-based NPs prepared from tetrameric oligoesters induce a minimal decrease of HeLa cell viability *in vitro* after 24 h of treatment, and no detectable decrease of cell viability upon 48 h of treatment at concentrations ranging from 1-50 μg/mL. Moreover, fluorescent analogues of **NP4Aa** are homogeneously internalised by HeLa cells after 6 hours of treatment with NPs.

Lastly, **OLGADMA 4Aa** was found amenable to polymerisation in the presence of a water-soluble azo-initiator V-50 yielding polymeric NPs, with implications for further development of the OLGA-based NPs aimed towards drug delivery applications.

The following chapter describes the synthesis and analysis of drug-loaded OLGA-based NPs.

Chapter 4: Synthesis and Analysis of Drug-loaded OLGA-based Nanoparticles

4.1 Introduction

The OLGA-based NPs described in Chapter 3 were designed as potential nanocarriers for small-molecule drugs. Given the aqueous insolubility of OLGADMAs and the establishment of the nanoprecipitation polymerisation method, it was hypothesised that the OLGA-based nanoplatform could be particularly suitable for the encapsulation of poorly soluble small-molecule therapeutics. This class of molecules occupies a significant portion of the chemical and pharmaceutical space with approximately 40% of the top drugs marketed in the US and Europe, 90% of new chemical entities, and 75% of compounds under development being poorly soluble.[331–334] Furthermore, the encapsulation of such hydrophobic molecules into stable nanocarriers can result in many therapeutic advantages including effective transport, lower toxicity, and control over the drug's pharmacokinetic profile.[335]

To study the drug encapsulation potential of OLGA-based NPs, the synthetic glucocorticoid dexamethasone was selected as a model small-molecule hydrophobic drug. Glucocorticoids are highly effective anti-inflammatory and immunosuppressant drugs which find application in a myriad of pathologies including auto-immune diseases, allergies, and cancer.[336] Being a small lipophilic molecule, dexamethasone can permeate the cell membrane, and bind to the glucocorticoid receptors in the cytoplasm to form a complex, which ultimately interacts with the DNA (*so-called* genomic mechanism of action).[337,338] Moreover, dexamethasone can act *via* non-genomic mechanisms comprising the binding to the membrane-associated glucocorticoid receptor present on cells such as T lymphocytes.

Dexamethasone is a poorly soluble molecule with an aqueous solubility of 89 mg/L at 25 °C.[339] To achieve systemic administration, the prodrug dexamethasone sodium phosphate, which is 500x more soluble than dexamethasone, is used.[340] Whilst this approach allows the administration of higher doses with a lower injection volume, the prodrug requires metabolism to yield dexamethasone in its native form and is predicted to showcase a lower permeability through biological membranes.[341]

Besides the prodrug approach, it has been hypothesised that the therapeutic use of glucocorticoids such as dexamethasone could greatly benefit from NP-based

delivery.[342,343] Within the field of polymer-based drug delivery, the encapsulation of dexamethasone within polymeric particles based on PLGA has been reported.[344,345]

In this work, the one-pot encapsulation of dexamethasone during the nanoprecipitation polymerisation of OLGADMAs was targeted. To test the feasibility of the approach, the stability of the dexamethasone molecule under nanoprecipitation polymerisation conditions was initially investigated, due to the presence of potential degradation factors such as the elevated reaction temperature and the presence of radicals as highly reactive species. The following chapter describes the synthesis and analysis of dexamethasone-loaded NPs and the comparison against dexamethasone-loaded PLGA-based NPs. The chapter concludes with a discussion of further examples of OLGA-based NPs prepared in the presence of small-molecule drugs such as betamethasone, prednisolone, and XBD173.

4.2 Initial Work Towards Dexamethasone-loaded OLGA-based Nanoparticles

4.2.1 Stability of Dexamethasone Under Reaction Conditions

The stability of dexamethasone under nanoprecipitation polymerisation conditions (70 °C in the presence of AIBN) was investigated to ascertain the feasibility of a one-pot NP formation and drug encapsulation approach. To this end, dexamethasone was subjected to typical nanoprecipitation polymerisation conditions in the absence of monomers. As expected, a white precipitate was rapidly formed upon injection of a THF solution containing dexamethasone and AIBN into water at 37 °C, resulting in a transparent supernatant. Subsequently, the sample was subjected to lyophilisation and the resulting powder was analysed by ^{1}H NMR spectroscopy and quantitation of the dexamethasone content. The ^{1}H NMR analysis performed in deuterated acetone revealed the exclusive presence of dexamethasone and AIBN (Figure 37). The quantitation of dexamethasone by UV-Vis spectroscopy revealed a 99% recovery of the drug from the procedure. Taken altogether, a good stability of dexamethasone under reaction conditions was ascertained. Furthermore, it was also confirmed that the presence of AIBN did not interfere with the structure of dexamethasone and the drug remained intact.

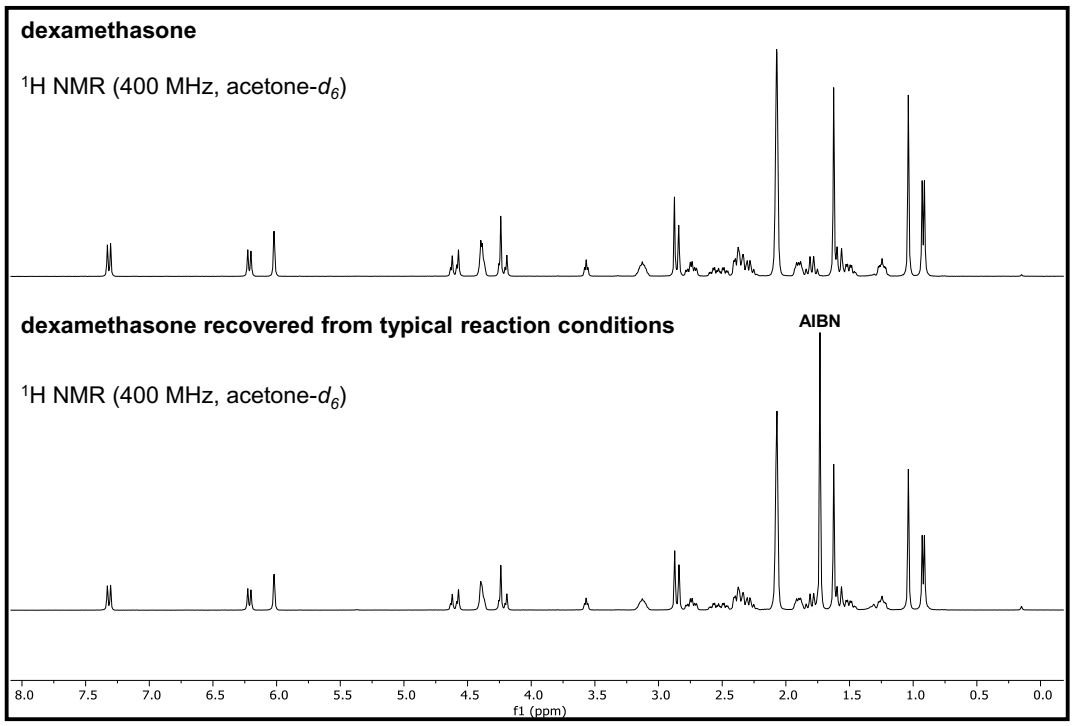


Figure 37. ^{1}H NMR (400 MHz, acetone-d_6) spectra of dexamethasone (above) and the powders obtained from subjecting dexamethasone to nanoprecipitation polymerisation conditions in the absence of monomers (below).

Whilst this type of experiment allowed us to ascertain the stability of dexamethasone in the presence of AIBN at 70 °C, a further investigation on the stability of the drug in the presence of the polymerising monomers is required to unequivocally confirm the integrity of the total amount of drug encapsulated within the NPs described in the following sections. This may be achieved via experiments involving the total degradation of the prepared drug-loaded OLGA-based NPs and the subsequent qualitative and quantitative characterisation of the released drug.

4.2.2 Optimisation of the Nanoprecipitation Polymerisation of **OLGADMA 4Aa** in the Presence of Dexamethasone

Having verified the stability of dexamethasone under typical reaction conditions and in the absence of polymerisable monomers it was considered imperative to confirm the ability to synthesise NPs with the drug present in the reaction mixture since such an experimental configuration was hypothesised to enable the NP formation and drug encapsulation in a single step.

For this purpose, a series of nanoprecipitation polymerisation reactions involving **OLGADMA 4Aa** performed in the presence of dexamethasone concentrations ranging from 10 wt% to 100 wt% of the monomer feed were conducted (Table 14). The resulting crude mixtures were subjected to standard purification procedures via centrifugal filtration, followed by separation of the cloudy supernatant from any sedimented residue eventually present on the bottom of the centrifugal filter. Aqueous NP suspensions were obtained from the nanoprecipitation polymerisation of **OLGADMA 4Aa** in the presence of dexamethasone at a concentration equal to 10 wt% and 25 wt% of the monomer feed. Notably, these experiments yielded suspensions which still contained particles larger than 1μm and were subjected to an additional purification step via syringe filtration. Expectedly, the estimated NP yields obtained via these experiments were considerably lower than those typically obtained in the absence of dexamethasone (~20%).

Additionally, when the concentration of dexamethasone was further increased to 37.5 wt%, 50 wt%, and 100 wt% of the monomer feed, large particles could be detected within the reaction mixture by visual inspection and DLS analysis. A further syringe filtration step was employed to remove the large particles within these samples, yielding transparent liquids characterised by scattering intensities comparable to that of filtered deionised water and containing a negligible quantity of solids. Therefore, such experiments were deemed unsuccessful in providing suitable NP suspensions.

Monomer composition*	Dexamethasone (wt% of monomer feed)	NP Suspension Obtained	Estimated NP Yield** (%)	z-average (nm)	PI
A	10	Yes	8	259.6	0.04
A	25	Yes	6	318.2	0.26
A	37.5	-	-	-	-
A	50	-	-	-	-
A	100	-	-	-	-
B	37.5	Yes	40	279.1	0.06
B	50	Yes	31	316.0	0.14
B	100	-	-	-	-

Table 14. Selected examples of experiments involving the encapsulation of dexamethasone under nanoprecipitation polymerisation conditions involving **OLGADMA 4Aa** and mixtures of **OLGADMA 4Aa** and PEGDA700. *A = **OLGADMA 4Aa**, B = **OLGADMA 4Aa** and PEGDA700 (1:1 ratio by weight). The optimal reaction composition is highlighted in blue. **Calculated as the ratio of the mass of the powders obtained via lyophilisation of the aqueous suspensions and the cumulative mass of **OLGADMA 4Aa**, PEGDA700 and dexamethasone employed for the experiment, expressed as a percentage.

Notably, when the monomer composition was modified from **OLGADMA 4Aa** to a mixture of **OLGADMA 4Aa** and **PEGDA700** (1:1 ratio by weight), a higher concentration of dexamethasone could be tolerated by the reaction system without inducing detrimental effects to the NP yield. Specifically, NP suspensions could be obtained in the presence of dexamethasone at a concentration of 37.5 wt% and 50 wt% of the monomer feed with estimated yields of 40% and 31% respectively. Moreover, the experiment involving dexamethasone at a concentration of 37.5% allowed the isolation of a suspension in which large particle contaminants were undetectable by DLS.

Given the results presented above, the use of the **OLGADMA 4Aa** and PEGDA700 mixture in combination with dexamethasone at a concentration of 37.5 wt% of monomers was identified as the optimal reaction composition for the synthesis of dexamethasone-loaded OLGA-based NPs and as such was employed as the preferred encapsulation method throughout the rest of this work.

4.2.3 Size-modulation of Dexamethasone-loaded Nanoparticles

The ability to tune the size of drug-loaded NPs is highly desirable for drug delivery applications as the NP size parameter assumes a critical role in many interactions of NPs with the biological milieu including vascular distribution, extravasation, binding to cells, cellular uptake, and intracellular trafficking.[346]

In this work, a dependence of the size of the prepared dexamethasone-loaded OLGA-based NPs on the duration of the nitrogen gas purging step of the standard procedure was identified. Particularly, it was ascertained that subjecting the reaction to longer purging durations induced the formation of smaller NPs. The potential explanation of this effect could be found in the decrease of the reaction mixture temperature evoked by purging the reaction mixture with N_2 at room temperature, an increased surface area of liquid available for THF evaporation, or a combination of these factors.

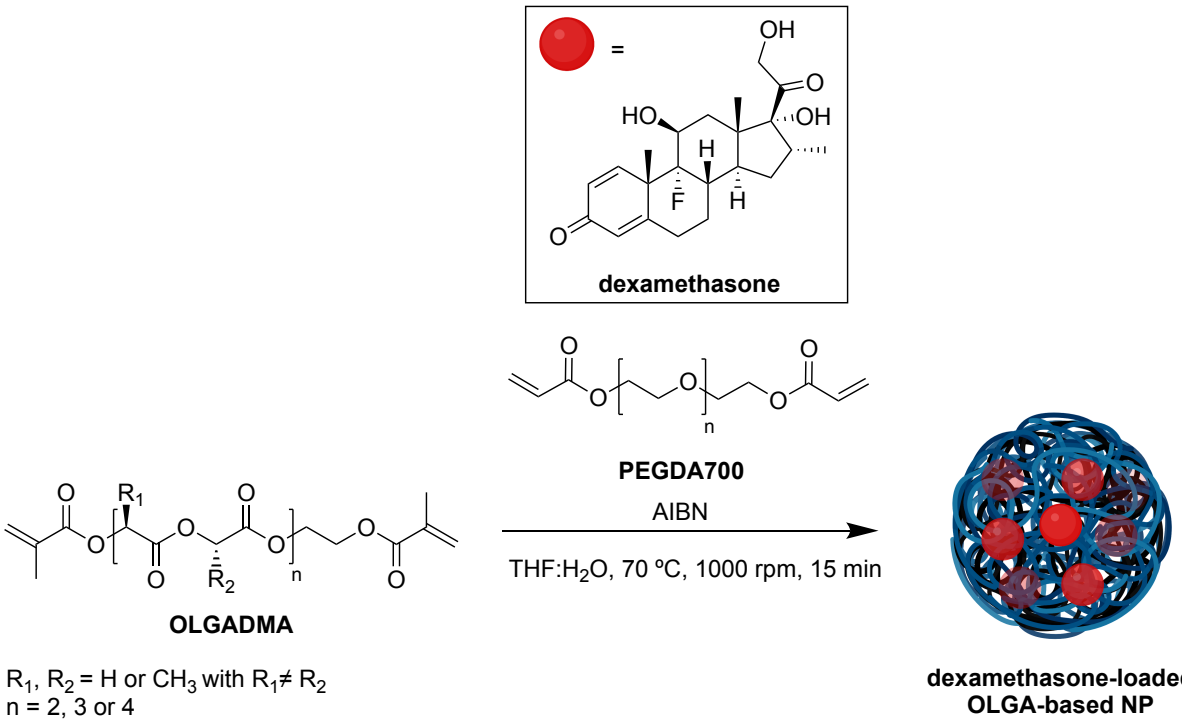
Dexamethasone-loaded NPs with sizes ranging from 104.9 ± 1.4 nm to 313.1 ± 7.0 nm were prepared using **OLGADMA 4Aa** and PEGDA700 and by subjecting the reaction mixture to a series of purging step durations, whilst maintaining constant the remaining reaction variables (Table 15). Expectedly, the duration of the purging time also affected the EE. Particularly, the highest EE was observed by limiting the purging step to a 5-minute window, whilst performing the purging step throughout the experiment halved the EE.

N_2 purge duration (min)	Z-average (nm ± SD)	PI ± SD	ζ-potential (mV ± SD)	EE (%)
0	313.1 ± 7.0	0.15 ± 0.02	-48.4 ± 1.3	66.6
1	303.1 ± 5.1	0.13 ± 0.02	-32.9 ± 0.1	70.0
5	279.1 ± 2.5	0.06 ± 0.05	-37.000 ± 0.001	72.4
10	178.4 ± 1.0	0.19 ± 0.06	-45.0 ± 0.8	54.6
15	104.9 ± 1.4	0.17 ± 0.04	-37.9 ± 1.4	36.3

Table 15. Analysis of dexamethasone-loaded NPs prepared via the nanoprecipitation polymerisation of **OLGADMA 4Aa** and PEGDA700, subjected to a variable duration of the N_2 gas purging step. The optimal N_2 purge duration is highlighted in blue. PI = polydispersity index, EE = encapsulation efficiency.

4.3 Standard Procedure for the Synthesis of Dexamethasone-Loaded OLGA-based Nanoparticles and Naming Conventions

The dexamethasone-loaded OLGA-based NPs presented in the following section were prepared using the standard procedure presented in Scheme 28. To this end, OLGADMAs and PEGDA700 are employed in a 1:1 ratio by weight, in the presence of dexamethasone at a fixed concentration equal to 37.5 wt% of the monomer feed.



Scheme 28. Standard procedure for the preparation of dexamethasone-loaded OLGA-based NPs. OLGADMA (40 wt%), PEGDA700 (40 wt%), AIBN (20 wt%), THF:H_2O (1:3), dexamethasone (37.5 wt% of monomer feed).

The dexamethasone-loaded OLGA-based NPs presented in the following section are denoted with alphanumerical code consisting of "DNP", followed by the type of OLGADMA employed for the synthesis of the NP. For instance, dexamethasone-loaded NPs prepared according to Scheme 28 and employing **OLGADMA 4Aa** will be denoted with **DNP4Aa**.

4.4 Synthesis and Analysis of DNP4Aa

The NPs **DNP4Aa** were synthesised from **OLGADMA 4Aa** using the standard procedure presented in the previous section, followed by a purification procedure via centrifugal filtration. The obtained NPs were analysed via DLS, ELS, TEM, and FTIR spectroscopy. Additionally, the sample was subjected to the determination of the EE and the estimation of the LE.

The DLS analysis of the aqueous suspension containing **DNP4Aa** revealed the presence of NPs with a size of 279.1 nm ± 2.5 nm expressed as z-average, having an intensity-weighted size distribution shown in Figure 38A. Furthermore, the PI value was 0.06 ± 0.05, indicating a sample with a narrow size distribution. The ζ-potential of **DNP4Aa** measured in deionised water was negative, having a value of -37.0 mV (Figure 38B). Compared to its analogue **NP4Aa** prepared in the absence of dexamethasone and presented in Chapter 3, **DNP4Aa** showcased a larger size, lower PI value, and a slightly more positive ζ-potential value.

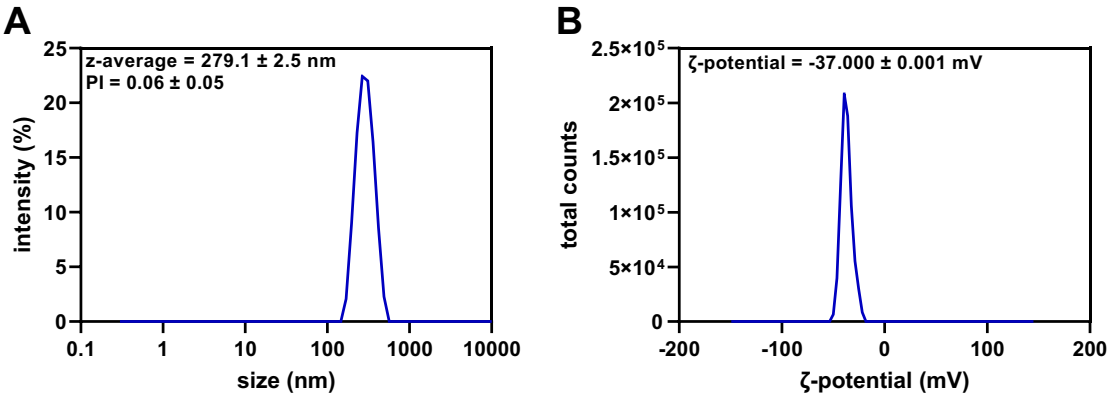


Figure 38. DLS and ELS analysis of **DNP4Aa**. A) intensity-weighted size distribution, and B) ζ-potential distribution in deionised water of **DNP4Aa**.

To further analyse **DNP4Aa**, the sample was visualised via TEM. The analysis revealed the presence of NPs having a spherical morphology as shown in Figure 39.

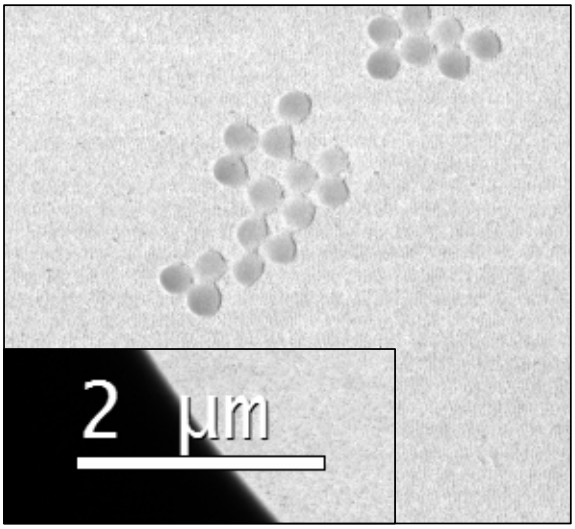


Figure 39. TEM micrograph of **DNP4Aa** (2000×, scale bar = 2 µm) showing the presence of uniform spherical NPs.

The lyophilisation of the aqueous suspension containing **DNP4Aa** afforded a white powder which was analysed via FTIR spectroscopy to investigate the chemical composition of the sample. The comparison of the FTIR spectrum of dexamethasone and **DNP4Aa** in powder form revealed the presence of vibrational bands in the OH, C=O, and C=C stretching regions of the NP spectrum which were suggestive of the presence of dexamethasone (Figure 40). Specifically, the band visible at 1662 cm^{-1} in the FTIR spectrum of **DNP4Aa** was assigned to the C=O stretch of the conjugated ketone of dexamethasone, whilst the bands at 1620 cm^{-1} and 1602 cm^{-1} were assigned to the C=C stretches of the conjugated trisubstituted and disubstituted double bonds of dexamethasone respectively. Additionally, the presence of dexamethasone in **DNP4Aa** was substantiated by the presence of a broad band visible in the OH stretch region which was assigned to the alcohol groups of dexamethasone. Moreover, the FTIR analysis of **DNP4Aa** confirmed the presence of a single vibration band at 1746 cm^{-1} which was assigned to the ester C=O stretch of the polymer portion of the NPs and appeared to partially obscure the C=O stretch band of the unconjugated ketone of dexamethasone, visible at 1700 cm^{-1} in FTIR spectrum of the free drug.

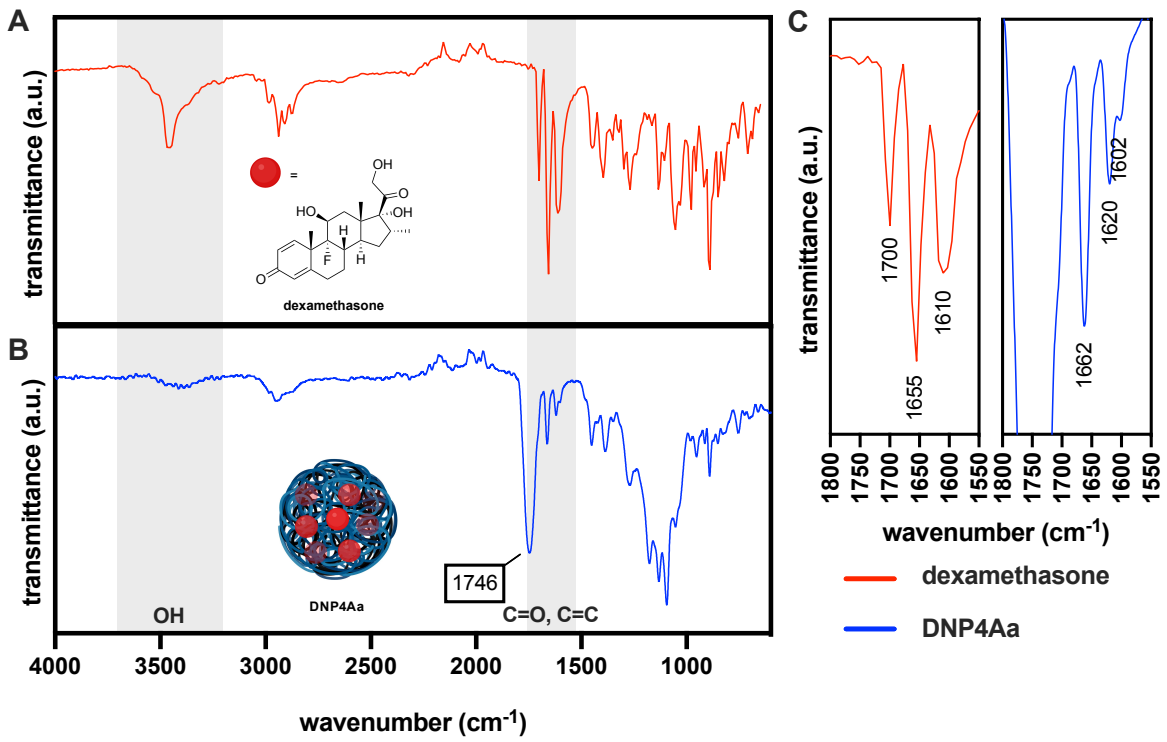


Figure 40. ATR FTIR spectra of dexamethasone and **DNP4Aa**. A) dexamethasone, B) **DNP4Aa**, and C) sections of FTIR spectra showing the region between 1550 cm^{-1} and 1800 cm^{-1}. The OH, C=O, and C=C stretching regions of the spectra are highlighted in grey.

The encapsulation efficiency (EE) of **DNP4Aa** was determined via the quantitation of unencapsulated dexamethasone by UV-Vis spectroscopy and amounted to 69.7%. The loading efficiency (LE) of **DNP4Aa,** estimated as the ratio of the dexamethasone content of the suspension and the total mass of the NPs measured upon lyophilisation, amounted to 47.8%.

4.5 Synthesis and Analysis of a Library of Dexamethasone-Loaded OLGA-based Nanoparticles

The synthesis of a library of dexamethasone-loaded OLGA-based NPs was attempted following the standard procedure for the synthesis of dexamethasone-loaded OLGA-based NPs and employing eight types of OLGADMAs presented in Chapter 2. The desired NP suspensions were successfully obtained from the reaction of six OLGADMAs (Table 16). Contamination with large particles was detected in the suspension of **DNP4Ab** which therefore subjected to an additional purification step via syringe filtration. **DNP4Bb** was isolated as the most concentrated suspension, whilst the reactions involving **OLGADMA 6B** and **OLGADMA 8B** yielded diluted NP suspensions.

NP suspension	OLGADMA monomer	Filtration required	Estimated Yield* (%)
DNP4Aa	**4Aa**	No	40
DNP4Ab	**4Ab**	Yes	31
DNP4Bb	**4Bb**	No	54
DNP6A	**6A**	No	25
DNP6B	**6B**	No	4
DNP8B	**8B**	No	3

Table 16. List of dexamethasone-loaded OLGA-based NPs synthesised in this work. *Calculated as the ratio of the mass of solids obtained by lyophilisation of the NP suspensions and the cumulative mass of OLGADMA, PEGDA700, and dexamethasone used in the experiment, expressed as a percentage.

As expected, reactions involving **OLGADMA 4Ba** and **OLGADMA 8A** failed to yield NP suspensions. Analogously to the findings detailed in Chapter 3, these reactions yielded a non-dispersible white precipitate and a transparent supernatant.

The prepared NPs were subjected to DLS, ELS, EE, and LE analysis (Table 17). The size of the NPs expressed as z-average ranged between 199.2 $\pm$ 5.7 and 320.9 $\pm$ 10.3

nm with PI values below 0.4. NPs prepared using tetramer OLGADMAs presented lower PI values indicating a narrower size distribution. The ζ-potential of the NPs was negative in deionised water, having values below -30 mV. The estimation of the encapsulation efficiency revealed values between 38.7% and 69.7%. The loading efficiencies were estimated to be between 22.6% and 59.1%.

As presented in Table 17, the size of dexamethasone-loaded OLGA-based NPs was generally higher than that of analogous empty OLGA-based NPs, except for **DNP4Bb** and **DNP6A** which were smaller. A possible explanation for these discrepancies might reside in a differential extent of a hypothetical effect of the drug on the rate of polymerisation of structurally diverse OLGADMAs, and/or different internal structures of the prepared NPs resulting from different polymer-drug interactions.

NPs	z-average (nm ± SD)	PI ± SD	ζ-potential (mV ± SD)	EE (%)	Estimated LE (%)	z-average of empty NPs* (nm ± SD)
DNP4Aa	279.1 ± 2.5	0.06 ± 0.05	-37.000 ± 0.001	69.7	47.8	227.9 ± 2.0
DNP4Ab	292.8 ± 9.6	0.08 ± 0.09	-39.33 ± 1.40	66.4	59.1	235.8 ± 0.7
DNP4Bb	320.9 ± 10.3	0.15 ± 0.02	-39.68 ± 0.40	45.2	22.6	366.0 ± 6.2
DNP6A	199.2 ± 5.7	0.19 ± 0.02	-48.76 ± 1.40	44.9	49.0	240.3 ± 5.1
DNP6B	251.0 ± 7.6	0.24 ± 0.05	-33.89 ± 1.25	54.5	49.0	171.70 ± 2.25
DNP8B	298.5 ± 7.4	0.35 ± 0.03	-30.910 ± 0.004	38.7	34.9	188.4 ± 3.8

Table 17. Analysis of the library of dexamethasone-loaded OLGA-based NPs synthesised in this work. *Size of empty OLGA-based NP expressed as z-average and described in Chapter 3.

Following the successful synthesis of a library of dexamethasone-loaded OLGA-based NPs, it was considered of interest to compare the properties of these NPs with those of dexamethasone-loaded PLGA-based NPs. The following section describes the preparation and analysis of dexamethasone-loaded PLGA-based NPs, followed by a comparative drug release study *in vitro*.

4.6 Synthesis and Analysis of Dexamethasone-loaded PLGA-based Nanoparticles

Control dexamethasone-loaded PLGA-based NPs were prepared using three types of PLGA polymers under conditions that mirrored the nanoprecipitation polymerisation reaction and conducted in the absence of AIBN (Table 18). For this purpose, **PLGA** and **PLGA-PEG** were obtained from commercial sources, whilst sequenced PLGA (**PLGA alt**) was synthesised according to established procedures, as detailed in Chapter 3.[326]

Nanoparticle	PLGA form used for preparation	Filtration required	Estimated Yield* (%)
DNP-PLGA	**PLGA**	yes	33
DNP-PLGA alt	**PLGA alt**	yes	32
DNP-PLGA-PEG	**PLGA-PEG**	no	79

Table 18. List of dexamethasone-loaded PLGA-based NPs prepared in this work. *Calculated as the ratio of the mass of solids obtained by lyophilisation of the NP suspensions and the cumulative mass of PLGA polymer, and dexamethasone, expressed as a percentage.

Consistently with the observations regarding PLGA-based NPs presented in Chapter 3, the preparation of **DNP-PLGA** and **DNP-PLGA alt** yielded suspensions containing large particles detected by DLS and required a further filtration step to achieve suitable samples. Conversely, **DNP-PLGA-PEG** was directly obtained as a homogeneous NP suspension. **DNP-PLGA-PEG** was obtained as the most concentrated suspension, whilst **DNP-PLGA** and **DNP-PLGA alt** were more diluted.

The analysis of dexamethasone-loaded PLGA-based NPs prepared in this work is presented in Table 19. Compared to dexamethasone-loaded OLGADMA-based NPs, PLGA-based NPs exhibited a smaller size, whilst the ζ-potential was comparatively negative in deionised water. The EE of **DNP-PLGA** and **DNP-PLGA alt** was lower than that of OLGADMA-based NPs, whilst a higher EE was achieved with **DNP-PLGA-**

PEG. The estimated LE of PLGA-based NPs was generally lower than that of OLGA-based NPs, except for **DNP4Bb**.

Nanoparticle	z-average (nm ± SD)	PI ± SD	ζ-potential (mV ± SD)	EE (%)	Estimated LE (%)
DNP-PLGA	95.5 ± 1.5	0.10 ± 0.02	-43.13 ± 0.87	30.0	25.0
DNP-PLGA (alt)	160.9 ± 2.8	0.09 ± 0.03	-35.60 ± 2.40	36.0	23.0
DNP-PLGA-PEG	111.0 ± 2.4	0.23 ± 0.06	-20.46 ± 1.90	74.5	25.5

Table 19. Analysis of dexamethasone-loaded PLGA-based NPs prepared in this work.

4.7 Comparative Drug Release Study

The library of dexamethasone-loaded NPs was screened in terms of their ability to release the encapsulated dexamethasone when subjected to a predetermined set of experimental conditions. The aim of this study was to:

(i) compare the drug release of OLGA-based NPs against PLGA-based NPs, as an established class of NPs for drug delivery applications,
(ii) identify potential differences in drug release among the prepared types of OLGA-based NPs.

In summary, dexamethasone-loaded NPs were subjected to an adaptation of the "sample and separate" method which consisted of the incubation of aqueous NP suspensions within centrifugal filters at 37 °C, followed by centrifugation, re-suspension, and quantitation of the dexamethasone content of the filtrates at different time points. This procedure was performed hourly over the first five hours of the study (phase 1), followed by daily intervals (phase 2). The experiment was performed over the course of a 7-day period.

Expectedly, the release of dexamethasone from PLGA-based NPs under experimental conditions revealed substantial differences between the PEGylated and the non-PEGylated NPs (Figure 41). Particularly, **DNP-PLGA-PEG** released dexamethasone at a higher rate than **DNP-PLGA** and **DNP-PLGA alt** throughout the study. Notably, **DNP-PLGA-PEG** NPs were able to release 3% to 23% of the encapsulated

dexamethasone daily, whilst **DNP-PLGA** and **DNP-PLGA alt** were releasing 0.1% to 16% and 0.1% to 12% respectively. Importantly, the cumulative release of dexamethasone over 7 days under experimental conditions was the highest for **DNP-PLGA-PEG** (56%), followed by **DNP-PLGA** (18%), and **DNP-PLGA alt** (13%).

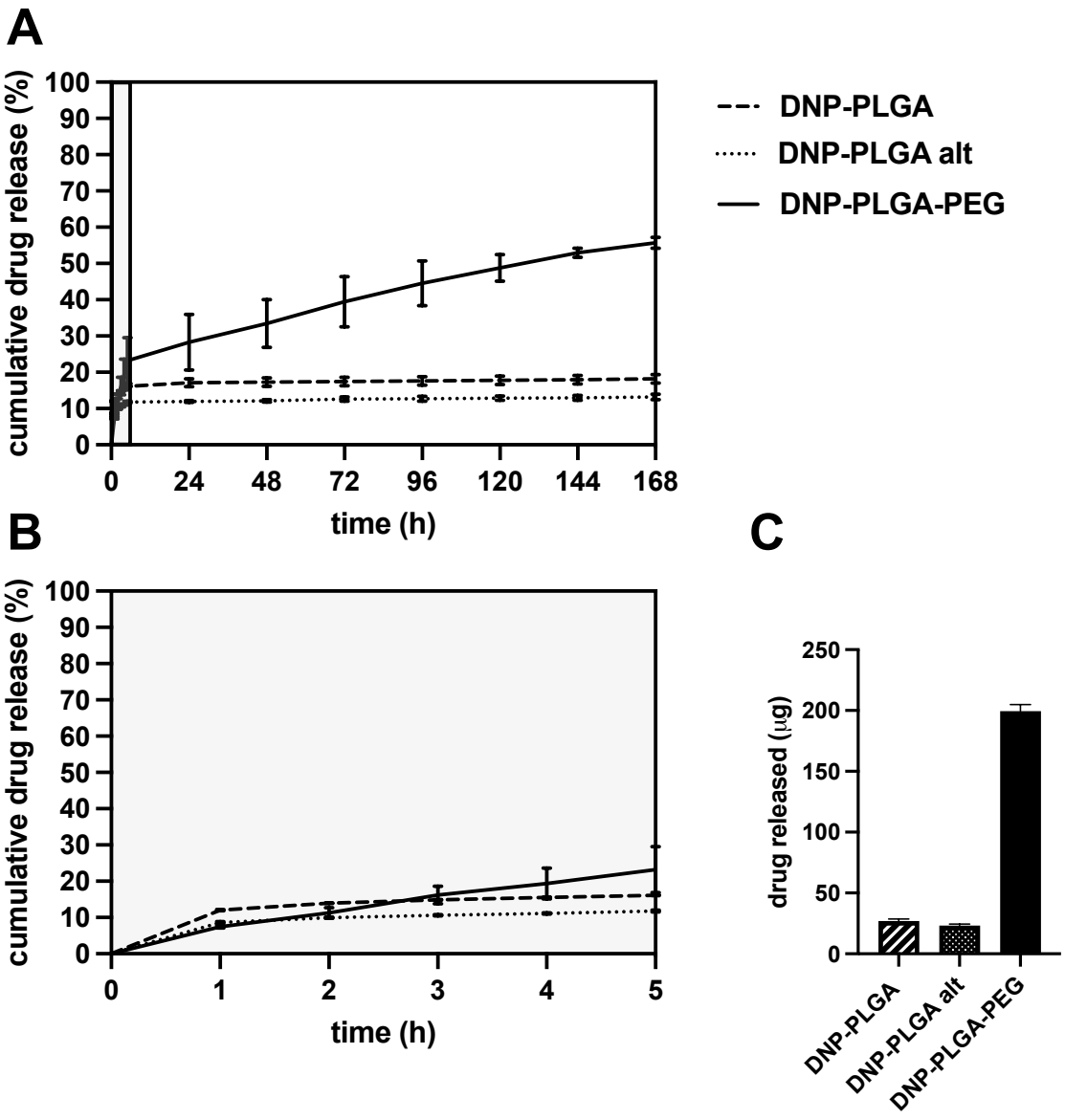


Figure 41. Cumulative release of dexamethasone from dexamethasone-loaded PLGA-based NPs **DNP-PLGA**, **DNP-PLGA alt**, and **DNP-PLGA-PEG** prepared in this work, subjected to experimental conditions over 7 days. A) Phase 1 and Phase 2 combined, B) Phase 1, and C) amount of released dexamethasone.

The release of dexamethasone from OLGA-based NPs was followed via an identical procedure (Figure 42). Interestingly, the different types of OLGA-based NPs exhibited a range of cumulative releases of dexamethasone ranging from 7% to 69%, measured after 7 days under the experimental conditions outlined above. **DNP4Bb** released the highest amount of encapsulated dexamethasone, whilst **DNP6B** released the smallest amount. Particularly, samples containing **DNP6B** were releasing between 0.1% and 6% of their dexamethasone content daily, and as such were the slowest-releasing NPs of the entire library of dexamethasone-loaded NPs investigated in this work.

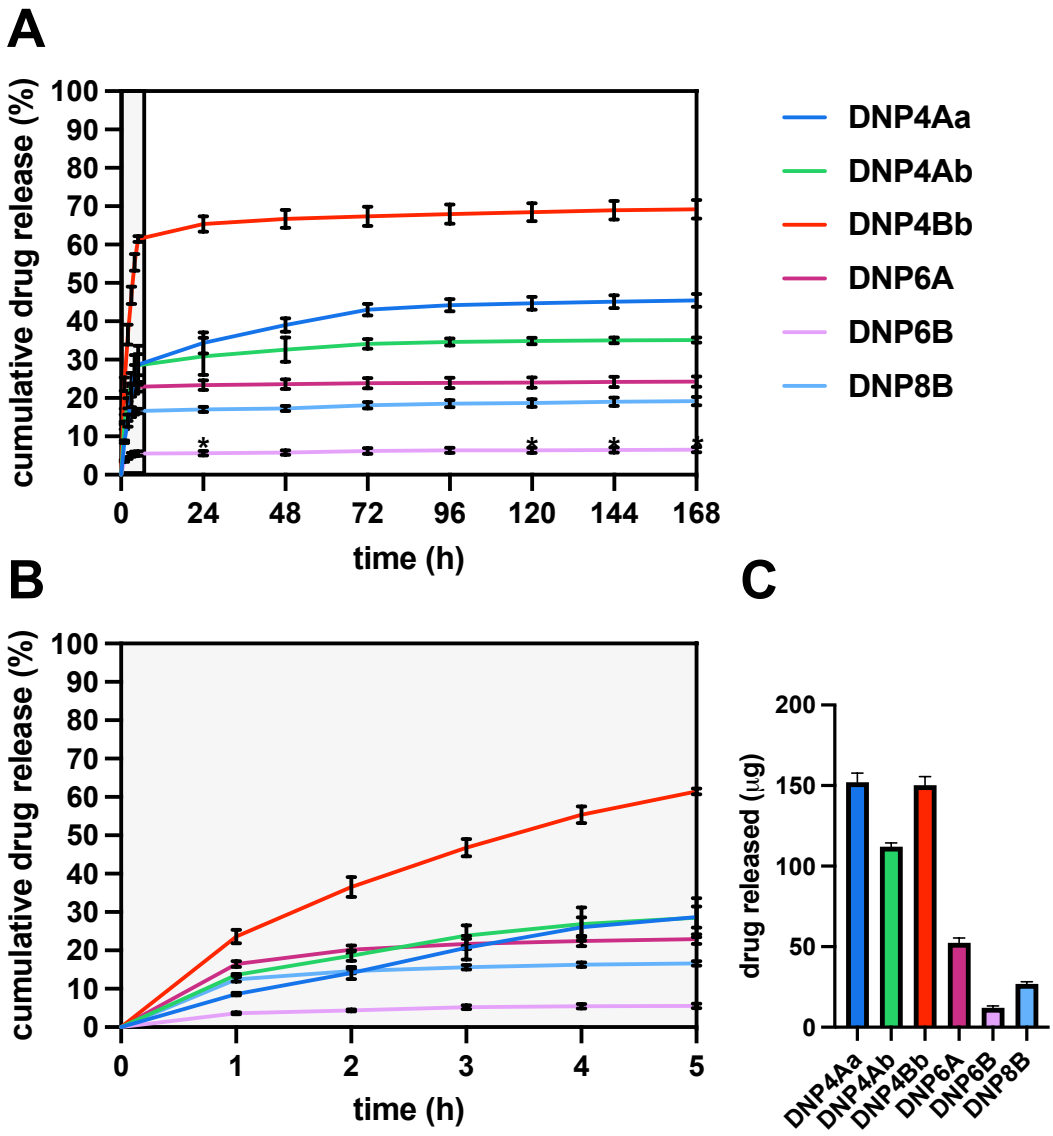


Figure 42. Cumulative release of dexamethasone from dexamethasone-loaded OLGA-based NPs prepared in this work, subjected to experimental conditions over 7 days. A) Phase 1 and Phase 2 combined, B) Phase 1, and C) amount of released dexamethasone. *Dexamethasone concentration below the limit of quantitation (LOQ).

Additionally, the content of the combined filtrates deriving from OLGA-based NPs was tested to establish the chemical composition of the released molecules. The ^{1}H NMR analysis of the combined filtrates established dexamethasone as the only detectable species released by dexamethasone-loaded OLGA-based NPs subjected to the outlined experimental conditions.

4.8 Stability of DNP4Aa, DNP4Ab, and DNP4Bb in Biological Medium

Synthetic chemistries often yield NPs that exhibit instability in biological fluids.[347] For instance, this instability can be evidenced by comparing the stability of NPs in water and a complete cell culture medium, which is a complex mixture containing a significant concentration of electrolytes and proteins. The presence of these species can alter the colloidal stability of NPs, ultimately resulting in profound effects on the behaviour of NPs *in vitro* and *in vivo*.[348] Specifically, NP aggregation *in vitro* can influence factors such as dosimetry, cellular uptake, and toxicity *in vitro*. Comparatively, aggregation of NPs *in vivo* can influence pharmacokinetics, biodistribution, and overall toxicity.

To evaluate the colloidal stability of dexamethasone-loaded OLGA-based NPs in the presence of physiological salts and proteins, **DNP4Aa**, **DNP4Ab**, and **DNP4Bb** were incubated at a temperature of 37 °C as suspensions in (i) deionised water, (ii) Dulbecco's Modified Eagle Medium (DMEM), and (iii) DMEM supplemented with 10% foetal bovine serum (FBS). The NPs were then analysed *via* DLS analysis to determine potential differences in the NP size (Figure 43).

As expected, the NPs suspended in water maintained their initial size, with only slight reductions in their PI after 2 h of incubation a 37 °C. In contrast, incubation in DMEM led to an average increase in size of 80%, alongside an increase in PI values, which is strongly suggestive of NP aggregation. Conversely, incubation in DMEM supplemented with FBS resulted in a minimal NP size increase which was in the range of 4-35 nm, alongside PI values below 0.3. Taken together, it can be hypothesised that the examined NPs rely on electrostatic stabilisation to maintain colloidal stability. This stabilisation is possibly challenged by dispersants having high salt concentrations

such as DMEM. Importantly, this destabilising effect appears to be lessened in the presence of proteins, possibly due to the formation of a stabilising protein corona.

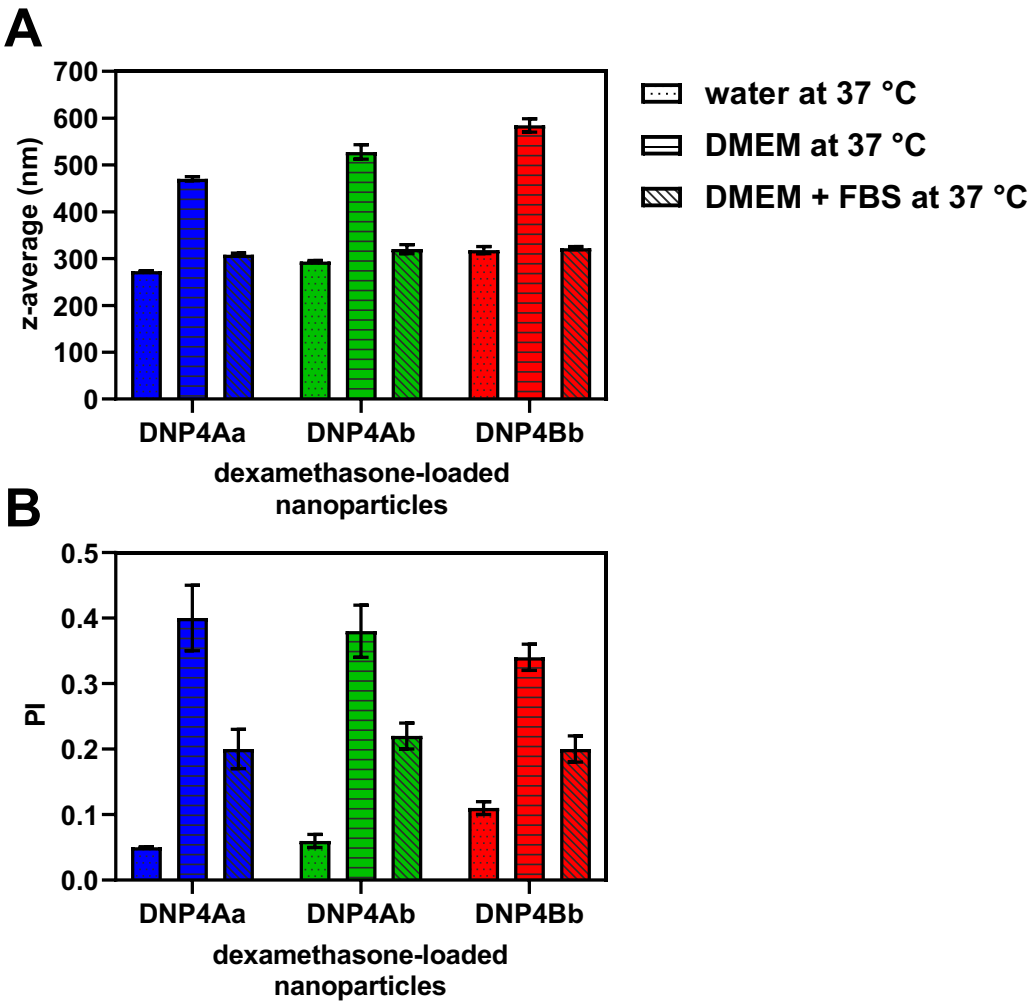


Figure 43. A) size expressed as z-average, and B) PI of **DNP4Aa**, **DNP4Ab**, and **DNP4Bb** after incubation in water, DMEM, and DMEM supplemented with 10% FBS over a period of 2 h.

4.9 Stability of DNP4Aa, DNP4Ab, and DNP4Bb Upon Storage at Room Temperature

Examining the stability of therapeutic NPs under various storage conditions is a crucial aspect of nanomedicine development.[349] For example, NPs loaded with small molecule drugs such as dexamethasone palmitate have been shown to exhibit a gradual size increase upon storage, most likely due to Ostwald ripening.[350]

To assess the colloidal stability of dexamethasone-loaded OLGA-based NPs, aqueous suspensions of **DNP4Aa**, **DNP4Ab**, and **DNP4Bb** were stored at variable room temperature (16-25 °C), exposed to moderate light, and in the absence of mechanical agitation. To this end, NP suspensions in transparent vials were stored on a laboratory bench over a period of 4 weeks. The NP suspensions were gently mixed and analysed by DLS and ELS once weekly (Figure 44).

Throughout the study, **DNP4Aa** and **DNP4Bb** exhibited good stability in terms of NP size with only slight size variations occurring within a 9 nm window, and relatively stable PI values. On the other hand, **DNP4Ab** showed a higher variability with z-average oscillations occurring within a window of 43 nm. Additionally, the PI values of **DNP4Ab** increased after week 2 of incubation however, these were maintained below the 0.4 value throughout the study.

The ELS analysis of the NPs revealed **DNP4Bb** as the most stable in terms of ζ-potential. Conversely, **DNP4Aa** and **DNP4Ab** showed a slight evolution towards more positive ζ-potential values.

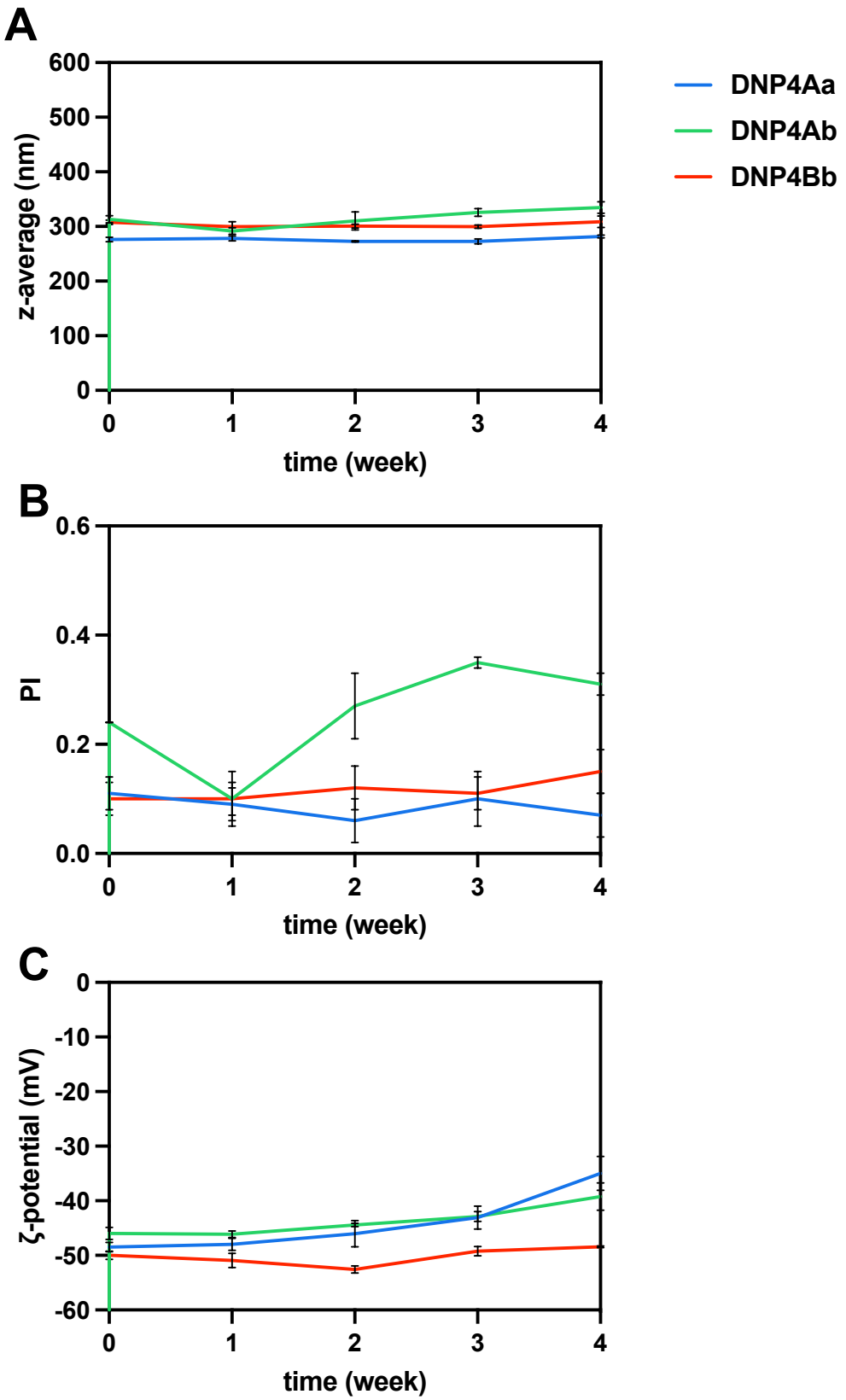


Figure 44. DLS and ELS analysis of aqueous suspensions containing **DNP4Aa**, **DNP4Ab**, and **DNP4Bb** stored at room temperature over a period of 4 weeks. A) size expressed as z-average, B) PI, and C) ζ-potential in deionised water.

4.10 Effect of DNP4Aa, DNP4Ab, and DNP4Bb on Cell Viability *In Vitro*

To evaluate the potential cytotoxic effects of dexamethasone-loaded OLGA-based NPs, viability assessments on HeLa cells following 24 and 48 hours of exposure to aqueous NP suspensions containing different concentrations of **DNP4Aa**, **DNP4Ab**, and **DNP4Bb** were performed (Figure 45). To this end, the Cell counting Kit-8 (CCK-8) assay was used to quantify cell viability. Notably, after incubating HeLa cells with NP suspensions for 24 hours, the normalised cell viability exceeded 90% across the tested NP types and concentrations. Furthermore, no significant decline in cell viability could be detected following a 48-hour incubation period with dexamethasone-loaded NPs.

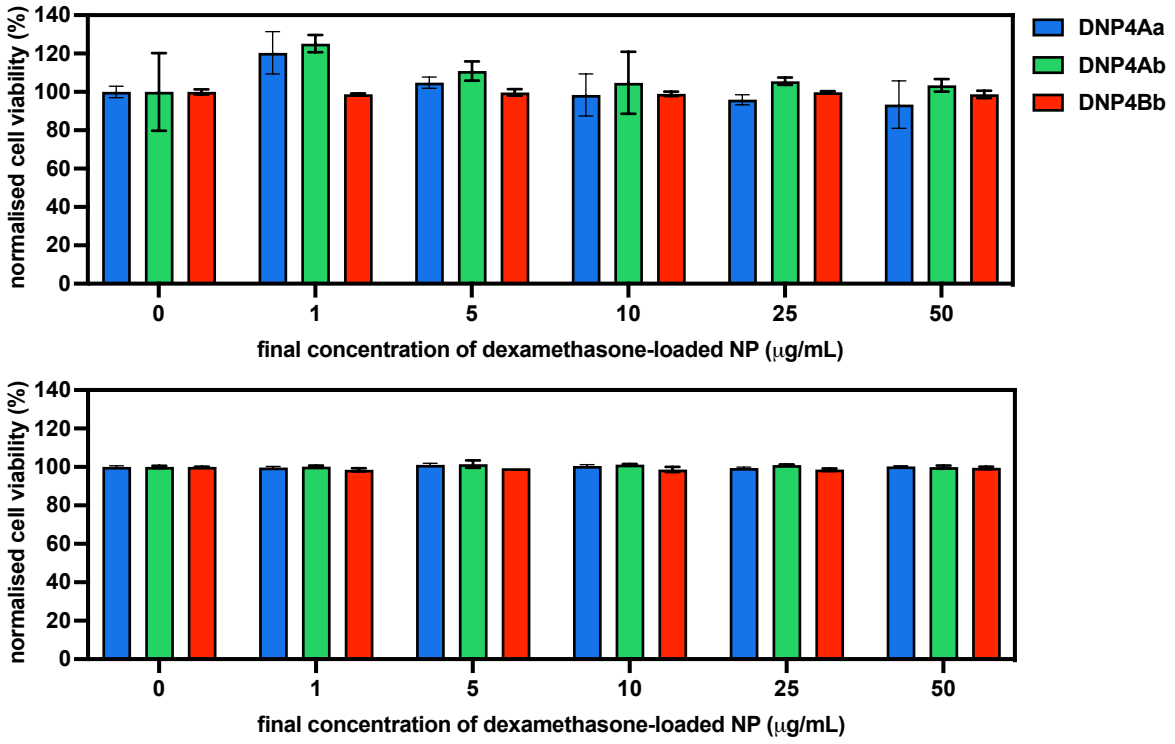


Figure 45. Normalised viability of HeLa cells upon treatment with aqueous suspensions of **DNP4Aa**, **DNP4Ab**, and **DNP4Bb** containing 0.01 – 0.5 mg/mL of NPs over a period of A) 24 h, and B) 48 h.

4.11 Further Observations Regarding Drug-Loaded OLGA-Based Nanoparticles

Having accomplished the synthesis of dexamethasone-loaded OLGA-based NPs, it became imperative to assess the ability to form OLGA-based NPs in the presence of additional types of small-molecule drugs to gain insight into the drug encapsulation versatility of the platform. To this end, nanoprecipitation polymerisations involving **OLGADMA 4Aa** and PEGDA700 were conducted in the presence of betamethasone, prednisolone, and XBD-173. The key findings resulting from these experiments are detailed in the following section.

4.11.1 Comparison of OLGA-based Nanoparticles Loaded with Dexamethasone, Betamethasone, and Prednisolone

To test whether the chemical nature of the drug payload could influence the size, PI, EE, and LE, OLGA-based NPs loaded with betamethasone and prednisolone were prepared from **OLGADMA 4Ab** under standard reaction conditions and compared against **DNP4Ab**. As visible from the chemical structures presented in Figure 46, the three glucocorticoid drugs share many structural similarities, including a four-membered fused ring system, the α,β-unsaturated ketone system, and three hydroxyl groups. Moreover, dexamethasone and betamethasone are epimers, differing only in the absolute configuration of the methyl group attached to the cyclopentane ring. Among the three drugs, prednisolone is the most soluble, followed by dexamethasone, and finally betamethasone.

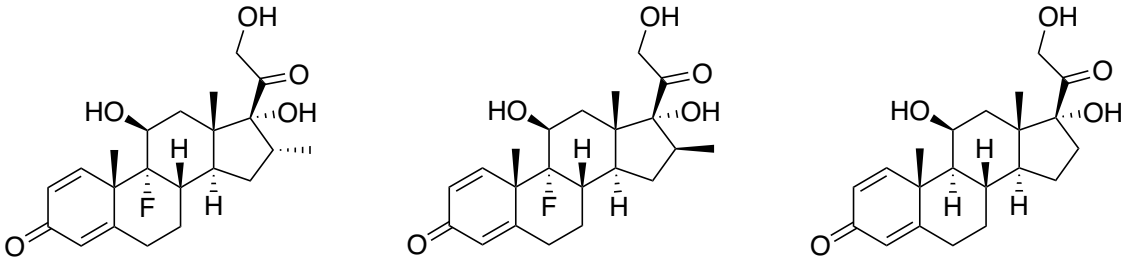


Figure 46. Chemical structure of dexamethasone, betamethasone, and prednisolone, alongside their aqueous solubility at 25 °C.[351]

Importantly, the size of NPs prepared in the presence of the three drugs was markedly different with the reaction involving dexamethasone yielding the smallest NPs and the reaction involving prednisolone yielding the largest NPs (Table 20). Similarly, the EE differed across the three examples. The NPs prepared in the presence of dexamethasone had the highest EE, whilst those prepared in the presence of prednisolone had the lowest EE. This observation has been rationalised in terms of the higher aqueous solubility of prednisolone in comparison to dexamethasone and betamethasone which might be correlated to a higher propensity for the partitioning of the drug to the aqueous phase during the process of NP formation. Surprisingly, regardless of the structural similarity and the low aqueous solubility of dexamethasone and betamethasone, the EE and LE of NPs prepared in the presence of the two drugs were substantially different. This observation could be suggestive of the existence of complex drug-nanoparticle and/or drug-monomer interactions which govern the encapsulation process. Furthermore, these interactions could potentially be influenced by the stereochemistry of the monomers involved in the polymerisation and drug encapsulation process.

Encapsulated drug	z-average (nm ± SD)	PI ± SD	ζ-potential (mV ± SD)	EE (%)	Estimated LE (%)
Dexamethasone	292.8 ± 9.6	0.08 ± 0.09	-39.3 ± 1.4	66.4	59.1
Betamethasone*	440.0 ± 7.0	0.08 ± 0.07	-34.3 ± 0.6	32.7	9.3
Prednisolone*	564.7 ± 17.9	0.34 ± 0.02	-36.1 ± 1.4	3.4	22.1

Table 20. OLGA-based NPs prepared in the presence of dexamethasone, betamethasone, and prednisolone using **OLGADMA 4Ab**. *Experiment and analytical characterisation performed in collaboration with Yicheng Wang and reported in the MSc thesis entitled “Synthesis and evaluation of tacticity defined oligoesters for polymer-based drug delivery applications”.

Given the results presented above, it was hypothesised that the chemical nature of the payload influences the size, EE, and LE of the resulting NPs which might be considered indicative of the existence of complex interactions occurring during the nanoprecipitation polymerisation reaction conducted in the presence of small molecules.

4.11.2 Synthesis of OLGA-based Nanoparticles in the Presence of XBD173

To further test the feasibility of drug encapsulation within OLGA-based NPs, the nanoprecipitation polymerisation of **OLGADMA 4Aa** and PEGDA700 was performed in the presence of the poorly soluble molecule XBD173, a translocator protein (TPSO) ligand explored in preclinical models (Figure 47).[352]

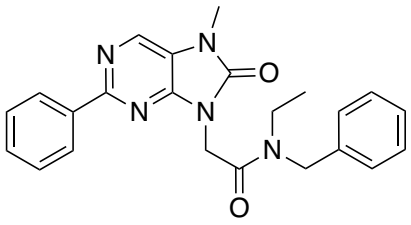


Figure 47. Chemical structure of XBD173, a translocator protein ligand explored in preclinical models.

The nanoprecipitation polymerisation procedure allowed the isolation of NPs having a size of 214.2 ± 5.2 nm alongside a PI of 0.013 ± 0.003, indicating a narrow size distribution (Figure 48A). The ζ-potential of such NPs was negative in deionised water, having a value of -32.86 ± 1.05 mV (Figure 48B). The TEM analysis of the sample confirmed the presence of spherical NPs (Figures 48C and 48D).

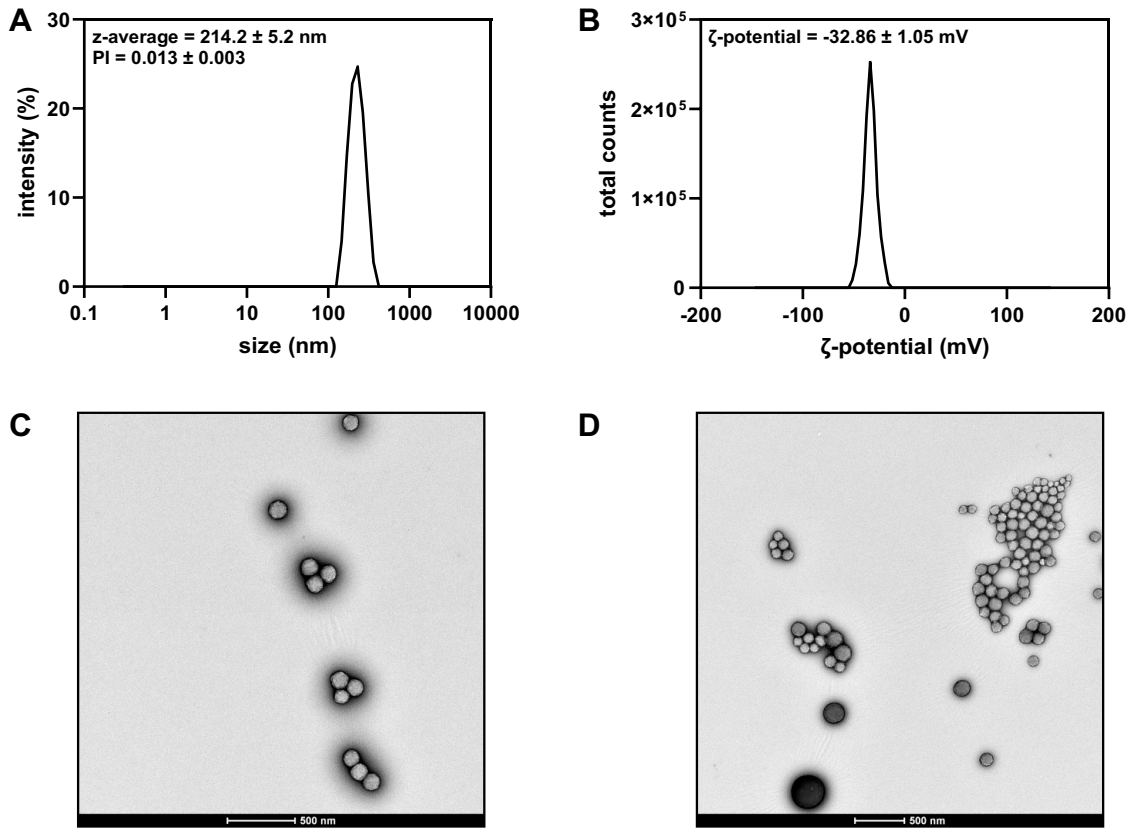


Figure 48. Analysis of NPs prepared via the nanoprecipitation polymerisation of **OLGADMA 4Aa** and PEGDA700, in the presence of XBD173. A) intensity-weighted size distribution, B) ζ-potential distribution in deionised water, C) TEM micrograph (15000×, scale bar = 500 nm, stained with 2% uranyl acetate), D) TEM micrograph (11000×, scale bar = 500 nm, stained with 2% uranyl acetate).

For comparison, the encapsulation of XBD173 within PLGA-based NPs prepared using PLGA-PEG was performed using conditions that mirror the nanoprecipitation polymerisation conditions and conducted in the absence of AIBN. The obtained NPs were smaller than those obtained via the nanoprecipitation polymerisation methodology, with a z-average of 108.5 ± 2.2 nm and a PI of 0.113 ± 0.009 (Figure 49A). The ζ-potential of the NPs was negative, with a value of -39.5 ± 0.7 mV in deionised water (Figure 49B). The TEM analysis of the sample confirmed the presence of spherical NPs (Figures 49C and 49D).

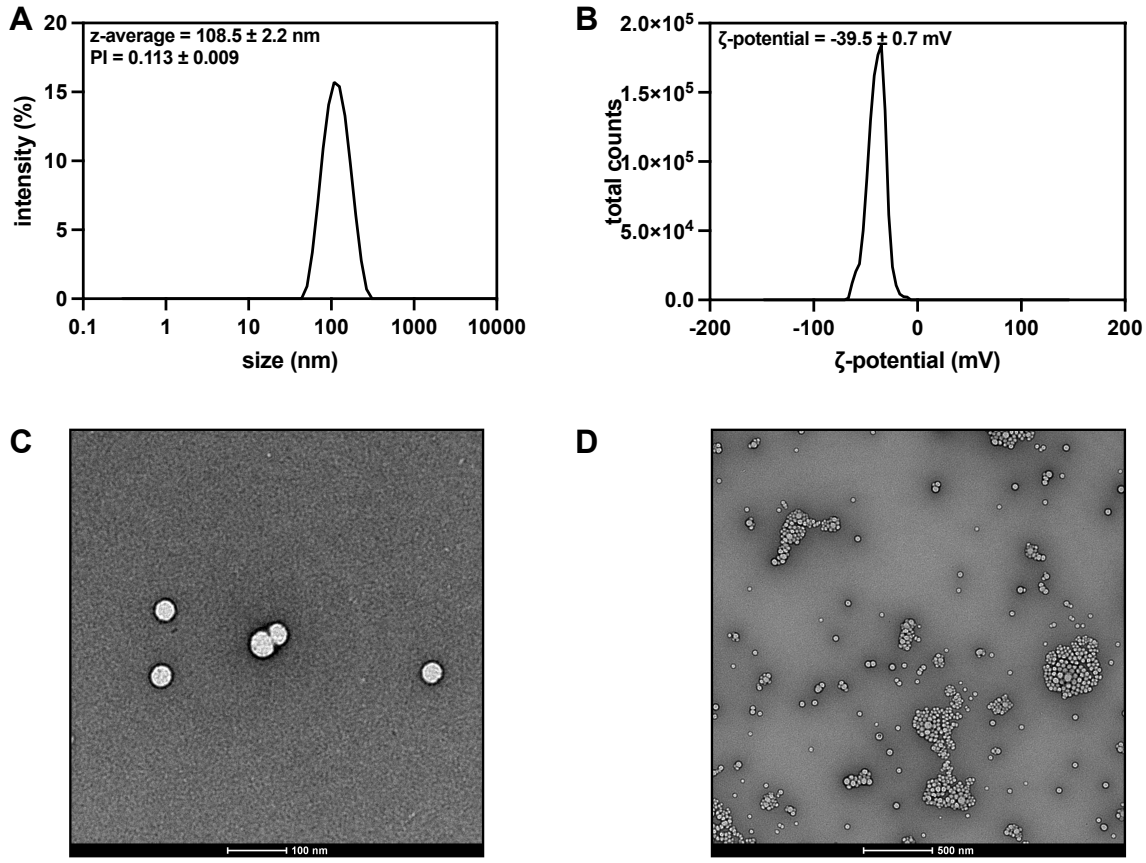


Figure 49. Analysis of PLGA-PEG NPs prepared in the presence of XBD173. A) intensity-weighted size distribution, B) ζ-potential distribution in deionised water, C) TEM micrograph (67000×, scale bar = 500 nm, stained with 2% uranyl acetate), D) TEM micrograph (15000×, scale bar = 500 nm, stained with 2% uranyl acetate).

A comparison of the obtained NP suspensions revealed PLGA-PEG NPs as the more concentrated suspension, and EE values of 11.6% and 10.5% for OLGA-based and PLGA-based NPs respectively (Table 21). Importantly, the estimated LE value for OLGA-based NPs was more than 2.5x higher than that of PLGA-based NPs.

Type of NP	EE (%)	LE (%)	Estimated NP Yield* (%)
OLGA-based	11.6	16.2	11.3
PLGA-based*	10.5	5.7	30

Table 21. EE, LE, and apparent yield of OLGA-based and PLGA-based NPs prepared in the presence of XBD173. *Prepared using the PLGA-PEG form of PLGA.

4.12 Chapter Summary

The encapsulation of dexamethasone within OLGA-based NPs was achieved through a one-pot procedure that enables simultaneous nanoprecipitation polymerisation and drug loading. A library of six types of dexamethasone-loaded OLGA-based NPs was prepared, which presented a higher EE than **DNP-PLGA** and **DNP-PLGA alt** prepared *via* a mirrored procedure. Moreover, the estimated LE of OLGA-based NPs was comparable to or higher than that of PLGA-based NPs.

The investigation of the drug release from NPs prepared from PLGA, PLGA alt, and PLGA-PEG revealed substantial differences in the rate of drug release and cumulative drug release, with DNP-PLGA-PEG releasing dexamethasone more rapidly than NPs based on non-PEGylated PLGA. Comparatively, OLGA-based NPs showcased the ability to release a variable fraction of the encapsulated dexamethasone over 7 days *in vitro*. Notably, the NPs could release between 7% and 69% of their dexamethasone content, possibly depending on the type of OLGADMA used for NP synthesis.

The dexamethasone-loaded NPs prepared from tetramer OLGADMAs exhibited excellent size-stability in protein-containing biological medium and could be stored at room temperature as aqueous suspensions for up to four weeks without suffering drastic variations of the NP size and ζ-potential. Additionally, these NPs demonstrated a minimal detrimental effect on the viability of HeLa cells upon 24 h and 48 h of *in vitro* treatment.

The final section of this chapter contains work aimed towards a further understanding of the drug encapsulation performance of OLGA-based NPs, performed *via* the synthesis and analysis of NPs prepared in the presence of betamethasone, prednisolone, and XBD173.

Chapter 5: Work Towards Stimuli-Responsive Crosslinked Polymeric Nanoparticles

5.1 Introduction

Having established the synthesis of crosslinked polymeric NPs from polymerisable compounds containing the PLGA and PEG chemical motifs, it was hypothesised that the developed synthetic platform based on the polymerisation of divinyl compounds could also be exploited to polymerise building blocks containing reactive moieties such as disulphides and diselenides. This would enable synthetic access to stimuli-responsive NPs which are potentially capable of stable encapsulation of therapeutic payloads and the triggered release of the payload upon interaction with reducing agents and oxidants.

The following chapter describes the synthesis of a disulphide-containing NP building block, its polymerisation and NP formation, and the preliminary evaluation of the stability of the resulting NPs in the presence of glutathione *in vitro*. The final section describes the evaluation of the stability of L-selenocystine in the presence of hydrogen peroxide, the synthesis of a diselenide-containing dimethacrylate prepared from L-selenocystine and concludes with the proposal of two strategies for the synthesis of diselenide-containing crosslinked polymeric NPs.

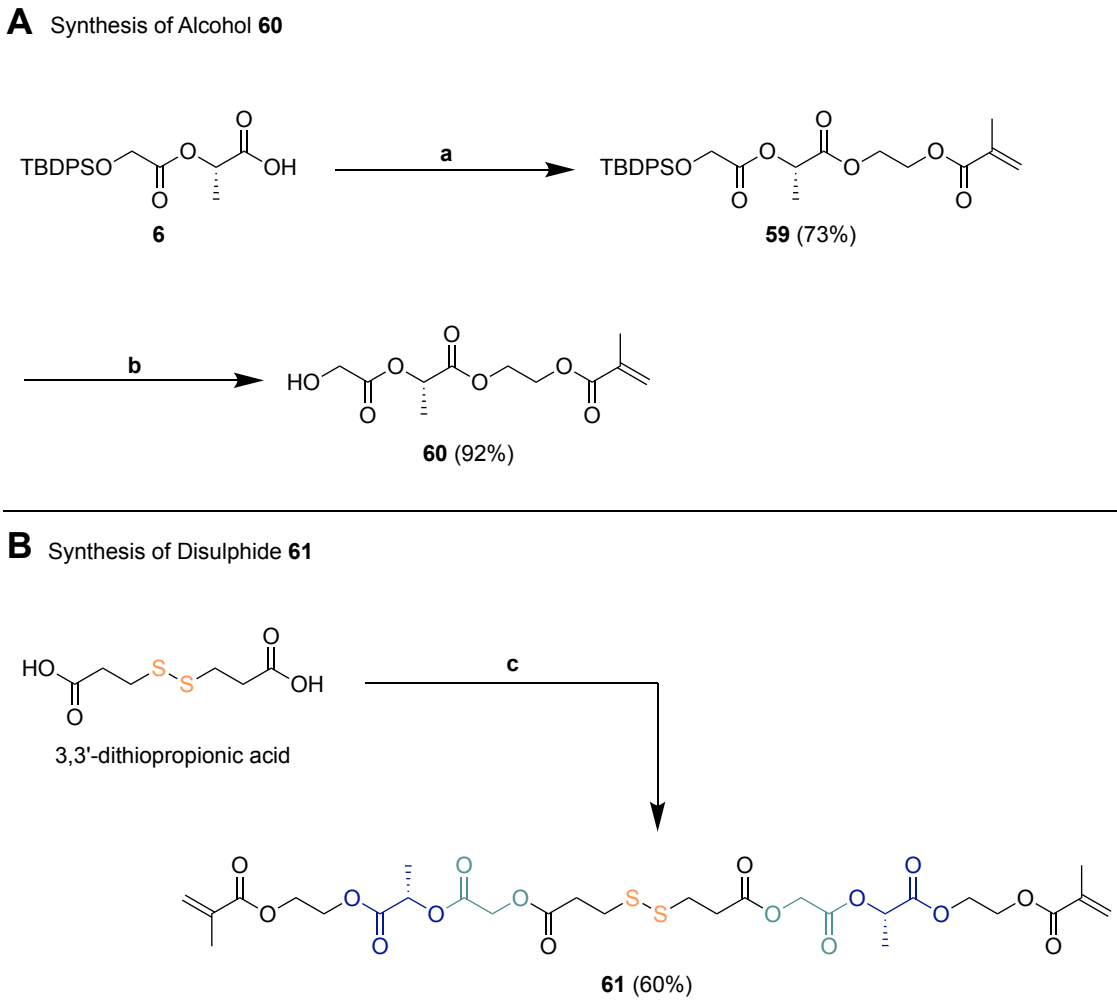
5.2 Work Towards Disulphide-Containing Crosslinked Polymeric Nanoparticles

The integration of disulphide linkages within OLGA-based NPs was identified as a critical advancement in the ongoing development of the OLGA-based nanoplatform towards potential drug delivery applications. Specifically, OLGA-based NPs comprising disulphide linkages could be able to maintain an elevated level of stability in extracellular environments, possibly superior to well-established nanocarriers such as PLGA-PEG micelles, whilst still retaining rapid degradation characteristics, typical to disulphide-containing NPs, within glutathione-enriched intracellular conditions. This combination of attributes would offer the prospect of precisely triggered drug release of small drug molecules in the first instance, establishing the foundation for the intracellular delivery of macromolecular payloads, as further discussed in Chapter 6. This chapter presents the preliminary investigations undertaken with the intent of setting the framework of a novel class of crosslinked polymeric NPs inspired by the combined chemistry of OLGADMAs and disulphides.

5.2.1 Design and Synthesis of Disulphide **61**

To access an oily, polymerisable dimethacrylate containing a disulphide moiety, a compound structurally resembling OLGADMAs was targeted. The hypothesis was that such a disulphide would have limited aqueous solubility and would thus promote the formation of NPs when subjected to nanoprecipitation polymerisation conditions, ultimately yielding disulphide-containing crosslinked polymeric NPs.

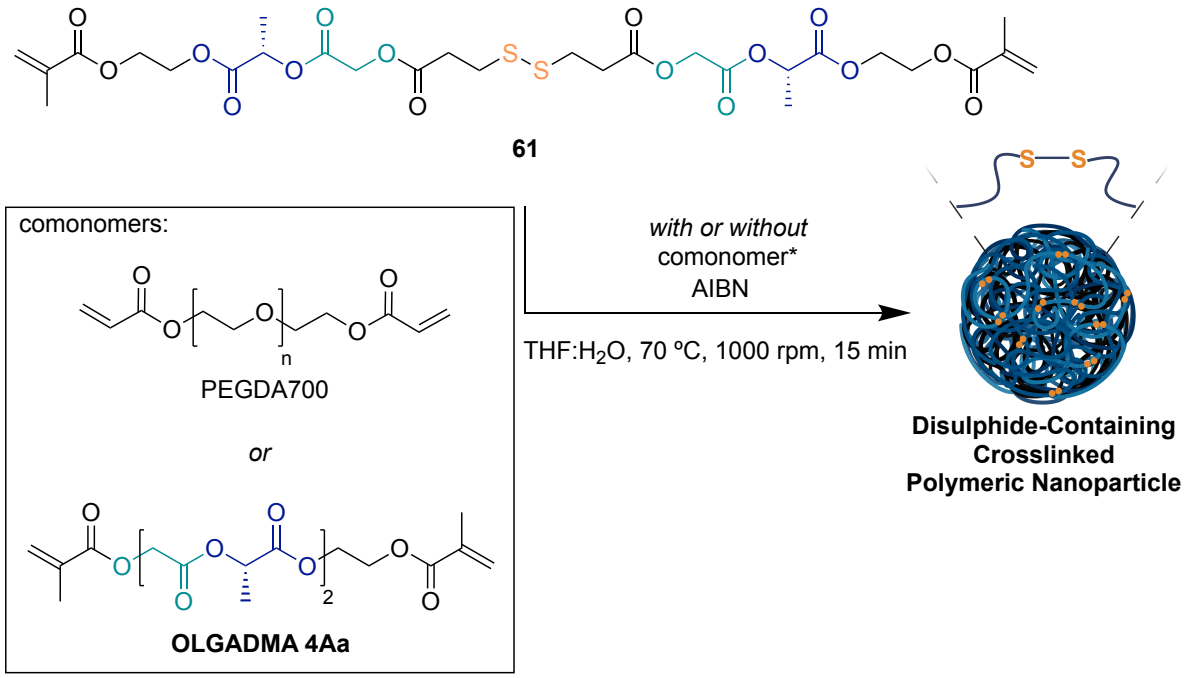
For this purpose, disulphide **61** was synthesised from alcohol **60**, obtained from previously synthesised acid **6**, and 3,3'-dithiopropionic acid, a commercially available disulphide source already employed for the synthesis of polymeric NPs for drug delivery applications in previous works (Scheme 29).[219,220] Specifically, the functionalisation of acid **6** with HEMA afforded methacrylate **59** with a 73% yield. The subsequent cleavage of the silyl ether present in methacrylate **59** provided the desired alcohol **60** in a 92% yield. In the following step, 3,3' dithiopropionic acid was reacted with 2.5 equivalents of alcohol **60** via carbodiimide coupling, to afford the desired disulphide **61** with a yield of 60%.



Scheme 29. A) Synthesis of alcohol **60**, and B) synthesis of disulphide **61**. a) HEMA (1.3 equiv), EDC HCl (1.3 equiv), DMAP (0.5 equiv), CH_2Cl_2, rt; b) TBAF (1.5 equiv), AcOH (3 equiv), THF, 0 °C to rt; c) **60** (2.5 equiv), EDC HCl (2.2 equiv), DMAP (0.5 equiv), CH_2Cl_2, rt.

5.2.2 Synthesis and Analysis of Disulphide-Containing Crosslinked Polymeric Nanoparticles

To evaluate the feasibility of generating crosslinked polymeric NPs, disulphide **61** was subjected to reactions under standard nanoprecipitation polymerisation conditions, both independently and in combination with PEGDA700, as well as with **OLGADMA 4Aa**. The experiments resulted in the formation of disulphide-containing crosslinked polymeric NPs as presented in Scheme 30.



Scheme 30. Synthesis of disulphide-containing crosslinked polymeric NPs via nanoprecipitation polymerisation of disulphide **61** independently or in the presence of a co-monomer. *The comonomer is either PEGDA700 or **OLGADMA 4Aa**.

The performed experiments led to the isolation of three types of NPs **NP-SS1**, **NP-SS2**, and **NP-SS3** which were purified and subsequently analysed using DLS and ELS analysis (Table 22). The measured sizes of these NPs were below 250 nm alongside PI values below 0.3. The ζ-potential of disulphide-containing NPs recorded in deionised water was negative. Particularly, **NP-SS2** presented a ζ-potential value of -14.0 ± 0.8 mV, whilst **NP-SS1** and **NP-SS3** both exhibited ζ-potentials of approximately -20 mV.

The **NP-SS3** was obtained as the most concentrated NP suspension, whilst reactions yielding **NP-SS1** and **NP-SS2** allowed the isolation of suspensions which contained a halved concentration of solids.

Nanoparticle	Comonomer	Estimated NP Yield* (%)	z-average (nm ± SD)	PI ± SD	ζ-potential (mV ± SD)
NP-SS1	-	25	179.20 ± 3.45	0.16 ± 0.03	-20.0 ± 0.7
NP-SS2	PEGDA700	25	145.6 ± 1.2	0.134 ± 0.003	-14.0 ± 0.8
NP-SS3	**OLGADMA 4Aa**	50	231.6 ± 5.5	0.25 ± 0.01	-20.3 ± 1.2

Table 22. The estimated yield, DLS analysis, and ELS analysis of **NP-SS1**, **NP-SS2**, and **NP-SS3**. *Calculated as the ratio of the mass of solids obtained via lyophilisation of aqueous NP suspensions and the cumulative mass of monomers employed for the synthesis of NPs, expressed as a percentage.

The analysis of the NPs was extended via TEM analysis, which revealed the presence of sub-micrometre NPs within the samples (Figure 50). Interestingly, **NP-SS2** exhibited obvious morphological differences when compared to **NP-SS1** and **NP-SS3,** which both displayed spherical morphology. Specifically, **NP-SS2** featured a corrugated surface reminiscent of popcorn, a morphology potentially arising from the aggregation of smaller particles during the NP formation process.

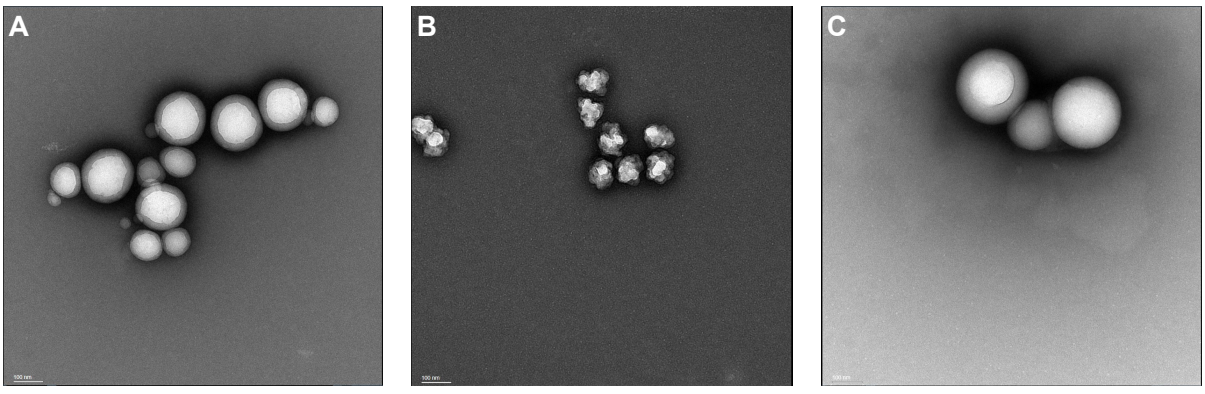


Figure 50. TEM micrographs of NPs prepared from disulphide **61**. A) **NP-SS1**, B) **NP-SS2**, and C) **NP-SS3** (stained with 2% uranyl acetate, 45000×, scale bar = 100 nm).

Having successfully prepared three types of NPs by subjecting disulphide **61** to nanoprecipitation polymerisation, it was considered imperative to screen these NPs for size and concentration stability in the presence of a physiologically relevant concentration of glutathione. For this purpose, a preliminary screening of the stability of disulphide-containing NPs in the presence of glutathione was performed as described in the following section.

5.2.3 Preliminary Evaluation of the Stability of Disulphide-Containing Crosslinked Polymeric Nanoparticles in the Presence of Glutathione

To verify the stability of **NP-SS1**, **NP-SS2**, and **NP-SS3** in the presence of glutathione, the NPs were incubated within aqueous glutathione solutions (15 mM) at the physiological temperature of 37 °C over a period of 24 h. Control samples were prepared by suspending the NPs in water. The samples were subsequently analysed via the comparison of the mean count rate, also known as scattering intensity since this parameter is proportional to both the number and the size of particles in suspension (Table 23).[353,354] A comparison of samples treated with glutathione and the controls revealed the glutathione-containing suspensions to exhibit lower scattering intensities in comparison with control samples. The difference in the mean count rate detected with the samples increased in the order of **NP-SS1** < **NP-SS2** < **NP-SS3**, with the latter showing the greatest discrepancy in the scattering intensity values by comparison with the control sample.

Nanoparticle	Mean Count Rate (kcps)	
	water	aq. glutathione (15 mM)
NP-SS1	336.04 ± 54.55	62.22 ± 12.91
NP-SS2	186.59 ± 63.84	19.19 ± 1.57
NP-SS3	402.38 ± 73.55	22.26 ± 4.51

Table 23. Comparison of count rates of disulphide-based NPs **NP-SS1**, **NP-SS2**, and **NP-SS3** suspended in water and aqueous solution of glutathione (15 mM) after incubation at 37 °C over a period of 24 h, measured by DLS. The measurements were performed at fixed attenuation and laser position over 60 s.

The above-presented results were considered indicative of the decrease of the NP size and/or NP concentration in the presence of glutathione. To further test this observation, the number-weighted size distributions of the samples were determined via DLS analysis (Figure 51). Interestingly, both the control and glutathione-treated samples containing **NP-SS1** showed the presence of particles with a mean size of around 120 nm. On the other hand, the comparison of the DLS analysis of suspensions containing **NP-SS2** and **NP-SS3** showed striking differences in the size distributions of the glutathione-containing and control samples. Particularly, the analysis of **NP-SS2** and **NP-SS3** incubated in water revealed a size distribution consistent with that of the freshly prepared NPs. Conversely, the analysis of the size distribution of **NP-SS2** and **NP-SS3** treated with glutathione revealed the absence of size distributions typical of the freshly prepared NPs.

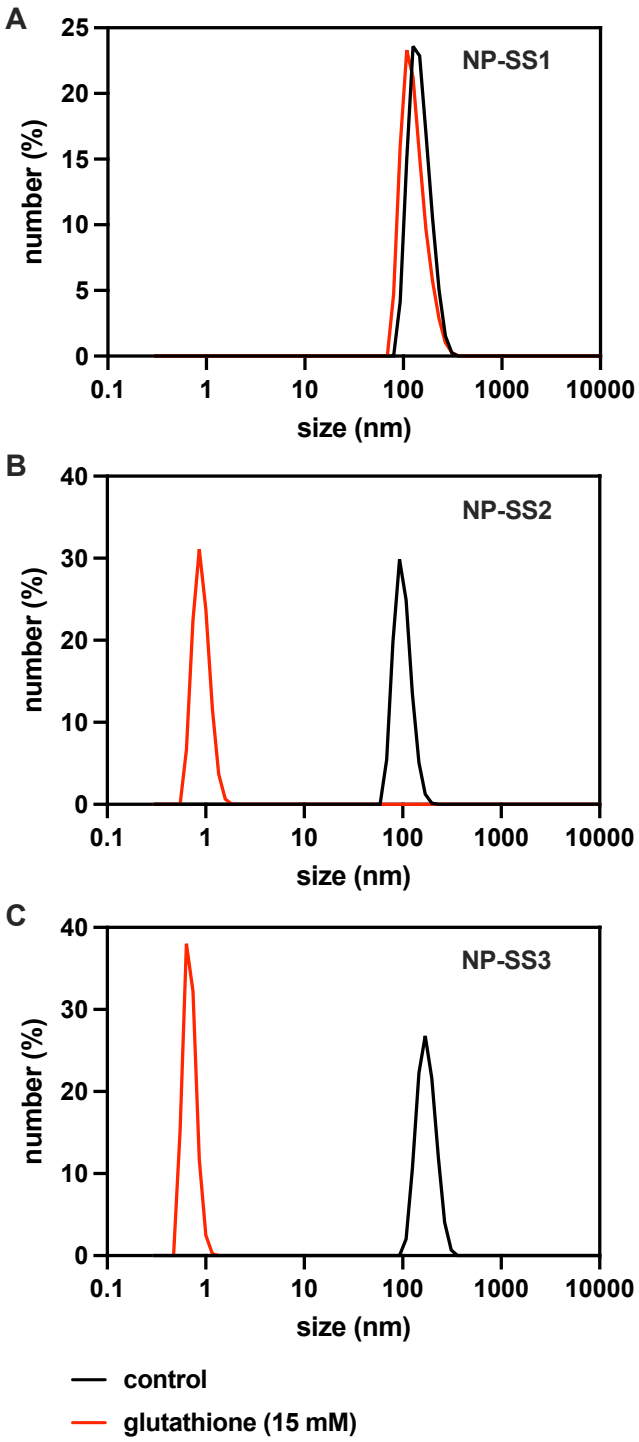


Figure 51. Comparison of number-weighted size distributions obtained via DLS analysis of disulphide-containing NPs subjected to 24 h of incubation in water (black line), and aqueous glutathione solution (15 mM) at 37 °C. A) sample prepared using **NP-SS1**, B) sample prepared using **NP-SS2**, and C) sample prepared using **NP-SS3**.

Taken altogether, it was concluded that **NP-SS1**, **NP-SS2**, and **NP-SS3** exhibit some form of instability in the presence of glutathione (15 mM). Whilst the employed concentration of glutathione is higher than that of reported intracellular concentrations (approximately 2-10 mM), the experiment described above allowed for a proof-of-concept study.[205] Future work will be aimed towards assessing the NP stability in the presence of lower concentrations of glutathione (e.g. 2 mM) and further physicochemical analysis of the NP stability via TEM and spectroscopic analysis. The combination of these techniques could allow for a detailed investigation of the nature of the NP-glutathione interaction and the stability of the disulphide linkages present within the NPs. Moreover, further analysis is required to dismiss the contribution of possible NP aggregation in the presence of glutathione resulting in a decrease in NP concentration, which may manifest as a decrease in the scattering intensity of the glutathione-treated suspensions.

5.3 Work Towards Diselenide-Containing Crosslinked Polymeric Nanoparticles

To expand the scope of potential applications beyond glutathione-triggered drug delivery, the incorporation of the diselenide chemical motif was identified as a potentially useful feature for the design of subsequent stimuli-responsive crosslinked polymeric NPs. Particularly, access to novel types of NPs incorporating the diselenide chemical motif might be advantageous for the treatment of inflammatory pathologies characterised by an upregulation of hydrogen peroxide, the most abundant ROS, identified as a potentially useful stimulus for the targeted delivery of therapeutics to diseased tissues.[188]

To this end, L-selenocystine was identified as a potentially valuable diselenide source for the synthesis of a novel dimethacrylate building block for NP synthesis (Figure 52). Specifically, L-selenocystine is the oxidised form of L-selenocysteine, a proteinogenic amino acid involved in redox biochemistry and is naturally present within biological systems.[355] Moreover, it may be amenable to facile chemical derivatisation via its amine and carboxylic acid groups to afford both ionisable and non-ionisable diselenide-containing monomers.

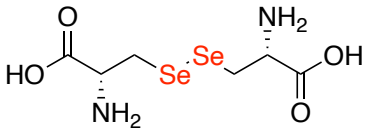


Figure 52. Chemical structure of L-selenocystine.

The following section describes a preliminary evaluation of the stability of L-selenocystine in the presence of hydrogen peroxide.

5.3.1 Evaluation of the Stability of L-Selenocystine in the Presence of Hydrogen Peroxide

To evaluate the feasibility of employing L-selenocystine as a diselenide source for the synthesis of building blocks for the construction of polymeric NPs with responsiveness towards hydrogen peroxide, the stability of the compound in the presence of the oxidant was analysed. To this end, L-selenocystine was solubilised in a solution of sodium hydroxide in deuterium oxide. The solution was then treated with hydrogen peroxide (3 equiv) and incubated at 37 °C. A control solution was prepared without the addition of hydrogen peroxide. After 24 h, the resulting solutions were analysed via ^{1}H NMR, ^{13}C NMR, and ^{77}Se NMR spectroscopy to determine the stability of L-selenocystine.

The analysis of the ^{1}H NMR, ^{13}C NMR, and ^{77}Se spectra of the control sample revealed the presence of resonances attributed to the starting material and were consistent with those previously reported.[356] The analysis of the spectra of the sample treated with hydrogen peroxide revealed the absence of detectable starting material. The integrity of the diselenide moiety was investigated via ^{77}Se NMR spectroscopy which revealed a resonance at δ 274 ppm for the control sample and was considered consistent with the chemical shift of an organic diselenide (Figure 53).[357] Conversely, the spectrum of the sample treated with hydrogen peroxide revealed a resonance at δ 1192 ppm. Given this, it was concluded that the L-selenocystine is unstable in the presence of hydrogen peroxide and was converted to one or more oxidised species, possibly including seleninic acids.

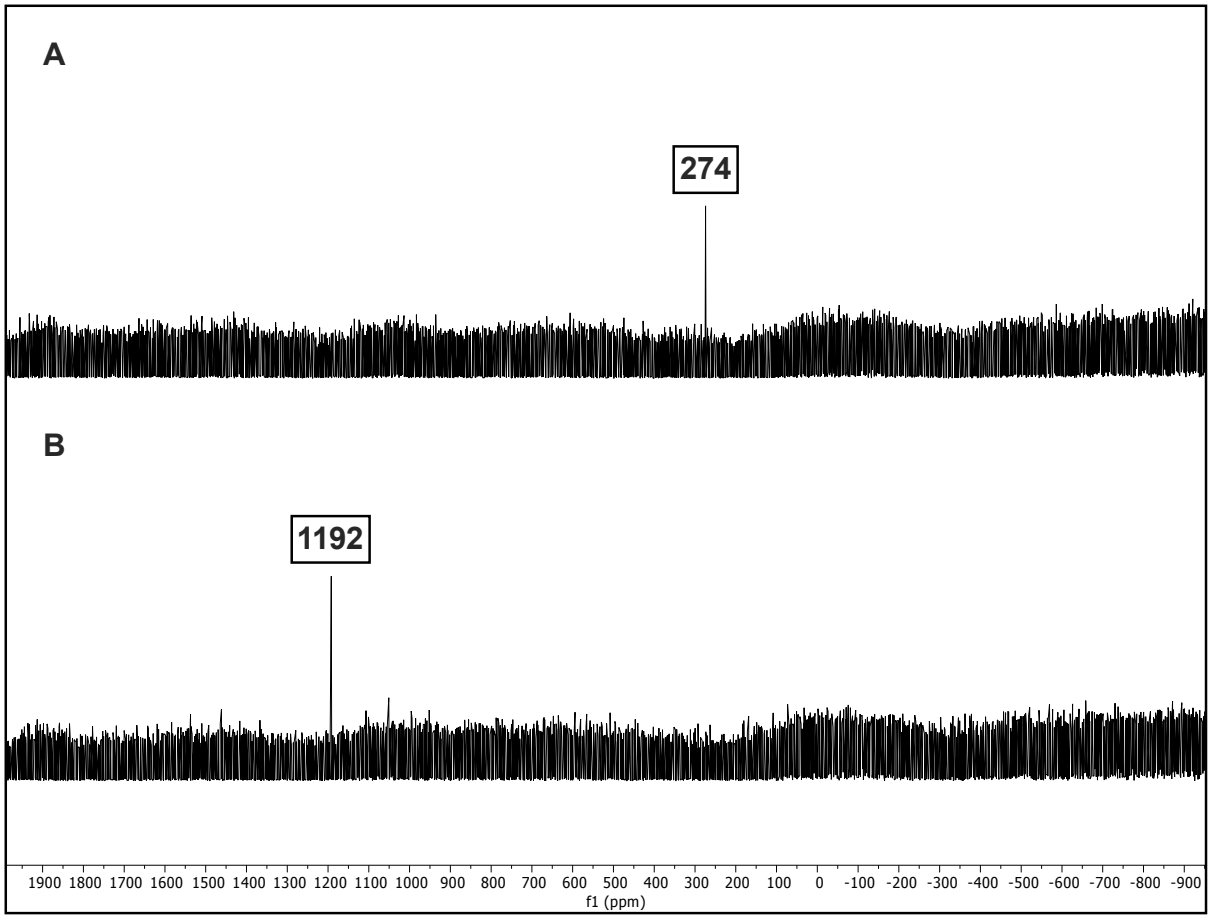
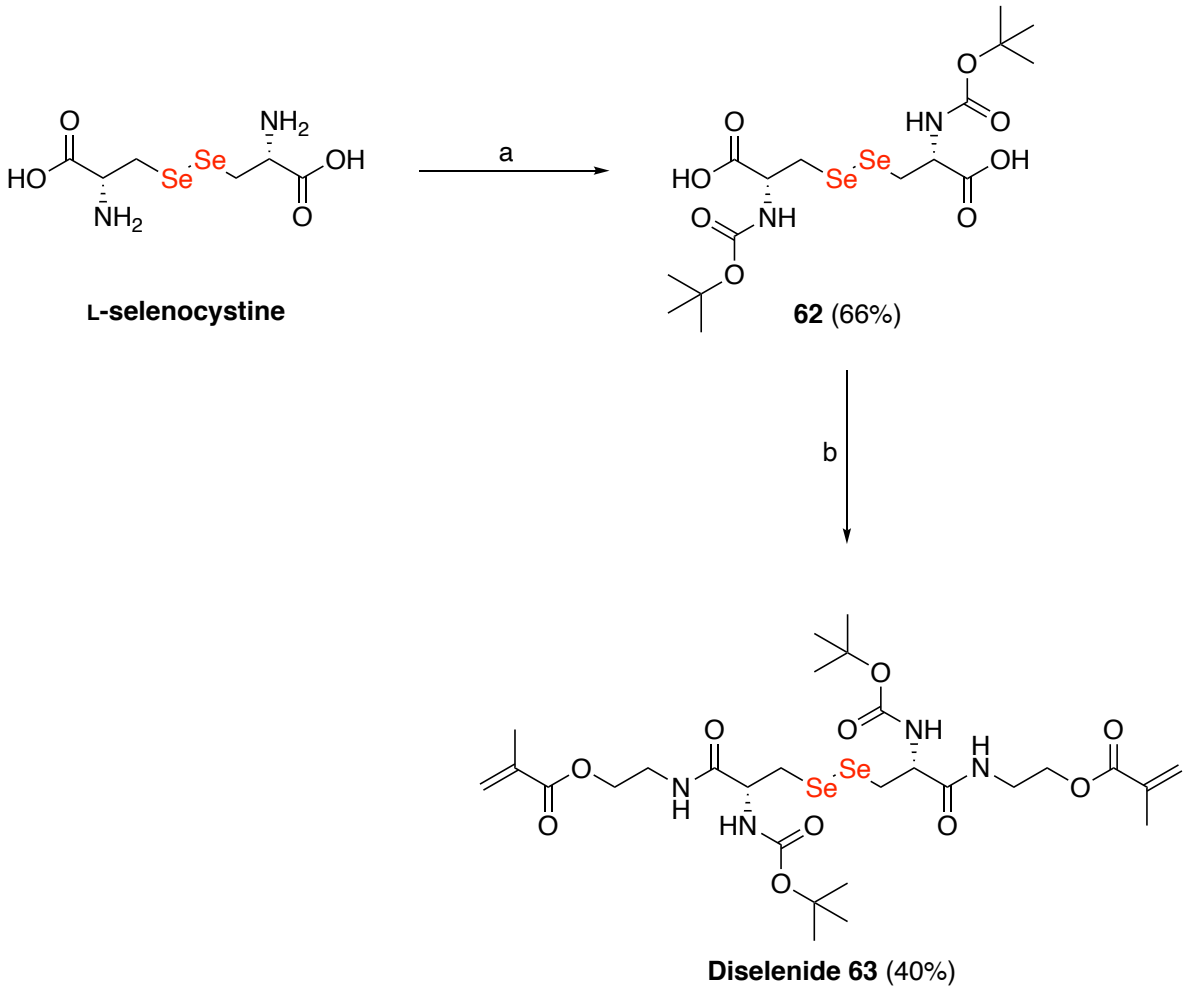


Figure 53. ^{77}Se NMR (76 MHz, D_2O/NaOH) spectrum of samples prepared using A) L-selenocystine subjected to 24 h of incubation at 37 °C, and B) L-selenocystine treated with H_2O_2 and subjected to 24 h of incubation at 37 °C.

Having ascertained the instability of L-selenocystine in the presence of hydrogen peroxide at 37 °C, it was hypothesised that the compound could be derivatised to a dimethacrylate which may be amenable to form NPs upon radical polymerisation, maintaining the reactivity towards hydrogen peroxide observed with the parent compound. The following section describes the synthesis of the novel diselenide **63** prepared from L-selenocystine.

5.3.2 Synthesis of Diselenide **63**

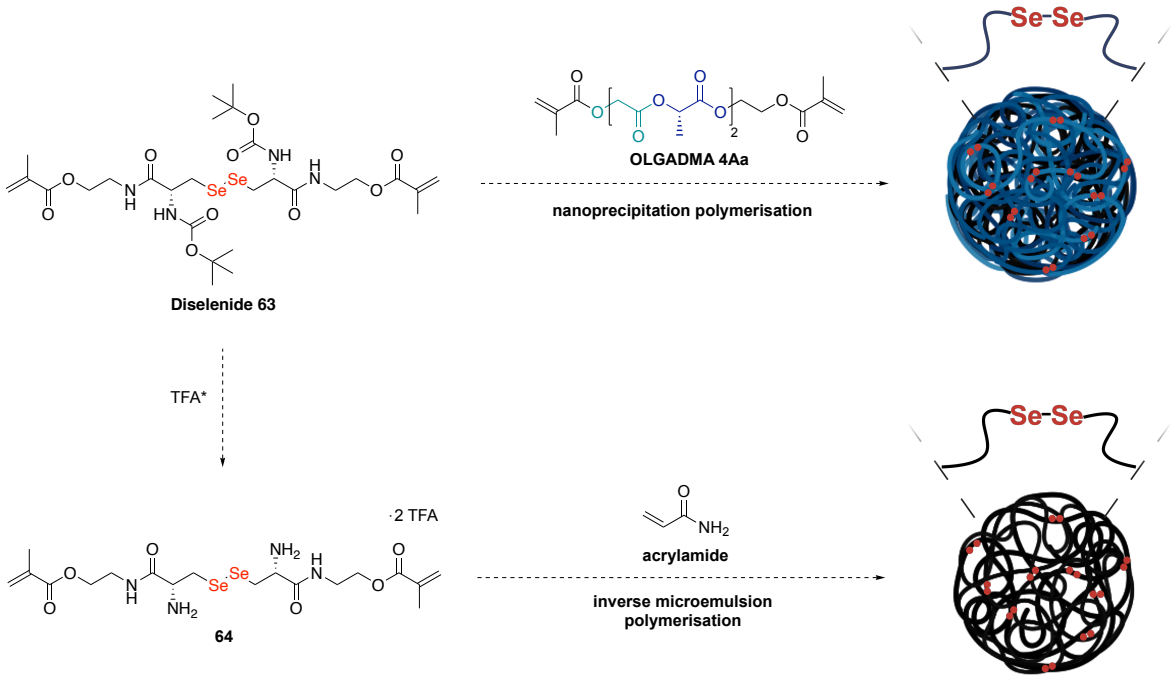
Diselenide **63** was synthesised from L-selenocystine over two steps (Scheme 31). In the first step, L-selenocystine was subjected to protection of the amine groups via reaction with di-tert-butyl-dicarbonate (Boc_2O) to afford the dicarbamate **62** in a 66% yield. In the following step, **62** was reacted with 2-aminoethyl methacrylate (HCl salt) in the presence of EDC, DMAP, and TEA to afford the desired diselenide **63** in a 40% yield. The compound was isolated as a viscous oil which appeared to have limited solubility in water.



Scheme 31. Synthesis of Diselenide **63** from L-selenocystine. a) Boc_2O (2.0 M solution in THF, 3 equiv), TEA (3 equiv), H_2O, 0 °C to rt; b) 2-aminoethyl methacrylate hydrochloride (3 equiv), EDC hydrochloride (3 equiv), DMAP (0.1 equiv), TEA (3.2 equiv), DMF, 0 °C to rt.

5.3.3 Proposed Routes Towards Diselenide-Containing Crosslinked Polymeric Nanoparticles

Following the successful synthesis of diselenide **63**, two main routes for the synthesis of diselenide-containing crosslinked polymeric NPs were hypothesised (Scheme 32).



Scheme 32. Proposed routes for the synthesis of crosslinked polymeric NPs from Diselenide **63**.

In the first instance, diselenide **63** is expected to be directly amenable to polymerisation under nanoprecipitation polymerisation conditions in the presence of OLGADMAs to yield diselenide-containing, OLGA-based crosslinked polymeric NPs. This setting may offer the potential for simultaneous NP formation and drug encapsulation, yielding drug-loaded NPs capable of releasing the therapeutic payload at higher rates upon interaction with hydrogen peroxide.

A further potential route was envisaged to be accessible upon deprotection of diselenide **63** with TFA to obtain the diamino compound **64** as the TFA salt. Given the salt form, **64** is expected to present good water solubility and may thus be amenable to polymerisations within inverse microemulsions and in the presence of hydrophilic monomers such as acrylamide to yield hydrophilic crosslinked polymeric NPs resembling nanogels. The polyacrylamide backbone of these NPs might confer good

swelling capabilities to the nanostructure and allow the encapsulation of macromolecular therapeutic payloads such as proteins and peptides via post-polymerisation encapsulation methods such as the “breathing in method” presented in Chapter 1. The resulting loaded NPs may be able to release their macromolecular payloads selectively in response to interaction with hydrogen peroxide.

5.4 Chapter Summary

A novel polymerisable disulphide inspired by OLGADMAs was designed and successfully synthesised. The disulphide can yield NPs once subjected to the nanoprecipitation polymerisation protocol alone or in the presence of either PEGDA700 or **OLGADMA 4Aa**. The resulting NP suspensions manifest a decrease in the scattering intensities upon incubation with glutathione (15 mM) at 37 °C over 24 h *in vitro*. Moreover, the DLS analysis of **NP-SS2** and **NP-SS3** reveals marked differences in the NP size distributions of glutathione-treated and control samples.

Moreover, L-selenocystine was identified as a potentially valuable diselenide source for the synthesis of diselenide-containing NP building blocks and was confirmed to present chemical instability relative to the diselenide moiety in the presence of hydrogen peroxide *in vitro*. Following this, a novel diselenide-containing dimethacrylate was synthesised and two strategies for its polymerisation into crosslinked polymeric NPs having potential utility for drug delivery applications were proposed.

Chapter 6: Conclusions and Future Work

A library of eight polymerisable oligoesters (OLGADMAs) inspired by the chemistry of sequenced PLGA was designed and synthesised. A rapid and surfactant-free methodology termed nanoprecipitation polymerisation was developed to polymerise OLGADMAs and form OLGA-based NPs in a single step. The nanoprecipitation polymerisation methodology allowed for simultaneous NP formation and drug encapsulation, as exemplified by the successful synthesis of a library of dexamethasone-loaded OLGA-based NPs. The estimated drug loading efficiencies achieved with OLGA-based NPs were found to be comparable to or higher than those achieved with PLGA-based NPs prepared via a mirrored procedure.

OLGA-based NPs exhibit size stability comparable to that of NPs prepared from PLGA and sequenced PLGA, whilst being markedly more size stable than PLGA-PEG NPs under aqueous conditions at 37 °C over 5 weeks. Contrary to suspensions containing PLGA-based NPs, the suspensions of OLGA-based NPs maintain their pH within a narrow window upon incubation at 37 °C which is suggestive of a lower quantity of percolating acids and superior hydrolytic stability.

Dexamethasone-loaded OLGA-based NPs released between 7% and 69% of the encapsulated dexamethasone over 7 days under experimental conditions *in vitro*, depending on the example. Moreover, NPs such as **DNP6B** were capable of releasing dexamethasone at rates as low as 0.1% per day. Whilst several factors could influence the discrepancies of the observed cumulative drug releases, it was hypothesised that the existence of different internal structures or differences in porosity amongst the OLGA-based NPs might be at the root of these observations.

Dexamethasone-loaded NPs prepared from tetramer OLGADMAs show a good level of colloidal stability in the FBS-supplemented biological medium which is favourable for *in vitro* applications. Moreover, aqueous suspensions containing **DNP4Aa** and

DNP4Bb can be stored on the bench for 4 weeks without suffering drastic size changes, indicating a good level of stability at room temperature.

The cell viability of HeLa cells treated with empty and dexamethasone-loaded OLGA-based NPs at concentrations up to 50 μg/mL exceeds 85% after 24h and 48 h of treatment, forecasting a good biocompatibility of the NPs. Moreover, fluorescent **NP4Aa** are homogeneously internalised by HeLa cells as confirmed by confocal microscopy.

Taken altogether, the developed OLGA-based NPs may find applications in prolonged and controlled-release drug delivery applications. Particularly, the NPs might offer the potential for stable encapsulation of significant quantities of hydrophobic drugs and release these drugs at slow rates over an extended period. Moreover, the OLGA-based NPs might be particularly suitable for the encapsulation of acid-sensitive therapeutic payloads, as highlighted by the increased stability, and limited acidification of the NP aqueous environment containing the NPs.

Work towards stimuli-responsive NP iterations inspired by OLGA-based NPs was initiated and disulphide-containing crosslinked polymeric NPs were synthesised which exhibit instability in the presence of 15 mM glutathione *in vitro*. A further dimethacrylate compound containing a diselenide moiety deriving from L-selenocystine was synthesised, and two synthetic routes to diselenide-containing crosslinked NPs achievable from its polymerisation were proposed.

Future synthetic work will focus on overcoming the limitations of the nanoprecipitation methodology and establishing novel synthetic platforms for the encapsulation of macromolecules such as proteins and nucleic acids within OLGA-based NPs. Specifically, it is critical to achieve the synthesis of OLGA-based NPs at room temperature, circumvent the requirement for the presence of large quantities of a radical initiator, and increase the yields of the NPs prepared via nanoprecipitation polymerisation. To this end, conducting the nanoprecipitation polymerisation in the presence of a photoinitiator such as lithium phenyl-2,4,6-trimethylbenzoylphosphinate

(LAP) has been identified as a possible alternative to AIBN that would allow to conduct the reactions at room temperature or lower (Figure 54).

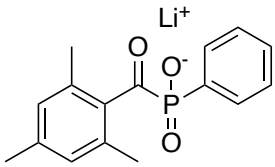
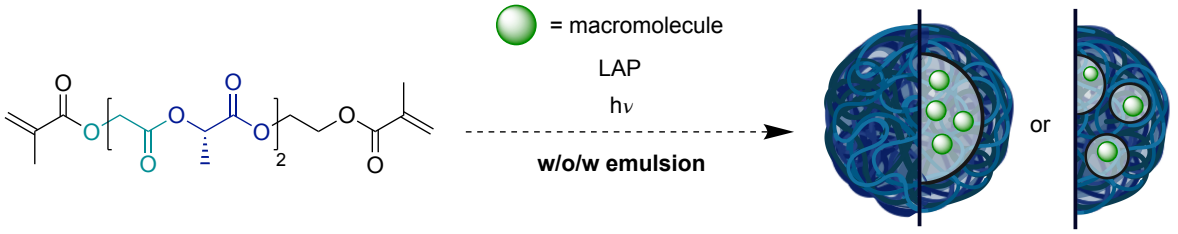


Figure 54. Chemical structure of the lithium phenyl-2,4,6-trimethylbenzoylphosphinate (LAP) photoinitator.

The decrease in the required reaction temperature might allow for conducting the reactions over extended periods, whilst maintaining the integrity of the OLGADMAs, and using a more modest amount of the initiator.

A further iteration of this methodology may comprise the formulation of double w/o/w emulsions with polymerisable monomers such as OLGADMAs constituting the oil phase. The polymerisation of these double emulsions may enable the preparation of OLGA-based nanocapsules which may house macromolecule therapies within their cores (Scheme 33).



Scheme 33. Proposed methodology for the synthesis of OLGA-based nanocapsules containing macromolecular payload.

Furthermore, the copolymerisation of OLGADMAs with co-monomers such as disulphide **61** or diselenide **63** within double emulsions may enable the preparation of stimuli-responsive OLGA-based nanocapsules capable of releasing macromolecular payloads in response to physiologically relevant concentrations of glutathione or hydrogen peroxide.

Lastly, to ascertain the feasibility of translating OLGA-based NPs for medical applications it is crucial to gain an understanding of the potential *in vivo* faith of these NPs. In this context, *in vitro* degradation studies involving the hydrolysis of the ester fraction of the NPs followed by chromatographic and DLS analysis of the resulting degradation products may harbour some predictive value in the first instance. Particularly, such an analysis could allow for the determination of the molecular weight and size of the presumably non-biodegradable C-C backbone resulting from the polymerisation of vinyl groups present within the monomers, giving a preliminary estimation of the potential for the elimination of these degradation products upon systemic administration of the NPs presented in this work.

Chapter 7: Experimental Section

7.1 General Information

7.1.1 Materials

PEGDA700, imidazole, and DBU were purchased from Fluorochem. PLGA-PEG (PLGA-PEG-COOH, acid terminated, L:G 50:50, M_n 50,000-5,000 Da) was purchased from PolySciTech. XBD173 was kindly provided by Dr. David Owen. All other chemicals were purchased from Sigma-Aldrich. Anhydrous solvents were obtained by filtration through drying columns (CH_2Cl_2, THF, MeCN, and DMF) or used as supplied (EtOAc, DMSO, hexane, and methanol). Amicon Ultra 0.5 mL Centrifugal Filter Units (100 kDa MWCO) and Amicon Ultra 15 mL Centrifugal Filter Units (100 kDa MWCO and 30 kDa MWCO) were purchased from Sigma-Aldrich. Formvar/Carbon supported copper grids (size 200 mesh) were purchased from Sigma-Aldrich. The CCK-8 assay was purchased from Abcam.

7.1.2 Instrumentation

Nuclear magnetic resonance spectra were recorded on 400 MHz spectrometers. Infrared spectra (ATR FTIR) were recorded in reciprocal centimetres (cm^{-1}) using an Agilent Cary 630 FTIR spectrometer. Drug quantitation was performed on an Agilent Cary 60 UV-Vis spectrophotometer. DLS and ELS analysis was performed on a Malvern Zetasizer Ultra instrument. TEM was performed on JEM-2100Plus, Tecnai 12 Spirit, and Talos F200X G2 electron microscopes. Centrifugations were performed using Eppendorf 5424 R and Sorvall ST8R centrifuges. Confocal microscopy was performed on a Leica SP8 DLS microscope. Absorbances for cell viability assays were measured on a CLARIOstar plate reader.

7.1.3 Dynamic Light Scattering (DLS)

Samples for analysis were typically prepared by mixing 50 μL of the NP suspension with the appropriate dispersant (1 mL), followed by gentle mixing by repetitive pipetting. If required, the samples were diluted or concentrated to obtain optimal concentration for analysis. Measurements were performed using disposable cuvettes,

at a temperature of 25 °C, and at a detection angle of 173°. The correlation functions were analysed automatically by the software (ZS Xplorer). The size of the particles is reported as the z-average ± standard deviation, obtained *via* three independent measurements, and expressed in nm. This z-average value is accompanied by the polydispersity index, reported as PI ± standard deviation.

7.1.4 Electrophoretic Light Scattering (ELS)

Samples for analysis were prepared by mixing aqueous nanoparticle suspensions with deionised water, followed by mixing *via* repetitive pipetting. The measurements were performed in a disposable folded capillary cell and at a temperature of 25 °C. The results are reported as the ζ-potential ± standard deviation (mV).

7.1.5 Transmission Electron Microscopy (TEM)

Samples for analysis were prepared by depositing aqueous NP suspensions (5 μL) onto glow discharged Formvar/Carbon supported copper grids (200 mesh) and allowing the particles to adsorb for 1 min before removing the excess sample by blotting gently with filter paper. The grids were then stained with 2% uranyl acetate (5 μL) for 1 min. The excess stain was removed by blotting with filter paper, and the grids were allowed to dry at room temperature before imaging. The TEM analysis of **NP4Aa** and **DNP4Aa** was performed using the same protocol detailed above, except for the deliberate omission of the staining step.

7.1.6 General Synthetic Procedures

Commercial reagents were used as supplied. All non-aqueous reactions were carried out under a nitrogen gas atmosphere with flame-dried glassware, using standard techniques. Flash column chromatography was performed using 230–400 mesh silica, with the indicated solvent system according to standard techniques. Analytical thin-layer chromatography (TLC) was performed on precoated, aluminium silica gel sheets. Visualisation of the developed chromatogram was performed by UV absorbance (254 nm) and staining with basic potassium permanganate stain. Chemical shifts for ^{1}H NMR spectra are recorded in parts per million from tetramethylsilane with the solvent resonance as the internal standard ($CHCl_3$: δ= 7.27 ppm, H_2O: δ=4.79 ppm, DMSO:

δ= 2.50 ppm). Data is reported as follows: chemical shift (multiplicity [s = singlet, d = doublet, t = triplet, q = quartet, quint = quintet, multiplet and br = broad], coupling constant (in Hz) and integration). ^{13}C NMR spectra were recorded with complete proton decoupling. Chemical shifts are reported in parts per million from tetramethylsilane with solvent resonance as the internal standard ($^{13}CDCl_3$: δ= 77.0 ppm).

7.1.6.1 Ester Formation

EDC HCl (1.3 equiv) was added to a solution of acid (1 equiv), alcohol (1.2 equiv) and DMAP (0.5 equiv) in dichloromethane. The mixture was left stirring overnight at rt and then concentrated *in vacuo*. Purification by flash chromatography (ethyl acetate/hexane) afforded the desired compounds.

7.1.6.2 Catalytic Hydrogenation

A mixture of benzyl ester and Pd/C (5 wt%) in ethyl acetate was left stirring under hydrogen gas (atmospheric pressure) overnight. The system was then purged with nitrogen gas and the mixtures filtered through a short plug of celite, eluting with dichloromethane. The resulting solution was concentrated *in vacuo* to afford the desired acids.

7.1.6.3 Silyl Ether Cleavage

TBAF (1.5 equiv) was added to a cold solution of silyl ether and glacial acetic acid (3 equiv) in THF and left stirring at 0 °C. The reaction was monitored by TLC, warming to room temperature if necessary. Upon completion, the reaction mixture was mixed with brine, extracted three times with diethyl ether, dried over Na_2SO_4 and concentrated *in vacuo*. Purification by flash chromatography (ethyl acetate/hexane or diethyl ether/hexane) afforded the desired alcohols.

7.1.6.4 Synthesis of Monomethacrylates

EDC HCl (1.3 equiv) was added to a solution of the appropriate acid (1 equiv), HEMA (1.3 equiv) and DMAP (0.5 equiv) in dichloromethane. The mixture was left stirring

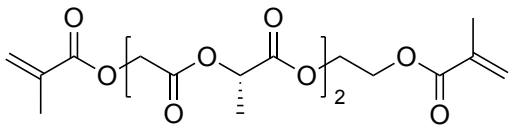
overnight at rt and then concentrated *in vacuo*. Purification by flash chromatography (ethyl acetate/hexane) afforded the desired monomethacrylates.

7.1.6.5 Synthesis of OLGADMAs

Methacryloyl chloride (2 equiv) was added to a cold solution of the appropriate alcohol and triethylamine (4 equiv) in dichloromethane at 0 °C. The reaction was monitored by TLC, warming to room temperature if necessary. Upon completion, the reaction mixture was partitioned between brine and dichloromethane, extracted with dichloromethane, dried over Na_2SO_4 and concentrated *in vacuo*. Purification by flash chromatography (ethyl acetate/hexane) afforded the desired OLGADMAs.

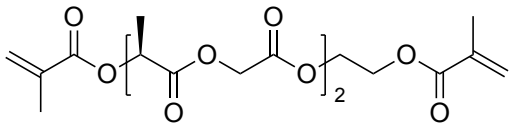
7.2 Experimental Details for Chapter 2

7.2.1 Synthesis and Characterisation of OLGADMAs



OLGADMA 4Aa

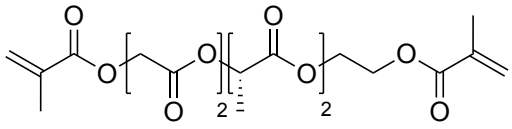
Preparation: The compound was prepared by subjecting **11** to the standard procedure for the synthesis of OLGADMAs. **Appearance**: colourless oil, Yield: 95%, **Characterisation**: R_f = 0.3 (30% EtOAc/hexane); IR (film)/cm^{-1} 2990, 2959, 1752 (C=O), 1722 (C=O), 1640, 1453, 1148, 909, 730; ^{1}H NMR (400 MHz, $CDCl_3$) δ 6.24 – 6.21 (m, 1H), 6.13 – 6.12 (m, 1H), 5.66 (quint, J = 1.6 Hz, 1H), 5.61 (quint, J = 1.6 Hz, 1H), 5.27 (q, J = 7.1 Hz, 1H), 5.18 (q, J = 7.0 Hz, 1H), 4.91 – 4.79 (m, 2H), 4.74 (d, J = 16.2 Hz, 1H), 4.64 (d, J = 16.0 Hz, 1H), 4.50 – 4.41 (m, 1H), 4.40 – 4.33 (m, 3H), 2.00 – 1.96 (m, 3H), 1.96 – 1.93 (m, 3H), 1.62 – 1.57 (m, 3H), 1.52 (d, J = 7.1 Hz, 3H); ^{13}C NMR (101 MHz, $CDCl_3$) δ 169.7, 169.5, 167.2, 167.0, 166.5, 166.5, 135.8, 135.2, 127.0, 126.2, 69.3, 68.9, 63.1, 61.9, 60.8, 60.6, 18.2, 18.2, 16.7; HRMS (ES+) m/z calcd for $C_{20}H_{26}O_{12}Na^+$ $[M+Na]^+$: 481.1316, Found: 481.1327.



OLGADMA 4Ab

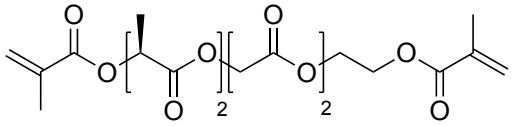
Preparation: The compound was prepared by subjecting **18** to the standard procedure for the synthesis of OLGADMAs. **Appearance:** colourless oil, **Yield**: 68%, **Characterisation:** R_f = 0.19 (30% EtOAc/hexane); IR (film)/cm^{-1} 2991, 2957, 1753 (C=O), 1717 (C=O), 1635, 1451, 1381, 1288, 1155, 1090, 943, 813; ^{1}H NMR (400 MHz, $CDCl_3$) δ 6.23 – 6.20 (m, 1H), 6.14 – 6.12 (m, 1H), 5.65 (quint, *J* = 1.5 Hz, 1H), 5.61 (quint, *J* = 1.5 Hz, 1H), 5.30 – 5.18 (m, 2H), 4.90 (d, *J* = 16.1 Hz, 1H), 4.80 (d, *J* = 16.0 Hz, 1H), 4.65 (d, *J* = 16.0 Hz, 1H), 4.62 (d, *J* = 16.0 Hz, 1H), 4.45 – 4.41 (m, 2H), 4.38 – 4.35 (m, 2H), 1.98 – 1.96 (m, 3H), 1.96 – 1.93 (m, 3H) , 1.62 (d, *J* = 7.1 Hz, 3H), 1.59 (d, *J* = 7.1 Hz, 3H); ^{13}C NMR (101 MHz, $CDCl_3$) δ 170.3, 169.4, 167.0,

166.9, 166.6, 135.7, 135.4, 126.7, 126.3, 69.1, 68.5, 63.1, 62.0, 60.9, 60.7, 18.2, 18.1, 16.9, 16.7; HRMS (TOF MS ES+) m/z calcd for $C_{20}H_{26}O_{12}Na^+$ $[M+Na]^+$: 481.1322, Found: 481.1308.



OLGADMA 4Ba

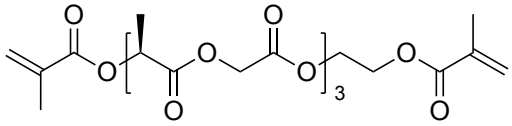
Preparation: The compound was prepared by subjecting **24** to the standard procedure for the synthesis of OLGADMAs. **Appearance:** colourless oil, **Yield:** 80%, **Characterisation:** R_f = 0.24 (30% EtOAc/hexane); IR (film)/cm^{-1} 2991, 2952, 1752 (C=O), 1722 (C=O), 1640, 1453, 1274, 1140, 946, 812; ^1H NMR (400 MHz, $CDCl_3$) δ 6.24 – 6.22 (m, 1H), 6.14 – 6.11 (m, 1H), 5.67 (quint, *J* = 1.6 Hz, 1H), 5.61 (quint, *J* = 1.6 Hz, 1H), 5.27 – 5.12 (m, 2H), 4.88 – 4.71 (m, 4H), 4.50 – 4.30 (m, 4H), 1.98 (dd, *J* = 1.6, 1.0 Hz, 3H), 1.94 (dd, *J* = 1.6, 1.0 Hz, 3H), 1.58 (d, *J* = 7.1 Hz, 3H), 1.53 (d, *J* = 7.1 Hz, 3H); ^{13}C NMR (101 MHz, $CDCl_3$) δ 169.8, 169.3, 167.2, 166.9, 166.5, 166.5, 135.7, 135.2, 127.1, 126.2, 69.2, 69.2, 63.0, 62.0, 60.7, 60.5, 18.2, 18.2, 16.7, 16.6; HRMS (ES+) m/z calcd for $C_{20}H_{26}O_{12}Na^+$ $[M+Na]^+$: 481.1316, Found: 481.1326.



OLGADMA 4Bb

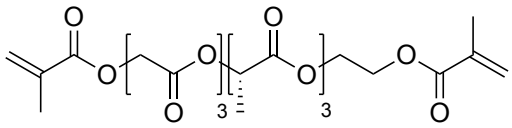
Preparation: The compound was prepared by subjecting **31** to the standard procedure for the synthesis of OLGADMAs. **Appearance:** colourless oil, **Yield:** 52%, **Characterisation:** R_f = 0.22 (25% EtOAc/hexane); IR (film)/cm^{-1} 2991, 2956, 1756 (C=O), 1719 (C=O), 1635, 1451, 1292, 1156, 1129, 1095, 946, 614; ^1H NMR (400 MHz, $CDCl_3$) δ 6.21 (s, 1H), 6.14 (s, 1H), 5.66 – 5.64 (m, 1H), 5.63 – 5.60 (m, 1H), 5.26 (q, *J* = 7.0 Hz, 1H), 5.17 (q, *J* = 7.1 Hz, 1H), 4.89 (d, *J* = 16.1 Hz, 1H), 4.78 – 4.66 (m, 3H), 4.46 – 4.40 (m, 2H), 4.40 – 4.35 (m, 2H), 1.99 – 1.96 (m, 3H), 1.96 – 1.94 (m, 3H), 1.62 (d, J = 7.0 Hz, 6H); ^{13}C NMR (101 MHz, $CDCl_3$) δ 170.2, 169.6, 167.0, 166.7, 166.7, 166.5, 135.7, 135.4, 126.6, 126.3, 68.7, 68.5, 63.2, 61.9, 60.9, 60.6, 18.2, 18.1,

16.7, 16.7; HRMS (TOF MS ES+) m/z calcd for $C_{20}H_{27}O_{12}^+$ [M+H]$^+$: 459.1503, Found: 459.1519.



OLGADMA 6A

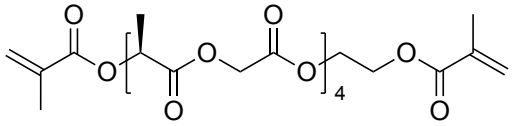
Preparation: The compound was prepared by subjecting **36** to the standard procedure for the synthesis of OLGADMAs. **Appearance:** colourless oil, **Yield:** 51%, **Characterisation:** R_f = 0.21; IR (film)/cm^{-1} 2993, 2956, 1758 (C=O), 1721 (C=O), 1636, 1452, 1288, 1165, 1130, 1095, 951; ^{1}H NMR (400 MHz, $CDCl_3$) δ 6.22 (s, 1H), 6.13 (s, 1H), 5.67 – 5.60 (m, 2H), 5.33 – 5.18 (m, 3H), 4.93 – 4.77 (m, 3H), 4.71 – 4.58 (m, 3H), 4.46 – 4.40 (m, 2H), 4.39 – 4.35 (m, 2H), 1.98 – 1.96 (m, 3H), 1.96 – 1.94 (m, 3H), 1.64 – 1.58 (m, 9H); ^{13}C NMR (101 MHz, $CDCl_3$) δ 170.3, 169.4, 169.4, 167.0, 166.8, 166.6, 166.4, 135.7, 135.4, 126.7, 126.3, 69.2, 69.1, 68.5, 63.2, 62.0, 60.9, 60.8, 60.7, 18.2, 18.1, 16.9, 16.7; HRMS (TOF MS ES+) m/z calcd for $C_{25}H_{33}O_{16}^+$ [M+H]$^+$: 589.1763, Found: 589.1785.



OLGADMA 6B

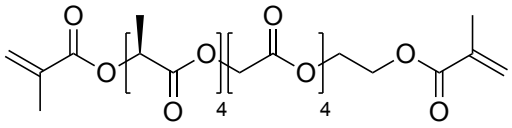
Preparation: The compound was prepared by subjecting **44** to the standard procedure for the synthesis of OLGADMAs. **Appearance:** colourless oil, **Yield:** 55%, **Characterisation:** R_f = 0.20 (40% EtOAc/hexane); IR (film)/cm^{-1} 2922, 2855, 1751 (C=O), 1720 (C=O), 1640, 1453, 1379, 1140, 954, 812; ^{1}H NMR (400 MHz, $CDCl_3$) δ 6.24 (quint, *J* = 1.0 Hz, 1H), 6.16 – 6.11 (m, 1H), 5.68 (quint, *J* = 1.6 Hz, 1H), 5.61 (quint, *J* = 1.6 Hz, 1H), 5.26 – 5.12 (m, 3H), 4.88 – 4.73 (m, 6H), 4.49 – 4.40 (m, 1H), 4.39 – 4.32 (m, 3H), 1.99 (dd, J = 1.6, 1.0 Hz, 3H), 1.95 (dd, J = 1.6, 1.0 Hz, 3H), 1.60 (d, J = 7.1 Hz, 3H), 1.59 (d, *J* = 7.1 Hz, 3H), 1.53 (d, J = 7.1 Hz, 3H); ^{13}C NMR (101 MHz, $CDCl_3$) δ 169.9, 169.5, 169.4, 167.0, 166.5, 166.4, 135.8, 135.2, 127.1, 126.2,

69.3, 69.1, 69.1, 63.0, 62.0, 60.9, 60.6, 60.5, 18.2, 18.2, 16.7, 16.6, 16.6; HRMS (TOF MS ES+) m/z calcd for $C_{25}H_{32}O_{16}Na^+$ $[M+Na]^+$: 611.1588, Found: 611.1575.



OLGADMA 8A

Preparation: The compound was prepared by subjecting **49** to the standard procedure for the synthesis of OLGADMAs. **Appearance:** colourless oil, **Yield:** 51%, **Characterisation**: R_f = 0.43 (45% EtOAc/ hexane); IR (film)/cm^{-1} 2922, 2855, 1759 (C=O), 1722 (C=O), 1640, 1453, 1174, 1095, 954; ^{1}H NMR (400 MHz, $CDCl_3$) δ 6.25 – 6.17 (m, 1H), 6.16 – 6.09 (m, 1H), 5.66 – 5.63 (m, 1H), 5.63 – 5.60 (m, 1H), 5.30 – 5.16 (m, 4H), 4.93 – 4.85 (m, 3H), 4.80 (d, *J* = 15.9 Hz, 1H), 4.69 – 4.59 (m, 4H), 4.46 – 4.40 (m, 2H), 4.39 – 4.34 (m, 2H), 1.97 (t, *J* = 1.3 Hz, 3H), 1.95 (t, *J* = 1.3 Hz, 3H), 1.63 – 1.58 (m, 12H); ^{13}C NMR (101 MHz, $CDCl_3$) δ 170.2, 169.4, 169.4, 167.0, 166.8, 166.6, 166.6, 166.4, 166.4, 135.7, 135.4, 126.7, 126.3, 69.2, 69.1, 69.0, 68.5, 63.1, 62.0, 60.9, 60.8, 60.6, 18.2, 18.1, 16.8, 16.7; HRMS (TOF MS ES+) m/z calcd for $C_{30}H_{42}NO_{20}^+$ $[M+NH_4]^+$: 736.2300, Found: 736.2309.



OLGADMA 8B

Preparation: The compound was prepared by subjecting **57** to the standard procedure for the synthesis of OLGADMAs. **Appearance:** colourless oil, **Yield:** 30%, **Characterisation:** R_f = 0.58 (60% EtOAc/hexane); IR (film)/cm^{-1} 2921, 2852, 1752 (C=O), 1718 (C=O), 1635, 1454, 1379, 1292, 1155, 1128, 1084, 947, 732; ^{1}H NMR (400 MHz, $CDCl_3$) δ 6.25 – 6.18 (m, 1H), 6.16 – 6.10 (m, 1H), 5.64 (quint, *J* = 1.5 Hz, 1H), 5.62 (quint, *J* = 1.6 Hz, 1H), 5.28 – 5.13 (m, 4H), 4.92 – 4.68 (m, 8H), 4.47 – 4.41 (m, 2H), 4.41 – 4.35 (m, 2H), 1.97 (t, *J* = 1.3 Hz, 3H), 1.95 (t, *J* = 1.3 Hz, 3H), 1.64 – 1.56 (m, 12H); ^{13}C NMR (101 MHz, $CDCl_3$) δ 170.4, 169.8, 169.6, 169.5, 166.7, 166.4, 166.4, 166.3, 135.8, 135.4, 126.6, 126.3, 68.9, 68.8, 68.5, 63.2, 61.9, 61.1, 60.8, 60.7,

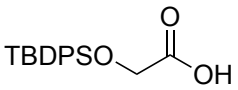
60.6, 18.2, 18.1, 16.8, 16.7, 16.6, 16.6; HRMS (TOF MS ES+) m/z calcd for $C_{30}H_{38}O_{20}Na^+$ $[M+Na]^+$: 741.1854, Found: 741.1853.

The overall yields and the amount of isolated OLGADMAs are presented in Table 24.

OLGADMA	overall yield* (%)	isolated weight (mg)
4Aa	29	239
4Ab	28	73
4Ba	33	38
4Bb	11	36
6A	9	24
6B	3	17
8A	13	37
8B	3	13

Table 24. Overall yield and isolated amounts of OLGADMAs prepared in this work. * Calculated from the partial yields of each single-step reaction, starting from protected monomers **1**-**4**.

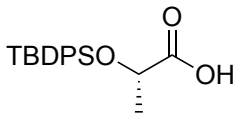
7.2.2 Synthesis and Characterisation of OLGADMA Precursors



1

Preparation: TBDPS chloride (6.24 mL, 24.0 mmol) was added dropwise to a solution of methyl glycolate (1.54 mL, 20.0 mmol) and imidazole (2.7 g, 40 mmol) in dichloromethane (80 mL) at 0°C. The reaction mixture was warmed to rt, left stirring for 2h and then quenched by the addition of aq. HCl (1 M, 50 mL). The organic phase was washed with water (2 × 100 mL), dried over Na_2SO_4 and concentrated *in vacuo*. The resulting crude mixture was dissolved in THF (180 mL) and aq. NaOH (1 M, 80

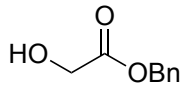
mL, 80 mmol) was added to the solution at 0°C. The mixture was then warmed to rt and stirred for 4 h. Water (100 mL) was added upon reaction completion and the THF was removed by concentration *in vacuo.* The aqueous phase was washed with diethyl ether (2 × 100 mL), and acidified with aq. HCl (1 M, 50 mL) until reaching pH 2 and extracted with ethyl acetate (3 × 50 mL). The organic phase was dried over Na_2SO_4 and concentrated *in vacuo* to afford the desired compound. **Appearance:** colourless oil; **Yield:** 55%; **Characterisation:** IR (film)/cm^{-1} 3071, 2929, 2855, 1726 (s. C=O), 1587, 1472, 1427, 1390, 1364, 1244, 1136, 1110, 998, 939, 820, 738, 697; ^{1}H NMR (400 MHz, $CDCl_3$) δ 7.72 – 7.62 (m, 4H), 7.51 – 7.38 (m, 6H), 4.26 (s, 2H), 1.12 (s, 9H); ^{13}C NMR (101 MHz, $CDCl_3$) δ 173.2, 135.5, 135.4, 135.3, 134.8, 131.7, 130.3, 129.6, 128.1, 127.8, 127.7, 61.9, 26.7, 19.1; The observed characterisation data was consistent with that previously reported[123]



2

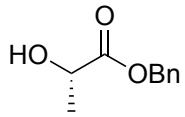
Preparation: TBDPS chloride (6.24 mL, 24.0 mmol) was added dropwise to a solution of methyl L-lactate (1.91 mL, 20.0 mmol) and imidazole (2.72 g, 40.0 mmol) in dichloromethane (80 mL) at 0 °C. The reaction mixture was warmed to rt, left stirring for 1 h and then quenched by the addition of 10% aq. HCl (50 mL). The organic phase was washed with brine (2 × 50 mL), dried over Na_2SO_4 and concentrated *in vacuo*. The resulting crude mixture was dissolved in THF (100 mL), aq. NaOH (1 M, 80 mL, 80 mmol) was added and the mixture was stirred 32 h at rt. Upon completion, water (100 mL) was added and the THF removed by concentration *in vacuo.* The aqueous phase was washed with diethyl ether (2 × 100 mL), acidified with 10% aq. HCl (50 mL) to reach pH 2 and extracted with ethyl acetate (3 × 50 mL). The organic phase was dried over Na_2SO_4 and concentrated *in vacuo* to afford the desired compound. **Appearance:** white solid; **MP:** 69-72 °C; **Yield:** 59%; **Characterisation:** IR (film)/cm^{-1} 3071, 2933, 2892, 2859, 1722 (s. C=O), 1472, 1427, 1364, 1300, 1244, 1140, 1110, 1058, 969, 823, 786, 738, 701; ^{1}H NMR (400 MHz, $CDCl_3$) δ 7.71 – 7.64 (m, 4H), 7.51 – 7.36 (m, 6H), 4.34 (q, J = 6.8 Hz, 1H), 1.36 (d, J = 6.8 Hz, 3H), 1.13 (s, 9H); ^{13}C

NMR (101 MHz, $CDCl_3$) δ 176.9, 135.7, 135.7, 132.8, 132.1, 130.2, 130.1, 127.9, 127.8, 69.1, 26.8, 21.0, 19.2. The observed characterisation data was consistent with that previously reported.[123]



3

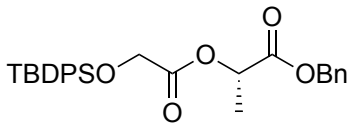
Preparation: DBU (0.17 mL, 1.1 mmol) was added dropwise to a mixture of glycolic acid (0.09 g, 1.2 mmol) and benzyl bromide (0.12 mL, 1.0 mmol) in acetonitrile (1 mL) at 0 °C. The reaction mixture was warmed to 70 °C, left stirring for 5h and then poured into ice cold water (10 mL). The aqueous phase was extracted with ethyl acetate (3 × 10 mL) and the combined organic extracts were washed with aq. HCl (1M, 10 mL), ice cold water (2 × 10 mL), dried over Na_2SO_4 and concentrated *in vacuo* to afford the desired compound. **Appearance:** colourless oil; **Yield:** 76%; R_f = 0.23 (50% Et_2O/hexane); **Characterisation:** IR (film)/cm^{-1} 3451 (br. OH), 1736 (C=O), 1498, 1453, 1192, 1084, 991, 738, 697; ^1H NMR (400 MHz, $CDCl_3$) δ 7.44 – 7.32 (m, 5H), 5.23 (s, 2H), 4.21 (s, 2H), 2.77 (br, 1H); ^{13}C NMR (101 MHz, $CDCl_3$) δ 173.2, 135.0, 128.6, 128.6, 128.4, 67.2, 60.6. The observed characterisation data for this compound was consistent with that previously reported.[123]



4

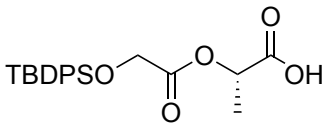
Preparation: DBU (3.30 mL, 22.0 mmol) was added dropwise to a mixture of L-lactic acid (>85% solution in water, 2.5 g, >24 mmol) and benzyl bromide (2.38 mL, 20.0 mmol) in acetonitrile (20 mL) at 0 °C. The reaction mixture was warmed to 70 °C, left stirring for 2 h 45 min and then poured into ice-cold water (20 mL). The aqueous phase was extracted with ethyl acetate (2 × 20 mL) and the combined organic extracts were washed with aq. HCl (10%, 20 mL), brine (20 mL), dried over Na_2SO_4 and concentrated *in vacuo*. The crude mixture was purified by vacuum distillation (165 °C at 0.22 mmHg)

to afford the desired compound. **Appearance:** colourless oil; **Yield:** 41%; R_f = 0.69 (50% ethyl acetate/hexane); **Characterisation:** IR (film)/cm^{-1} 3462 (br. OH), 2982, 1737 (C=O), 1498, 1453, 1375, 1264, 1215, 1126, 1043, 954, 753, 701; ^{1}H NMR (400 MHz, $CDCl_3$) δ 7.42 – 7.33 (m, 5H), 5.22 (s, 2H), 4.33 (q, J = 6.9 Hz, 1H), 2.77 (s, 1H), 1.45 (d, J = 6.9 Hz, 3H); ^{13}C NMR (101 MHz, $CDCl_3$) δ 175.5, 135.2, 128.6, 128.5, 128.2, 67.2, 66.8, 20.3. The observed characterisation data for this compound was consistent with that previously reported.[123]



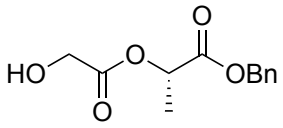
5

Preparation: The compound was prepared by subjecting **1** and **4** to the standard ester formation procedure. **Appearance:** colourless oil**, Yield:** 62%**, Characterisation:** R_f = 0.18 (5% EtOAc/hexane); IR (film)/cm^{-1} 3041, 2937, 2855, 1751 (C=O), 1453, 1267, 1192, 1133, 820, 700, 506; ^{1}H NMR (400 MHz, $CDCl_3$) δ 7.73 – 7.67 (m, 4H), 7.48 – 7.31 (m, 11H), 5.24 – 5.14 (m, 3H), 4.37 (d, *J* = 16.8 Hz, 1H), 4.31 (d, *J* = 16.7 Hz, 1H), 1.46 (d, *J* = 7.1 Hz, 3H), 1.10 (s, 9H); ^{13}C NMR (101 MHz, $CDCl_3$) δ 170.6, 170.3, 135.6, 135.5, 135.2, 132.7, 129.9, 128.6, 128.4, 128.1, 127.8, 68.7, 67.0, 62.0, 26.6, 19.2, 16.9. The spectroscopic data was consistent with that previously reported.[123]



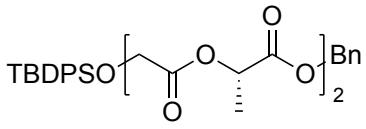
6

Preparation: The compound was prepared by subjecting **5** to the standard catalytic hydrogenation procedure. **Appearance:** colourless oil**, Yield:** 100%**, Characterisation:** IR (film)/cm^{-1} broad OH vibration, 3049, 2937, 2862, 1745 (C=O), 1729 (C=O), 1431, 1192, 1140, 820, 700; ^{1}H NMR (400 MHz, $CDCl_3$) δ 7.73 – 7.67 (m, 4H), 7.46 – 7.37 (m, 6H), 5.15 (q, *J* = 7.1 Hz, 1H), 4.38 (d, *J* = 16.9 Hz, 1H), 4.33 (d, *J* = 16.9 Hz, 1H), 1.51 (d, *J* = 7.1 Hz, 3H), 1.10 (s, 9H); ^{13}C NMR (101 MHz, $CDCl_3$) δ 176.1, 170.6, 135.6, 135.5, 132.6, 132.6, 129.9, 127.8, 68.2, 61.9, 26.6, 19.2, 16.7; HRMS (APCI) m/z calcd for $C_{21}H_{25}O_5Si^-$ [M-H]$^-$: 385.1477; Found: 385.1465.



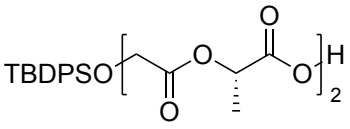
7

Preparation: The compound was prepared by subjecting **5** to the standard silyl ether cleavage procedure. **Appearance:** colourless oil**, Yield:** 93%**, Characterisation:** R_f = 0.17 (60% Et_2O/hexane); IR (film)/cm^{-1} 3473 (br, OH), 2944, 1744 (C=O), 1453, 1267, 1192, 1095, 745; ^1H NMR (400 MHz, $CDCl_3$) δ 7.43 – 7.32 (m, 5H), 5.26 (q, *J* = 7.1 Hz, 1H), 5.23 – 5.16 (m, 2H), 4.30 (d, *J* = 17.4 Hz, 1H), 4.24 (d, *J* = 17.4 Hz, 1H), 2.32 (br, 1H), 1.55 (d, *J* = 7.1 Hz, 3H); ^{13}C NMR (101 MHz, $CDCl_3$) δ 172.7, 170.0, 135.0, 128.6, 128.5, 128.1, 69.4, 67.2, 60.5, 16.8. The spectroscopic data was consistent with that previously reported.[123]



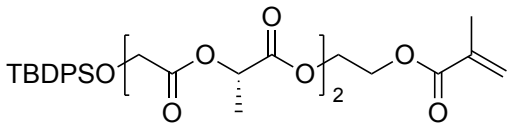
8

Preparation: The compound was prepared by subjecting **6** and **7** to the standard ester formation procedure. **Appearance:** colourless oil**, Yield:** 84%**, Characterisation:** R_f = 0.26 (20% EtOAc/hexane); IR (film)/cm^{-1} 3041, 2987, 2855, 1751 (C=O), 1453, 1267, 1177, 1088, 820, 700; ^1H NMR (400 MHz, $CDCl_3$) δ 7.73 – 7.67 (m, 4H), 7.48 – 7.31 (m, 11H), 5.26 – 5.14 (m, 4H), 4.87 (d, *J* = 16.0 Hz, 1H), 4.63 (d, *J* = 16.0 Hz, 1H), 4.38 (d, *J* = 16.8 Hz, 1H), 4.31 (d, *J* = 16.8 Hz, 1H), 1.53 (d, *J* = 7.1 Hz, 3H), 1.53 (d, *J* = 7.1 Hz, 3H), 1.09 (s, 9H); ^{13}C NMR (101 MHz, $CDCl_3$) δ 170.6, 169.8, 166.6, 135.6, 135.5, 135.1, 132.7, 129.9, 128.6, 128.5, 128.2, 127.8, 69.5, 68.4, 67.2, 61.9, 60.7, 26.6, 19.2, 16.8, 16.8.



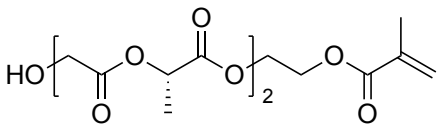
9

Preparation: The compound was prepared by subjecting **8** to the standard catalytic hydrogenation procedure. **Appearance:** pale yellow oil**, Yield:** 99%**, Characterisation:** IR (film)/cm^{-1} broad OH vibration observed, 3069, 2932, 1744 (C=O), 1590, 1185, 1130, 740, 702 ; ^{1}H NMR (400 MHz, $CDCl_3$) δ 7.76 – 7.66 (m, 4H), 7.47 – 7.37 (m, 6H), 5.25 – 5.13 (m, 2H), 4.88 (d, *J* = 16.1 Hz, 1H), 4.64 (d, *J* = 16.1 Hz, 1H), 4.38 (d, *J* = 16.8, 1H), 4.32 (d, *J* = 16.9 Hz, 1H), 1.57 (d, *J* = 7.2 Hz, 3H), 1.53 (d, *J* = 7.1 Hz, 3H), 1.09 (s, 9H); ^{13}C NMR (101 MHz, $CDCl_3$) δ 175.2, 170.7, 169.9, 166.6, 135.6, 135.5, 132.6, 129.9, 127.8, 68.9, 68.4, 61.9, 60.7, 26.6, 19.2, 16.8, 16.6; HRMS (APCI) m/z calcd for $C_{26}H_{31}O_9Si^-$ [M-H]$^-$: 515.1743, Found: 515.1730.



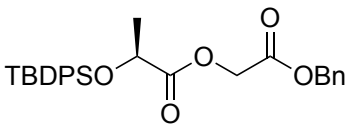
10

Preparation: The compound was prepared by subjecting **9** to the standard standard procedure for the synthesis of monomethacrylates. **Appearance:** colourless oil**, Yield:** 68%**, Characterisation:** R_f = 0.20 (20% EtOAc/hexane); IR (film)/cm^{-1} 3080, 2952, 2862, 1759 (C=O), 1720 (C=O), 1640, 1453, 1274, 1095, 946, 820, 700; ^{1}H NMR (400 MHz, $CDCl_3$) δ 7.74 – 7.65 (m, 4H), 7.48 – 7.35 (m, 6H), 6.16 – 6.09 (m, 1H), 5.63 – 5.58 (m, 1H), 5.23 – 5.13 (m, 2H), 4.87 (d, *J* = 16.0 Hz, 1H), 4.63 (d, *J* = 16.0 Hz, 1H), 4.51 – 4.27 (m, 6H), 1.98 – 1.91 (m, 3H), 1.53 (d, *J* = 7.1, 3H), 1.52 (d, *J* = 7.1 Hz, 3H), 1.09 (s, 9H); ^{13}C NMR (101 MHz, $CDCl_3$) δ 170.6, 169.8, 169.8, 167.0, 166.6, 135.7, 135.6, 135.5, 132.6, 129.9, 127.8, 126.2, 69.3, 68.4, 63.1, 61.9, 61.9, 60.7, 26.6, 19.2, 18.2, 16.8, 16.7.



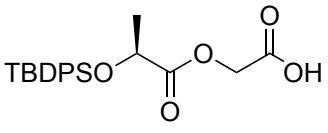
11

Preparation: The compound was prepared by subjecting **10** to the standard silyl ether cleavage procedure. **Appearance:** colourless oil**, Yield:** 86%**, Characterisation:** R_f = 0.24 (50% EtOAc/hexane); IR (film)/cm^{-1} 3503 (br. OH), 2959, 1751 (C=O), 1720 (C=O), 1640, 1453, 1177, 1095; ^{1}H NMR (400 MHz, $CDCl_3$) δ 6.15 – 6.11 (m, 1H), 5.63 – 5.59 (m, 1H), 5.30 (q, *J* = 7.1 Hz, 1H), 5.19 (q, *J* = 7.1 Hz, 1H), 4.87 (d, *J* = 16.0 Hz, 1H), 4.67 (d, *J* = 16.0 Hz, 1H), 4.52 – 4.42 (m, 1H), 4.42 – 4.22 (m, 5H), 2.56 – 2.17 (br, 1H), 1.98 – 1.92 (m, 3H), 1.61 (d, J = 7.1 Hz, 3H), 1.53 (d, J = 7.1 Hz, 3H); ^{13}C NMR (101 MHz, $CDCl_3$) δ 172.6, 169.7, 169.6, 167.0, 166.4, 135.8, 126.2, 69.4, 69.0, 63.1, 62.0, 60.8, 60.5, 18.2, 16.8, 16.8; HRMS (TOF MS ES+) m/z calcd for $C_{16}H_{23}O_{11}^+$ $[M+H]^+$: 391.1240; Found: 391.1228



12

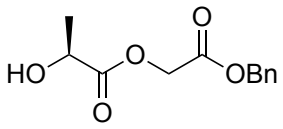
Preparation: The compound was prepared by subjecting **2** and **3** to the standard ester formation procedure. **Appearance:** colourless oil**, Yield:** 74%**, Characterisation:** R_f = 0.30 (5% EtOAc/hexane); IR (film)/cm^{-1} 3071, 2933, 2858, 1759 (C=O), 1427, 1394, 1177, 1133, 969, 782, 741, 700; ^{1}H NMR (400 MHz, $CDCl_3$) δ 7.72 – 7.65 (m, 4H), 7.48 – 7.28 (m, 11H), 5.18 (s, 2H), 4.62 (d, *J* = 15.9 Hz, 1H), 4.47 (d, *J* = 15.9 Hz, 1H), 4.39 (q, *J* = 6.8 Hz, 1H), 1.41 (d, *J* = 6.8 Hz, 3H), 1.10 (s, 9H); ^{13}C NMR (101 MHz, $CDCl_3$) δ 173.1, 167.3, 135.9, 135.7, 135.0, 133.4, 133.0, 129.8, 128.6, 128.5, 128.4, 127.6, 127.6, 68.7, 67.0, 60.6, 26.8, 21.2, 19.2; HRMS (TOF MS ES+) m/z calcd for $C_{28}H_{32}O_5NaSi^+$ $[M+Na]^+$: 499.1917; Found: 499.1909.



13

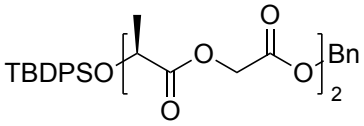
Preparation: The compound was prepared by subjecting **12** to the standard catalytic hydrogenation procedure. **Appearance:** colourless oil**, Yield:** 95%**, Characterisation:** IR (film)/cm^{-1} broad OH vibration visible, 3069, 2932, 2857, 1728 (C=O), 1588, 1424, 1132, 1105, 820, 738, 698, 609, 504, 483; ^{1}H NMR (400 MHz,

$CDCl_3$) δ 7.73 – 7.64 (m, 4H), 7.49 – 7.34 (m, 6H), 4.60 (d, *J* = 16.4 Hz, 1H), 4.50 (d, *J* = 16.4 Hz, 1H), 4.40 (q, *J* = 6.8 Hz, 1H), 1.43 (d, *J* = 6.8 Hz, 3H), 1.10 (s, 9H); ^{13}C NMR (101 MHz, $CDCl_3$) δ 173.0, 172.4, 135.9, 135.7, 133.4, 132.9, 129.8, 127.7, 127.6, 68.6, 60.0, 26.8, 21.2, 19.2; HRMS (TOF MS ES+) m/z calcd for $C_{21}H_{26}O_5NaSi^+$ $[M+Na]^+$: 409.1447; Found: 409.1461.



14

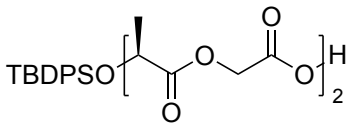
Preparation: The compound was prepared by subjecting **12** to the standard silyl ether cleavage procedure. **Appearance:** colourless oil**, Yield:** 93%**, Characterisation:** R_f = 0.16 (30% EtOAc/hexane); IR (film)/cm^{-1} 3488 (br, OH), 3034, 2985, 2944, 1744 (C=O), 1453, 1278, 1181, 1125, 752, 700; ^{1}H NMR (400 MHz, $CDCl_3$) δ 7.44 – 7.31 (m, 5H), 5.21 (s, 2H), 4.80 (d, *J* = 15.9 Hz, 1H), 4.71 (d, *J* = 15.9 Hz, 1H), 4.42 (q, *J* = 6.9 Hz, 1H), 2.16 (br, 1H), 1.48 (d, *J* = 7.0 Hz, 3H); ^{13}C NMR (101 MHz, $CDCl_3$) δ 175.1, 167.1, 134.8, 128.7, 128.5, 67.3, 66.7, 61.2, 20.3.



15

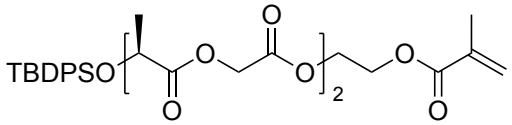
Preparation: The compound was prepared by subjecting **13** and **14** to the standard ester formation procedure. **Appearance:** colourless oil**, Yield:** 89%**, Characterisation:** R_f = 0.24 (15% EtOAc/hexane); IR (film)/cm^{-1} 3069, 2933, 2857, 1753 (C=O), 1451, 1424, 1277, 1174, 1128, 1101, 969, 740, 701, 611, 507; ^{1}H NMR (400 MHz, $CDCl_3$) δ 7.71 – 7.65 (m, 4H), 7.49 – 7.31 (m, 11H), 5.24 (q, *J* = 7.1 Hz, 1H), 5.19 (s, 2H), 4.80 (d, *J* = 15.9 Hz, 1H), 4.68 (d, *J* = 16.0 Hz, 1H), 4.62 (d, *J* = 15.9 Hz, 1H), 4.45 (d, *J* = 16.0 Hz, 1H), 4.38 (q, *J* = 6.8 Hz, 1H), 1.53 (d, *J* = 7.1 Hz, 3H), 1.43 (d, *J* = 6.8 Hz, 3H), 1.10 (s, 9H); ^{13}C NMR (101 MHz, $CDCl_3$) δ 173.0, 169.5, 166.9, 166.8, 135.9, 135.7, 134.8, 133.4, 132.9, 129.8, 128.7, 128.5, 127.7, 127.6,

69.0, 68.6, 67.3, 61.1, 60.1, 26.8, 21.3, 19.2, 16.7; HRMS (TOF MS ES+) m/z calcd for $C_{33}H_{38}O_9NaSi^+$ [M+Na]$^+$: 629.2183; Found: 629.2181.



16

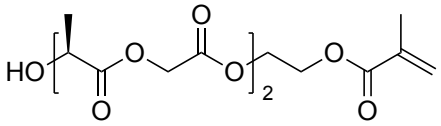
Preparation: The compound was prepared by subjecting **15** to the standard catalytic hydrogenation procedure. **Appearance:** pale yellow oil**, Yield:** 97%**, Characterisation:** IR (film)/cm^{-1} broad OH vibration, 3071, 2929, 2858, 1763 (C=O), 1427, 1185, 1133, 1110, 704; ^{1}H NMR (400 MHz, $CDCl_3$) δ 7.71 – 7.63 (m, 4H), 7.50 – 7.34 (m, 6H), 5.24 (q, *J* = 7.1 Hz, 1H), 4.80 (d, *J* = 16.4 Hz, 1H), 4.73 – 4.61 (m, 2H), 4.46 (d, *J* = 16.0 Hz, 1H), 4.39 (q, *J* = 6.8 Hz, 1H), 1.56 (d, *J* = 7.1 Hz, 3H), 1.43 (d, *J* = 6.8 Hz, 3H), 1.10 (s, 9H); ^{13}C NMR (101 MHz, $CDCl_3$) δ 173.1, 171.0, 169.4, 166.9, 135.9, 135.7, 133.4, 132.9, 129.8, 127.7, 127.6, 69.0, 68.6, 60.5, 60.3, 26.8, 21.3, 19.2, 16.7; HRMS (TOF MS ES+) m/z calcd for $C_{26}H_{32}O_9NaSi$ [M+Na]$^+$: 539.1713, Found: 539.1709.



17

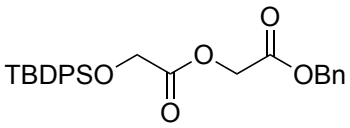
Preparation: The compound was prepared by subjecting **16** to the standard procedure for the synthesis of monomethacrylates. **Appearance:** colourless oil**, Yield:** 89%**, Characterisation:** R_f = 0.25 (30% EtOAc/hexane); IR (film)/cm^{-1} 3048, 2931, 2857, 1728 (C=O), 1588, 1468, 1426, 1136, 1109, 820, 700; ^{1}H NMR (400 MHz, $CDCl_3$) δ 7.71 – 7.64 (m, 4H), 7.48 – 7.34 (m, 6H), 6.15 – 6.11 (m, 1H), 5.61 (quint, *J* = 1.6 Hz, 1H), 5.24 (q, *J* = 7.1 Hz, 1H), 4.79 (d, *J* = 15.9 Hz, 1H), 4.68 (d, *J* = 16.0 Hz, 1H), 4.61 (d, *J* = 16.0 Hz, 1H), 4.50 – 4.33 (m, 6H), 1.97 – 1.93 (m, 3H), 1.56 (d, *J* = 7.1 Hz, 3H), 1.43 (d, *J* = 6.8 Hz, 3H), 1.10 (s, 9H); ^{13}C NMR (101 MHz, $CDCl_3$) δ 173.0, 169.5, 167.0, 166.9, 166.8, 135.9, 135.7, 133.4, 132.9, 129.8, 127.7, 127.6, 126.3,

69.0, 68.6, 63.1, 62.0, 60.9, 60.2, 26.8, 21.3, 19.2, 18.2, 16.7; HRMS (TOF MS ES+) m/z calcd for $C_{32}H_{40}O_{11}NaSi^+$ [M+Na]$^+$: 651.2238, Found: 651.2240.



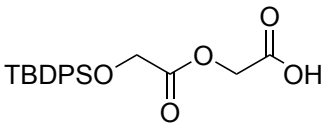
18

Preparation: The compound was prepared by subjecting **17** to the standard silyl ether cleavage procedure. **Appearance:** colourless oil, **Yield:** 76%, **Characterisation:** R_f = 0.37 (60% EtOAc/hexane); IR (film)/cm^{-1} 3500 (br. OH), 2986, 2957, 1750 (C=O), 1719 (C=O), 1635, 1451, 1384, 1292, 1169, 1128, 1096, 950; ^{1}H NMR (400 MHz, $CDCl_3$) δ 6.16 – 6.09 (m, 1H), 5.60 (quint, *J* = 1.6 Hz, 1H), 5.26 (q, *J* = 7.1 Hz, 1H), 4.86 (d, *J* = 16.0 Hz, 1H), 4.79 (d, *J* = 15.9 Hz, 1H), 4.72 (d, *J* = 16.0 Hz, 1H), 4.62 (d, *J* = 16.0 Hz, 1H), 4.46 – 4.33 (m, 5H), 3.34 – 2.44 (br, 1H), 1.94 (t, *J* = 1.2 Hz, 3H), 1.59 (d, *J* = 7.1 Hz, 3H), 1.49 (d, *J* = 7.0 Hz, 3H); ^{13}C NMR (101 MHz, $CDCl_3$) δ 174.8, 169.4, 167.0, 166.8, 166.6, 135.7, 126.3, 69.1, 66.7, 63.1, 62.0, 60.9, 60.8, 20.3, 18.2, 16.7; HRMS (TOF MS ES+) m/z calcd for $C_{16}H_{22}O_{11}Na^+$ [M+Na]$^+$: 413.1060, Found: 413.1066.



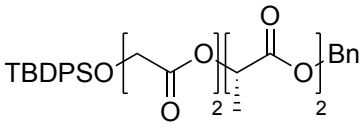
19

Preparation: The compound was prepared by subjecting **1** and **3** to the standard ester formation procedure. **Appearance:** colourless oil**, Yield:** 78%**, Characterisation:** R_f = 0.15 (5% EtOAc/hexane); IR (film)/cm^{-1} 3071, 2929, 2855, 1755 (C=O), 1472, 1427, 1267, 1133, 823, 738, 697; ^{1}H NMR (400 MHz, $CDCl_3$) δ 7.73 – 7.67 (m, 4H), 7.48 – 7.32 (m, 11H), 5.20 (s, 2H), 4.68 (s, 2H), 4.37 (s, 2H), 1.10 (s, 9H); ^{13}C NMR (101 MHz, $CDCl_3$) δ 170.6, 167.3, 135.5, 135.0, 134.8, 132.6, 129.9, 128.6, 128.5, 128.4, 127.8, 67.1, 61.9, 60.7, 26.6, 19.2; HRMS (TOF MS ES+) m/z calcd for $C_{27}H_{30}O_5NaSi^+$ [M+Na]$^+$: 485.1760; Found: 485.1742.



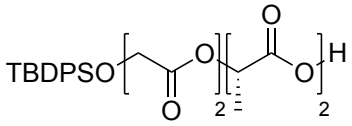
20

Preparation: The compound was prepared by subjecting **19** to the standard catalytic hydrogenation procedure. **Appearance:** colourless oil**, Yield:** 100%**, Characterisation:** IR (film)/cm^{-1} broad OH vibration visible, 3071, 2929, 2855, 1763 (C=O), 1729 (C=O), 1580, 1431, 1259, 1200, 1110, 931, 805, 700; ^{1}H NMR (400 MHz, $CDCl_3$) δ 7.75 – 7.66 (m, 4H), 7.47 – 7.37 (m, 6H), 4.69 (s, 2H), 4.38 (s, 2H), 1.10 (s, 9H); ^{13}C NMR (101 MHz, $CDCl_3$) δ 171.8, 170.6, 135.5, 134.8, 132.6, 130.0, 127.8, 61.8, 60.0, 26.6, 19.2; HRMS (TOF MS ES+) m/z calcd for $C_{20}H_{24}O_5NaSi^+$ $[M+Na]^+$: 395.1291; Found: 395.1291.



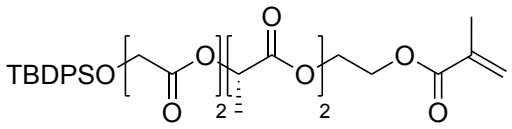
21

Preparation: The compound was prepared by subjecting **20** and **32** to the standard ester formation procedure. **Appearance:** colourless oil**, Yield:** 97%**, Characterisation:** R_f = 0.26 (20% EtOAc/hexane); IR (film)/cm^{-1} 3069, 2931, 2857, 1752 (C=O), 1451, 1173, 970; ^{1}H NMR (400 MHz, $CDCl_3$) δ 7.74 – 7.67 (m, 4H), 7.47 – 7.33 (m, 11H), 5.25 – 5.13 (m, 4H), 4.77 (d, *J* = 16.1 Hz, 1H), 4.66 (d, *J* = 16.1 Hz, 1H), 4.37 (d, *J* = 16.8 Hz, 1H), 4.37 (d, *J* = 16.8, 1H), 1.54 (d, *J* = 7.1 Hz, 3H), 1.52 (d, *J* = 7.1 Hz, 3H), 1.10 (s, 9H); ^{13}C NMR (101 MHz, $CDCl_3$) δ 170.5, 169.9, 169.5, 166.9, 135.5, 135.0, 132.6, 132.6, 129.9, 128.6, 128.5, 128.2, 127.8, 69.3, 69.1, 67.2, 61.8, 60.4, 26.6, 19.2, 16.7, 16.6; HRMS (TOF MS ES+) m/z calcd for $C_{33}H_{42}NO_9Si^+$ $[M+NH_4]^+$: 624.2629; Found: 624.2637.



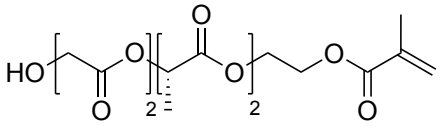
22

Preparation: The compound was prepared by subjecting **21** to the standard catalytic hydrogenation procedure. **Appearance:** yellowish oil**, Yield:** 94%**, Characterisation:** IR (film)/cm^{-1} broad OH vibration observed, 3070, 2932, 2857, 1744 (C=O), 1589, 1426, 1186, 1131, 1102, 821, 741, 703; ^{1}H NMR (400 MHz, $CDCl_3$) δ 7.75 – 7.64 (m, 4H), 7.49 – 7.35 (m, 6H), 5.28 – 5.14 (m, 2H), 4.77 (d, *J* = 16.1 Hz, 1H), 4.67 (d, *J* = 16.1 Hz, 1H), 4.37 (d, *J* = 16.7 Hz, 1H), 4.37 (d, *J* = 16.7 Hz, 1H), 1.57 (d, *J* = 7.1 Hz, 6H), 1.09 (s, 9H); ^{13}C NMR (101 MHz, $CDCl_3$) δ 175.2, 170.6, 169.4, 166.9, 135.5, 132.6, 129.9, 127.8, 69.1, 68.7, 61.8, 60.4, 26.6, 19.2, 16.6; HRMS (TOF MS ES+) m/z calcd for $C_{26}H_{36}NO_9Si^+$ $[M+NH_4]^+$: 534.2159, Found: 534.2155.



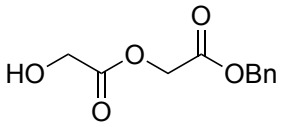
23

Preparation: The compound was prepared by subjecting **22** to the standard procedure for the synthesis of monomethacrylates. **Appearance:** colourless oil**, Yield:** 70%**, Characterisation:** R_f = 0.30 (25% EtOAc/hexane); IR (film)/cm^{-1} 3071, 2933, 2855, 1751(C=O), 1720 (C=O), 1636, 1453, 1129, 1095, 823, 741, 700, 611; ^{1}H NMR (400 MHz, $CDCl_3$) δ 7.75 – 7.63 (m, 4H), 7.51 – 7.33 (m, 6H), 6.16 – 6.09 (m, 1H), 5.61 (quint, *J* = 1.5 Hz, 1H), 5.31 – 5.11 (m, 2H), 4.77 (d, *J* = 16.1 Hz, 1H), 4.66 (d, *J* = 16.1 Hz, 1H), 4.53 – 4.29 (m, 6H), 1.97 – 1.93 (m, 3H), 1.57 (d, *J* = 7.1 Hz, 3H), 1.54 (d, *J* = 7.1 Hz, 3H), 1.09 (s, 9H); ^{13}C NMR (101 MHz, $CDCl_3$) δ 170.5, 169.9, 169.4, 167.0, 166.9, 135.7, 135.5, 132.6, 129.9, 127.8, 126.3, 69.1, 69.0, 63.0, 62.0, 61.8, 60.3, 26.6, 19.2, 18.2, 16.7, 16.6.



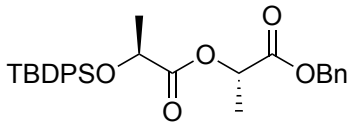
24

Preparation: The compound was prepared by subjecting **23** to the standard silyl ether cleavage procedure. **Appearance:** colourless oil**, Yield:** 84%**, Characterisation:** R_f = 0.20 (50% EtOac/hexane); IR (film)/cm^{-1} 3503 (br, OH), 2952, 1744 (C=O), 1720 (C=O), 1640, 1453, 1386, 1162, 1088, 954; ^{1}H NMR (400 MHz, $CDCl_3$) δ 6.18 – 6.08 (m, 1H), 5.61 (quint, *J* = 1.6 Hz, 1H), 5.28 – 5.14 (m, 2H), 4.86 (d, *J* = 16.1 Hz, 1H), 4.78 (d, *J* = 16.0 Hz, 1H), 4.50 – 4.29 (m, 6H), 2.22 (s, 1H), 1.95 (dd, *J* = 1.6, 1.0 Hz, 3H), 1.60 (d, *J* = 7.1 Hz, 3H), 1.54 (d, *J* = 7.1 Hz, 3H); ^{13}C NMR (101 MHz, $CDCl_3$) δ 172.6, 169.8, 169.3, 167.0, 166.6, 135.8, 126.3, 69.3, 69.2, 63.0, 62.0, 60.8, 60.4, 18.2, 16.7, 16.7.



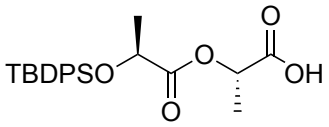
25

Preparation: The compound was prepared by subjecting **19** to the standard silyl ether cleavage procedure. **Appearance:** colourless oil**, Yield:** 90%**, Characterisation:** R_f = 0.20 (40% EtOAc/hexane); IR (film)/cm^{-1} 3309 (br, OH), 2952, 1744 (C=O), 1580, 1431, 1401, 1200, 1092, 1039, 700; ^{1}H NMR (400 MHz, $CDCl_3$) δ 7.45 – 7.31 (m, 5H), 5.22 (s, 2H), 4.78 (s, 2H), 4.31 (s, 2H), 2.33 (br, 1H); ^{13}C NMR (101 MHz, $CDCl_3$) δ 172.7, 167.1, 134.8, 128.7, 128.4, 67.4, 61.1, 60.4; HRMS (APCI) m/z calcd for $C_{11}H_{11}O_5^-$ [M-H]$^-$: 223.0612; Found: 223.0611.



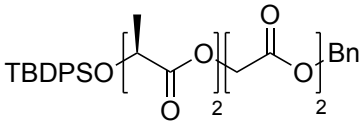
26

Preparation: The compound was prepared by subjecting **2** and **4** to the standard ester formation procedure. **Appearance:** colourless oil**, Yield:** 57%**, Characterisation:** R_f = 0.20 (5% EtOAc/hexane); IR (film)/cm^{-1} 3071, 2933, 2858, 1751 (C=O), 1587, 1453, 1427, 1267, 1185, 1129, 972, 823, 738, 700; ^{1}H NMR (400 MHz, $CDCl_3$) δ 7.73 – 7.64 (m, 4H), 7.50 – 7.27 (m, 11H), 5.17 (d, *J* = 12.3 Hz, 1H), 5.11 (d, *J* = 12.3 Hz, 1H) 4.99 (q, *J* = 7.1 Hz, 1H), 4.33 (q, *J* = 6.7 Hz, 1H), 1.38 (d, *J* = 6.7 Hz, 3H), 1.34 (d, *J* = 7.1 Hz, 3H), 1.10 (s, 9H); ^{13}C NMR (101 MHz, $CDCl_3$) δ 173.1, 170.3, 135.9, 135.7, 135.2, 133.4, 133.1, 129.8, 128.6, 128.4, 128.2, 127.6, 127.5, 68.5, 67.0, 26.8, 21.1, 19.2, 16.7; HRMS (TOF MS ES+) m/z calcd for $C_{29}H_{34}O_5SiNa^+$ $[M+Na]^+$: 513.2073; Found: 513.2070.



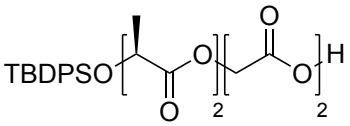
27

Preparation: The compound was prepared by subjecting **26** to the standard catalytic hydrogenation procedure. **Appearance:** colourless oil**, Yield:** 100%**, Characterisation:** IR (film)/cm^{-1}broad OH vibration observed, 3071, 2933, 2858, 1763 (C=O), 1722 (C=O), 1587, 1461, 1427, 1185, 1107, 972, 909, 820, 734, 700; ^{1}H NMR (400 MHz, $CDCl_3$) δ 7.72 – 7.66 (m, 4H), 7.47 – 7.34 (m, 6H), 4.95 (q, *J* = 7.1 Hz, 1H), 4.34 (q, *J* = 6.7 Hz, 1H), 1.42 (d, *J* = 6.7 Hz, 3H), 1.39 (d, *J* = 7.2 Hz, 3H), 1.10 (s, 9H); ^{13}C NMR (101 MHz, $CDCl_3$) δ 176.1, 173.1, 136.0, 135.7, 133.4, 133.0, 129.8, 127.6, 127.6, 68.5, 68.1, 26.8, 21.1, 19.2, 16.6; HRMS (TOF MS ES+) m/z calcd for $C_{22}H_{28}O_5NaSi^+$ $[M+Na]^+$: 423.1604; Found: 423.1598.



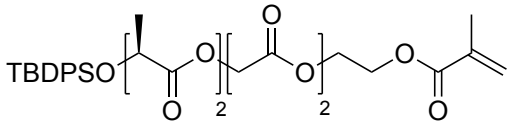
28

Preparation: The compound was prepared by subjecting **27** and **25** to the standard ester formation procedure. **Appearance:** colourless oil**, Yield:** 86%**, Characterisation:** R_f = 0.25 (30% Et_2O/hexane); IR (film)/cm^{-1} 3070, 2931, 2857, 1750 (C=O), 1451, 1170, 971, 702; ^1H NMR (400 MHz, $CDCl_3$) δ 7.72 – 7.66 (m, 4H), 7.50 – 7.32 (m, 11H), 5.20 (s, 2H), 5.01 (q, *J* = 7.1 Hz, 1H), 4.85 (d, *J* = 16.1 Hz, 1H), 4.79 – 4.63 (m, 3H), 4.35 (q, *J* = 6.7 Hz, 1H), 1.45 – 1.39 (m, 6H), 1.10 (s, 9H); ^{13}C NMR (101 MHz, $CDCl_3$) δ 173.1, 169.8, 166.8, 166.6, 136.0, 135.7, 134.8, 133.4, 133.0, 129.8, 128.7, 128.6, 128.4, 127.6, 127.6, 68.5, 68.3, 67.3, 61.1, 60.5, 26.8, 21.1, 19.2, 16.6; HRMS (TOF MS ES+) m/z calcd for $C_{33}H_{38}O_9NaSi^+$ $[M+Na]^+$: 629.2183; Found: 629.2194.



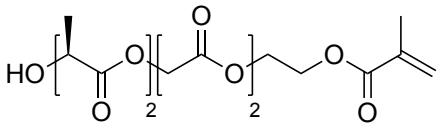
29

Preparation: The compound was prepared by subjecting **28** to the standard catalytic hydrogenation procedure. **Appearance:** yellowish oil**, Yield:** 100%**, Characterisation:** IR (film)/cm^{-1} broad OH vibration, 3329, 2931, 2855, 1760, 1587, 1425, 1176, 1131, 108, 972, 704, 507; ^1H NMR (400 MHz, $CDCl_3$) δ 7.74 – 7.62 (m, 4H), 7.49 – 7.32 (m, 6H), 5.01 (q, *J* = 7.1 Hz, 1H), 4.84 (d, *J* = 16.2 Hz, 1H), 4.80 – 4.63 (m, 3H), 4.35 (q, *J* = 6.7 Hz, 1H), 1.44 – 1.40 (m, 6H), 1.10 (s, 9H); ^{13}C NMR (101 MHz, $CDCl_3$) δ 173.2, 171.4, 169.9, 166.6, 136.0, 135.7, 133.4, 133.0, 129.8, 127.6, 127.6, 68.5, 68.3, 60.5, 26.8, 21.1, 19.2, 16.6; HRMS (APCI) m/z calcd for $C_{26}H_{31}O_9Si^-$ $[M-H]^-$: 515.1743, Found: 515.1732.



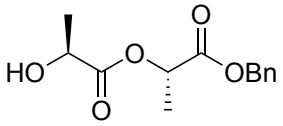
30

Preparation: The compound was prepared by subjecting **29** to the standard procedure for the synthesis of monomethacrylates. **Appearance:** colourless oil**, Yield:** 72%**, Characterisation:** R_f = 0.33 (50% Et_2O/hexane); IR (film)/cm^{-1} 3070, 2934, 2956, 2858, 1759 (C=O), 1722 (C=O), 1636, 1425, 1159, 1130. 1107, 972, 704, 508; ^{1}H NMR (400 MHz, $CDCl_3$) δ 7.73 – 7.64 (m, 4H), 7.49 – 7.33 (m, 6H), 6.16 – 6.09 (m, 1H), 5.61 (quint, *J* = 1.6 Hz, 1H), 5.01 (q, *J* = 7.1 Hz, 1H), 4.84 (d, *J* = 16.1 Hz, 1H), 4.77 – 4.64 (m, 3H), 4.46 – 4.40 (m, 2H), 4.39 – 4.31 (m, 3H), 1.97 – 1.93 (m, 3H), 1.46 – 1.39 (m, 6H), 1.10 (s, 9H); ^{13}C NMR (101 MHz, $CDCl_3$) δ 173.0, 169.8, 167.0, 166.8, 166.6, 135.9, 135.7, 133.4, 133.0, 129.8, 127.6, 127.6, 126.3, 68.5, 68.2, 63.2, 61.9, 60.9, 60.5, 26.8, 21.1, 19.2, 18.2, 16.6; HRMS (TOF MS ES+) m/z calcd for $C_{32}H_{41}O_{11}Si^+$ $[M+H]^+$: 629.2418, Found: 629.2429.



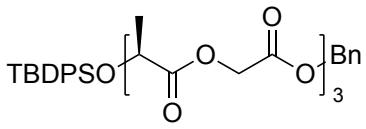
31

Preparation: The compound was prepared by subjecting **30** to the standard silyl ether cleavage procedure. **Appearance:** colourless oil**, Yield:** 60%**, Characterisation:** R_f = 0.28 (70% Et_2O/hexane); IR (film)/cm^{-1} 3500 (br, OH), 2987, 2958, 1753, 1720, 1635, 1388, 1295, 1166, 1129, 1097, 943; ^{1}H NMR (400 MHz, $CDCl_3$) δ 6.16 – 6.10 (m, 1H), 5.61 (quint, *J* = 1.6 Hz, 1H), 5.32 – 5.23 (m, 1H), 4.89 (d, *J* = 16.1 Hz, 1H), 4.79 – 4.68 (m, 3H), 4.50 – 4.29 (m, 5H), 2.87 – 2.70 (m, 1H), 1.95 (t, *J* = 1.3 Hz, 3H), 1.61 (d, *J* = 7.1 Hz, 3H), 1.50 (d, *J* = 6.9 Hz, 3H); ^{13}C NMR (101 MHz, $CDCl_3$) δ 175.0, 169.5, 167.0, 166.8, 166.5, 135.7, 126.3, 69.0, 66.7, 63.2, 61.9, 61.0, 60.7, 20.4, 18.2, 16.7; HRMS (TOF MS ES+) m/z calcd for $C_{16}H_{23}O_{11}^+$ $[M+H]^+$: 391.1240, Found: 391.1226.



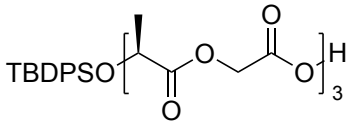
32

Preparation: The compound was prepared by subjecting **26** to the standard silyl ether cleavage procedure. **Appearance:** colourless oil**, Yield:** 64%**, Characterisation:** R_f = 0.12 (30% EtOAc/hexane); IR (film)/cm^{-1} 3490 (br, OH), 2987, 2939, 1737 (C=O), 1498, 1452, 1266, 1188, 1122, 1092, 1042, 743, 697; ^{1}H NMR (400 MHz, $CDCl_3$) δ 7.44 – 7.31 (m, 5H), 5.31 – 5.13 (m, 3H), 4.35 (q, *J* = 7.0 Hz, 1H), 2.55 (br, 1H), 1.55 (d, *J* = 7.1 Hz, 3H), 1.45 (d, *J* = 6.9 Hz, 3H); ^{13}C NMR (101 MHz, $CDCl_3$) δ 175.1, 170.0, 135.0, 128.6, 128.5, 128.2, 69.4, 67.2, 66.7, 20.4, 16.8; HRMS (TOF MS ES+) m/z calcd for $C_{13}H_{16}O_5Na^+$ [M+Na]$^+$: 275.0895; Found: 275.0900.



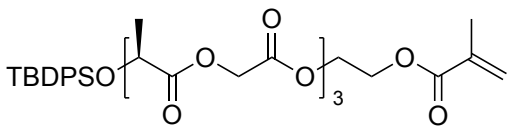
33

Preparation: The compound was prepared by subjecting **16** and **14** to the standard ester formation procedure. **Appearance:** colourless oil**, Yield:** 68%**, Characterisation:** R_f = 0.49 (30% EtOAc/hexane); IR (film)/cm^{-1} 3069, 2931, 2857, 1758 (C=O), 1588, 1452, 1424, 1389, 1175, 1131, 1101, 703; ^{1}H NMR (400 MHz, $CDCl_3$) δ 7.71 – 7.64 (m, 4H), 7.49 – 7.31 (m, 11H), 5.29 – 5.17 (m, 4H), 4.86 (d, *J* = 16.1 Hz, 1H), 4.82 (d, *J* = 15.9 Hz, 1H), 4.68 (d, *J* = 16.0 Hz, 1H), 4.66 – 4.60 (m, 2H), 4.45 (d, *J* = 16.0 Hz, 1H), 4.38 (q, *J* = 6.7 Hz, 1H), 1.56 (d, *J* = 7.1 Hz, 3H), 1.56 (d, *J* = 7.1 Hz, 3H), 1.43 (d, *J* = 6.7 Hz, 3H), 1.10 (s, 9H); ^{13}C NMR (101 MHz, $CDCl_3$) δ 173.0, 169.5, 169.4, 166.9, 166.8, 166.4, 135.9, 135.7, 134.8, 133.4, 132.9, 129.8, 128.6, 128.5, 127.6, 127.6, 69.3, 69.2, 68.9, 68.6, 67.3, 61.1, 60.8, 60.2, 26.8, 21.2, 19.2, 16.7, 16.7; HRMS (TOF MS ES+) m/z calcd for $C_{38}H_{44}O_{13}NaSi^+$ [M+Na]$^+$: 759.2449; Found: 759.2456.



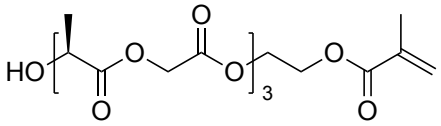
34

Preparation: The compound was prepared by subjecting **33** to the standard catalytic hydrogenation procedure. **Appearance:** yellowish oil**, Yield:** 90%**, Characterisation:** IR (film)/cm^{-1} broad OH vibration visible, 3069, 2930, 2855, 1750 (C=O), 1589, 1454, 1384, 1130, 702; ^{1}H NMR (400 MHz, $CDCl_3$) δ 7.71 – 7.65 (m, 4H), 7.49 – 7.33 (m, 6H), 5.31 – 5.20 (m, 2H), 4.87 (d, *J* = 16.1 Hz, 1H), 4.81 (d, *J* = 16.3 Hz, 1H), 4.72 – 4.61 (m, 3H), 4.46 (d, *J* = 16.0 Hz, 1H), 4.39 (q, *J* = 6.7 Hz, 1H), 1.59 (d, *J* = 7.1 Hz, 3H), 1.57 (d, *J* = 7.0 Hz, 3H), 1.43 (d, *J* = 6.8 Hz, 3H), 1.10 (s, 9H); ^{13}C NMR (101 MHz, $CDCl_3$) δ 173.1, 171.5, 169.5, 169.3, 166.9, 166.5, 135.9, 135.7, 133.3, 132.9, 129.8, 127.7, 127.6, 69.2, 68.9, 68.6, 60.8, 60.6, 60.3, 26.8, 21.2, 19.2, 16.7, 16.7; HRMS (TOF MS ES+) m/z calcd for $C_{31}H_{42}NO_{13}Si^+$ $[M+NH_4]^+$: 664.2425, Found: 664.2437.



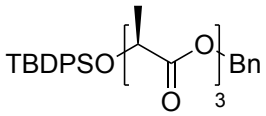
35

Preparation: The compound was prepared by subjecting **34** to the standard procedure for the synthesis of monomethacrylates. **Appearance:** colourless oil**, Yield:** 58%**, Characterisation:** R_f = 0.55 (70% Et_2O/hexane); IR (film)/cm^{-1} 3071, 2992, 2955, 2858, 1761, 1722, 1636, 1425, 1173, 1132, 1102, 705, 509; ^{1}H NMR (400 MHz, $CDCl_3$) δ 7.73 – 7.63 (m, 4H), 7.51 – 7.33 (m, 6H), 6.13 (quint, *J* = 1.1 Hz, 1H), 5.62 (quint, *J* = 1.6 Hz, 1H), 5.31 – 5.19 (m, 2H), 4.87 (d, *J* = 16.0 Hz, 1H), 4.80 (d, *J* = 16.0 Hz, 1H), 4.72 – 4.58 (m, 3H), 4.49 – 4.33 (m, 6H), 1.97 – 1.92 (m, 3H), 1.59 (d, *J* = 7.1 Hz, 3H), 1.57 (d, *J* = 7.1 Hz, 3H), 1.43 (d, *J* = 6.7 Hz, 3H), 1.10 (s, 9H); ^{13}C NMR (101 MHz, $CDCl_3$) δ 173.0, 169.5, 169.4, 167.0, 166.8, 166.5, 135.9, 135.7, 133.4, 132.9, 129.8, 127.7, 127.6, 126.3, 69.2, 68.9, 68.6, 63.2, 62.0, 60.9, 60.7, 60.2, 26.8, 21.3, 19.2, 18.2, 16.7, 16.7; HRMS (TOF MS ES+) m/z calcd for $C_{37}H_{50}NO_{15}Si^+$ $[M+NH_4]^+$: 776.2950, Found: 776.2955.



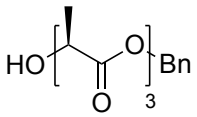
36

Preparation: The compound was prepared by subjecting **35** to the standard silyl ether cleavage procedure. **Appearance:** colourless oil**, Yield:** 82%**, Characterisation:** R_f = 0.22 (50% EtOAc/hexane); IR (film)/cm^{-1} 3531 (br, OH), 2993, 2957, 1755 (C=O), 1720 (C=O), 1635, 1386, 1279, 1176, 1130, 1096, 955; ^{1}H NMR (400 MHz, $CDCl_3$) δ 6.17 – 6.10 (m, 1H), 5.63 – 5.56 (m, 1H), 5.33 – 5.22 (m, 2H), 4.94 – 4.57 (m, 6H), 4.47 – 4.32 (m, 5H), 2.75 (d, *J* = 5.3 Hz, 1H), 1.95 (s, 3H), 1.60 (d, *J* = 7.2 Hz, 3H), 1.59 (d, J = 7.0 Hz, 3H), 1.50 (d, *J* = 7.0 Hz, 3H); ^{13}C NMR (101 MHz, $CDCl_3$) δ 174.9, 169.4, 167.0, 166.8, 166.6, 166.4, 135.7, 126.3, 69.2, 69.1, 66.7, 63.2, 62.0, 60.9, 60.8, 60.8, 20.3, 18.2, 16.7, 16.7; HRMS (ES+) m/z calcd for $C_{21}H_{28}O_{15}Na^+$ $[M+Na]^+$: 543.1326, Found: 543.1334.



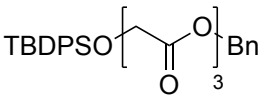
37

Preparation: The compound was prepared by subjecting **27** and **4** to the standard ester formation procedure. **Appearance:** colourless oil**, Yield:** 91%**, Characterisation:** R_f = 0.23 (10% EtOAc/hexane); IR (film)/cm^{-1} 3068, 2930, 2856, 1750 (C=O), 1588, 1452, 1184, 1127, 1091, 971, 738, 698; ^{1}H NMR (400 MHz, $CDCl_3$) δ 7.73 – 7.64 (m, 4H), 7.53 – 7.28 (m, 11H), 5.22 – 5.10 (m, 3H), 4.95 (q, *J* = 7.1 Hz, 1H), 4.33 (q, *J* = 6.7 Hz, 1H), 1.51 (d, *J* = 7.1 Hz, 3H), 1.42 (d, *J* = 6.7 Hz, 3H), 1.34 (d, *J* = 7.1 Hz, 3H), 1.10 (s, 9H); ^{13}C NMR (101 MHz, $CDCl_3$) δ 173.1, 170.1, 169.9, 136.0, 135.7, 135.1, 133.4, 133.1, 129.8, 128.6, 128.5, 128.2, 127.6, 127.6, 69.1, 68.5, 68.2, 67.1, 26.8, 21.1, 19.2, 16.8, 16.5; HRMS (TOF MS ES+) m/z calcd for $C_{32}H_{38}O_7NaSi^+$ $[M+Na]^+$: 585.2285; Found: 585.2293.



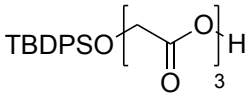
38

Preparation: The compound was prepared by subjecting **37** to the standard silyl ether cleavage procedure. **Appearance:** colourless oil**, Yield:** 88%**, Characterisation:** R_f = 0.20 (30% EtOAc/hexane); IR (film)/cm^{-1} 3490 (br, OH), 2917, 2849, 1737 (C=O), 1495, 1462, 1239, 1091, 740; ^{1}H NMR (400 MHz, $CDCl_3$) δ 7.43 – 7.31 (m, 5H), 5.25 – 5.12 (m, 4H), 4.36 (q, *J* = 6.9 Hz, 1H), 2.65 (s, 1H), 1.55 (d, *J* = 7.1 Hz, 3H), 1.55 (d, *J* = 7.1 Hz, 3H), 1.50 (d, *J* = 6.9 Hz, 3H); ^{13}C NMR (101 MHz, $CDCl_3$) δ 175.1, 169.9, 169.6, 128.6, 128.5, 128.3, 69.3, 69.1, 67.2, 66.7, 20.5, 16.8, 16.7; HRMS (TOF MS ES+) m/z calcd for $C_{16}H_{21}O_7^+$ $[M+H]^+$: 325.1287; Found: 325.1286.



39

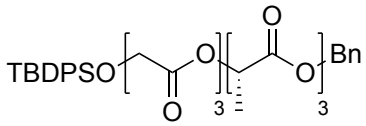
Preparation: The compound was prepared by subjecting **20** and **3** to the standard ester formation procedure. **Appearance:** colourless oil**, Yield:** 20%**, Characterisation:** R_f = 0.40 (30% EtOAc/hexane); IR (film)/cm^{-1} 3071, 2929, 2855, 1755 (C=O), 1587, 1423, 1394, 1267, 1170, 1133, 1073, 823; ^{1}H NMR (400 MHz, $CDCl_3$) δ 7.73 – 7.66 (m, 4H), 7.49 – 7.32 (m, 11H), 5.21 (s, 2H), 4.75 (s, 2H), 4.73 (s, 2H), 4.37 (s, 2H), 1.10 (s, 9H); ^{13}C NMR (101 MHz, $CDCl_3$) δ 170.5, 166.9, 135.5, 134.9, 132.6, 129.9, 128.7, 128.6, 128.4, 127.8, 67.3, 61.8, 61.1, 60.3, 26.6, 19.2; HRMS (TOF MS ES+) m/z calcd for $C_{29}H_{32}O_7NaSi^+$ $[M+Na]^+$: 543.1815; Found: 543.1811.



40

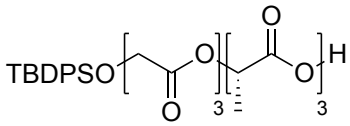
Preparation: The compound was prepared by subjecting **39** to the standard catalytic hydrogenation procedure. **Appearance:** colourless oil**, Yield:** 98%**, Characterisation:** IR (film)/cm^{-1} broad OH vibration observed, 2926, 2849, 1721(C=O), 1423, 1102, 1082, 809; ^{1}H NMR (400 MHz, $CDCl_3$) δ 7.72 – 7.66 (m, 4H),

7.49 – 7.35 (m, 6H), 4.75 (s, 2H), 4.74 (s, 2H), 4.38 (s, 2H), 1.10 (s, 9H); ^{13}C NMR (101 MHz, $CDCl_3$) δ 171.0, 170.6, 166.8, 135.6, 132.6, 130.0, 127.8, 61.8, 60.4, 60.3, 26.6, 19.2; HRMS (TOF MS ES+) m/z calcd for $C_{22}H_{26}O_7NaSi^+$ $[M+Na]^+$: 453.1346; Found: 453.1351.



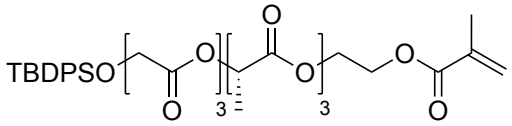
41

Preparation: The compound was prepared by subjecting **40** and **38** to the standard ester formation procedure. **Appearance:** colourless oil**, Yield:** 70%**, Characterisation:** R_f = 0.42 (30% EtOAc/hexane); IR (film)/cm^{-1} 3069, 2934, 2857, 1754 (C=O), 1452, 1425, 1387, 1269, 1184, 1133, 1094, 703; ^{1}H NMR (400 MHz, $CDCl_3$) δ 7.72 – 7.67 (m, 4H), 7.48 – 7.31 (m, 11H), 5.25 – 5.11 (m, 5H), 4.82 (d, *J* = 16.1 Hz, 1H), 4.79 – 4.68 (m, 3H), 4.37 (s, 2H), 1.60 (d, *J* = 7.1 Hz, 3H), 1.54 (d, *J* = 7.1 Hz, 3H), 1.53 (d, *J* = 7.1 Hz, 3H), 1.09 (s, 9H); ^{13}C NMR (101 MHz, $CDCl_3$) δ 170.5, 169.9, 169.5, 169.4, 166.8, 166.5, 135.6, 132.6, 129.9, 128.6, 128.5, 128.2, 127.8, 69.3, 69.1, 67.2, 61.8, 60.8, 60.3, 26.6, 19.2, 16.7, 16.7, 16.6.



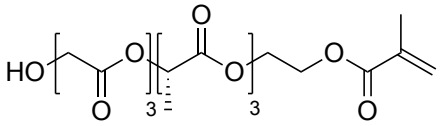
42

Preparation: The compound was prepared by subjecting **41** to the standard catalytic hydrogenation procedure. **Appearance:** yellowish oil**, Yield:** 100%**, Characterisation:** IR (film)/cm^{-1} broad OH vibration observable, 3070, 2928, 2856, 1747 (C=O), 1589, 1454, 1426, 1385, 1191, 1132, 1108, 821, 704; ^{1}H NMR (400 MHz, $CDCl_3$) δ 7.73 – 7.65 (m, 4H), 7.48 – 7.36 (m, 6H), 5.26 – 5.14 (m, 3H), 4.81 (d, *J* = 16.1 Hz, 1H), 4.77 – 4.67 (m, 3H), 4.37 (s, 2H), 1.60 (d, *J* = 7.1 Hz, 3H), 1.59 (d, *J* = 7.1 Hz, 3H), 1.57 (d, *J* = 7.2 Hz, 3H), 1.09 (s, 9H); ^{13}C NMR (101 MHz, $CDCl_3$) δ 174.4, 170.6, 169.5, 169.5, 166.8, 166.5, 135.5, 132.6, 129.9, 127.8, 69.3, 69.1, 68.7, 61.8, 60.8, 60.3, 26.6, 19.2, 16.6, 16.6; HRMS (TOF MS ES+) m/z calcd for $C_{38}H_{44}O_{13}NaSi^+$ $[M+Na]^+$: 759.2449, Found: 759.2455.



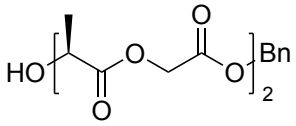
43

Preparation: The compound was prepared by subjecting **42** to the standard procedure for the synthesis of monomethacrylates. **Appearance:** colourless oil**, Yield:** 73%**, Characterisation:** R_f = 0.24 (35% EtOAc/hexane); IR (film)/cm^{-1} 3069, 2952, 2857, 1755 (C=O), 1721 (C=O), 1451, 1425, 1382, 1169, 1133, 1094, 704; ^{1}H NMR (400 MHz, $CDCl_3$) δ 7.72 – 7.67 (m, 4H), 7.48 – 7.36 (m, 6H), 6.15 – 6.11 (m, 1H), 5.61 (quint, *J* = 1.6 Hz, 1H), 5.26 – 5.12 (m, 3H), 4.86 – 4.70 (m, 4H), 4.49 – 4.34 (m, 6H), 1.98 – 1.93 (m, 3H), 1.60 (d, *J* = 7.1, 3H), 1.59 (d, *J* = 7.1 Hz, 3H), 1.53 (d, *J* = 7.1 Hz, 3H), 1.09 (s, 9H); 13C NMR (101 MHz, CDCl3) δ 170.5, 169.9, 169.5, 169.4, 167.0, 166.8, 166.5, 135.5, 132.6, 129.9, 127.8, 126.2, 69.2, 69.1, 69.1, 63.0, 62.0, 61.8, 60.8, 60.2, 26.6, 19.2, 18.2, 16.7, 16.6, 16.6; HRMS (TOF MS ES+) m/z calcd for $C_{37}H_{46}O_{15}NaSi^+$ $[M+Na]^+$: 781.2504, Found: 781.2492.



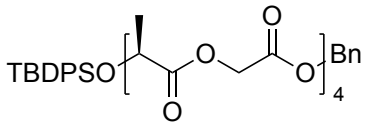
44

Preparation: The compound was prepared by subjecting **43** to the standard silyl ether cleavage procedure. **Appearance:** colourless oil**, Yield:** 75%**, Characterisation:** R_f = 0.24 (50% EtOAc/hexane); IR (film)/cm^{-1} 3520 (br, OH), 2993, 2952, 1750 (C=O), 1720 (C=O), 1633, 1386, 1176, 954; ^{1}H NMR (400 MHz, $CDCl_3$) δ 6.16 – 6.10 (m, 1H), 5.61 (quint, *J* = 1.6 Hz, 1H), 5.28 – 5.13 (m, 3H), 4.91 – 4.72 (m, 4H), 4.50 – 4.25 (m, 6H), 1.95 (t, *J* = 1.3 Hz, 3H), 1.60 (d, *J* = 7.1, 3H), 1.59 (d, *J* = 7.1 Hz, 3H), 1.53 (d, *J* = 7.1 Hz, 3H); ^{13}C NMR (101 MHz, $CDCl_3$) δ 172.6, 169.9, 169.5, 169.4, 167.0, 166.6, 166.4, 135.8, 126.2, 69.3, 69.1, 69.1, 63.0, 62.0, 60.9, 60.7, 60.4, 18.2, 16.7, 16.6, 16.6.



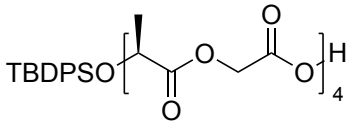
45

Preparation: The compound was prepared by subjecting **15** to the standard silyl ether cleavage procedure. **Appearance:** colourless oil**, Yield:** 89%**, Characterisation:** R_f = 0.25 (30% EtOAc/hexane); IR (film)/cm^{-1} 3514 (br, OH), 2926. 2851, 1751 (C=O), 1587, 1349, 1278. 1177, 1133, 1099, 752, 700; ^{1}H NMR (400 MHz, $CDCl_3$) δ 7.43 – 7.32 (m, 5H), 5.28 (q, *J* = 7.1 Hz, 1H), 5.20 (s, 2H), 4.87 (d, *J* = 16.0 Hz, 1H), 4.82 (d, *J* = 15.9 Hz, 1H), 4.72 (d, *J* = 16.1 Hz, 1H), 4.64 (d, *J* = 15.9 Hz, 1H), 4.42 (q, *J* = 6.9 Hz, 1H), 2.35 (br, 1H), 1.58 (d, *J* = 7.1 Hz, 3H), 1.50 (d, *J* = 6.9 Hz, 3H); ^{13}C NMR (101 MHz, $CDCl_3$) δ 174.9, 169.4, 166.9, 166.6, 134.8, 128.7, 128.5, 69.2, 67.3, 66.7, 61.1, 60.8, 20.3, 16.7; HRMS (TOF MS ES+) m/z calcd for $C_{17}H_{20}O_9Na^+$ [M+Na]$^+$: 391.1005; Found: 391.1006.



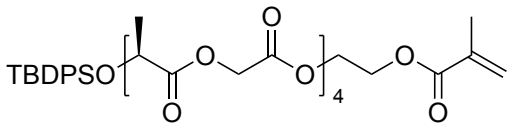
46

Preparation: The compound was prepared by subjecting **16** and **45** to the standard ester formation procedure. **Appearance:** colourless oil**, Yield:** 81%**, Characterisation:** R_f = 0.57 (35% EtOAc/hexane); IR (film)/cm^{-1} 3070, 2927, 2856, 1753 (C=O), 1588, 1451, 1423, 1387, 1275, 1171, 1128, 1091, 740, 701; ^{1}H NMR (400 MHz, $CDCl_3$) δ 7.72 – 7.64 (m, 4H), 7.48 – 7.32 (m, 11H), 5.31 – 5.18 (m, 5H), 4.92 – 4.79 (m, 3H), 4.73 – 4.60 (m, 4H), 4.46 (d, *J* = 16.0 Hz, 1H), 4.38 (q, *J* = 6.7 Hz, 1H), 1.59 (d, *J* = 7.1 Hz, 3H), 1.57 (d, *J* = 7.1 Hz, 3H), 1.56 (d, *J* = 7.1 Hz, 3H), 1.43 (d, *J* = 6.7 Hz, 3H), 1.10 (s, 9H); ^{13}C NMR (101 MHz, $CDCl_3$) δ 173.0, 169.5, 169.4, 169.4, 166.9, 166.8, 166.5, 166.4, 135.9, 135.7, 134.8, 133.4, 132.9, 129.8, 128.6, 128.5, 127.6, 127.6, 69.2, 69.1, 68.9, 68.6, 67.3, 61.1, 60.8, 60.7, 60.2, 26.8, 21.3, 19.2, 16.7; HRMS (TOF MS ES+) m/z calcd for $C_{43}H_{50}O_{17}NaSi^+$ [M+Na]$^+$: 889.2715; Found: 889.2730.



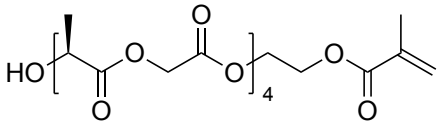
47

Preparation: The compound was prepared by subjecting **46** to the standard catalytic hydrogenation procedure. **Appearance:** yellowish oil**, Yield:** 99%**, Characterisation:** IR (film)/cm^{-1} broad OH vibration visible, 2926, 2855, 1751 (C=O), 1588, 1452, 1423, 1275, 1171, 1128, 1092, 741, 702; ^{1}H NMR (400 MHz, $CDCl_3$) δ 7.70 – 7.65 (m, 4H), 7.48 – 7.34 (m, 6H), 5.32 – 5.19 (m, 3H), 4.91 – 4.79 (m, 3H), 4.72 – 4.61 (m, 4H), 4.46 (d, *J* = 16.0 Hz, 1H), 4.38 (q, *J* = 6.7 Hz, 1H), 1.59 (d, *J* = 7.1 Hz, 6H), 1.56 (d, *J* = 7.1 Hz, 3H), 1.42 (d, *J* = 6.7 Hz, 3H), 1.10 (s, 9H); ^{13}C NMR (101 MHz, $CDCl_3$) δ 173.1, 171.1, 169.5, 169.4, 169.3, 166.9, 166.5, 166.5, 135.9, 135.7, 133.4, 132.9, 129.8, 127.7, 127.6, 69.2, 69.1, 69.0, 68.6, 60.8, 60.8, 60.5, 60.3, 26.8, 21.3, 19.2, 16.7, 16.7; HRMS (TOF MS ES+) m/z calcd for $C_{36}H_{44}O_{17}NaSi^{+}$ $[M+Na]^{+}$: 799.2245; Found: 799.2250.



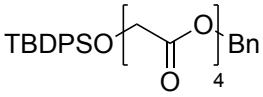
48

Preparation: The compound was prepared by subjecting **47** to the standard procedure for the synthesis of monomethacrylates. **Appearance:** colourless oil**, Yield:** 69%**, Characterisation:** R_f = 0.62 (8% MeCN/CH_2Cl_2); IR (film)/cm^{-1} 3080, 2992, 2954, 2857, 1753 (C=O), 1720 (C=O), 1635, 1423, 1277, 1169, 1128, 1093, 964, 742, 704, 612, 508; ^{1}H NMR (400 MHz, $CDCl_3$) δ 7.71 – 7.64 (m, 4H), 7.47 – 7.34 (m, 6H), 6.16 – 6.11 (m, 1H), 5.62 (quint, *J* = 1.6 Hz, 1H), 5.32 – 5.18 (m, 3H), 4.92 – 4.58 (m, 7H), 4.49 – 4.34 (m, 6H), 1.95 (dd, *J* = 1.6, 1.0 Hz, 3H), 1.59 (d, *J* = 7.1 Hz, 6H), 1.56 (d, *J* = 7.1 Hz, 3H), 1.42 (d, *J* = 6.8 Hz, 3H), 1.10 (s, 9H); ^{13}C NMR (101 MHz, $CDCl_3$) δ 173.0, 169.5, 169.4, 167.0, 166.8, 166.5, 166.4, 135.9, 135.7, 133.4, 132.9, 129.8, 127.6, 127.6, 126.3, 69.2, 69.1, 68.9, 68.6, 63.1, 62.0, 60.9, 60.8, 60.7, 60.2, 26.8, 21.3, 19.2, 18.2, 16.7; HRMS (TOF MS ES^{+}) m/z calcd for $C_{42}H_{52}O_{19}NaSi^{+}$ $[M+Na]^{+}$: 911.2770, Found: 911.2783.



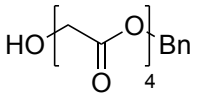
49

Preparation: The compound was prepared by subjecting **48** to the standard silyl ether cleavage procedure. **Appearance:** colourless oil**, Yield:** 76%**, Characterisation:** R_f = 0.27 (60% EtOAc/hexane); IR (film)/cm^{-1} 3501 (br, OH), 2993, 2953, 2925, 1756 (C=O), 1720 (C=O), 1635, 1385, 1175, 1130, 1095, 956; ^{1}H NMR (400 MHz, $CDCl_3$) δ 6.16 – 6.05 (m, 1H), 5.65 – 5.54 (m, 1H), 5.30 – 5.22 (m, 3H), 4.92 – 4.59 (m, 8H), 4.45 – 4.33 (m, 5H), 2.64 – 2.37 (br, 1H), 1.97 – 1.90 (m, 3H), 1.62 – 1.57 (m, 9H), 1.49 (d, *J* = 7.0 Hz, 3H); ^{13}C NMR (101 MHz, $CDCl_3$) δ 174.9, 169.4, 167.0, 166.8, 166.6, 166.4, 135.7, 126.3, 69.1, 69.1, 66.7, 63.1, 62.0, 60.9, 60.8, 20.3, 18.2, 16.7, 16.7; HRMS (TOF MS ES+) m/z calcd for $C_{26}H_{34}O_{19}Na^+$ $[M+Na]^+$: 673.1592, Found: 673.1584.



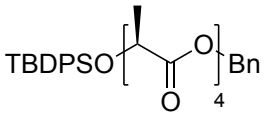
50

Preparation: The compound was prepared by subjecting **20** and **25** to the standard ester formation procedure. **Appearance:** colourless oil**, Yield:** 81%**, Characterisation:** R_f = 0.25 (30% EtOAc/hexane); IR (film)/cm^{-1} 3069, 2932, 2857, 1759 (C=O), 1588, 1424, 1394, 1270, 1165, 1136, 822, 703; ^{1}H NMR (400 MHz, $CDCl_3$) δ 7.72 – 7.67 (m, 4H), 7.48 – 7.35 (m, 11H), 5.21 (s, 2H), 4.81 (s, 2H), 4.75 (s, 2H), 4.74 (s, 2H), 4.37 (s, 2H), 1.10 (s, 9H); ^{13}C NMR (101 MHz, $CDCl_3$) δ 170.5, 166.8, 166.8, 166.5, 135.5, 134.8, 132.6, 129.9, 128.6, 128.6, 128.4, 127.8, 67.3, 61.8, 61.2, 60.7, 60.2, 26.6, 19.2; HRMS (TOF MS ES+) m/z calcd for $C_{31}H_{34}O_9NaSi^+$ $[M+Na]^+$: 601.1870; Found: 601.1862.



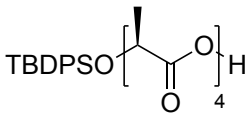
51

Preparation: The compound was prepared by subjecting **50** to the standard silyl ether cleavage procedure. **Appearance:** colourless oil**, Yield:** 60%**, Characterisation:** R_f = 0.28 (55% EtOAc/hexane); IR (film)/cm^{-1} 3500 (br, OH), 2953, 1743 (C=O), 1422, 1394, 1273, 1154, 1095, 1074, 737, 697; ^{1}H NMR (400 MHz, $CDCl_3$) δ 7.43 – 7.32 (m, 5H), 5.21 (s, 2H), 4.86 (s, 2H), 4.84 (s, 2H), 4.75 (s, 2H), 4.32 (s, 2H), 2.18 (br, 1H); ^{13}C NMR (101 MHz, $CDCl_3$) δ 172.6, 166.8, 166.6, 166.5, 134.8, 128.7, 128.4, 67.4, 61.2, 60.8, 60.7, 60.4; HRMS (TOF MS ES+) m/z calcd for $C_{15}H_{16}O_9Na^+$ [M+Na]$^+$: 363.0692; Found: 363.0701.



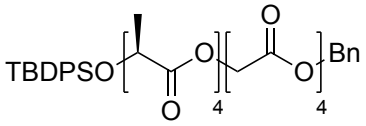
52

Preparation: The compound was prepared by subjecting 27 and 32 to the standard ester formation procedure. **Appearance:** colourless oil**, Yield:** 63%**, Characterisation:** R_f = 0.32 (15% EtOAc/hexane); IR (film)/cm^{-1} 3069, 290, 2931, 2856, 1751 (C=O), 1452, 1184, 1128, 1093, 702; ^{1}H NMR (400 MHz, $CDCl_3$) δ 7.74 – 7.65 (m, 4H), 7.46 – 7.31 (m, 11H), 5.23 – 5.10 (m, 4H), 4.95 (q, *J* = 7.1 Hz, 1H), 4.33 (q, *J* = 6.7 Hz, 1H), 1.52 (d, *J* = 7.1 Hz, 3H), 1.51 (d, *J* = 7.1 Hz, 3H), 1.42 (d, *J* = 6.7 Hz, 3H), 1.40 (d, *J* = 7.1 Hz, 3H), 1.10 (s, 9H); ^{13}C NMR (101 MHz, $CDCl_3$) δ 173.1, 169.9, 169.7, 135.9, 135.7, 135.1, 133.4, 133.0, 129.8, 128.6, 128.5, 128.2, 127.6, 127.6, 69.2, 68.8, 68.5, 68.2, 67.2, 26.8, 21.1, 19.2, 16.7, 16.6; HRMS (TOF MS ES+) m/z calcd for $C_{35}H_{42}O_9NaSi^+$ [M+Na]$^+$: 657.2496; Found: 657.2501.



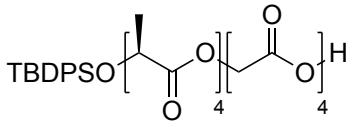
53

Preparation: The compound was prepared by subjecting **52** to the standard catalytic hydrogenation procedure. **Appearance:** colourless oil**, Yield:** 100%**, Characterisation:** IR (film)/cm^{-1} 3069, 2991, 2932, 2857, 1755 (C=O), 1588, 1452, 1376, 1187, 1129, 095, 703; ^{1}H NMR (400 MHz, $CDCl_3$) δ 7.73 – 7.65 (m, 4H), 7.49 – 7.34 (m, 6H), 5.16 (q, *J* = 7.1 Hz, 2H), 4.95 (q, *J* = 7.1 Hz, 1H), 4.34 (q, *J* = 6.7 Hz, 1H), 1.56 (d, *J* = 7.1 Hz, 3H), 1.56 (d, *J* = 7.1 Hz, 3H), 1.42 (d, *J* = 6.8 Hz, 3H), 1.40 (d, *J* = 7.2 Hz, 3H), 1.10 (s, 9H); ^{13}C NMR (101 MHz, $CDCl_3$) δ 174.9, 173.2, 170.0, 169.6, 135.9, 135.7, 133.4, 133.0, 129.8, 127.6, 127.6, 68.8, 68.7, 68.5, 68.3, 26.8, 21.1, 19.2, 16.6, 16.6; HRMS (TOF MS ES+) m/z calcd for $C_{28}H_{36}O_9NaSi^+$ $[M+Na]^+$: 567.2026; Found: 567.2033.



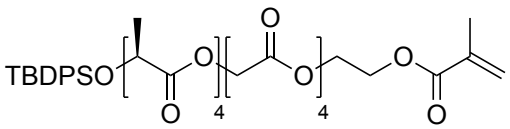
54

Preparation: The compound was prepared by subjecting **53** and **51** to the standard ester formation procedure. **Appearance:** colourless oil**, Yield:** 45 %**, Characterisation:** R_f = 0.43 (35% EtOAc/hexane); IR (film)/cm^{-1} 3069. 2938, 2857, 1752 (C=O), 1451, 1424, 1391, 1158, 1128, 1089, 740, 703; ^{1}H NMR (400 MHz, $CDCl_3$) δ 7.72 – 7.65 (m, 4H), 7.47 – 7.33 (m, 11H), 5.26 – 5.19 (m, 3H), 5.15 (q, *J* = 7.1 Hz, 1H), 4.95 (q, *J* = 7.1 Hz, 1H), 4.92 – 4.64 (m, 8H), 4.33 (q, *J* = 6.7 Hz, 1H), 1.59 (d, *J* = 8.2 Hz, 3H), 1.57 (d, *J* = 8.1 Hz, 3H), 1.42 (d, *J* = 6.8 Hz, 3H), 1.40 (d, *J* = 7.1 Hz, 3H), 1.10 (s, 9H); ^{13}C NMR (101 MHz, $CDCl_3$) δ 173.1, 170.0, 169.7, 169.5, 166.8, 166.4, 166.4, 166.3, 135.9, 135.7, 134.8, 133.4, 133.0, 129.8, 128.7, 128.4, 127.6, 127.6, 68.9, 68.8, 68.4, 68.2, 67.4, 61.2, 60.8, 60.7, 60.6, 26.8, 21.1, 19.2, 16.7, 16.6, 16.6; HRMS (TOF MS ES+) m/z calcd for $C_{43}H_{50}O_{17}NaSi^+$ $[M+Na]^+$: 889.2715; Found: 889.2733.



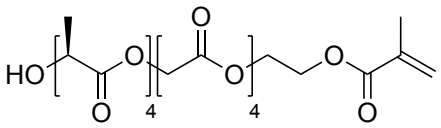
55

Preparation: The compound was prepared by subjecting **54** to the standard catalytic hydrogenation procedure. **Appearance:** yellowish oil**, Yield:** 96%**, Characterisation:** IR (film)/cm^{-1} 3071, 2953, 2857, 1758 (C=O), 1425, 1165, 1131, 1095, 705; ^{1}H NMR (400 MHz, $CDCl_3$) δ 7.76 – 7.62 (m, 4H), 7.48 – 7.31 (m, 6H), 5.22 (q, *J* = 7.1 Hz, 1H), 5.16 (q, *J* = 7.1 Hz, 1H), 4.95 (q, *J* = 7.1 Hz, 1H), 4.91 – 4.81 (m, 5H), 4.79 – 4.68 (m, 3H), 4.33 (q, *J* = 6.7 Hz, 1H), 1.59 (d, *J* = 7.2 Hz, 3H), 1.57 (d, *J* = 7.2 Hz, 4H), 1.42 (d, *J* = 6.8 Hz, 3H), 1.39 (d, *J* = 7.1 Hz, 3H), 1.09 (s, 9H); ^{13}C NMR (101 MHz, $CDCl_3$) δ 173.3, 170.6, 170.0, 169.7, 169.5, 166.5, 166.4, 166.4, 135.9, 135.7, 133.4, 133.0, 129.8, 127.6, 127.6, 68.9, 68.8, 68.5, 68.3, 60.8, 60.7, 60.6, 26.8, 21.1, 19.2, 16.6, 16.6, 16.5; HRMS (TOF MS ES+) m/z calcd for $C_{36}H_{44}O_{17}NaSi^{+}$ $[M+Na]^{+}$: 799.2245; Found: 799.2256.



56

Preparation: The compound was prepared by subjecting **55** to the standard procedure for the synthesis of monomethacrylates. **Appearance:** colourless oil**, Yield:** 75%**, Characterisation:** R_f = 0.60 (8% MeCN/CH_2Cl_2); IR (film)/cm^{-1} 3071, 2928, 2857, 1757 (C=O), 1722 (C=O), 1636, 1451, 1425, 1384, 1158, 1130, 1093, 705; ^{1}H NMR (400 MHz, $CDCl_3$) δ 7.72 – 7.65 (m, 4H), 7.49 – 7.33 (m, 6H), 6.16 – 6.12 (m, 1H), 5.62 (quint, *J* = 1.6 Hz, 1H), 5.22 (q, *J* = 7.1 Hz, 1H), 5.16 (q, *J* = 7.1 Hz, 1H), 4.95 (q, *J* = 7.1 Hz, 1H), 4.89 (d, *J* = 16.1 Hz, 1H), 4.85 – 4.73 (m, 6H), 4.69 (d, *J* = 16.1 Hz, 1H), 4.48 – 4.40 (m, 2H), 4.40 – 4.30 (m, 3H), 1.95 (dd, *J* = 1.6, 1.0 Hz, 3H), 1.59 (d, *J* = 7.1 Hz, 3H), 1.57 (d, *J* = 7.1 Hz, 3H), 1.42 (d, *J* = 6.7 Hz, 3H), 1.40 (d, J = 7.1 Hz, 3H), 1.09 (s, 9H); ^{13}C NMR (101 MHz, $CDCl_3$) δ 173.1, 169.9, 169.7, 169.5, 167.0, 166.7, 166.4, 166.4, 166.3, 135.9, 135.7, 133.4, 133.0, 129.8, 127.6, 127.5, 126.3, 68.9, 68.8, 68.4, 68.2, 63.2, 61.9, 61.0, 60.8, 60.7, 60.6, 26.8, 21.1, 19.2, 18.2, 16.7, 16.6, 16.5; HRMS (TOF MS ES+) m/z calcd for $C_{42}H_{52}O_{19}NaSi^{+}$ $[M+Na]^{+}$: 911.2770, Found: 911.2791.



57

Preparation: The compound was prepared by subjecting **56** to the standard silyl ether cleavage procedure. **Appearance:** colourless oil**, Yield:** 82%**, Characterisation:** R_f = 0.18 (55% EtOAc/hexane); IR (film)/cm^{-1} 3460 (br, OH), 1745 (C=O), 1720 (C=O), 1634, 1167, 720 ; ^{1}H NMR (400 MHz, $CDCl_3$) δ 6.13 (quint, *J* = 1.0 Hz, 1H), 5.62 (quint, *J* = 1.6 Hz, 1H), 5.31 – 5.13 (m, 3H), 4.97 – 4.66 (m, 8H), 4.46 – 4.42 (m, 2H), 4.40 – 4.33 (m, 3H), 1.95 (dd, *J* = 1.6, 1.0 Hz, 3H), 1.64 – 1.57 (m, 9H), 1.50 (d, *J* = 6.9 Hz, 3H); ^{13}C NMR (101 MHz, $CDCl_3$) δ 169.9, 169.5, 169.4, 167.3, 167.0, 166.6, 166.5, 135.8, 135.2, 127.2, 126.3, 69.3, 69.2, 69.1, 63.1, 62.1, 60.9, 60.7, 60.5, 18.2, 18.2, 16.7, 16.7, 16.6; HRMS (TOF MS ES+) m/z calcd for $C_{26}H_{34}O_{19}Na^+$ $[M+Na]^+$: 673.1592, Found: 673.1577.

7.3 Experimental Details for Chapter 3

7.3.1 Influence of the Reaction Duration on the Size of OLGA-based Nanoparticles

OLGADMA 4Aa and PEGDA700 were subjected to nanoprecipitation polymerisation under standard conditions. Pairs of samples of the reaction mixture (0.2 mL) were taken at determined time points, quickly diluted into ice-cold deionised water (0.6 mL) with exposure to air and analysed by DLS or lyophilised for 48 h to remove water. The obtained powders were then suspended in deuterated DMSO and subjected to ^{1}H NMR spectroscopy analysis.

7.3.2 Standard Nanoprecipitation Polymerisation Conditions

In a typical run, a solution of OLGADMA (8 mg), PEGDA700 (8 mg), and AIBN (4 mg) in THF (1.6 mL) was rapidly injected into water (4.8 mL) at 70 ºC, stirring at 1000 rpm, with the system open to the air and under N_2 gas flow. The reaction mixture was immediately purged with N_2 gas for 5 minutes and left stirring under a N_2 gas atmosphere for a further 10 min. The mixture was then exposed to air and cooled in an ice bath over 2 min. The resulting suspension was purified by centrifugal filtration within centrifugal filter units (MWCO 100 kDa), via two centrifugations at 3200 rcf over 5 minutes, passing through water (~12 mL). The retentate containing the NPs was then carefully pipetted into a volumetric flask and diluted to a final volume of 5 mL with deionised water.

Safety note: We acknowledge the potential hazards deriving from a quick injection of substantial quantities of an organic solution of AIBN (H242) into water at 70 °C. Unwanted events were not observed in any of the reactions. The highest amount of AIBN used in this work was 4 mg per reaction.

7.3.3 Preparation of PLGA-based NPs

A solution of the appropriate PLGA polymer (16 mg) in THF (1.6 mL) was rapidly injected into water (4.8 mL) at 70 ºC, stirring at 1000 rpm, with the system open to the air and under N_2 gas flow. The reaction mixture was immediately purged with N_2 gas for 5 minutes and left stirring under a N_2 gas atmosphere for a further 10 min. The mixture was then exposed to air and cooled in an ice bath over 2 min. The resulting suspension was purified by centrifugal filtration within centrifugal filter units (MWCO 100 kDa), via two centrifugations at 3200 rcf over 5 minutes, passing through water (~12 mL). The retentate containing the NPs was then carefully pipetted into a volumetric flask and diluted to a final volume of 5 mL with deionised water.

7.3.4 Comparative Stability Study of OLGA-based and PLGA-based Nanoparticles

Aqueous suspensions of OLGA-based NPs and PLGA-based NPs (2 mL, 1 mg/mL) were placed in centrifuge tubes equipped with a stir bar, sealed with parafilm, incubated at 37 °C, and left stirring at 500 rpm over a period of 5 weeks. At determined time points, the samples were subjected to pH determination and analysed by DLS and ELS.

7.3.5 Effect of **NP4Aa**, **NP4Ab,** and **NP4Bb** on Cell Viability *In Vitro*

HeLa cells were seeded in 96-well plates (5×10^3 cells per well) in 100 µL of DMEM supplemented with 10% fetal bovine serum (FBS), 1% penicillin and streptomycin, and incubated for 24 h at 37 ºC and 5% CO_2. The media was then removed, fresh media was added (90 µL), and the cells were treated with aliquots (10 µL) of aqueous suspensions of **NP4Aa**, **NP4Ab**, and **NP4Bb** with NP concentrations of 0.5, 0.25, 0.1, 0.05, and 0.01 mg/mL. Control cells were treated with water (10 µL). The cells were then incubated for 24 h and 48 h at 37 ºC and 5% CO_2. The cell viability was measured using the Cell Counting Kit-8 (CCK-8) assay, according to the manufacturer's instructions, assigning 100% viability to cells treated with water.

7.3.6 Synthesis of Fluorescent **NP4Aa**

Fluorescent **NP4Aa** were synthesised using the standard nanoprecipitation polymerisation conditions with the addition of fluorescein O-methacrylate at a concentration equal to 1 wt% of the monomer feed. This procedure was followed by the standard purification protocol performed via centrifugal filtration.

7.3.7 Cellular Uptake of Fluorescent **NP4Aa**

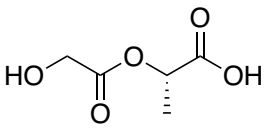
HeLa cells were seeded into an 8-well chambered coverslip for cell imaging (5×10^4 cells per chamber) in 300 μL of DMEM supplemented with 10% FBS and incubated at 37 °C and 5% CO_2. The media was removed after 48 h of incubation and 300 μL of OptiMEM was added to each chamber, followed by the addition of an aqueous suspension of fluorescent **NP4Aa** to achieve a NP content of 40, 60, and 100 μg/mL per chamber. The cells were then incubated at 37 °C and 5% CO_2 for 6 h after which the media was removed, the cells washed fourfold with sterile PBS and treated with Lysotracker Red (75 nM) for 30 min at 37 °C. Then, the cells were washed thrice with PBS and fixed with 300 μL of a 4% paraformaldehyde solution for 15 min. The paraformaldehyde solution was then removed, the cells washed twice with PBS and stained with Hoescht stain for 15 min in the dark. The stain was then removed, the cells were washed twice with PBS, and stored in sterile PBS until imaging. The cells were imaged at 40× using the oil immersion technique.

7.3.8 Nanoprecipitation Polymerisation of **OLGADMA 4Aa** in the Presence of the Water-Soluble Initiator V-50

A solution of **OLGADMA 4Aa** (8 mg) in THF (0.8 mL) was rapidly injected into an aqueous solution of V-50 (2 mg in 2.4 mL) at 70 ºC, stirring at 1000 rpm, with the system open to the air and under N_2 gas flow. The reaction mixture was immediately purged with N_2 gas for 5 minutes and left stirring under a N_2 gas atmosphere for a further 10 min. The mixture was then exposed to air and cooled in an ice bath over 2 min. The resulting suspension was purified by centrifugal filtration within centrifugal filter units (MWCO 100 kDa), via two centrifugations at 3200 rcf over 5 minutes, passing through water (~12 mL). The retentate containing the NPs was then carefully

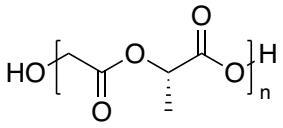
pipetted into a volumetric flask and diluted to a final volume of 5 mL with deionised water.

7.3.9 Synthesis and Characterisation of **PLGA alt**



58

Preparation: The compound was prepared from **7** following the standard procedure for catalytic hydrogenation. **Appearance:** colourless oil, **Yield:** 97%, **Characterisation:** IR (film)/cm^{-1} 3445 (OH), broad OH (acid), 1729 (C=O), 1200, 1094; ^{1}H NMR (400 MHz, $CDCl_3$) δ 6.57 (br. 1H), 5.24 (q, *J* = 7.1 Hz, 1H), 4.32 (d, *J* = 17.4 Hz, 1H), 4.26 (d, *J* = 17.4 Hz, 1H), 1.57 (d, *J* = 7.1 Hz, 3H); ^{13}C NMR (101 MHz, $CDCl_3$) δ 174.9, 172.8, 69.0, 60.4, 16.7; HRMS (ESI(-)-FTMS) m/z calcd for [M-H]$^{-}$: 147.0299, Found: 147.0299. The spectroscopic data was consistent with that previously reported.[326]



PLGA alt

Preparation: DMAP (7.3 mg, 0.06 mmol) was added to a solution of **58** (100.0 mg, 0.7 mmol) in EtOAc (0.2 mL) and CH_2Cl_2 (0.2 mL) at rt and the solution was cooled to 0 °C. Then, DCC (217.0 mg, 1.05 mmol) was added slowly over 2 min. The reaction mixture was then warmed to rt and allowed to stir for 24 h. The mixture was then diluted with CH_2Cl_2, filtered through a short plug of celite, and the resulting solution precipitated into cold methanol. The resulting suspension was filtered to afford the desired polymer. **Appearance:** white solid, **Characterisation:** IR (film)/cm^{-1} 2996, 2946, 1756 (C=O), 1175, 1094; ^{1}H NMR (400 MHz, $CDCl_3$) δ 5.26 (q, J = 7.0 Hz, 1H), 4.89 (d, J = 16.0 Hz, 1H), 4.66 (d, J = 16.0 Hz, 1H), 1.60 (d, J = 7.1 Hz, 3H); ^{13}C NMR (101 MHz, $CDCl_3$) δ 169.39, 166.44, 69.15, 60.82, 16.74; GPC (THF) M_n : 5954, M_w:

7158, PDI: 1.20. The observed spectroscopic data was consistent with that previously reported.[326]

7.4 Experimental Details for Chapter 4

7.4.1 Stability of Dexamethasone Under Typical Nanoprecipitation Polymerisation Conditions

A solution of dexamethasone (6 mg) and AIBN (4 mg) in THF (1.6 mL) was quickly injected into water (4.8 mL) at 70 ºC, stirring at 1000 rpm, with the system open to air and under N_2 gas flow. The mixture was immediately subjected to nitrogen gas purging over 5 minutes and then left under a N_2 gas atmosphere for a further 10 min. The mixture was then opened to air, cooled in an ice bath for 2 min and lyophilised over 48 h. The resulting powders were subjected to ^{1}H NMR analysis and dexamethasone quantitation to determine the chemical composition and the content of dexamethasone.

7.4.2 Standard Procedure for the Synthesis of Dexamethasone-loaded OLGA-based Nanoparticles

In a typical run, a solution of OLGADMA (8 mg), PEGDA700 (8 mg), AIBN (4 mg), and dexamethasone (6 mg) in THF (1.6 mL) was rapidly injected into water (4.8 mL) at 70 ºC, stirring at 1000 rpm, with the system open to the air and under N_2 gas flow. The reaction mixture was immediately purged with N_2 gas over 5 minutes and then left stirring under N_2 gas atmosphere for a further 10 min. The mixture was then exposed to air and cooled in an ice bath for 2 min. The resulting suspension was purified by centrifugal filtration within centrifugal filter units (MWCO 30 kDa), via two centrifugations at 3200 rcf over 5 minutes, passing through water (~12 mL). The retentate containing the NPs was then carefully pipetted into a volumetric flask and diluted to a final volume of 5 mL with deionised water.

7.4.3 Synthesis of Dexamethasone-loaded PLGA-based Nanoparticles

In a typical run, a solution of the PLGA polymer (16 mg) and dexamethasone (6 mg) in THF (1.6 mL) was rapidly injected into water (4.8 mL) at 70 ºC, stirring at 1000 rpm, with the system open to the air and under N_2 gas flow. The reaction mixture was immediately purged with N_2 gas over 5 minutes and then left stirring under N_2 gas atmosphere for a further 10 min. The reaction mixture was then exposed to air and cooled in an ice bath for 2 min. The resulting suspension was purified by centrifugal

filtration within centrifugal filter units (MWCO 30 kDa), via two centrifugations at 3200 rcf over 5 minutes, passing through water (~12 mL). The retentate containing the NPs was then carefully pipetted into a volumetric flask and diluted to a final volume of 5 mL with deionised water.

7.4.4 Quantitation of Dexamethasone

Analytical curves were constructed measuring the absorption of standard aqueous solutions of dexamethasone (25, 20, 15, 10, 5, 1, and 0.5 μg/mL) at 240 nm using a quartz cuvette. Limits of detection (LOD) and quantification (LOQ) were calculated as 3.3 σ/S and 10 σ/S, respectively, where σ is the standard deviation of intercept and S is the slope of the calibration plot. The measurements were performed in triplicate for the quantitation of dexamethasone in the various experiments.

7.4.5 Determination of the Encapsulation Efficiency of Dexamethasone

The reaction vial and centrifugal filters used for the NP synthesis and the purification step were soaked in methanol over 12 h and combined with the aqueous filtrates obtained from the NP purification step. The resulting solution was diluted with methanol and water to achieve a 1:1 v/v hydromethanolic solution. The resulting solution was subjected to dexamethasone quantitation via the measurement of the absorbance at 240 nm to quantify the unencapsulated dexamethasone. The encapsulation efficiency was calculated according to the equation presented below.

$$\mathrm{EE}(\%)=\frac{\text{weight of dexamethasone feed - weight of unencapsulated dexamethasone}}{\text{weight of dexamethasone feed}}\times 100$$

7.4.6 Estimation of the Loading Efficiency of Dexamethasone

The nanoparticle suspensions containing dexamethasone were lyophilised over 48 h and the resulting powders accurately weighted. The loading efficiency was estimated according to the equation presented below.

$$\mathrm{LE}(\%)=\frac{\text{weight of dexamethasone feed - weight of unencapsulated dexamethasone}}{\text{weight of nanoparticles}}\times 100$$

7.4.7 Comparative Drug Release Study

Aqueous suspensions of dexamethasone-loaded NPs (400 µL) were placed into centrifugal filters (MWCO 100 kDa), sealed with parafilm, and incubated at 37 °C. The samples were then centrifuged (14000 rcf, 5 min, 37 °C) at predetermined time points and the resulting filtrates were collected. The content of the filter was then re-suspended by the addition of water (400 µL), sonicated in a bath sonicator (2 min), and re-incubated at 37 °C. The released dexamethasone was quantified from the individual filtrates allowing for the construction of cumulative release curves.

7.4.8 Stability of **DNP4Aa**, **DNP4Ab**, and **DNP4Bb** in Biological Medium

Aqueous suspensions of **DNP4Aa**, **DNP4Ab**, and **DNP4Bb** (20 µL) were mixed with the dispersant (900 µL of either water, DMEM, and DMEM supplemented with 10% FBS) and left to equilibrate at room temperature for 15 min. The samples were then incubated at 37 ºC for 2 hours and subsequently analysed by DLS. Prior to DLS analysis, the samples containing FBS were centrifuged (15000 rcf at room temperature for 20 minutes), the supernatant discarded, and the sediment re-suspended in FBS-free DMEM (900 µL) by simple inversion of the centrifuge tube.

7.4.9 Stability of **DNP4Aa**, **DNP4Ab**, and **DNP4Bb** Upon Storage at Room Temperature

Aqueous suspensions of **DNP4Aa**, **DNP4Ab**, and **DNP4Bb** (0.1 mg/mL) were left to equilibrate at room temperature over 2 h and subsequently analysed via DLS and ELS for the determination of the size, PI, and ζ-potential. The samples were then sealed in vials, stored on the bench at rt over a period of 4 weeks, and analysed via DLS and ELS weekly.

7.4.10 Synthesis of OLGA-based Nanoparticles in the Presence of XBD173

A solution of **OLGADMA 4Aa** (4.0 mg), PEGDA700 (4.0 mg), AIBN (2.0 mg), and XBD173 (1.5 mg) in THF (0.8 mL) was rapidly injected into water (2.4 mL) at 70 ºC, stirring at 1000 rpm, with the system open to the air and under N_2 gas flow. The reaction mixture was immediately purged with N_2 gas over 5 minutes and then left

stirring under N_2 gas atmosphere for a further 10 min. The mixture was then exposed to air and cooled in an ice bath for 2 min. The resulting suspension was purified by centrifugal filtration within centrifugal filter units (MWCO 30 kDa), via two centrifugations at 3200 rcf over 5 minutes, passing through water (~12 mL). The retentate containing the NPs was then carefully pipetted into a volumetric flask, diluted to a final volume of 2.5 mL with deionised water, and filtered through a syringe filter (0.45 μm).

7.4.11 Synthesis of PLGA-based Nanoparticles in the Presence of XBD173

A solution of PLGA-PEG (8.0 mg) and XBD173 (1.5 mg) in THF (0.8 mL) was rapidly injected into water (2.4 mL) at 70 ºC, stirring at 1000 rpm, with the system open to the air and under N_2 gas flow. The reaction mixture was immediately purged with N_2 gas over 5 minutes and then left stirring under N_2 gas atmosphere for a further 10 min. The mixture was then exposed to air and cooled in an ice bath for 2 min. The resulting suspension was purified by centrifugal filtration within centrifugal filter units (MWCO 30 kDa), via two centrifugations at 3200 rcf over 5 minutes, passing through water (~12 mL). The retentate containing the NPs was then carefully pipetted into a volumetric flask, diluted to a final volume of 2.5 mL with deionised water, and filtered through a syringe filter (0.45 μm).

7.4.12 Quantitation of XBD173

Analytical curves were constructed measuring the absorption of standard solutions of XBD173 in DMSO (25, 20, 15, 10, 5, 1, and 0.5 μg/mL) at 326 nm using a quartz cuvette. Limits of detection (LOD) and quantification (LOQ) were calculated as 3.3 σ/S and 10 σ/S, respectively, where σ is the standard deviation of intercept and S is the slope of the calibration plot. The measurements were performed in triplicate for the quantitation of XBD173 in the various experiments.

7.4.13 Estimation of the Encapsulation Efficiency and the Loading Efficiency of XBD173

Sodium hydroxide was added to the aqueous suspension of NPs prepared in the presence of XBD173 to achieve a 0.5 M sodium hydroxide solution. After 24 h, the solution was diluted with four volumes of DMSO, centrifuged (3 min), filtered through a syringe filter (0.2 μm), and subjected to quantitation of the encapsulated XBD173 by UV-Vis spectroscopy.

The encapsulation efficiency was estimated according to the equation presented below.

$$EE(\%) = \frac{\text{weight of encapsulated XBD173}}{\text{weight of XBD173 feed}} \times 100$$

The loading efficiency was estimated according to the equation presented below.

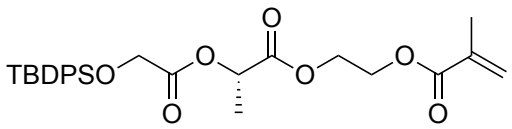
$$LE(\%) = \frac{\text{weight of encapsulated XBD173}}{\text{weight of nanoparticles}} \times 100$$

7.4.14 Effect of **DNP4Aa**, **DNP4Ab**, and **DNP4Bb** on Cell Viability *In Vitro*

HeLa cells were seeded in 96-well plates (5×10^3 cells per well) in 100 μL of DMEM supplemented with 10% foetal bovine serum (FBS), 1% penicillin and streptomycin, and incubated for 24 h at 37 ºC and 5% CO_2. Following this, the media was removed, fresh media was added (90 μL), and the cells were treated with aliquots (10 μL) of aqueous suspensions of **DNP4Aa**, **DNP4Ab**, and **DNP4Bb** having NP concentrations of 0.5, 0.25, 0.1, 0.05, and 0.01 mg/mL. Control cells were treated with water (10 μL). The cells were then incubated for 24 h and 48 h at 37 ºC and 5% CO_2. The cell viability was measured using the Cell Counting Kit-8 (CCK-8) assay, according to the manufacturer's instructions, assigning 100% viability to cells treated with water.

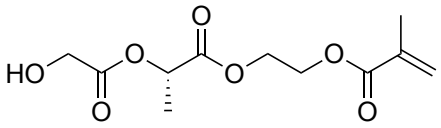
7.5 Experimental Details for Chapter 5

7.5.1 Synthesis and Characterisation of Disulphide **61**



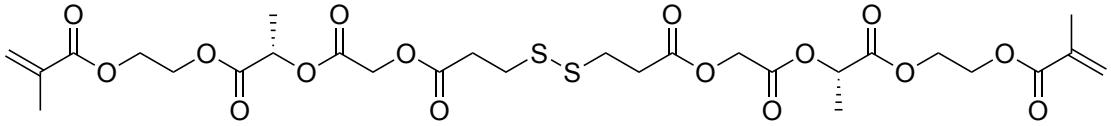
59

Preparation: The compound was prepared by subjecting acid **6** to derivatisation with HEMA according to the standard procedure for the synthesis of monomethacrylates. **Appearance:** colourless oil, **Yield**: 73%, **Characterisation:** R_f = 0.5 (40% Et_2O/hexane); IR (film)/cm^{-1} 2932, 2857, 1760 (C=O), 1722 (C=O), 1136, 820; 1H NMR (400 MHz, $CDCl_3$) δ 7.74 – 7.65 (m, 4H), 7.51 – 7.36 (m, 6H), 6.17 – 6.09 (m, 1H), 5.62 – 5.55 (m, 1H), 5.13 (q, J = 7.1 Hz, 1H), 4.48 – 4.31 (m, 6H), 2.00 – 1.90 (m, 3H), 1.45 (d, J = 7.1 Hz, 3H), 1.09 (s, 9H); ^{13}C NMR (101 MHz, $CDCl_3$) δ 170.5, 170.2, 135.6, 135.5, 132.7, 129.9, 127.8, 126.3, 68.6, 62.8, 62.0, 61.9, 26.6, 19.2, 18.2, 16.8; HRMS (TOF MS ES+) m/z calcd for $C_{27}H_{34}O_7NaSi^+$ $[M+Na]^+$: 521.1972, Found: 521.1974.



60

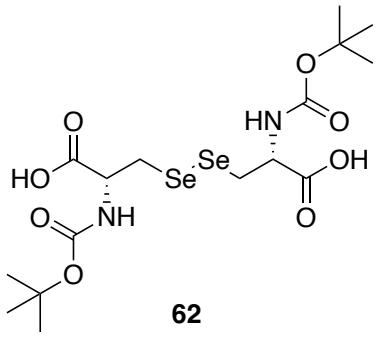
Preparation: The compound was prepared by subjecting **59** to the standard silyl ether cleavage procedure. **Appearance:** colourless oil, **Yield:** 92%, **Characterisation:** R_f = 0.24 (60% Et_2O/hexane); IR (film)/cm^{-1} 3492 (br, OH), 2959, 1748 (C=O), 1719 (C=O), 1635, 1164, 1099, 950; ^1H NMR (400 MHz, $CDCl_3$) δ 6.23 – 6.05 (m, 1H), 5.69 – 5.55 (m, 1H), 5.22 (q, J = 7.1 Hz, 1H), 4.51 – 4.33 (m, 4H), 4.28 (d, J = 17.2 Hz, 1H), 4.23 (d, J = 17.2 Hz, 1H), 2.30 (br, 1H), 1.96 – 1.92 (m, 3H), 1.53 (d, J = 7.1 Hz, 3H); ^{13}C NMR (101 MHz, $CDCl_3$) δ 172.6, 170.0, 167.0, 135.8, 126.3, 69.2, 63.1, 61.9, 60.5, 18.2, 16.8; HRMS (TOF MS ES+) m/z calcd for $C_{11}H_{16}O_7Na^+$ $[M+Na]^+$: 283.0794; Found: 283.0789.



61

Preparation: EDC HCl (21.0 mg, 0.11 mmol) was added to a solution of **60** (35.0 mg, 0.13 mmol), 3,3'-dithiopropionic acid (11.0 mg, 0.05 mmol), and DMAP (3 mg, 0.025 mmol) in CH_2Cl_2 (1 mL) at rt. The reaction was allowed to proceed at rt for 24 h and then concentrated *in vacuo*. An attempt of purification by flash chromatography (60% EtOAc/hexane) afforded a mixture of compounds containing **61**. To purify the compound, the mixture was dissolved in CH_2Cl_2 (10 mL) and washed with aq. HCl (5 mL), sat. aq. $NaHCO_3$ (5 mL), and saturated brine (5 mL). The resulting solution was dried over Na_2SO_4 and concentrated *in vacuo* to afford the desired compound. **Appearance:** colourless oil; **Yield:** 60%, **Characterisation:** R_f = 0.78 (60% EtOAc/hexane); IR (film)/cm^{-1} 2919, 1746 (C=O), 1719 (C=O), 1162, 1133, 1095; ^{1}H NMR (400 MHz, $CDCl_3$) δ 6.17 – 6.10 (m, 2H), 5.64 – 5.57 (m, 2H), 5.19 (q, J = 7.1 Hz, 2H), 4.77 (d, J = 16.1 Hz, 2H), 4.69 (d, J = 16.1 Hz, 2H), 4.51 – 4.33 (m, 8H), 3.00 – 2.92 (m, 4H), 2.91 – 2.83 (m, 4H), 2.00 – 1.92 (m, 6H), 1.53 (d, J = 7.1 Hz, 6H); ^{13}C NMR (101 MHz, $CDCl_3$) δ 170.9, 169.8, 167.0, 166.9, 135.8, 126.2, 69.3, 63.1, 62.0, 60.5, 33.6, 32.7, 18.2, 16.8; HRMS (TOF MS ES+) m/z calcd for $C_{28}H_{39}O_{16}S_2^+$ $[M+H]^+$: 695.1680; Found: 695.1682.

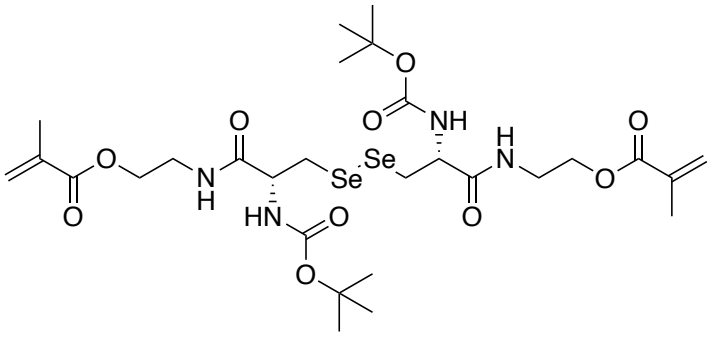
7.5.2 Synthesis and Characterisation of Diselenide **63**



62

Preparation: L-Selenocystine (0.167 g, 0.5 mmol) was suspended in water (2.5 mL) and chilled to 0 °C. Triethylamine (209 µL, 1.5 mmol) followed by Boc_2O (2.0 M solution

in THF, 0.750 mL, 1.5 mmol) were added at 0 °C. The reaction was allowed to proceed on ice for 5 min, then stirred at rt for 24 h. The mixture was then diluted with ice cold water (10 mL), acidified with ice-cold aq. HCl (10%, 3 mL), then quickly extracted with ethyl acetate (3 × 30 mL). The combined organic layers were washed with brine (20 mL), dried over Na_2SO_4, and concentrated *in vacuo*. The obtained solid was repeatedly washed with hexane and then dried under reduced pressure to afford the desired compound. **Appearance:** Yellow solid, **Yield:** 66%, **Characterisation**: R_f = 0.60 (1 % AcOH/ethyl acetate); IR (film)/cm^{-1} 3360, 2979, 1699, 1665, 1504; ^{1}H NMR (400 MHz, $(CD_3)_2SO$) δ 12.80 (s, 2H), 7.20 (d, J = 8.2 Hz, 2H), 4.14 (m, 2H), 3.29 (dd, J = 12.4, 4.8 Hz, 2H), 3.10 (dd, J = 12.3, 9.8 Hz, 2H), 1.38 (s, 18H); ^{13}C NMR (101 MHz, $(^{13}CD_3)_2SO$) δ 172.5, 155.3, 78.3, 54.2, 30.9, 28.2. The observed spectroscopic data was consistent with that previously reported.[358]



63

Preparation: Triethylamine (0.13 mL, 0.92 mmol) was added dropwise to a solution of **62** (152 mg, 0.29 mmol), 2-aminoethyl methacrylate (142 mg, 0.86 mmol) and DMAP (3.50 mg, 0.029 mmol) in DMF (2 mL) at 0 °C. The mixture was left stirring at 0 °C for 15 min and EDC hydrochloride (165 mg, 0.86 mmol, 3 equiv) was added. The reaction was allowed to proceed at rt for 24 h. Upon completion, the reaction mixture was partitioned between saturated brine (10 mL) and ethyl acetate (10 mL), the phases separated, and the aqueous layer extracted with ethyl acetate (2 × 10 mL). The combined organic phases were quickly washed with aq. HCl (10 %, 10 mL), sat. aq. NaHCO3 (10 mL), dried over Na_2SO_4 and concentrated *in vacuo*. Purification by filtration through a short silica plug (100% ethyl acetate) afforded the desired compound. **Appearance:** viscous yellow oil; **Yield:** 40%; **Characterisation:** R_f = 0.26 (80% diethyl ether/hexane); ^{1}H NMR (400 MHz, $(CD_3)_2SO$) δ 8.11 – 8.03 (m, 2H), 7.05 (d, J = 8.3 Hz, 2H), 6.07 – 6.04 (m, 2H), 5.68 – 5.65 (m, 2H), 4.19–4.05 (m, 6H), 3.22

(dd, J = 12.3, 5.4 Hz, 2H), 3.09 – 3.01 (m, 2H), 1.89 – 1.85 (m, 6H), 1.37 (s, 18H); ^{13}C NMR (101 MHz, $(^{13}CD_3)_2SO$) δ 170.7, 166.5, 155.1, 135.7, 125.9, 78.3, 62.8, 55.0, 37.7, 32.4, 28.1, 18.0; HRMS (TOF MS ES+) m/z calcd for $C_{28}H_{47}N_4O_{10}{}^{80}Se_2{}^+$ $[M+H]^+$: 759.1623; Found 759.1651.

7.5.3 Synthesis of Disulphide-Containing Crosslinked Polymeric Nanoparticles

In a typical run, a solution of disulphide **61** (16 mg), or a mixture of disulphide **61** (8 mg) and co-monomer (8 mg), in THF (1.6 mL) was rapidly injected into water (4.8 mL) at 70 ºC, stirring at 1000 rpm, with the system open to the air and under N_2 gas flow. The reaction mixture was immediately purged with N_2 gas over 5 minutes and then left stirring under N_2 gas atmosphere for a further 10 min. The mixture was then exposed to air and cooled in an ice bath for 2 min. The resulting suspension was purified by centrifugal filtration within centrifugal filter units (MWCO 100 kDa), via two centrifugations at 3200 rcf over 5 minutes, passing through water (~12 mL). The retentate containing the NPs was then carefully pipetted into a volumetric flask and diluted to a final volume of 5 mL with deionised water.

References

1. Langer, R. Drug delivery and targeting. *Nature* **392**, 5–10 (1998).

2. Allen, T. M. & Cullis, P. R. Drug Delivery Systems: Entering the Mainstream. *Science* **303**, 1818–1822 (2004).

3. Langer, R. New Methods of Drug Delivery. *Science* **249**, 1527–1533 (1990).

4. Vargason, A. M., Anselmo, A. C. & Mitragotri, S. The evolution of commercial drug delivery technologies. *Nat. Biomed. Eng.* **5**, 951–967 (2021).

5. Strategies to Modify the Drug Release from Pharmaceutical Systems. 15–28 (2015) doi:10.1016/b978-0-08-100092-2.00002-3.

6. Palomba, S., Falbo, A., Cello, A. D., Materazzo, C. & Zullo, F. Nexplanon: the new implant for long-term contraception. A comprehensive descriptive review. *Gynecol. Endocrinol.* **28**, 710–721 (2012).

7. Shen, J., Choi, S., Qu, W., Wang, Y. & Burgess, D. J. In vitro-in vivo correlation of parenteral risperidone polymeric microspheres. *J. Control. Release* **218**, 2–12 (2015).

8. Rainer, M. K. Risperidone long-acting injection: a review of its long term safety and efficacy. *Neuropsychiatr. Dis. Treat.* **4**, 919–927 (2008).

9. Dhand, C. *et al.* Role of size of drug delivery carriers for pulmonary and intravenous administration with emphasis on cancer therapeutics and lung-targeted drug delivery. *RSC Adv.* **4**, 32673–32689 (2014).

10. Rafiyath, S. M. *et al.* Comparison of safety and toxicity of liposomal doxorubicin vs. conventional anthracyclines: a meta-analysis. *Exp. Hematol. Oncol.* **1**, 10 (2012).

11. Gao, J., Karp, J. M., Langer, R. & Joshi, N. The Future of Drug Delivery. *Chem. Mater.* **35**, 359–363 (2023).

12. Park, H., Otte, A. & Park, K. Evolution of drug delivery systems: From 1950 to 2020 and beyond. *J. Control. Release* **342**, 53–65 (2022).

13. Vert, M. *et al.* Terminology for biorelated polymers and applications (IUPAC Recommendations 2012). *Pure Appl. Chem.* **84**, 377–410 (2012).

14. Trotta, F. & Mele, A. Nanosponges. 1–26 (2019) doi:10.1002/9783527341009.ch1.

15. Jong, W. H. D. & Borm, P. J. Drug delivery and nanoparticles: Applications and hazards. *Int. J. Nanomed.* **3**, 133–149 (2008).

16. Kreuter, J. Nanoparticles—a historical perspective. *Int. J. Pharm.* **331**, 1–10 (2007).

17. Mitchell, M. J. *et al.* Engineering precision nanoparticles for drug delivery. *Nature Reviews Drug Discovery* **20**, 101–124 (2021).

18. Shi, J., Votruba, A. R., Farokhzad, O. C. & Langer, R. Nanotechnology in drug delivery and tissue engineering: From discovery to applications. *Nano Letters* **10**, 3223–3230 (2010).

19. Farokhzad, O. C. & Langer, R. Impact of Nanotechnology on Drug Delivery. *ACS Nano* **3**, 16–20 (2009).

20. Tenchov, R., Bird, R., Curtze, A. E. & Zhou, Q. Lipid Nanoparticles From Liposomes to mRNA Vaccine Delivery, a Landscape of Research Diversity and Advancement. *ACS Nano* **15**, 16982–17015 (2021).

21. Anselmo, A. C. & Mitragotri, S. Nanoparticles in the clinic: An update post COVID-19 vaccines. *Bioengineering and Translational Medicine* **6**, 1–20 (2021).

22. Ali, M. R. K., Wu, Y. & El-Sayed, M. A. Gold-Nanoparticle-Assisted Plasmonic Photothermal Therapy Advances Toward Clinical Application. *J. Phys. Chem. C* **123**, 15375–15393 (2019).

23. Gupta, A. K. & Gupta, M. Synthesis and surface engineering of iron oxide nanoparticles for biomedical applications. *Biomaterials* **26**, 3995–4021 (2005).

24. Wagner, A. M., Knipe, J. M., Orive, G. & Peppas, N. A. Quantum dots in biomedical applications. *Acta Biomater.* **94**, 44–63 (2019).

25. Wagner, V., Dullaart, A., Bock, A.-K. & Zweck, A. The emerging nanomedicine landscape. *Nat. Biotechnol.* **24**, 1211–1217 (2006).

26. Liz-Marzán, L. M. *et al.* What Do We Mean When We Say Nanomedicine? *ACS Nano* **16**, 13257–13259 (2022).

27. Anselmo, A. C. & Mitragotri, S. Nanoparticles in the clinic. *Bioeng. Transl. Med.* **1**, 10–29 (2016).

28. CUMMINGS, G. C. *et al.* Dose requirements of ICI 35,868 (Propofol, 'Diprivan') in a new formulation for induction of anaesthesia. *Anaesthesia* **39**, 1168–1171 (1984).

29. Green, M. R. *et al.* Abraxane®, a novel Cremophor®-free, albumin-bound particle form of paclitaxel for the treatment of advanced non-small-cell lung cancer. *Ann. Oncol.* **17**, 1263–1268 (2006).

30. Allen, T. M. & Martin, F. J. Advantages of liposomal delivery systems for anthracyclines. *Semin. Oncol.* **31**, 5–15 (2004).

31. Working, P. K. *et al.* Pharmacokinetics, Biodistribution and Therapeutic Efficacy of Doxorubicin Encapsulated in Stealth® Liposomes (Doxil®). *J. Liposome Res.* **4**, 667–687 (1994).

32. Sparreboom, A. *et al.* Comparative Preclinical and Clinical Pharmacokinetics of a Cremophor-Free, Nanoparticle Albumin-Bound Paclitaxel (ABI-007) and Paclitaxel Formulated in Cremophor (Taxol). *Clin. Cancer Res.* **11**, 4136–4143 (2005).

33. Anselmo, A. C. & Mitragotri, S. Nanoparticles in the clinic: An update. *Bioeng. Transl. Med.* **4**, e10143 (2019).

34. Barenholz, Y. Doxil® - The first FDA-approved nano-drug: Lessons learned. *Journal of Controlled Release* **160**, 117–134 (2012).

35. Coyne, D. W. & Auerbach, M. Anemia management in chronic kidney disease: Intravenous iron steps forward. *Am. J. Hematol.* **85**, 311–312 (2010).

36. Thompson, K. A. & Goodale, D. B. The Recent Development of Propofol (DIPRIVAN®). *Intensiv. Care Med.* **26**, S400–S404 (2000).

37. Bovier, P. A. Epaxal®: a virosomal vaccine to prevent hepatitis A infection. *Expert Rev. Vaccines* **7**, 1141–1150 (2008).

38. Boswell, G. W., Buell, D. & Bekersky, I. AmBisome (Liposomal Amphotericin B): A Comparative Review. *J. Clin. Pharmacol.* **38**, 583–592 (1998).

39. Schmidt-Erfurth, U. & Hasan, T. Mechanisms of Action of Photodynamic Therapy with Verteporfin for the Treatment of Age-Related Macular Degeneration. *Surv. Ophthalmol.* **45**, 195–214 (2000).

40. Kamaly, N., Xiao, Z., Valencia, P. M., Radovic-Moreno, A. F. & Farokhzad, O. C. Targeted polymeric therapeutic nanoparticles: Design, development and clinical translation. *Chemical Society Reviews* **41**, 2971–3010 (2012).

41. Germain, M. *et al.* Delivering the power of nanomedicine to patients today. *J. Control. Release* **326**, 164–171 (2020).

42. Kulkarni, J. A. *et al.* The current landscape of nucleic acid therapeutics. *Nat. Nanotechnol.* **16**, 630–643 (2021).

43. Akinc, A. *et al.* The Onpattro story and the clinical translation of nanomedicines containing nucleic acid-based drugs. *Nat. Nanotechnol.* **14**, 1084–1087 (2019).

44. Bonvalot, S. *et al.* NBTXR3, a first-in-class radioenhancer hafnium oxide nanoparticle, plus radiotherapy versus radiotherapy alone in patients with locally advanced soft-tissue sarcoma (Act.In.Sarc): a multicentre, phase 2–3, randomised, controlled trial. *Lancet Oncol.* **20**, 1148–1159 (2019).

45. Guerrini, G., Magrì, D., Gioria, S., Medaglini, D. & Calzolai, L. Characterization of nanoparticles-based vaccines for COVID-19. *Nat. Nanotechnol.* **17**, 570–576 (2022).

46. Creech, C. B., Walker, S. C. & Samuels, R. J. SARS-CoV-2 Vaccines. *JAMA* **325**, 1318–1320 (2021).

47. Milane, L. & Amiji, M. Clinical approval of nanotechnology-based SARS-CoV-2 mRNA vaccines: impact on translational nanomedicine. *Drug Deliv. Transl. Res.* **11**, 1309–1315 (2021).

48. Higuchi, T. & Kuramoto, R. Study of possible complex formation between macromolecules and certain pharmaceuticals. I. Polyvinylpyrrolidone with sulfathiazole, procaine hydrochloride, sodium salicylate, benzyl penicillin, chloramphenicol, mandelic acid, caffeine, theophylline, and cortisone. *J. Am. Pharm. Assoc.* **43**, 393–397 (1954).

49. Folkman, J. & Long, D. M. The use of silicone rubber as a carrier for prolonged drug therapy. *J. Surg. Res.* **4**, 139–142 (1964).

50. Khanna, S. C., Jecklin, T. & Speiser, P. Bead Polymerization Technique for Sustained-Release Dosage Form. *J. Pharm. Sci.* **59**, 614–618 (1970).

51. Roseman, T. J. & Higuchi, W. I. Release of Medroxyprogesterone Acetate from a Silicone Polymer. *J. Pharm. Sci.* **59**, 353–357 (1970).

52. Roseman, T. J. Release of steroids from a silicone polymer. *J. Pharm. Sci.* **61**, 46–50 (1972).

53. Batz, H., Franzmann, G. & Ringsdorf, H. Model Reactions for Synthesis of Pharmacologically Active Polymers by Way of Monomeric and Polymeric Reactive Esters. *Angew. Chem. Int. Ed. Engl.* **11**, 1103–1104 (1972).

54. Theeuwes, F., Hussain, A. & Higuchi, T. Quantitative analytical method for determination of drugs dispersed in polymers using differential scanning calorimetry. *J. Pharm. Sci.* **63**, 427–429 (1974).

55. Birrenbach, G. & Speiser, P. P. Polymerized Micelles and Their Use as Adjuvants in Immunology. *J. Pharm. Sci.* **65**, 1763–1766 (1976).

56. LANGER, R. & FOLKMAN, J. Polymers for the sustained release of proteins and other macromolecules. *Nature* **263**, 797–800 (1976).

57. Peppas, N. A. & Merrill, E. W. Development of semicrystalline poly(vinyl alcohol) hydrogels for biomedical applications. *J. Biomed. Mater. Res.* **11**, 423–434 (1977).

58. Heller, J. Controlled release of biologically active compounds from bioerodible polymers. *Biomaterials* **1**, 51–57 (1980).

59. Langer, R. S. & Peppas, N. A. Present and future applications of biomaterials in controlled drug delivery systems. *Biomaterials* **2**, 201–214 (1981).

60. Langer, R. Implantable controlled release systems. *Pharmacol. Ther.* **21**, 35–51 (1983).

61. Heller, J. & Himmelstein, K. J. [31] Poly(ortho ester) biodegradable polymer systems. *Methods Enzym.* **112**, 422–436 (1985).

62. Hoffman, A. S. The origins and evolution of “controlled” drug delivery systems. *J. Control. Release* **132**, 153–163 (2008).

63. Patel, T., Zhou, J., Piepmeier, J. M. & Saltzman, W. M. Polymeric nanoparticles for drug delivery to the central nervous system. *Adv. Drug Deliv. Rev.* **64**, 701–705 (2012).

64. Kamaly, N., Yameen, B., Wu, J. & Farokhzad, O. C. Degradable controlled-release polymers and polymeric nanoparticles: Mechanisms of controlling drug release. *Chemical Reviews* **116**, 2602–2663 (2016).

65. Ryu, S. *et al.* Visualization of the distribution of nanoparticle-formulated AZD2811 in mouse tumor model using matrix-assisted laser desorption ionization mass spectrometry imaging. *Sci. Rep.* **10**, 15535 (2020).

66. Sanna, V., Pala, N. & Sechi, M. Targeted therapy using nanotechnology: focus on cancer. *Int. J. Nanomed.* **9**, 467–483 (2014).

67. Kim, S. C. *et al.* In vivo evaluation of polymeric micellar paclitaxel formulation: toxicity and efficacy. *J. Control. Release* **72**, 191–202 (2001).

68. Harada, M. *et al.* Improved anti-tumor activity of stabilized anthracycline polymeric micelle formulation, NC-6300. *Cancer Sci.* **102**, 192–199 (2011).

69. Osada, A. NC-6004, a novel cisplatin nanoparticle, in combination with pembrolizumab for head and neck cancer. *Integr. Clin. Med.* **3**, (2019).

70. Nishiyama, N., Matsumura, Y. & Kataoka, K. Development of polymeric micelles for targeting intractable cancers. *Cancer Sci.* **107**, 867–874 (2016).

71. Wang, R., Billone, P. S. & Mullett, W. M. Nanomedicine in Action: An Overview of Cancer Nanomedicine on the Market and in Clinical Trials. *J. Nanomater.* **2013**, 1–12 (2013).

72. Rijcken, C. J. F. *et al.* Design, development and clinical translation of CriPec®-based core-crosslinked polymeric micelles. *Adv. Drug Deliv. Rev.* **191**, 114613 (2022).

73. Weiss, G. J. *et al.* First-in-human phase 1/2a trial of CRLX101, a cyclodextrin-containing polymer-camptothecin nanopharmaceutical in patients with advanced solid tumor malignancies. *Investig. N. Drugs* **31**, 986–1000 (2013).

74. Piha-Paul, S. A. *et al.* First-in-human, phase I/IIa study of CRLX301, a nanoparticle drug conjugate containing docetaxel, in patients with advanced or metastatic solid malignancies. *Investigational New Drugs* **39**, 1047–1056 (2021).

75. Creemers, J. H. A. *et al.* Assessing the safety, tolerability and efficacy of PLGA-based immunomodulatory nanoparticles in patients with advanced NY-ESO-1-positive cancers: a first-in-human phase I open-label dose-escalation study protocol. *BMJ Open* **11**, e050725 (2021).

76. Rideau, E., Dimova, R., Schwille, P., Wurm, F. R. & Landfester, K. Liposomes and polymersomes: a comparative review towards cell mimicking. *Chem. Soc. Rev.* **47**, 8572–8610 (2018).

77. Shae, D. *et al.* Endosomolytic polymersomes increase the activity of cyclic dinucleotide STING agonists to enhance cancer immunotherapy. *Nat. Nanotechnol.* **14**, 269–278 (2019).

78. Ahmad, Z., Shah, A., Siddiq, M. & Kraatz, H.-B. Polymeric micelles as drug delivery vehicles. *RSC Adv.* **4**, 17028–17038 (2014).

79. Ghezzi, M. *et al.* Polymeric micelles in drug delivery: An insight of the techniques for their characterization and assessment in biorelevant conditions. *J. Control. Release* **332**, 312–336 (2021).

80. Wang, J., Li, B., Qiu, L., Qiao, X. & Yang, H. Dendrimer-based drug delivery systems: history, challenges, and latest developments. *J. Biol. Eng.* **16**, 18 (2022).

81. Dufès, C., Uchegbu, I. F. & Schätzlein, A. G. Dendrimers in gene delivery. *Adv. Drug Deliv. Rev.* **57**, 2177–2202 (2005).

82. Caminade, A.-M. & Turrin, C.-O. Dendrimers for drug delivery. *J. Mater. Chem. B* **2**, 4055–4066 (2014).

83. Kabanov, A. V. & Vinogradov, S. V. Nanogels as pharmaceutical carriers: Finite networks of infinite capabilities. *Angewandte Chemie - International Edition* **48**, 5418–5429 (2009).

84. Gao, Y., Newland, B., Zhou, D., Matyjaszewski, K. & Wang, W. Controlled Polymerization of Multivinyl Monomers: Formation of Cyclized/Knotted Single-Chain Polymer Architectures. *Angew. Chem. Int. Ed.* **56**, 450–460 (2017).

85. Oyama, T. Encyclopedia of Polymeric Nanomaterials. 1–11 (2014) doi:10.1007/978-3-642-36199-9_181-1.

86. Elsabahy, M. & Wooley, K. L. Design of polymeric nanoparticles for biomedical delivery applications. *Chem. Soc. Rev.* **41**, 2545–2561 (2012).

87. Fujii, S. Polymeric core-crosslinked particles prepared via a nanoemulsion-mediated process: from particle design and structural characterization to in vivo behavior in chemotherapy. *Polym. J.* 1–13 (2023) doi:10.1038/s41428-023-00793-6.

88. Thurmond, K. B., Kowalewski, T. & Wooley, K. L. Shell Cross-Linked Knedels: A Synthetic Study of the Factors Affecting the Dimensions and Properties of Amphiphilic Core-Shell Nanospheres. *J. Am. Chem. Soc.* **119**, 6656–6665 (1997).

89. Joralemon, M. J., O'Reilly, R. K., Hawker, C. J. & Wooley, K. L. Shell Click-Crosslinked (SCC) Nanoparticles: A New Methodology for Synthesis and Orthogonal Functionalization. *J. Am. Chem. Soc.* **127**, 16892–16899 (2005).

90. Xu, H., Meng, F. & Zhong, Z. Reversibly crosslinked temperature-responsive nano-sized polymersomes: synthesis and triggered drug release. *J. Mater. Chem.* **19**, 4183–4190 (2009).

91. Cheng, R. *et al.* Reduction and temperature dual-responsive crosslinked polymersomes for targeted intracellular protein delivery. *J. Mater. Chem.* **21**, 19013–19020 (2011).

92. Thambi, T. *et al.* Biostable and bioreducible polymersomes for intracellular delivery of doxorubicin. *Polym. Chem.* **5**, 4627–4634 (2014).

93. Liu, X., Yaszemski, M. J. & Lu, L. Expansile crosslinked polymersomes for pH sensitive delivery of doxorubicin. *Biomater. Sci.* **4**, 245–249 (2015).

94. Zhang, X., Malhotra, S., Molina, M. & Haag, R. Micro- and nanogels with labile crosslinks-from synthesis to biomedical applications. *Chemical Society Reviews* **44**, 1948–1973 (2015).

95. Liu, B. & Thayumanavan, S. Importance of Evaluating Dynamic Encapsulation Stability of Amphiphilic Assemblies in Serum. *Biomacromolecules* **18**, 4163–4170 (2017).

96. Liechty, W. B., Kryscio, D. R., Slaughter, B. V. & Peppas, N. A. Polymers for Drug Delivery Systems. *Annu. Rev. Chem. Biomol. Eng.* **1**, 149–173 (2010).

97. Vilar, G., Tulla-Puche, J. & Albericio, F. Polymers and drug delivery systems. *Curr. drug Deliv.* **9**, 367–94 (2011).

98. Turos, E. *et al.* Antibiotic-conjugated polyacrylate nanoparticles: New opportunities for development of anti-MRSA agents. *Bioorg. Med. Chem. Lett.* **17**, 53–56 (2007).

99. Bettencourt, A. & Almeida, A. J. Poly(methyl methacrylate) particulate carriers in drug delivery. *J. Microencapsul.* **29**, 353–367 (2012).

100. Gombotz, W. R. & Pettit, D. K. Biodegradable Polymers for Protein and Peptide Drug Delivery. *Bioconjugate Chem.* **6**, 332–351 (1995).

101. Vert, M., Li, S. M., Spenlehauer, G. & Guerin, P. Bioresorbability and biocompatibility of aliphatic polyesters. *J. Mater. Sci.: Mater. Med.* **3**, 432–446 (1992).

102. Brannigan, R. P. & Dove, A. P. Synthesis, properties and biomedical applications of hydrolytically degradable materials based on aliphatic polyesters and polycarbonates. *Biomater. Sci.* **5**, 9–21 (2016).

103. Anderson, J. M. & Shive, M. S. Biodegradation and biocompatibility of PLA and PLGA microspheres. *Adv. Drug Deliv. Rev.* **28**, 5–24 (1997).

104. Gao, D., Xu, H., Philbert, M. A. & Kopelman, R. Bioeliminable Nanohydrogels for Drug Delivery. *Nano Lett.* **8**, 3320–3324 (2008).

105. Wang, S. *et al.* Multifunctional Biodegradable Polyacrylamide Nanocarriers for Cancer Theranostics□A “See and Treat” Strategy. *ACS Nano* **6**, 6843–6851 (2012).

106. Fredenberg, S., Wahlgren, M., Reslow, M. & Axelsson, A. The mechanisms of drug release in poly(lactic-co-glycolic acid)-based drug delivery systems—A review. *Int. J. Pharm.* **415**, 34–52 (2011).

107. Frazza, E. J. & Schmitt, E. E. A new absorbable suture. *J. Biomed. Mater. Res.* **5**, 43–58 (1971).

108. Reed, A. M. & Gilding, D. K. Biodegradable polymers for use in surgery — poly(glycolic)/poly(lactic acid) homo and copolymers: 2. In vitro degradation. *Polymer* **22**, 494–498 (1981).

109. Engelberg, I. & Kohn, J. Physico-mechanical properties of degradable polymers used in medical applications: A comparative study. *Biomaterials* **12**, 292–304 (1991).

110. Nair, L. S. & Laurencin, C. T. Biodegradable polymers as biomaterials. *Prog. Polym. Sci.* **32**, 762–798 (2007).

111. Ovitt, T. M. & Coates, G. W. Stereoselective ring-opening polymerization ofrac-lactide with a single-site, racemic aluminum alkoxide catalyst: Synthesis of stereoblock poly(lactic acid). *J. Polym. Sci. Part A: Polym. Chem.* **38**, 4686–4692 (2000).

112. Joziasse, C. A. P. *et al.* The influence of morphology on the (hydrolytic degradation of as-polymerized and hot-drawn poly(L-lactide)). *Colloid Polym. Sci.* **276**, 968–975 (1998).

113. Södergård, A. & Stolt, M. Properties of lactic acid based polymers and their correlation with composition. *Prog. Polym. Sci.* **27**, 1123–1163 (2002).

114. Jain, R. A. The manufacturing techniques of various drug loaded biodegradable poly(lactide-co-glycolide) (PLGA) devices. *Biomaterials* **21**, 2475–2490 (2000).

115. Sheridan, M. H., Shea, L. D., Peters, M. C. & Mooney, D. J. Bioabsorbable polymer scaffolds for tissue engineering capable of sustained growth factor delivery. *J. Control. Release* **64**, 91–102 (2000).

116. Mundargi, R. C., Babu, V. R., Rangaswamy, V., Patel, P. & Aminabhavi, T. M. Nano/micro technologies for delivering macromolecular therapeutics using poly(d,l-lactide-co-glycolide) and its derivatives. *J. Control. Release* **125**, 193–209 (2008).

117. Danhier, F. *et al.* PLGA-based nanoparticles: An overview of biomedical applications. *Journal of Controlled Release* **161**, 505–522 (2012).

118. Miller, R. A., Brady, J. M. & Cutright, D. E. Degradation rates of oral resorbable implants (polylactates and polyglycolates): Rate modification with changes in PLA/PGA copolymer ratios. *J. Biomed. Mater. Res.* **11**, 711–719 (1977).

119. Vey, E. *et al.* Degradation mechanism of poly(lactic-co-glycolic) acid block copolymer cast films in phosphate buffer solution. *Polym. Degrad. Stab.* **93**, 1869–1876 (2008).

120. Vey, E. *et al.* The impact of chemical composition on the degradation kinetics of poly(lactic-co-glycolic) acid copolymers cast films in phosphate buffer solution. *Polym. Degrad. Stab.* **97**, 358–365 (2012).

121. Li, J. *et al.* of Poly (lactic- co -glycolic acid) through Precise Control of Monomer Sequence. *ACS Symposium Series* (2014) doi:10.1021/bk-2014-1170.ch018.

122. Yoo, J., Viswanath, D. & Won, Y. Y. Strategy for Synthesis of Statistically Sequence-Controlled Uniform PLGA and Effects of Sequence Distribution on Interaction and Drug Release Properties. *ACS Macro Letters* **10**, 1510–1516 (2021).

123. Stayshich, R. M. & Meyer, T. Y. New insights into poly(lactic- co -glycolic acid) microstructure: Using repeating sequence copolymers to decipher complex NMR and thermal behavior. *Journal of the American Chemical Society* **132**, 10920–10934 (2010).

124. Li, J., Stayshich, R. M. & Meyer, T. Y. Exploiting sequence to control the hydrolysis behavior of biodegradable PLGA copolymers. *Journal of the American Chemical Society* **133**, 6910–6913 (2011).

125. Li, J., Rothstein, S. N., Little, S. R., Edenborn, H. M. & Meyer, T. Y. The effect of monomer order on the hydrolysis of biodegradable poly(lactic-co-glycolic acid) repeating sequence copolymers. *Journal of the American Chemical Society* **134**, 16352–16359 (2012).

126. Washington, M. A. *et al.* The impact of monomer sequence and stereochemistry on the swelling and erosion of biodegradable poly(lactic-co-glycolic acid) matrices. *Biomaterials* **117**, 66–76 (2017).

127. Washington, M. A. *et al.* Monomer sequence in PLGA microparticles: Effects on acidic microclimates and in vivo inflammatory response. *Acta Biomaterialia* **65**, 259–271 (2018).

128. Kulkarni, R. K., Moore, E. G., Hegyeli, A. F. & Leonard, F. Biodegradable poly(lactic acid) polymers. *J. Biomed. Mater. Res.* **5**, 169–181 (1971).

129. Avgoustakis, K. Encyclopedia of Biomedical Polymers and Polymeric Biomaterials. 6491–6500 (2015) doi:10.1081/e-ebpp-120013950.

130. Siepmann, J., Elkharraz, K., Siepmann, F. & Klose, D. How Autocatalysis Accelerates Drug Release from PLGA-Based Microparticles: A Quantitative Treatment. *Biomacromolecules* **6**, 2312–2319 (2005).

131. Machatschek, R. & Lendlein, A. Fundamental insights in PLGA degradation from thin film studies. *J. Control. Release* **319**, 276–284 (2020).

132. Kemme, M., Prokesch, I. & Heinzel-Wieland, R. Comparative study on the enzymatic degradation of poly(lactic-co-glycolic acid) by hydrolytic enzymes based on the colorimetric quantification of glycolic acid. *Polym. Test.* **30**, 743–748 (2011).

133. Wu, X. S. & Wang, N. Synthesis, characterization, biodegradation, and drug delivery application of biodegradable lactic/glycolic acid polymers. Part II: Biodegradation. *J. Biomater. Sci., Polym. Ed.* **12**, 21–34 (2001).

134. Therin, M., Christel, P., Li, S., Garreau, H. & Vert, M. In vivo degradation of massive poly(α-hydroxy acids): Validation of In vitro findings. *Biomaterials* **13**, 594–600 (1992).

135. Vert, M., Mauduit, J. & Li, S. Biodegradation of PLA/GA polymers: increasing complexity. *Biomaterials* **15**, 1209–1213 (1994).

136. Alexis, F. Factors affecting the degradation and drug-release mechanism of poly(lactic acid) and poly[(lactic acid)-co-(glycolic acid)]. *Polym. Int.* **54**, 36–46 (2005).

137. Li, S. Hydrolytic degradation characteristics of aliphatic polyesters derived from lactic and glycolic acids. *J. Biomed. Mater. Res.* **48**, 342–353 (1999).

138. Tracy, M. A. *et al.* Factors affecting the degradation rate of poly(lactide-co-glycolide) microspheres in vivo and in vitro. *Biomaterials* **20**, 1057–1062 (1999).

139. Lu, L., Garcia, C. A. & Mikos, A. G. In vitro degradation of thin poly(DL-lactic-co-glycolic acid) films. *J. Biomed. Mater. Res.* **46**, 236–244 (1999).

140. Stayshich, R. M. & Meyer, T. Y. New insights into poly(lactic- co -glycolic acid) microstructure: Using repeating sequence copolymers to decipher complex NMR and thermal behavior. *Journal of the American Chemical Society* **132**, 10920–10934 (2010).

141. Li, J., Rothstein, S. N., Little, S. R., Edenborn, H. M. & Meyer, T. Y. The effect of monomer order on the hydrolysis of biodegradable poly(lactic-co-glycolic acid) repeating sequence copolymers. *Journal of the American Chemical Society* **134**, 16352–16359 (2012).

142. Nowalk, J. A., Swisher, J. H. & Meyer, T. Y. Consequences of isolated critical monomer sequence errors for the hydrolysis behaviors of sequenced degradable polyesters. *Polymer Chemistry* **10**, 4930–4934 (2019).

143. Eger, E. M. & Agarwal, S. Poly(lactic-co-glycolic acid) Networks with Dynamic Covalent Bonds: Synthesis and Characterization. *ACS Appl. Polym. Mater.* **5**, 5141–5148 (2023).

144. Phong, L., Han, E. S. C., Xiong, S., Pan, J. & Loo, S. C. J. Properties and hydrolysis of PLGA and PLLA cross-linked with electron beam radiation. *Polym. Degrad. Stab.* **95**, 771–777 (2010).

145. Michlovská, L. *et al.* Hydrolytic stability of end-linked hydrogels from PLGA–PEG–PLGA macromonomers terminated by α,ω-itaconyl groups. *RSC Adv.* **6**, 16808–16816 (2016).

146. Zahoranova, A. *et al.* Hybrid Hydrogel Networks by Photocrosslinking of Thermoresponsive α,ω-Itaconyl-PLGA-PEG-PLGA Micelles in Water: Influence of the Lithium Phenyl-2,4,6-Trimethylbenzoylphosphinate Photoinitinator. *Macromol. Chem. Phys.* **221**, 2000165 (2020).

147. Wang, Y., Qin, B., Xia, G. & Choi, S. H. FDA's Poly (Lactic-Co-Glycolic Acid) Research Program and Regulatory Outcomes. *AAPS Journal* **23**, (2021).

148. Operti, M. C. *et al.* PLGA-based nanomedicines manufacturing: Technologies overview and challenges in industrial scale-up. *International Journal of Pharmaceutics* **605**, 120807 (2021).

149. Knop, K., Hoogenboom, R., Fischer, D. & Schubert, U. S. Poly(ethylene glycol) in Drug Delivery: Pros and Cons as Well as Potential Alternatives. *Angew. Chem. Int. Ed.* **49**, 6288–6308 (2010).

150. Ju, Y. *et al.* Impact of anti-PEG antibodies induced by SARS-CoV-2 mRNA vaccines. *Nat. Rev. Immunol.* **23**, 135–136 (2023).

151. Chen, E. *et al.* Premature Drug Release from Polyethylene Glycol (PEG)-Coated Liposomal Doxorubicin via Formation of the Membrane Attack Complex. *ACS Nano* **14**, 7808–7822 (2020).

152. Torchilin, V. P. Polymer-coated long-circulating microparticulate pharmaceuticals. *J. Microencapsul.* **15**, 1–19 (1998).

153. Wen, P. *et al.* Stealth and pseudo-stealth nanocarriers. *Adv. Drug Deliv. Rev.* **198**, 114895 (2023).

154. Makadia, H. K. & Siegel, S. J. Poly Lactic-co-Glycolic Acid (PLGA) as biodegradable controlled drug delivery carrier. *Polymers* **3**, 1377–1397 (2011).

155. Li, Y.-P. *et al.* PEGylated PLGA nanoparticles as protein carriers: synthesis, preparation and biodistribution in rats. *J. Control. Release* **71**, 203–211 (2001).

156. Cheng, J. *et al.* Formulation of functionalized PLGA–PEG nanoparticles for in vivo targeted drug delivery. *Biomaterials* **28**, 869–876 (2007).

157. Wang, P. *et al.* Modified PLGA–PEG–PLGA thermosensitive hydrogels with suitable thermosensitivity and properties for use in a drug delivery system. *J. Mater. Chem. B* **5**, 1551–1565 (2017).

158. Ghahremankhani, A. A., Dorkoosh, F. & Dinarvand, R. PLGA-PEG-PLGA tri-block copolymers as an in-situ gel forming system for calcitonin delivery. *Polym. Bull.* **59**, 637–646 (2007).

159. Jeong, B., Bae, Y. H. & Kim, S. W. Drug release from biodegradable injectable thermosensitive hydrogel of PEG–PLGA–PEG triblock copolymers. *J. Control. Release* **63**, 155–163 (2000).

160. Cui, S., Yu, L. & Ding, J. Thermogelling of Amphiphilic Block Copolymers in Water: ABA Type versus AB or BAB Type. *Macromolecules* **52**, 3697–3715 (2019).

161. Fonseca, C., Simões, S. & Gaspar, R. Paclitaxel-loaded PLGA nanoparticles: preparation, physicochemical characterization and in vitro anti-tumoral activity. *J. Control. Release* **83**, 273–286 (2002).

162. Cartiera, M. S. *et al.* Partial Correction of Cystic Fibrosis Defects with PLGA Nanoparticles Encapsulating Curcumin. *Mol. Pharm.* **7**, 86–93 (2010).

163. Guo, J. *et al.* Aptamer-functionalized PEG–PLGA nanoparticles for enhanced anti-glioma drug delivery. *Biomaterials* **32**, 8010–8020 (2011).

164. Zou, L. *et al.* Administration of PLGA nanoparticles carrying shRNA against focal adhesion kinase and CD44 results in enhanced antitumor effects against ovarian cancer. *Cancer Gene Ther.* **20**, 242–250 (2013).

165. Nance, E. *et al.* Brain-Penetrating Nanoparticles Improve Paclitaxel Efficacy in Malignant Glioma Following Local Administration. *ACS Nano* **8**, 10655–10664 (2014).

166. Pahuja, R. *et al.* Trans-Blood Brain Barrier Delivery of Dopamine-Loaded Nanoparticles Reverses Functional Deficits in Parkinsonian Rats. *ACS Nano* **9**, 4850–4871 (2015).

167. Singh, Y. *et al.* Subcutaneously Administered Ultrafine PLGA Nanoparticles Containing Doxycycline Hydrochloride Target Lymphatic Filarial Parasites. *Mol. Pharm.* **13**, 2084–2094 (2016).

168. Díez-Martínez, R. *et al.* Auranofin-loaded nanoparticles as a new therapeutic tool to fight streptococcal infections. *Sci. Rep.* **6**, 19525 (2016).

169. Gao, S. *et al.* Nanoparticles Encapsulating Nitrosylated Maytansine To Enhance Radiation Therapy. *ACS Nano* **14**, 1468–1481 (2020).

170. Hu, H. *et al.* Fabrication, Optimization, and Evaluation of Paclitaxel and Curcumin Coloaded PLGA Nanoparticles for Improved Antitumor Activity. *ACS Omega* **8**, 976–986 (2023).

171. Fredman, G. *et al.* Targeted nanoparticles containing the proresolving peptide Ac2-26 protect against advanced atherosclerosis in hypercholesterolemic mice. *Sci. Transl. Med.* **7**, 275ra20 (2015).

172. Farokhzad, O. C. *et al.* Targeted nanoparticle-aptamer bioconjugates for cancer chemotherapy in vivo. *Proc. Natl. Acad. Sci.* **103**, 6315–6320 (2006).

173. Grosso, A. D. *et al.* Brain-targeted enzyme-loaded nanoparticles: A breach through the blood-brain barrier for enzyme replacement therapy in Krabbe disease. *Sci. Adv.* **5**, eaax7462 (2019).

174. Palanikumar, L. *et al.* pH-responsive high stability polymeric nanoparticles for targeted delivery of anticancer therapeutics. *Commun. Biol.* **3**, 95 (2020).

175. Woodrow, K. A. *et al.* Intravaginal gene silencing using biodegradable polymer nanoparticles densely loaded with small-interfering RNA. *Nat. Mater.* **8**, 526–533 (2009).

176. Gajbhiye, K. R., Gajbhiye, V., Siddiqui, I. A., Pilla, S. & Soni, V. Ascorbic acid tethered polymeric nanoparticles enable efficient brain delivery of galantamine: An in vitro-in vivo study. *Sci. Rep.* **7**, 11086 (2017).

177. Yang, T. *et al.* Ligand-switchable nanoparticles resembling viral surface for sequential drug delivery and improved oral insulin therapy. *Nat. Commun.* **13**, 6649 (2022).

178. Xiong, M.-H. *et al.* Lipase-Sensitive Polymeric Triple-Layered Nanogel for “On-Demand” Drug Delivery. *J. Am. Chem. Soc.* **134**, 4355–4362 (2012).

179. Liu, B. & Thayumanavan, S. Substituent Effects on the pH Sensitivity of Acetals and Ketals and Their Correlation with Encapsulation Stability in Polymeric Nanogels. *Journal of the American Chemical Society* **139**, 2306–2317 (2017).

180. Wei, H., Cheng, S.-X., Zhang, X.-Z. & Zhuo, R.-X. Thermo-sensitive polymeric micelles based on poly(N-isopropylacrylamide) as drug carriers. *Prog. Polym. Sci.* **34**, 893–910 (2009).

181. Wang, Y. *et al.* Light-Responsive Nanoparticles for Highly Efficient Cytoplasmic Delivery of Anticancer Agents. *ACS Nano* **11**, 12134–12144 (2017).

182. Wei, P., Sun, M., Yang, B., Xiao, J. & Du, J. Ultrasound-responsive polymersomes capable of endosomal escape for efficient cancer therapy. *J. Control. Release* **322**, 81–94 (2020).

183. Griset, A. P. *et al.* Expansile Nanoparticles: Synthesis, Characterization, and in Vivo Efficacy of an Acid-Responsive Polymeric Drug Delivery System. *J. Am. Chem. Soc.* **131**, 2469–2471 (2009).

184. Aryal, S., Hu, C.-M. J. & Zhang, L. Polymer−Cisplatin Conjugate Nanoparticles for Acid-Responsive Drug Delivery. *ACS Nano* **4**, 251–258 (2010).

185. Ibrahim, A. *et al.* Reduction-Responsive Polymer Prodrug Micelles with Enhanced Endosomal Escape Capability for Efficient Intracellular Translocation and Drug Release. *ACS Appl. Bio Mater.* **2**, 5099–5109 (2019).

186. Wan, D., Li, C. & Pan, J. Polymeric Micelles with Reduction-Responsive Function for Targeted Cancer Chemotherapy. *ACS Appl. Bio Mater.* **3**, 1139–1146 (2020).

187. Rehor, A., Hubbell, J. A. & Tirelli, N. Oxidation-Sensitive Polymeric Nanoparticles. *Langmuir* **21**, 411–417 (2005).

188. Lux, C. de G. *et al.* Biocompatible Polymeric Nanoparticles Degrade and Release Cargo in Response to Biologically Relevant Levels of Hydrogen Peroxide. *J. Am. Chem. Soc.* **134**, 15758–15764 (2012).

189. Volpatti, L. R. *et al.* Glucose-Responsive Nanoparticles for Rapid and Extended Self-Regulated Insulin Delivery. *ACS Nano* **14**, 488–497 (2020).

190. Gillies, R. J., Raghunand, N., Karczmar, G. S. & Bhujwalla, Z. M. MRI of the tumor microenvironment. *J. Magn. Reson. Imaging* **16**, 430–450 (2002).

191. Cardone, R. A., Casavola, V. & Reshkin, S. J. The role of disturbed pH dynamics and the Na+/H+ exchanger in metastasis. *Nat. Rev. Cancer* **5**, 786–795 (2005).

192. Webb, B. A., Chimenti, M., Jacobson, M. P. & Barber, D. L. Dysregulated pH: A perfect storm for cancer progression. *Nature Reviews Cancer* **11**, 671–677 (2011).

193. Deirram, N., Zhang, C., Kermaniyan, S. S., Johnston, A. P. R. & Such, G. K. pH-Responsive Polymer Nanoparticles for Drug Delivery. *Macromol. Rapid Commun.* **40**, 1800917 (2019).

194. Casey, J. R., Grinstein, S. & Orlowski, J. Sensors and regulators of intracellular pH. *Nat. Rev. Mol. Cell Biol.* **11**, 50–61 (2010).

195. Gao, W., Chan, J. M. & Farokhzad, O. C. pH-Responsive Nanoparticles for Drug Delivery. *Mol. Pharm.* **7**, 1913–1920 (2010).

196. Yameen, B. *et al.* Insight into nanoparticle cellular uptake and intracellular targeting. *J. Control. Release* **190**, 485–499 (2014).

197. Rica, R. de la, Aili, D. & Stevens, M. M. Enzyme-responsive nanoparticles for drug release and diagnostics. *Adv. Drug Deliv. Rev.* **64**, 967–978 (2012).

198. Duncan, R. Development of HPMA copolymer–anticancer conjugates: Clinical experience and lessons learnt. *Adv. Drug Deliv. Rev.* **61**, 1131–1148 (2009).

199. Huo, M., Yuan, J., Tao, L. & Wei, Y. Redox-responsive polymers for drug delivery: from molecular design to applications. *Polym. Chem.* **5**, 1519–1528 (2013).

200. Guo, X. *et al.* Advances in redox-responsive drug delivery systems of tumor microenvironment. *Journal of Nanobiotechnology* **16**, 1–10 (2018).

201. Hsu, P.-H. & Almutairi, A. Recent progress of redox-responsive polymeric nanomaterials for controlled release. *J. Mater. Chem. B* **9**, 2179–2188 (2021).

202. Schafer, F. Q. & Buettner, G. R. Redox environment of the cell as viewed through the redox state of the glutathione disulfide/glutathione couple. *Free Radic. Biol. Med.* **30**, 1191–1212 (2001).

203. Wu, G., Fang, Y. Z., Yang, S., Lupton, J. R. & Turner, N. D. Glutathione Metabolism and Its Implications for Health. *Journal of Nutrition* **134**, 489–492 (2004).

204. Kuppusamy, P. *et al.* Noninvasive imaging of tumor redox status and its modification by tissue glutathione levels. *Cancer Research* **62**, 307–312 (2002).

205. Cheng, R. *et al.* Glutathione-responsive nano-vehicles as a promising platform for targeted intracellular drug and gene delivery. *Journal of Controlled Release* **152**, 2–12 (2011).

206. Iyer, R. *et al.* Glutathione-responsive biodegradable polyurethane nanoparticles for lung cancer treatment. *J. Control. Release* **321**, 363–371 (2020).

207. Saito, G., Swanson, J. A. & Lee, K.-D. Drug delivery strategy utilizing conjugation via reversible disulfide linkages: role and site of cellular reducing activities. *Adv. Drug Deliv. Rev.* **55**, 199–215 (2003).

208. Yuan, C. *et al.* Composite supramolecular nanoassemblies with independent stimulus sensitivities. *Chem. Sci.* **5**, 229–234 (2013).

209. Phillips, D. J. & Gibson, M. I. Biodegradable Poly(disulfide)s Derived from RAFT Polymerization: Monomer Scope, Glutathione Degradation, and Tunable Thermal Responses. *Biomacromolecules* **13**, 3200–3208 (2012).

210. Fernandes, P. A. & Ramos, M. J. Theoretical Insights into the Mechanism for Thiol/Disulfide Exchange. *Chem. A Eur. J.* **10**, 257–266 (2004).

211. Black, S. P., Sanders, J. K. M. & Stefankiewicz, A. R. Disulfide exchange: exposing supramolecular reactivity through dynamic covalent chemistry. *Chem. Soc. Rev.* **43**, 1861–1872 (2013).

212. Kumar, P., Liu, B. & Behl, G. A Comprehensive Outlook of Synthetic Strategies and Applications of Redox-Responsive Nanogels in Drug Delivery. *Macromolecular Bioscience* **19**, 1–28 (2019).

213. Kanjilal, P., Dutta, K. & Thayumanavan, S. Thiol-Disulfide Exchange as a Route for Endosomal Escape of Polymeric Nanoparticles. *Angew. Chem.* **134**, (2022).

214. Tian, Y., Bian, S. & Yang, W. A redox-labile poly(oligo(ethylene glycol)methacrylate)-based nanogel with tunable thermosensitivity for drug delivery. *Polymer Chemistry* **7**, 1913–1921 (2016).

215. Zhang, L., Xi, L., Shi, G., Zhu, C. & Ni, C. Reduction-responsive zwitterionic nanogels based on carboxymethyl chitosan for enhancing cellular uptake in drug release. *Colloid and Polymer Science* **294**, 629–637 (2016).

216. Zhan, Y. *et al.* Thermo/redox/pH-triple sensitive poly(N-isopropylacrylamide-co-acrylic acid) nanogels for anticancer drug delivery. *Journal of Materials Chemistry B* **3**, 4221–4230 (2015).

217. Mackiewicz, M. *et al.* Nanohydrogel with N,N′-bis(acryloyl)cystine crosslinker for high drug loading. *International Journal of Pharmaceutics* **523**, 336–342 (2017).

218. Ding, J. *et al.* One-step preparation of reduction-responsive poly(ethylene glycol)-poly(amino acid)s nanogels as efficient intracellular drug delivery platforms. *Polymer Chemistry* **2**, 2857–2864 (2011).

219. Oh, J. K., Siegwart, D. J. & Matyjaszewski, K. Synthesis and biodegradation of nanogels as delivery carriers for carbohydrate drugs. *Biomacromolecules* **8**, 3326–3331 (2007).

220. Wen, Y. & Oh, J. K. Dual-stimuli reduction and acidic pH-responsive bionanogels: Intracellular delivery nanocarriers with enhanced release. *RSC Advances* **4**, 229–237 (2014).

221. Tian, Y., Bian, S. & Yang, W. A redox-labile poly(oligo(ethylene glycol)methacrylate)-based nanogel with tunable thermosensitivity for drug delivery. *Polymer Chemistry* **7**, 1913–1921 (2016).

222. Jung, K. O. *et al.* Biodegradable nanogels prepared by atom transfer radical polymerization as potential drug delivery carriers: Synthesis, biodegradation, in vitro release, and bioconjugation. *Journal of the American Chemical Society* **129**, 5939–5945 (2007).

223. Ryu, J. H. *et al.* Self-cross-linked polymer nanogels: A versatile nanoscopic drug delivery platform. *Journal of the American Chemical Society* **132**, 17227–17235 (2010).

224. Zhang, Q., Aleksanian, S., Noh, S. M. & Oh, J. K. Thiol-responsive block copolymer nanocarriers exhibiting tunable release with morphology changes. *Polymer Chemistry* **4**, 351–359 (2013).

225. Zhang, X. *et al.* A facile approach for dual-responsive prodrug nanogels based on dendritic polyglycerols with minimal leaching. *Journal of Controlled Release* **174**, 209–216 (2014).

226. Ding, J. *et al.* Enhanced endocytosis of acid-sensitive doxorubicin derivatives with intelligent nanogel for improved security and efficacy. *Biomaterials Science* **1**, 633–646 (2013).

227. Kildahl, N. K. Bond energy data summarized. *Journal of Chemical Education* **73**, 423–424 (1995).

228. Xu, H., Cao, W. & Zhang, X. Selenium-containing polymers: Promising biomaterials for controlled release and enzyme mimics. *Accounts of Chemical Research* **46**, 1647–1658 (2013).

229. Tian, Y. *et al.* Near-infrared light-responsive nanogels with diselenide-cross-linkers for on-demand degradation and triggered drug release. *Particle and Particle Systems Characterization* **32**, 547–551 (2015).

230. Ma, N., Li, Y., Xu, H., Wang, Z. & Zhang, X. Dual redox responsive assemblies formed from diselenide block copolymers. *Journal of the American Chemical Society* **132**, 442–443 (2010).

231. Han, P. *et al.* Red light responsive diselenide-containing block copolymer micelles. *Journal of Materials Chemistry B* **1**, 740–743 (2013).

232. Sun, C., Ji, S., Li, F. & Xu, H. Diselenide-Containing Hyperbranched Polymer with Light-Induced Cytotoxicity. *ACS Applied Materials and Interfaces* **9**, 12924–12929 (2017).

233. Gao, Y. & Dong, C. M. Triple redox/temperature responsive diselenide-containing homopolypeptide micelles and supramolecular hydrogels thereof. *Journal of Polymer Science, Part A: Polymer Chemistry* **56**, 1067–1077 (2018).

234. Liang, J. & Liu, B. ROS-responsive drug delivery systems. *Bioeng. Transl. Med.* **1**, 239–251 (2016).

235. Trachootham, D., Alexandre, J. & Huang, P. Targeting cancer cells by ROS-mediated mechanisms: A radical therapeutic approach? *Nature Reviews Drug Discovery* **8**, 579–591 (2009).

236. Brieger, K., Schiavone, S., Miller, F. J. & Krause, K. H. Reactive oxygen species: From health to disease. *Swiss Medical Weekly* **142**, 1–14 (2012).

237. Saravanakumar, G., Kim, J. & Kim, W. J. Reactive-Oxygen-Species-Responsive Drug Delivery Systems: Promises and Challenges. *Advanced Science* **4**, (2017).

238. Cheng, X. *et al.* Dual pH and oxidation-responsive nanogels crosslinked by diselenide bonds for controlled drug delivery. *Polymer* **101**, 370–378 (2016).

239. Tan, K. H. *et al.* Selenium-Modified Microgels as Bio-Inspired Oxidation Catalysts. *Angew. Chem. Int. Ed.* **58**, 9791–9796 (2019).

240. Tian, Y., Lei, M., Yan, L. & An, F. Diselenide-crosslinked zwitterionic nanogels with dual redox-labile properties for controlled drug release. *Polymer Chemistry* **11**, 2360–2369 (2020).

241. Li, C. *et al.* PEGylated poly(diselenide-phosphate) nanogel as efficient self-delivery nanomedicine for cancer therapy. *Polymer Chemistry* **6**, 6498–6508 (2015).

242. Hailemeskel, B. Z. *et al.* Synthesis and characterization of diselenide linked poly(ethylene glycol) nanogel as multi-responsive drug carrier. *Applied Surface Science* **449**, 15–22 (2018).

243. Cheng, X. *et al.* Dual pH and oxidation-responsive nanogels crosslinked by diselenide bonds for controlled drug delivery. *Polymer* **101**, 370–378 (2016).

244. Deepagan, V. G. *et al.* In situ diselenide-crosslinked polymeric micelles for ROS-mediated anticancer drug delivery. *Biomaterials* **103**, 56–66 (2016).

245. Fessi, H., Puisieux, F., Devissaguet, J. P., Ammoury, N. & Benita, S. *Rapid Communication Nanocapsule formation by interfacial polymer deposition following solvent displacement*. 55 (1989).

246. Lassalle, V. & Ferreira, M. L. PLA Nano- and Microparticles for Drug Delivery: An Overview of the Methods of Preparation. *Macromol. Biosci.* **7**, 767–783 (2007).

247. Rivas, C. J. M. *et al.* Nanoprecipitation process: From encapsulation to drug delivery. *Int. J. Pharm.* **532**, 66–81 (2017).

248. Miladi, K., Sfar, S., Fessi, H. & Elaissari, A. Polymer Nanoparticles for Nanomedicines, A Guide for their Design, Preparation and Development. 17–53 (2017) doi:10.1007/978-3-319-41421-8_2.

249. Vitale, S. A. & Katz, J. L. Liquid Droplet Dispersions Formed by Homogeneous Liquid−Liquid Nucleation: “The Ouzo Effect.” *Langmuir* **19**, 4105–4110 (2003).

250. Ganachaud, F. & Katz, J. L. Nanoparticles and Nanocapsules Created Using the Ouzo Effect: Spontaneous Emulsification as an Alternative to Ultrasonic and High-Shear Devices. *ChemPhysChem* **6**, 209–216 (2005).

251. Lepeltier, E., Bourgaux, C. & Couvreur, P. Nanoprecipitation and the “Ouzo effect”: Application to drug delivery devices. *Adv. Drug Deliv. Rev.* **71**, 86–97 (2014).

252. Couvreur, P., Barratt, G., Fattal, E., Legrand, P. & Vauthier, C. Nanocapsule Technology: A Review. *Crit. Rev. Ther. Drug Carr. Syst.* **19**, 36 (2002).

253. Legrand, P. *et al.* Influence of polymer behaviour in organic solution on the production of polylactide nanoparticles by nanoprecipitation. *Int. J. Pharm.* **344**, 33–43 (2007).

254. Beck-Broichsitter, M., Nicolas, J. & Couvreur, P. Solvent selection causes remarkable shifts of the “Ouzo region” for poly(lactide- co -glycolide) nanoparticles prepared by nanoprecipitation. *Nanoscale* **7**, 9215–9221 (2015).

255. Stainmesse, S., Orecchioni, A.-M., Nakache, E., Puisieux, F. & Fessi, H. Formation and stabilization of a biodegradable polymeric colloidal suspension of nanoparticles. *Colloid Polym. Sci.* **273**, 505–511 (1995).

256. Hornig, S., Heinze, T., Becer, C. R. & Schubert, U. S. Synthetic polymeric nanoparticles by nanoprecipitation. *J. Mater. Chem.* **19**, 3838–3840 (2009).

257. Aubry, J., Ganachaud, F., Addad, J. P. C. & Cabane, B. Nanoprecipitation of polymethylmethacrylate by solvent shifting: 1. Boundaries. *Langmuir* **25**, 1970–1979 (2009).

258. Govender, T., Stolnik, S., Garnett, M. C., Illum, L. & Davis, S. S. PLGA nanoparticles prepared by nanoprecipitation: drug loading and release studies of a water soluble drug. *J. Control. Release* **57**, 171–185 (1999).

259. Peltonen, L., Aitta, J., Hyvönen, S., Karjalainen, M. & Hirvonen, J. Improved entrapment efficiency of hydrophilic drug substance during nanoprecipitation of poly(l)lactide nanoparticles. *AAPS PharmSciTech* **5**, 115 (2009).

260. Dong, Y. & Feng, S.-S. Methoxy poly(ethylene glycol)-poly(lactide) (MPEG-PLA) nanoparticles for controlled delivery of anticancer drugs. *Biomaterials* **25**, 2843–2849 (2004).

261. Verger, M. L.-L., Fluckiger, L., Kim, Y.-I., Hoffman, M. & Maincent, P. Preparation and characterization of nanoparticles containing an antihypertensive agent. *Eur. J. Pharm. Biopharm.* **46**, 137–143 (1998).

262. Domínguez-Ríos, R. *et al.* Cisplatin-loaded PLGA nanoparticles for HER2 targeted ovarian cancer therapy. *Colloids Surf. B: Biointerfaces* **178**, 199–207 (2019).

263. Liu, Q. *et al.* Enhanced antitumor efficacy, biodistribution and penetration of docetaxel-loaded biodegradable nanoparticles. *Int. J. Pharm.* **430**, 350–358 (2012).

264. Ven, H. V. de *et al.* PLGA nanoparticles and nanosuspensions with amphotericin B: Potent in vitro and in vivo alternatives to Fungizone and AmBisome. *J. Control. Release* **161**, 795–803 (2012).

265. Desgouilles, S. *et al.* The Design of Nanoparticles Obtained by Solvent Evaporation: A Comprehensive Study. *Langmuir* **19**, 9504–9510 (2003).

266. Hariharan, S., Bala, I. & Kumar, M. N. V. R. PLGA Nanoparticles in Drug Delivery: The State of the Art. *Crit. Rev. Ther. Drug Carr. Syst.* **21**, 36 (2004).

267. Song, C. X. *et al.* Formulation and characterization of biodegradable nanoparticles for intravascular local drug delivery. *J. Control. Release* **43**, 197–212 (1997).

268. Jaiswal, J., Gupta, S. K. & Kreuter, J. Preparation of biodegradable cyclosporine nanoparticles by high-pressure emulsification-solvent evaporation process. *J. Control. Release* **96**, 169–178 (2004).

269. Ueda, M. & Kreuter, J. Optimization of the preparation of loperamide-loaded poly (L-lactide) nanoparticles by high pressure emulsification-solvent evaporation. *J. Microencapsul.* **14**, 593–605 (1997).

270. Kızılbey, K. Optimization of Rutin-Loaded PLGA Nanoparticles Synthesized by Single-Emulsion Solvent Evaporation Method. *ACS Omega* **4**, 555–562 (2019).

271. Ubrich, N., Bouillot, P., Pellerin, C., Hoffman, M. & Maincent, P. Preparation and characterization of propranolol hydrochloride nanoparticles: a comparative study. *J. Control. Release* **97**, 291–300 (2004).

272. Lamprecht, A. *et al.* Biodegradable monodispersed nanoparticles prepared by pressure homogenization-emulsification. *Int. J. Pharm.* **184**, 97–105 (1999).

273. Vinogradov, S., Batrakova, E. & Kabanov, A. Poly(ethylene glycol)-polyethyleneimine NanoGel(TM) particles: Novel drug delivery systems for antisense oligonucleotides. *Colloids and Surfaces B: Biointerfaces* **16**, 291–304 (1999).

274. Vinogradov, S. V., Zeman, A. D., Batrakova, E. V. & Kabanov, A. V. Polyplex Nanogel formulations for drug delivery of cytotoxic nucleoside analogs. *Journal of Controlled Release* **107**, 143–157 (2005).

275. Gou, M. *et al.* Efficient inhibition of C-26 colon carcinoma by VSVMP gene delivered by biodegradable cationic nanogel derived from polyethyleneimine. *ACS Nano* **4**, 5573–5584 (2010).

276. Santis, S. D., Diociaiuti, M., Cametti, C. & Masci, G. Hyaluronic acid and alginate covalent nanogels by template cross-linking in polyion complex micelle nanoreactors. *Carbohydrate Polymers* **101**, 96–103 (2014).

277. Steinhilber, D. *et al.* Surfactant free preparation of biodegradable dendritic polyglycerol nanogels by inverse nanoprecipitation for encapsulation and release of pharmaceutical biomacromolecules. *Journal of Controlled Release* **169**, 289–295 (2013).

278. Zhang, Y. *et al.* One-Step “click Chemistry”-Synthesized Cross-Linked Prodrug Nanogel for Highly Selective Intracellular Drug Delivery and Upregulated Antitumor Efficacy. *ACS Applied Materials and Interfaces* **8**, 10673–10682 (2016).

279. Liu, J., Uhlir, C., Shah, P. K., Sun, F. & Stansbury, J. W. Controlled nanogel and macrogel structures from self-assembly of a stimuli-responsive amphiphilic block copolymer. *RSC Advances* **6**, 64791–64798 (2016).

280. Bhatia, S. *et al.* Adaptive Flexible Sialylated Nanogels as Highly Potent Influenza A Virus Inhibitors. *Angewandte Chemie - International Edition* 12417–12422 (2020) doi:10.1002/anie.202006145.

281. Zhao, L. *et al.* Facile one-pot synthesis of glucose-sensitive nanogel via thiol-ene click chemistry for self-regulated drug delivery. *Acta Biomaterialia* **9**, 6535–6543 (2013).

282. Bhattacharya, K. *et al.* REDOX Responsive Fluorescence Active Glycopolymer Based Nanogel: A Potential Material for Targeted Anticancer Drug Delivery. *ACS Applied Bio Materials* **2**, 2587–2599 (2019).

283. Rao, J. P. & Geckeler, K. E. Polymer nanoparticles: Preparation techniques and size-control parameters. *Prog. Polym. Sci.* **36**, 887–913 (2011).

284. Ma, J. *et al.* Liposomes-Camouflaged Redox-Responsive Nanogels to Resolve the Dilemma between Extracellular Stability and Intracellular Drug Release. *Macromolecular Bioscience* **18**, 1–10 (2018).

285. Graham, N. B. & Cameron, A. Nanogels and microgels: The new polymeric materials playground. *Pure and Applied Chemistry* **70**, 1271–1275 (1998).

286. Biffis, A., Graham, N. B., Siedlaczek, G., Stalberg, S. & Wulff, G. The synthesis, characterization and molecular recognition properties of imprinted microgels. *Macromolecular Chemistry and Physics* **202**, 163–171 (2001).

287. Chen, Z. *et al.* Molecularly imprinted soluble nanogels as a peroxidase-like catalyst in the oxidation reaction of homovanillic acid under aqueous conditions. *Applied Catalysis A: General* **328**, 252–258 (2007).

288. Yan, M. *et al.* A novel intracellular protein delivery platform based on single-protein nanocapsules. *Nat. Nanotechnol.* **5**, 48–53 (2010).

289. Tian, H. *et al.* Growth-Factor Nanocapsules That Enable Tunable Controlled Release for Bone Regeneration. *ACS Nano* **10**, 7362–7369 (2016).

290. Zhao, M. *et al.* Clickable Protein Nanocapsules for Targeted Delivery of Recombinant p53 Protein. *J. Am. Chem. Soc.* **136**, 15319–15325 (2014).

291. Yan, M., Ge, J., Liu, Z. & Ouyang, P. Encapsulation of single enzyme in nanogel with enhanced biocatalytic activity and stability. *Journal of the American Chemical Society* **128**, 11008–11009 (2006).

292. Beloqui, A., Kobitski, A. Y., Nienhaus, G. U. & Delaittre, G. A simple route to highly active single-enzyme nanogels. *Chem. Sci.* **9**, 1006–1013 (2017).

293. Basak, S. *et al.* Simultaneous Cross-Linking and Cross-Polymerization of Enzyme Responsive Polyethylene Glycol Nanogels in Con fi ned Aqueous Droplets for Reduction of Low-Density Lipoprotein Oxidation. (2020) doi:10.1021/acs.biomac.0c01238.

294. Landfester, K., Willert, M. & Antonietti, M. Preparation of polymer particles in nonaqueous direct and inverse miniemulsions. *Macromolecules* **33**, 2370–2376 (2000).

295. Antonietti, M. & Landfester, K. Polyreactions in miniemulsions. *Progress in Polymer Science (Oxford)* **27**, 689–757 (2002).

296. Capek, I. On inverse miniemulsion polymerization of conventional water-soluble monomers. *Advances in Colloid and Interface Science* **156**, 35–61 (2010).

297. Porras, M., Solans, C., González, C. & Gutiérrez, J. M. Properties of water-in-oil (W/O) nano-emulsions prepared by a low-energy emulsification method. *Colloids and Surfaces A: Physicochemical and Engineering Aspects* **324**, 181–188 (2008).

298. Landfester, K., Bechthold, N., Förster, S. & Antonietti, M. Evidence for the preservation of the particle identity in miniemulsion polymerization. *Macromolecular Rapid Communications* **20**, 81–84 (1999).

299. Medeiros, S. F., Santos, A. M., Fessi, H. & Elaissari, A. Synthesis of biocompatible and thermally sensitive poly(N-vinylcaprolactam) nanogels via inverse miniemulsion polymerization: Effect of the surfactant concentration. *Journal of Polymer Science, Part A: Polymer Chemistry* **48**, 3932–3941 (2010).

300. Landfester, K. Synthesis of Colloidal Particles in Miniemulsions. *Annual Review of Materials Research* **36**, 231–279 (2006).

301. Klinger, D., Aschenbrenner, E. M., Weiss, C. K. & Landfester, K. Enzymatically degradable nanogels by inverse miniemulsion copolymerization of acrylamide with dextran methacrylates as crosslinkers. *Polymer Chemistry* **3**, 204–216 (2012).

302. Peres, L. B. *et al.* pH-responsive physically and chemically cross-linked glutamic-acid-based hydrogels and nanogels. *European Polymer Journal* **101**, 341–349 (2018).

303. Nagarajan, R. & Ruckenstein, E. Molecular theory of microemulsions. *Langmuir* **16**, 6400–6415 (2000).

304. Pavel, F. M. Microemulsion polymerization. *Journal of Dispersion Science and Technology* **25**, 1–16 (2004).

305. Candau, F., Leong, Y. S. & Fitch, R. M. No Title. *J. Polym. Sci.: Polym. Chem. Ed.* **23**, 193–214 (1985).

306. Candau, F., Leong, Y. S., Pouyet, G. & Candau, S. Inverse microemulsion polymerization of acrylamide: Characterization of the water-in-oil microemulsions and the final microlatexes. *Journal of Colloid And Interface Science* **101**, 167–183 (1984).

307. Lacík, I., Bartoň, J. & Warr, G. G. Use of fluorescence to study inverse microemulsion polymerization of acrylamide. *Macromolecular Chemistry and Physics* **196**, 2223–2236 (1995).

308. Leong, Y. S. & Candau, F. Inverse microemulsion polymerization. *Journal of Physical Chemistry* **86**, 2269–2271 (1982).

309. Gao, D., Xu, H., Philbert, M. A. & Kopelman, R. Ultrafine hydrogel nanoparticles: Synthetic approach and therapeutic application in living cells. *Angewandte Chemie - International Edition* **46**, 2224–2227 (2007).

310. Shi, L., Khondee, S., Linz, T. H. & Berkland, C. Poly(N-vinylformamide) nanogels capable of pH-sensitive protein release. *Macromolecules* **41**, 6546–6554 (2008).

311. Khorasani, R. & Pourmahdian, S. Synthesis and characterization of hydrogel nanoparticles through inverse microemulsion polymerization of 2-Acrylamido-2-methyl-1-propanesulfonic Acid. *Journal of Macromolecular Science, Part A: Pure and Applied Chemistry* **51**, 240–248 (2014).

312. McAllister, K. *et al.* Polymeric nanogels produced via inverse microemulsion polymerization as potential gene and antisense delivery agents. *Journal of the American Chemical Society* **124**, 15198–15207 (2002).

313. Odian, G. *Principles of Polymerization*. (John Wiley & Sons, Inc., 2004). doi:10.1002/047147875x.

314. Sanson, N. & Rieger, J. Synthesis of nanogels/microgels by conventional and controlled radical crosslinking copolymerization. *Polymer Chemistry* **1**, 965–977 (2010).

315. Duracher, D., Elaïssari, A. & Pichot, C. Preparation of poly(N-isopropylmethacrylamide) latexes kinetic studies and characterization. *Journal of Polymer Science, Part A: Polymer Chemistry* **37**, 1823–1837 (1999).

316. Arshady, R. Suspension, emulsion, and dispersion polymerization: A methodological survey. *Colloid & Polymer Science* **270**, 717–732 (1992).

317. Blackburn, W. H., Dickerson, E. B., Smith, M. H., McDonald, J. F. & Lyon, L. A. Peptide-functionalized nanogels for targeted siRNA delivery. *Bioconjugate Chemistry* **20**, 960–968 (2009).

318. Pakulska, M. M. *et al.* Encapsulation-free controlled release: Electrostatic adsorption eliminates the need for protein encapsulation in PLGA nanoparticles. *Sci. Adv.* **2**, e1600519 (2016).

319. Ossipov, D., Kootala, S., Yi, Z., Yang, X. & Hilborn, J. Orthogonal chemoselective assembly of hyaluronic acid networks and nanogels for drug delivery. *Macromolecules* **46**, 4105–4113 (2013).

320. Wu, M. *et al.* Reduction/photo dual-responsive polymeric prodrug nanoparticles for programmed siRNA and doxorubicin delivery. *Biomater. Sci.* **6**, 1457–1468 (2018).

321. Zhao, X. *et al.* Polymerization-Induced Self-Assembly to Produce Prodrug Nanoparticles with Reduction-Responsive Camptothecin Release and pH-Responsive Charge-Reversible Property. *Macromol. Rapid Commun.* **41**, 2000260 (2020).

322. Wang, Y. *et al.* Tuning the efficacy of esterase-activatable prodrug nanoparticles for the treatment of colorectal malignancies. *Biomaterials* **270**, 120705 (2021).

323. Wang, X., Cheng, R., Cheng, L. & Zhong, Z. Lipoyl Ester Terminated Star PLGA as a Simple and Smart Material for Controlled Drug Delivery Application. *Biomacromolecules* **19**, 1368–1373 (2018).

324. Wang, X., Qiu, M., Deng, C., Cheng, R. & Zhong, Z. Targeted and Reduction-Sensitive Cross-Linked PLGA Nanotherapeutics for Safer and Enhanced Chemotherapy of Malignant Melanoma. *ACS Biomater. Sci. Eng.* **6**, 2621–2629 (2020).

325. Liu, X., II, A. L. M., Yaszemski, M. J. & Lu, L. Biodegradable and crosslinkable PPF–PLGA–PEG self-assembled nanoparticles dual-decorated with folic acid ligands and Rhodamine B fluorescent probes for targeted cancer imaging. *RSC Adv.* **5**, 33275–33282 (2015).

326. Stayshich, R. M. & Meyer, T. Y. Preparation and Microstructural Analysis of Poly(lactic-alt-glycolic acid). *Journal of Polymer Science: Part A: Polymer Chemistry* **46**, 4704–4711 (2008).

327. Stayshich, R. M. & Meyer, T. Y. New insights into poly(lactic- co -glycolic acid) microstructure: Using repeating sequence copolymers to decipher complex NMR and thermal behavior. *Journal of the American Chemical Society* **132**, 10920–10934 (2010).

328. Bertrand, N. *et al.* Mechanistic understanding of in vivo protein corona formation on polymeric nanoparticles and impact on pharmacokinetics. *Nature Communications* **8**, (2017).

329. Zweers, M. L. T., Engbers, G. H. M., Grijpma, D. W. & Feijen, J. In vitro degradation of nanoparticles prepared from polymers based on dl-lactide, glycolide and poly(ethylene oxide). *J. Control. Release* **100**, 347–356 (2004).

330. Swider, E. *et al.* Förster Resonance Energy Transfer-Based Stability Assessment of PLGA Nanoparticles in Vitro and in Vivo. *ACS Appl. Bio Mater.* **2**, 1131–1140 (2019).

331. Takagi, T. *et al.* A Provisional Biopharmaceutical Classification of the Top 200 Oral Drug Products in the United States, Great Britain, Spain, and Japan. *Mol. Pharm.* **3**, 631–643 (2006).

332. Di, L., Fish, P. V. & Mano, T. Bridging solubility between drug discovery and development. *Drug Discov. Today* **17**, 486–495 (2012).

333. Williams, H. D. *et al.* Strategies to Address Low Drug Solubility in Discovery and Development. *Pharmacol. Rev.* **65**, 315–499 (2013).

334. Rodriguez-Aller, M., Guillarme, D., Veuthey, J.-L. & Gurny, R. Strategies for formulating and delivering poorly water-soluble drugs. *J. Drug Deliv. Sci. Technol.* **30**, 342–351 (2015).

335. Louage, B., Tack, L., Wang, Y. & Geest, B. G. D. Poly(glycerol sebacate) nanoparticles for encapsulation of hydrophobic anti-cancer drugs. *Polym. Chem.* **8**, 5033–5038 (2017).

336. Bordag, N. *et al.* Glucocorticoid (dexamethasone)-induced metabolome changes in healthy males suggest prediction of response and side effects. *Sci. Rep.* **5**, 15954 (2015).

337. Mitre-Aguilar, I. B., Cabrera-Quintero, A. J. & Zentella-Dehesa, A. Genomic and non-genomic effects of glucocorticoids: implications for breast cancer. *Int. J. Clin. Exp. Pathol.* **8**, 1–10 (2014).

338. Ahmed, M. H. & Hassan, A. Dexamethasone for the Treatment of Coronavirus Disease (COVID-19): a Review. *SN Compr. Clin. Med.* **2**, 2637–2646 (2020).

339. Rožanc, J., Žižek, M., Milojević, M., Maver, U. & Finšgar, M. Dexamethasone-Loaded Bioactive Coatings on Medical Grade Stainless Steel Promote Osteointegration. *Pharmaceutics* **13**, 568 (2021).

340. Samtani, M. N. & Jusko, W. J. Stability of dexamethasone sodium phosphate in rat plasma. *Int. J. Pharm.* **301**, 262–266 (2005).

341. Salt, A. N., Hartsock, J. J., Piu, F. & Hou, J. Dexamethasone and dexamethasone phosphate entry into perilymph compared for middle ear applications in Guinea Pigs. *Audiology and Neurotology* **23**, 245–257 (2018).

342. Simón-Vázquez, R. *et al.* Improving dexamethasone drug loading and efficacy in treating arthritis through a lipophilic prodrug entrapped into PLGA-PEG nanoparticles. *Drug Deliv. Transl. Res.* **12**, 1270–1284 (2022).

343. Lammers, T. *et al.* Dexamethasone nanomedicines for COVID-19. *Nat. Nanotechnol.* **15**, 622–624 (2020).

344. Gómez-Gaete, C., Tsapis, N., Besnard, M., Bochot, A. & Fattal, E. Encapsulation of dexamethasone into biodegradable polymeric nanoparticles. *Int. J. Pharm.* **331**, 153–159 (2007).

345. Gómez-Gaete, C., Fattal, E., Silva, L., Besnard, M. & Tsapis, N. Dexamethasone acetate encapsulation into Trojan particles. *J. Control. Release* **128**, 41–49 (2008).

346. Hickey, J. W., Santos, J. L., Williford, J.-M. & Mao, H.-Q. Control of polymeric nanoparticle size to improve therapeutic delivery. *J. Control. Release* **219**, 536–547 (2015).

347. Pino, P. D. *et al.* Protein corona formation around nanoparticles - From the past to the future. *Materials Horizons* **1**, 301–313 (2014).

348. Moore, T. L. *et al.* Nanoparticle colloidal stability in cell culture media and impact on cellular interactions. *Chemical Society Reviews* **44**, 6287–6305 (2015).

349. Đorđević, S. *et al.* Current hurdles to the translation of nanomedicines from bench to the clinic. *Drug Delivery and Translational Research* **12**, 500–525 (2022).

350. Lu, X. *et al.* Nanoparticles Containing Anti-inflammatory Agents as Chemotherapy Adjuvants: Optimization and In Vitro Characterization. *AAPS J.* **10**, 133–140 (2008).

351. Solubility data extracted from DrugBank. https://go.drugbank.com.

352. Owen, D. R. *et al.* Human pharmacokinetics of XBD173 and etifoxine distinguish their potential for pharmacodynamic effects mediated by translocator protein. *Br. J. Clin. Pharmacol.* **88**, 4230–4236 (2022).

353. Ragheb, R. & Nobbmann, U. Multiple scattering effects on intercept, size, polydispersity index, and intensity for parallel (VV) and perpendicular (VH) polarization detection in photon correlation spectroscopy. *Sci. Rep.* **10**, 21768 (2020).

354. Gambles, M. T., Fan, B., Borecki, A. & Gillies, E. R. Hybrid Polyester Self-Immolative Polymer Nanoparticles for Controlled Drug Release. *ACS Omega* **3**, 5002–5011 (2018).

355. Johansson, L., Gafvelin, G. & Arnér, E. S. J. Selenocysteine in proteins—properties and biotechnological use. *Biochim. Biophys. Acta (BBA) - Gen. Subj.* **1726**, 1–13 (2005).

356. Xie, Y., Short, M. D., Cassidy, P. B. & Roberts, J. C. Selenazolidines as Novel Organoselenium Delivery Agents. *Bioorg. Med. Chem. Lett.* **11**, 2911–2915 (2001).

357. Duddeck, H. 77Se NMR Spectroscopy and Its Applications in Chemistry. *Annu. Rep. NMR Spectrosc.* **52**, 105–166 (2004).

358. Moriello, A. S. *et al.* Elongation of the Hydrophobic Chain as a Molecular Switch: Discovery of Capsaicin Derivatives and Endogenous Lipids as Potent Transient Receptor Potential Vanilloid Channel 2 Antagonists. *Journal of Medicinal Chemistry* **61**, 8255–8281 (2018).

Figures and schemes presented in this thesis were created using Biorender, GraphPad Prism, and ChemDraw.